# Transition metal modified titanium dioxide photocatalysts for the removal of nitric oxide

**Neil Bowering, BSc(Hons)**


Thesis submitted to the University of Nottingham for the degree

of Doctor of Philosophy, April 2004

**Contents** i

**Acknowledgements** vii

**Abstract** viii

**List of abbreviations** x

**1 Introduction** 1

1.1 Air pollution 1

1.2 Environmental impact of $NO_x$ emissions 2

1.3 Control of $NO_x$ emissions 4

1.4 Selective catalytic reduction of $NO_x$ 5

1.4.1 Thermally activated catalytic reactions 5

1.4.2 Photocatalytic reactions 6

1.5 Aims of the research 8

1.6 Thesis overview 9

1.7 References 10

**2 Literature Review** 11

2.1 Introduction 11

2.2 Terms and definitions in catalysis and photocatalysis 12

2.2.1 Thermal catalysis 12

2.2.2 Photocatalysis 14

2.2.3 Heterogeneous photocatalysis 15

2.3 Theory of semiconductor photocatalysis 17

2.3.1 Basic principles 17

2.3.2 Band bending and the formation of a Schottky barrier 20

2.4 Titanium dioxide photocatalysis 23

2.4.1 Properties of titanium dioxide 23

2.4.2 Supported $TiO_2$ photocatalysts- Effect of film thickness 27

2.5 Effect of transition metal modification on photocatalytic behaviour 28

2.6 Environmental applications of semiconductor photocatalysis 32

2.6.1 Photocatalytic degradation of organic pollutants 32

2.6.1.1 Water and oxygen adsorption on $TiO_2$ surfaces 35

2.6.1.2 Oxidation of alkanes and alkenes 37

2.6.1.3 Oxidation of alcohols 42

2.6.2 Photocatalytic elimination of nitric oxide 45

2.6.2.1 Introduction 45

2.6.2.2 NO photooxidation reactions 47

2.6.2.3 NO decomposition reactions 52

2.6.2.4 NO reduction reactions 57

2.7 Summary 63

2.8 References 65

**3 Experimental 70**

3.1 Introduction 70

3.2 Preparation of $TiO_2$ and modified $TiO_2$ photocatalysts 70

3.3 Estimation of film thickness 72

3.4 Photoreactor 74

3.4.1 Photoreactor design 74

3.4.2 Reaction chamber 75

3.4.3 Photoreactions 77

3.4.4 Quantification of the reaction data 82

3.5 Characterisation techniques and sample handling 85

3.5.1 X-ray diffraction (XRD) 85

3.5.2 Transmission electron microscopy (TEM) 88

3.5.3 X-ray photoelectron spectroscopy (XPS) 89

3.5.4 Differential scanning calorimetry (DSC) 91

3.6 References 91

**4 Characterisation 92**

4.1 Introduction 92

4.2 Results 93

4.2.1 Characterisation of unmodified P25 93

4.2.1.1 XRD 93

4.2.1.2 TEM 97

4.2.1.3 XPS 98

4.2.1.4 DSC 101

4.2.2 Characterisation of silver modified P25 photocatalysts 103

4.2.2.1 Introduction 103

4.2.2.2 XRD 103

4.2.2.3 TEM 109

4.2.2.4 XPS 110

4.2.3 Characterisation of rhodium modified P25 photocatalysts 118

4.2.3.1 Introduction 118

4.2.3.2 XRD 118

4.2.3.3 TEM 120

4.2.3.4 XPS 121

4.3 Discussion 126

4.3.1 Unmodified P25 photocatalysts 126

4.3.2 Silver modified P25 photocatalysts 129

4.3.3 Rhodium modified P25 photocatalysts 136

4.4 Conclusions 139

4.5 References 141

**5 Photocatalytic reactions over Degussa P25 photocatalysts 142**

5.1 Introduction 142

5.2 Results 144

5.2.1 UV lamp emissions 144

5.2.2 Reproducibility experiments 145

5.2.3 Effect of thermal processing 147

5.2.4 Effect of varying NO concentration 149

5.2.5 Effect of varying CO concentration 151

5.3 Discussion 152

5.3.1 Effect of thermal processing 152

5.3.2 Effect of varying NO concentration 162

5.3.3 Effect of varying CO concentration 167

5.4 Conclusions 170

5.5 References 171

**6 Photocatalytic reactions over silver modified Degussa P25 photocatalysts 173**

6.1 Introduction 173

6.2 Results 175

6.2.1 0.1Ag-P25 photocatalysts – Effect of calcination temperature 175

6.2.2 1Ag-P25 photocatalysts – Effect of calcination temperature 178

6.2.3 5Ag-P25 photocatalysts – Effect of calcination temperature 180

6.2.4 Effect of varying NO concentration 182

6.2.5 Effect of varying CO concentration 184

6.3 Discussion 186

6.3.1 Effect of silver species on photocatalytic behaviour 186

6.3.2 Effect of varying NO concentration 196

6.3.3 Effect of varying CO concentration 200

6.4 Conclusions 202

6.5 References 203

**7 Photocatalytic reactions over rhodium modified Degussa P25 photocatalysts. 205**

7.1 Introduction 205

7.2 Results 206

7.2.1 Rh-P25 photocatalysts – Dried at 70°C 206

7.2.2 Rh-P25 photocatalysts – Calcined at 200°C 209

7.2.3 Rh-P25 photocatalysts – UV reduced 211

7.2.4 Rh-P25 photocatalysts – Hydrogen reduced 213

7.2.5 Effect of varying NO concentration 216

7.2.6 Effect of varying CO concentration 218

7.3 Discussion 219

7.3.1 Effect of rhodium 219

7.3.2 Effect of varying NO concentration 230

7.3.3 Effect of varying CO concentration 233

7.4 Conclusions 236

7.5 References 237

**8 Conclusions 239**

8.1 Overview of results 239

8.2 Conclusions from unmodified P25 photocatalysts 240

8.3 Conclusions from silver modified P25 photocatalysts 241

8.4 Conclusions from rhodium modified P25 photocatalysts 242

**9 Future Work 244**

# Acknowledgements

I would like to take this opportunity to thank Dr Gavin Walker and Dr Philip Harrison under whose supervision this work has been carried out. Their continued support, guidance and encouragement throughout the project has been much appreciated.

I also wish to thank members of the research and technical staff from the School of Mechanical, Materials, Manufacturing Engineering and Management and School of Chemistry who have given invaluable assistance. In particular thanks are given to Mr Keith Dinsdale and Dr Emily Smith for their expertise in the acquisition of TEM and XPS data, respectively.

Special thanks are given to all my family, in particular my Mother and Father, for this would not have been possible without their endless support and encouragement. Sincere thanks are given to Deborah for her understanding and patience during the preparation of this manuscript.

Finally, I would like to thank the countless people who have ensured that my postgraduate days in Nottingham will always be remembered. Although too many to mention, special thanks are given to Frank, Stuart, Karen and Matt.

# Abstract

Photocatalytic NO decomposition and reduction reactions, using CO as a reducing gas, have been investigated over $TiO_2$, Ag-$TiO_2$ and Rh-$TiO_2$ photocatalysts, using a purpose built continuous flow photoreactor. The transition metal modified $TiO_2$ photocatalysts were prepared using wet impregnation techniques, and the effect of thermal processing parameters on their photocatalytic behaviour was studied. Prepared photocatalysts were characterised using a number of complementary techniques, including XRD, TEM, DSC, and XPS. The findings from these techniques were used to explain the observed photocatalytic properties.

The activity and selectivity of the photocatalysts were found to be dependant on a number of factors; thermal pretreatment temperature, type and amount of the modifying element, chemical nature of the modifying element and the reaction conditions used. It was found, for $TiO_2$ photocatalysts, that increasing the pretreatment calcination temperature resulted in lower NO conversion rates, due to removal of surface bound hydroxyl groups. A similar trend was observed for Ag-P25 photocatalysts, but the reduction in activity was greater due to the presence of larger silver clusters, which acted as recombination centres for photogenerated electron-hole pairs. The activity of the Ag-P25 photocatalysts decreased as the silver loadings increased, whilst the activity of the Rh-P25 photocatalysts remained largely unaffected by the metal concentration.

Over $TiO_2$ and Ag-$TiO_2$ systems, the NO conversion rate was lower for the reduction reactions compared to decomposition reactions. This was attributed to the preferential adsorption of the CO molecules, blocking NO adsorption sites. Contrasting behaviour was observed over Rh-P25 systems and NO conversions as high as 87 % were recorded in the presence of CO.

Silver modified catalysts were highly selective for $N_2$ formation (90 %) whilst rhodium modified catalysts were more selective for $N_2O$ formation. These results are discussed with respect to the possible surface reactions and the chemical intermediates that may be formed.

# List of abbreviations

| | |
|---|---|
| BET | Brunauer-Emmett-Teller surface area |
| DSC | Differential scanning calorimetry |
| EDX | Energy dispersive X-ray analysis |
| EPR | Electron paramagnetic resonance |
| ESR | Electron spin resonance |
| EXAFS | Extended X-ray atomic fine structure |
| FQE | Formal quantum efficiency |
| FTIR | Fourier transform infrared spectroscopy |
| IPA | Isopropyl alcohol |
| P25 | Degussa P25 type $TiO_2$ |
| PEG | Polyethylene glycol |
| PPM | Parts per million |
| SCCM | Standard centimetre cubed per minute / $cm^3$ $min^{-1}$ |
| SCR | Selective catalytic reduction |
| TCE | Trichloroethylene |
| TDW | Triply deionised water |
| TEM | Transmission electron microscopy |
| TOF-SIMS | Time of flight secondary ion mass spectrometry |
| TON | Turnover number |
| UNECE | United nation economic commission for Europe |
| UV | Ultra violet |
| VOC | Volatile organic compounds |
| XPS | X-ray photoelectron spectroscopy |
| XRD | X-ray diffraction |

# 1 Introduction

## 1.1 Air pollution

In 1967 the European Council provided the following definition of air pollution.[1]

"*Air pollution occurs when the presence of a foreign substance or large variation in the proportion of its components is liable to cause a harmful effect according to the scientific knowledge of the time, or to create a discomfort.*"

Although this definition allows for the inclusion of irritants such as noise as well as the more obvious harmful effects from chemical compounds, it is a very general definition that also encompasses the fact that air pollution can be responsible for detrimental effects to plants, animals, and human life. It can also cause accelerated rates of corrosion to buildings. Within the boundaries of this definition is pollution from natural sources such as volcanic eruptions that can propel tons of gases and ash into the atmosphere, which can subsequently be carried long distances by wind. Trees, plants and rotting vegetation are other sources of natural pollution since they release hydrocarbon gases into the atmosphere. However, a more serious type of air pollution in urban areas is anthropogenic pollution. Common sources of such air pollution include the combustion of fossil fuels, e.g. from industrial processes and emissions from road transport vehicles. The pollutants of main concern include carbon monoxide, nitrogen oxides ($NO_x$) and hydrocarbons.

## 1.2 Environmental impact of $NO_x$ emissions

The oxides of nitrogen, collectively termed $NO_x$, consist of nitrogen dioxide ($NO_2$) and nitrogen monoxide (nitric oxide, NO). These gases form at high temperatures in air during fuel combustion, and are produced primarily by road transport and the energy production industry. Although industries and automobile manufacturers have to conform to increasingly more stringent regulations which limit harmful emissions, air pollution levels are still very high around industrial sites and areas of high traffic use. The map of $NO_x$ levels in the UK, shown in figure 1.1, quite clearly illustrates that pollution levels are highest around industrial regions and areas of high traffic use, as all the major cities and motorways can be identified from high $NO_x$ levels.

$NO_x$ gases present serious environmental and health hazards. They are a cause of acid rain, which forms when $NO_x$ is oxidised in air to produce nitric acid ($HNO_3$). Acid rain can disrupt plant growth, destroy aquatic environments, cause damage to buildings and other structures, and affect human health. $NO_x$ emissions also contribute to ground-level ozone, or smog, resulting from the reaction between $NO_x$ and volatile organic compounds (VOCs) in the presence of sunlight. Ground-level ozone can lead to serious respiratory problems in humans.

$NO_x$ emissions are a complex global problem. They are primarily produced in industrialised and developing nations, particularly those with high road transport levels. Once emitted, $NO_x$ becomes a transboundary pollutant, capable of causing widespread damage. For example, forests in Scandinavia have been damaged due to acid rain from pollutants emitted in the United Kingdom and other parts of Europe.[2]

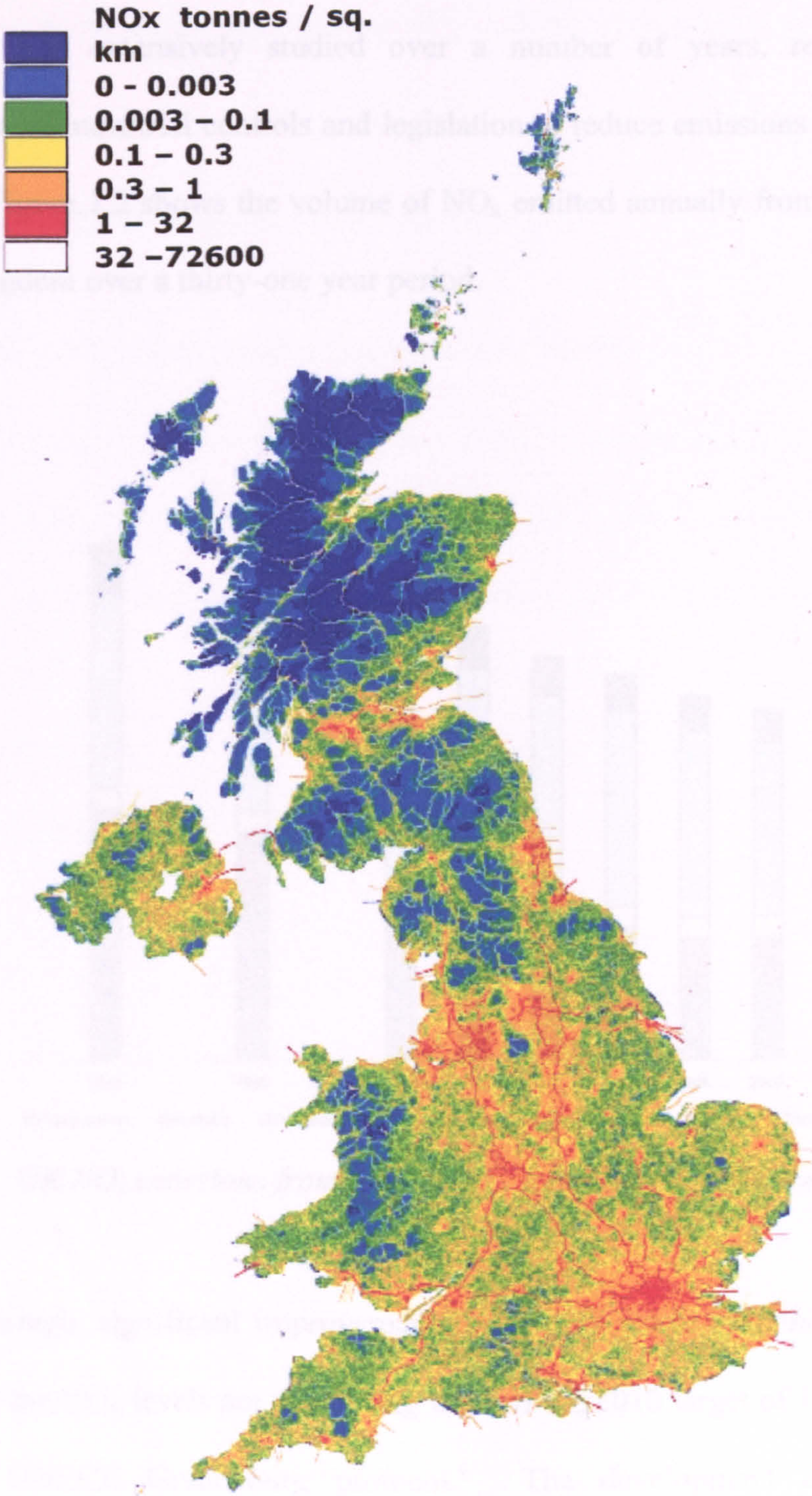


*Figure 1.1. Map of the UK showing the levels of atmospheric $NO_x$ pollution. Reproduced from Dore.*[3]

## 1.3 Control of $NO_x$ emissions

The worldwide effects of $NO_x$ on health and the environment have been recognised and extensively studied over a number of years, resulting in the introduction of industrial controls and legislation to reduce emissions of this harmful pollutant. Figure 1.2 shows the volume of $NO_x$ emitted annually from sources in the United Kingdom over a thirty-one year period.

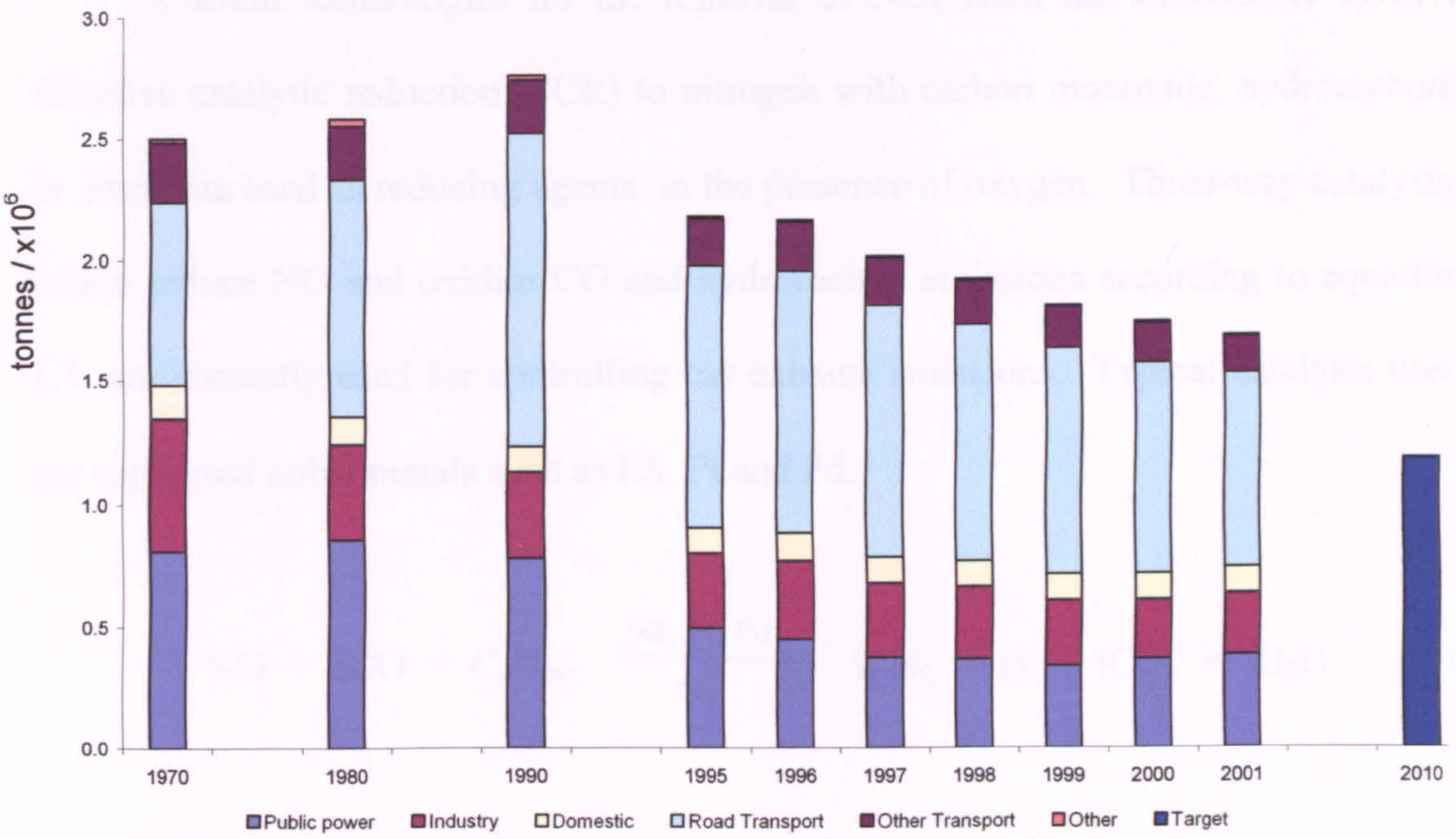


*Figure 1.2. UK $NO_x$ emissions from 1970-2001. Reproduced from Dore.*[3]

Although, significant improvements have been made over the past 10 years (figure 1.2) the $NO_x$ levels are still a long way off the 2010 target of 1.181 Mt, set by the 1988 UNECE Gothenburg protocol.[4] The development and mandatory installation of catalytic converters in all vehicles in Europe since 1993 have reduced emissions due to road transport, and measures have also been taken in industry with a variety of emission controls, such as fuel additives and selective catalytic reduction, to meet required target levels. Despite the introduction of progressively stricter

legislation, increased industrial activity and transport worldwide mean that $NO_x$ emissions remain a serious problem. There is, therefore, considerable interest in the development of new methods to remove $NO_x$ from the atmosphere.

## 1.4 Selective catalytic reduction of $NO_x$

### 1.4.1 Thermally activated catalytic reactions

Current technologies for the removal of $NO_x$ from the atmosphere involve selective catalytic reduction (SCR) to nitrogen with carbon monoxide, hydrocarbons or ammonia used as reducing agents, in the presence of oxygen. Three-way catalysts, which reduce NO and oxidise CO and hydrocarbon emissions according to equation 1.1, are currently used for controlling car exhaust emissions. Typical catalysts used are supported noble metals such as Rh, Pt and Pd.

$$NO + zCO + C_xH_{2y} \xrightarrow[O_2]{Rh,\ Pt,\ Pd} \tfrac{1}{2}N_2 + (x+y)CO_2 + {}_yH_2O \qquad (1.1)$$

For the removal of $NO_x$ from industrial emissions the SCR of $NO_x$ over supported Rh, Pt and Pd catalysts with ammonia as the reducing ga,s is commonly used. A problem with this system is that un-reacted ammonia needs to be removed as this is also a regulated pollutant. Studies of SCR of NO over Rh based catalysts have found that NO adsorbed on Rh sites is susceptible to reduction because the Rh pushes electron density into the antibonding orbital of adsorbed NO.[5] A further problem with thermal SCR of atmospheric $NO_x$ is that the reactions only proceed at temperatures significantly higher than room temperature.

### 1.4.2 Photocatalytic reactions

Most of the primary light absorbers used in photocatalytic reactions are semiconductors, with the most commonly reported being $TiO_2$. This is because it is photostable, non-toxic, inexpensive and electrons can be excited into the conduction band of $TiO_2$ via the absorption of UV light. The electron-hole pair created in the $TiO_2$ can be used to catalyse reduction or oxidation reactions of adsorbed species. Photoactive $TiO_2$ materials have been used to promote a variety of reactions, but most applications are for the complete oxidation of organic pollutants.[6-8] The band-gap of anatase phase $TiO_2$ is 3.2eV and the oxidation and reduction potentials of the valance and conduction bands are +2.95 V and -0.25 V, respectively. Hence, both photooxidation and photoreduction of NO are feasible reactions as NO reduction and oxidation potentials are +3.36 V and -0.934 V, respectively.

Recently, there have been a number of commercial photocatalytic products introduced onto the UK market. Pilkington Activ$^{TM}$, which is marketed as a self-cleaning glass, has a $TiO_2$ coating that photocatalytically oxidises organic dirt deposits. Rain water then washes the loosened dirt away due to the hydrophilic nature of the $TiO_2$ coating in the presence of sunlight. In February 2004 patents were filed for Ecopaint (developed my Millennium Chemicals, Grimsby, UK.). It is designed to reduce atmospheric levels of nitrogen oxides, by utilising $TiO_2$ photocatalysis. $TiO_2$ particles ($\phi$ = 30 nm) are embedded into a polysiloxane based paint. Calcium carbonate is also added to neutralise $HNO_3$ that is produced during photooxidation of NO. Also, a European consortium of private enterprises, research institutions and the European commission's joint research centre (JRC) are currently involved in the PICADA project (photocatalytic innovative coverings applications for depollution

assessment, 2002-2005). The aim is to develop and test "smart" construction materials and coatings, containing $TiO_2$, that are active for the elimination of $NO_x$.

As discussed above, current photocatalytic technology for air pollution control uses $TiO_2$ photocatalysts to oxidise the pollutants according to reaction 1.2. $NO_x$ is converted to $HNO_3$, which blocks the active sites and thus deactivates the catalyst.[9,10] The catalyst can be regenerated by washing with water to remove the acid, however this adds an extra complication to the process and creates a waste product which will require disposal. It would clearly be more desirable to have a catalyst system which, whilst oxidising carbon monoxide and hydrocarbons, selectively reduced $NO_x$ to nitrogen gas (as occurs over the Rh, Pd, Pt thermal catalysts, reaction 1.1), thus avoiding deactivation of the catalyst by $HNO_3$, which can take place when reaction 1.2 occurs.

$$NO + zCO + C_xH_{2y} \xrightarrow[h\nu]{TiO_2,\ O_2} HNO_3 + (x+z)CO_2 + yH_2O \qquad (1.2)$$

Reduction of $NO_x$ to nitrogen and oxygen has been achieved photocatalytically over copper(I) and silver(I) ion-exchanged zeolites.[11-13] It was found that the mechanism of reduction over both types of catalyst was via electron transfer from the photoexcited state of the metal ion to an antibonding orbital of adsorbed NO.[11,14] This is a similar mechanism to that found for rhodium based thermal catalysts. A drawback for both the copper and silver systems is that they have a large band gap energy and therefore require short wavelength UV radiation for excitation, thus prohibiting the use of solar energy.

## 1.5 Aims of the research

It is thought that by combining the knowledge of photo and thermal catalysis it would be possible to develop novel photocatalysts that will be a significant improvement on current $NO_x$ SCR photocatalysts in terms of selectivity, cost, reduced maintenance and longer lifetimes.

Noble metals (e.g. platinum) have been impregnated onto $TiO_2$ photocatalysts before, however, the only purpose was to improve the efficiency of the photocatalyst through enhancing charge transfer, and not to alter the overall reaction.[7,15] It was envisaged that silver and rhodium clusters supported on $TiO_2$ will not only enhance charge transfer to adsorbed molecules but also the metal centres will promote reduction of $NO_x$, because of electron transfer into the antibonding orbital of NO. Thus, the selectivity of the titania-based photocatalysts will be modified, producing $NO_x$ SCR photocatalysts.

Two types of NO elimination reactions are reported in this thesis; decomposition of NO in the absence of $O_2$ and the reduction of NO with CO as the reducing gas. The reaction variables that were investigated include, varying the NO concentration from 455 ppm to 1818 ppm, both in the presence and absence of CO. For the reduction reactions, the effect of changing the CO concentration, whilst maintaining a constant concentration of NO, was also investigated. For all of the different reaction parameters, the photocatalytic behaviour of three photocatalyst systems ($TiO_2$, Ag-$TiO_2$ and Rh-$TiO_2$) was determined using a continuous flow type photoreactor.

## 1.6 Thesis overview

Chapter 2 – A critical review of the literature relevant to the work presented in this thesis is presented. The main focus is gas-phase photocatalytic oxidation and reduction reactions of NO over $TiO_2$ photocatalysts.

Chapter 3 – Details the experimental procedures used in the work reported in this thesis.

Chapter 4 – Characterisation of the photocatalysts prepared. The results from XRD, TEM, XPS and DSC experiments, used to characterise P25, Ag-P25 and Rh-P25 photocatalysts, are presented. The results from each of the techniques are discussed and brought together to give a clearer understanding as to the nature of the materials.

Chapter 5 - Results from NO decomposition and reduction reactions over unmodified P25 photocatalysts are presented and discussed with respect to the characterisation results. Parameters investigated include effect of pretreatment temperature and gas compositions.

Chapter 6 - Results from NO decomposition and reduction reactions over Ag-P25 photocatalysts are presented and discussed with respect to the characterisation results. Parameters investigated include effect of pretreatment temperature and gas compositions.

Chapter 7 - Results from NO decomposition and reduction reactions over Rh-P25 photocatalysts are presented and discussed with respect to the characterisation results. Parameters investigated include effect of preparation methodology and gas compositions.

Chapter 8 – Conclusions drawn from the results presented in chapters 4-7 are presented.

## 1.7 References


(1) Loveday, M. *NSCA Pollution Handbook*; National Society for Clean Air & Environmental Protection: UK, 1997.

(2) Berge, E.; Bartnicki, J.; Olendrzynski, K.; Tsyro, S. G. *J. Environ. Manag.* **1999**, *57*, 31.

(3) Dore, C. J. "15th Annual report from the UK National Atmospheric Emmissions Inventory (NAEI) - UK Emissions of air pollutants from 1970 to 2001," National Environmental Technology Centre, 2003.

(4) UNECE "Control of Emissions of Nitrogen Oxides or their Transboundary Fluxes,", 1988.

(5) Ward, T. R.; Alemany, P.; Hoffmann, R. *J. Phys. Chem.* **1993**, *97*, 7691.

(6) Alberici, R. M.; Jardim, W. E. *Appl. Catal. B Environ.* **1997**, *14*, 55.

(7) Ollis, D. F.; Al-Ekabi, H. *Photocatalytic purification and treatment of water and air*; Elsecier: Amsterdam, 1993.

(8) Peral, J.; Domenech, X.; Ollis, D. F. *J. Chem. Technol. Biotechnol.* **1997**, *70*, 117.

(9) Negishi, N.; Takeuchi, K.; Ibusuki, T. *J. Mater. Sci.* **1998**, *33*, 5789.

(10) Ibusuki, T.; Takeuchi, K. *J. Mol. Catal.* **1994**, *88*, 93.

(11) Anpo, M.; Matsuoka, M.; Hanou, K.; Mishima, H.; Yamashita, H.; Patterson, H. H. *Coord. Chem. Rev.* **1998**, *171*, 175.

(12) Economidis, N. V.; Pena, D. A.; Smirniotis, P. G. *Appl. Catal. B Environ.* **1999**, *23*, 123.

(13) Matsuoka, M.; Matsuda, E.; Tsuji, K.; Yamashita, H.; Anpo, M. *Chem. Lett.* **1995**, 375.

(14) Ebitani, K.; Morokuma, M.; Kim, J. H.; Morikawa, A. *J. Chem. Soc. Faraday Trans.* **1994**, *90*, 377.

(15) Lewis, N. S.; Rosenbluth, M. L. *Photocatalysis - Fundamentals and Applications*, 1st ed.; Wiley, Chichester, 1989.

# 2 Literature Review

## 2.1 Introduction

This chapter presents a focussed review of the literature, for which the subject matter is of relevance to the photocatalytic reactions reported in this thesis. For this reason, only reports concerning gas-phase oxidation and reduction reactions are covered.

Since the introduction of the term "photocatalysis", in the early 20$^{th}$ century, to represent the field of chemistry that focussed on catalytic reactions occurring under the action of light, there have been many attempts to give an unambiguous definition. However, the term is still often misused and misinterpreted; hence this review starts by attempting to make clear the appropriate use of the terms "photocatalysis" and "photocatalyst" by presenting a critical review of the suggested definitions (and sub-definitions of the terms, sections 2.2.1-2.2.3)

Section 2.3 briefly describes the fundamental theory of semiconductor photocatalysis, whilst sections 2.4 and 2.5 provide a more detailed review of titanium dioxide based photocatalysts. Environmental applications of semiconductor photocatalysis are presented in section 2.6, with an emphasis on gas phase oxidation and reduction reactions. A review of photocatalytic oxidation reactions of alkanes, alkenes and alcohols is included in section 2.6.1 as the fundamental mechanistic details are similar to those observed for photocatalytic reactions of NO. The literature concerning the photocatalytic elimination of NO (2.6.2) is categorised into three types of reactions; oxidation (2.6.2.2), decomposition (2.6.2.3) and reduction (2.6.2.4). A summary of the literature, highlighting where the research opportunities lie, is presented in 2.7.

## 2.2 Terms and definitions in catalysis and photocatalysis

### 2.2.1 Thermal catalysis[1]

In order to understand what is meant by the term "photocatalysis" it is first necessary to define the term catalysis, and explain the effect a catalyst may have on a chemical reaction.

A catalyst can be described as "a substance that increases the rate at which a chemical system approaches equilibrium, without itself being consumed in the process." During the course of a reaction, the catalyst is likely to be chemically altered by interactions with the reactants. However, once the reaction is complete the catalyst returns to its original chemical state, hence there is no net change.

A reaction between molecules can only occur once the potential energy barrier has been overcome. The height of the potential barrier is termed the activation energy or enthalpy of activation for the reaction. The function of a catalyst is to lower the activation energy by providing an alternative lower energy route for the reaction to follow. Therefore, when taking into account reaction rate theory, the above definition of a catalyst can be modified into: "a substance that lowers the free enthalpy of activation of a reaction." Figure 2.1 and equations 2.1-2.3 (where R is a reactant, C is the catalyst and P is a product) exemplify the difference between an uncatalysed (equation 2.1) and a catalytic thermal reaction (equations 2.2 and 2.3) in terms of the potential energy profiles for the two reactions. E is the activation energy for the uncatalysed reaction and $E_{cat}$ is the lower activation energy for the reaction in the presence of a catalyst. The new reaction path in the presence of a catalyst may (and often does) include the formation of a catalyst-substrate intermediate complex

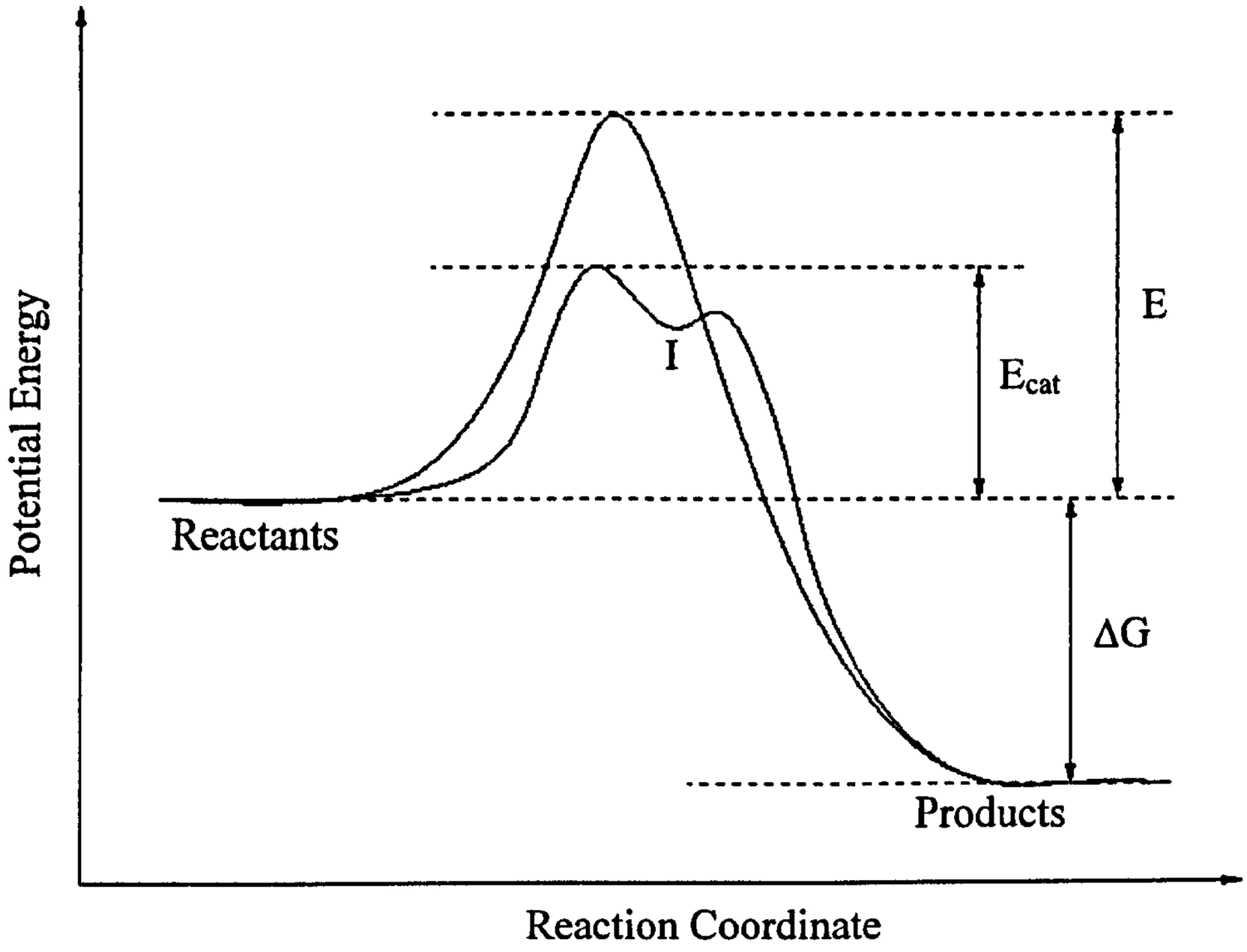


*Figure 2.1. Potential energy profile for a catalysed and uncatalysed reaction*

$$R \longrightarrow P \qquad (2.1)$$

$$R + C \rightleftharpoons (R....C) \qquad (2.2)$$

$$(R....C) \longrightarrow P + C \qquad (2.3)$$

(equation 2.2), as indicated by the minimum (I in figure 2.1) in the energy profile of the catalysed reaction.

It should be noted that the change in free energy ($\Delta G$) is the same for both the catalysed and uncatalysed reactions and only the activation energies differ. Hence the catalyst accelerates both the forward and reverse reactions to the same extent, such that only the kinetics and not the thermodynamics of the reactions are affected.

A value that is often used to describe catalytic reactions is "turnover number" (TON) which is defined as "*the number of moles of product formed (or reactants used) per mole of catalyst.*" For a reaction to be deemed to be catalytic TON must be greater than unity. When calculating TON values for heterogeneous catalysts, the concentration of the catalyst has to be replaced by the number of moles of active sites on the catalyst surface.

### 2.2.2 Photocatalysis

It is possible that the term "photocatalysis" may be misconstrued, as it could reasonably be interpreted to mean the use of photons as the catalysts for a reaction. This concept is fundamentally incorrect, as photons can only act as reactants and are thus consumed in the chemical process. For this reason, the use and definition of the term "photocatalysis" is a subject under constant debate, although the term is widely used in the literature to describe a variety of reactions that are accelerated by the presence of light and a catalyst. There have been many attempts to give definitive meaning to the word photocatalysis and the one provided by one of the IUPAC commissions is:

*"A catalytic reaction involving light absorption by a catalyst or a substrate,"*

where a "catalytic reaction" takes the same definition as discussed previously. This definition may be used to describe the action of a photocatalyst without undue constraint as to the often unknown mechanistic details of the chemical process. The statement makes no attempt to describe the role of the photons in the reaction and as such includes the process of "photosensitisation", which is defined as;[2]

*"a process whereby a photochemical change occurs in one molecular entity as a result of initial photon absorption by another molecular species, known as the photosensitiser"*

### 2.2.3 Heterogeneous photocatalysis

Heterogeneous photocatalysis involves photoreactions occurring at the surface of a catalyst and the mechanism of such reactions may take one of two general pathways. If the initial photon is absorbed by an adsorbate molecule, resulting in a photoexcited state for that molecule which then interacts with the ground state of the catalyst, the process is referred to as a "catalysed photoreaction". However, if the initial photoexcitation occurs in the catalyst substrate and the photoexcited catalyst then interacts with the ground state of an adsorbed molecule, the process is referred to as a "sensitised photoreaction" and the catalyst may be deemed to be a photocatalyst. Most cases of heterogeneous photocatalysis reported in the literature are in fact referring to semiconductor photocatalysis (i.e. semiconductor-sensitised photoreactions) and it is reactions of this type that are reported in this thesis.

As discussed previously, in order for a chemical process to be classed as a catalysed reaction, it has to be demonstrated that the TON for the process it greater than unity. TON values greater than unity are rarely reported for most examples of heterogeneous photocatalytic reactions, due to the complexity in accurately determining the number of photogenerated active sites (see below). However, reactions of this type are still believed to be catalytic if it can be demonstrated that they proceed at steady rate, in the presence of photons and reactants, over extended periods of time.

It has been shown that when semiconducting metal oxides such as $TiO_2$ and $ZnO_2$ are used as sensitisers for photoreactions (as is often the case due to their moderate band-gap energies), OH groups bound to the surface often act as active sites (this concept will be discussed further below). Therefore, for the basis of calculation of TON, the number of active sites is often assumed to be the product of the surface

density of OH groups (typically $10^{12}$-$10^{15}$ $cm^{-2}$ for a $TiO_2$ surface) and the specific surface area. However, BET surface areas are measured using bulk powders, while in reality the catalyst is often deposited as a film or dispersed in solution, in which case the actual surface area depends on the degree of aggregation. For both these cases specific surface area measurements overestimate the available surface area, thus leading to an underestimate for TON. In addition, it does not follow that all surface OH groups will necessarily act as active sites for the reaction. This again would have the effect of yielding a TON value that is lower than the actual value. For these reasons, it is assumed that most studies of semiconductor-assisted photoreactions are actually examples of photocatalysis, especially if it can be shown that there is no loss in photoactivity with extended use.

It should also be noted that semiconductor-assisted photoreactions are sometimes confusingly categorised as either "photocatalytic" or "photosynthetic" processes, according to whether the $\Delta G^{o}$ value for the reaction is negative or positive, respectively.[2] According to the above distinction a photocatalytic reaction is one that, in the absence of a semiconductor and photons of energy greater than or equal to the band-gap energy, $\Delta G^{o}$ for the reaction is negative (i.e. a thermodynamically feasible reaction).[3] Alternatively, if $\Delta G^{o}$ for the reaction is positive (i.e. a thermodynamically unfeasible reaction occurring only in the presence of a suitable semiconductor and photons of appropriate energy), the semiconductor-sensitised photoreaction is an example of a photosynthetic process.[3] Table 2.1 lists some reported examples of the two processes. According to the definition of a catalyst, the rates of both the forward and reverse reactions are accelerated equally and therefore, any semiconductor-assisted photoreaction may be deemed to be both photosynthetic and photocatalytic, depending on whether the

forward or reverse reaction is being described. It is, therefore, felt that these further sub-definitions are not required (and should not be used) as they do not help in clarifying the definition of photocatalysis, but rather, introduce more ambiguity.

| Reaction | $\Delta G^o$ / kJ mol$^{-1}$ | Reference |
|---|---|---|
| Photosynthesis | | |
| $H_2O + H_2O \rightarrow 2H_2 + O_2$ | 475 | 4 |
| $2CO_2 + 4H_2O \rightarrow 2CH_3OH + 3H_2O$ | 1401 | 5 |
| $2N_2 + 6H_2O \rightarrow 4NH_3 + 3O_2$ | 1355 | 6 |
| Photocatalysis | | |
| $3O_2 + 2CH_3OH \rightarrow 4H_2O + 2CO_2$ | -1401 | 7,8 |
| $2NO \rightarrow N_2 + O_2$ | -180 | 9 |
| $6H_2O + C_6H_{12}O_6 \rightarrow 12H_2 + 6CO_2$ | -535 | 10,11 |

*Table 2.1. Examples of semiconductor-sensitised photosynthetic and photocatalytic processes.*

## 2.3 Theory of semiconductor photocatalysis

### 2.3.1 Basic principles

In the literature, the most commonly reported sensitisers used in heterogeneous photocatalysis are n-type semiconducting materials due to their favourable combination of electronic structure, light absorption properties, charge transfer characteristics and relatively long lifetimes of the photoexcited states. Common examples are $TiO_2$, ZnO, CdS and ZnS. In this part of the review, the basic theory of semiconductor photocatalysis will be presented along with a brief discussion of possible electron-hole pair trapping mechanisms.

Unlike metals which have a continuum of electronic states, the electronic structure of semiconductors can be characterised by a region void of energy levels,

known as the band gap, which extends from the top of the filled valence band to the bottom of the vacant conduction band. When illuminated by radiation of energy ($h\nu$) greater than or equal to the band gap, electrons (-) are promoted to the conduction band, leaving positive holes (+) in the valence band. As shown in figure 2.2, several pathways are available for the generated electrons and holes. They can either recombine in the bulk material or migrate to the semiconductor surface before recombination, in both cases releasing the absorbed energy as heat. More importantly, the electrons and holes may migrate to the surface of the photocatalyst and undergo redox reactions with adsorbed molecules. Negative electrons may reduce electron acceptors (A) and positive holes may oxidise electron donors (D).

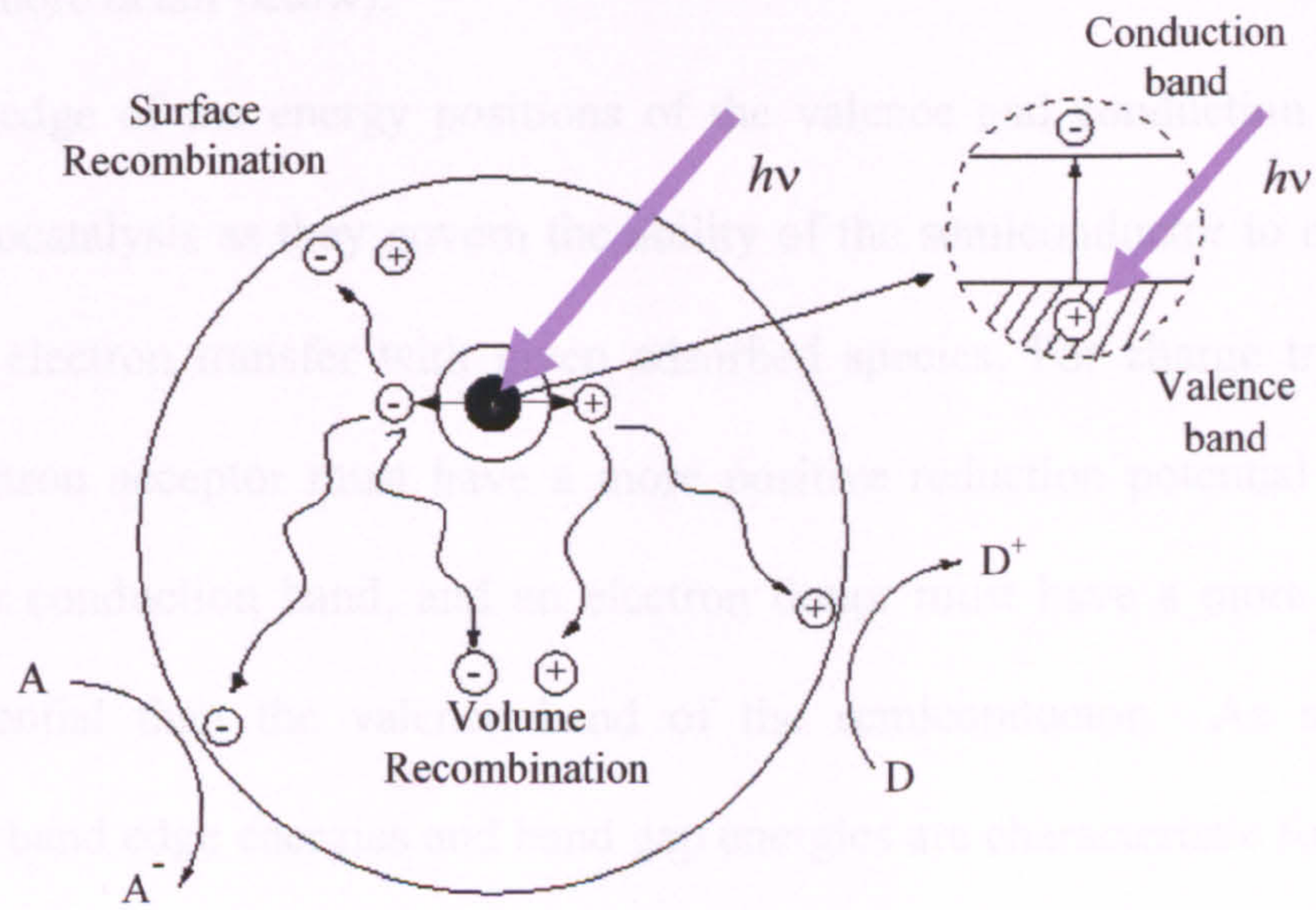


*Figure 2.2. Schematic of photogeneration of electron-hole pairs in a semiconductor along with possible relaxation processes. A – electron acceptor, D – electron donor (adapted from Linsebigler[12])*

The time scale for recombination to occur is in the order of a few nanoseconds, whilst interfacial charge transfer reactions may take hundreds of nanoseconds.[13,14] Recombination of the photoexcited electron-hole pairs will prevent

a photocatalytic reaction and therefore needs to be retarded for efficient charge transfer processes to occur on the surface of the photocatalyst.

In the preparation of semiconductor materials, ideal crystal lattices are rarely formed, but rather surface and bulk irregularities are naturally present in the materials. The surface irregularities result in localised regions of electron states (metastable surface states) that differ from the bulk materials. These can serve as charge carrier traps, thus increasing the lifetime of separated electrons and holes and ultimately result in more efficient photoreactions. Another mechanism for suppressing electron-hole recombination reactions is surface modification of the photocatalyst by addition of metals, which can also act as trapping sites for photogenerated electrons (discussed in more detail below).

Knowledge of the energy positions of the valence and conduction bands is useful in photocatalysis as they govern the ability of the semiconductor to engage in photoinduced electron transfer with given adsorbed species. For charge transfer to occur, an electron acceptor must have a more positive reduction potential than the semiconductor conduction band, and an electron donor must have a more negative reduction potential than the valence band of the semiconductor. As shown in figure 2.3, the band edge energies and band gap energies are characteristic for a given semiconductor and therefore, different semiconductors will be effective for catalysing different surface photoreactions, depending upon the redox potentials of the reactants.

For example, the photooxidation of water in the presence of $WO_3$ is a thermodynamically feasible reaction, but the same reaction is not possible in the presence of CdSe. The photo-reduction of water, instead, could occur more easily in the presence of CdSe, due to the position of its conduction band.

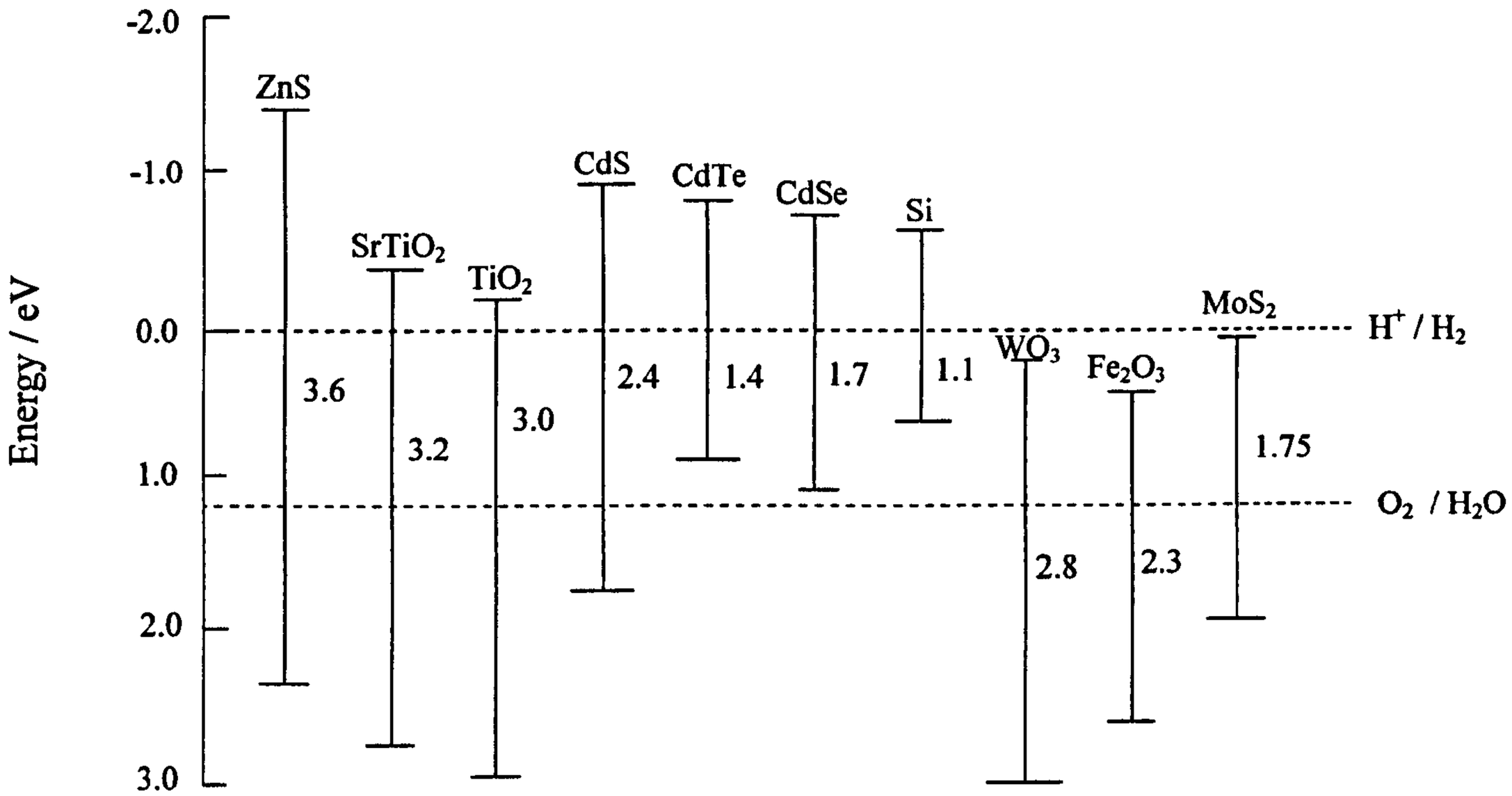


*Figure 2.3. Band edge positions, relative to the normal hydrogen electrode, for some semiconductors in contact with an aqueous electrolyte. (Adapted from Schiavello[15]).*

## 2.3.2 Band bending and the formation of a Schottky barrier

When a semiconductor is in contact with another phase (i.e. liquid, gas or metal), which is always the case for a semiconductor photocatalyst, a redistribution of electronic charges occurs along with the formation of an electronic double layer or a space charge layer. As discussed above, surface states of semiconductors can serve as trapping sites for the mobile charge carriers and hence the surface may become positively or negatively charged depending on the number and type of trapping sites. For positively charged n-type semiconductors, electron transfer occurs from surface to the bulk and positive holes are confined on the surface (depletion layer), causing a change in the electrostatic potential and a bending of the bands upward towards the surface. For a negatively charged surface, the reverse occurs and electrons accumulate on the surface (and bands bend downward towards the surface) forming an accumulation layer. The opposite situation arises for p-type semiconductors.

Figure 2.4 illustrates the space charge layers produced from the mobility of charge carriers across a n-type semiconductor-solution interface along with the flat band potential diagram in the absence of a space charge layer (figure 2.4 (A)).

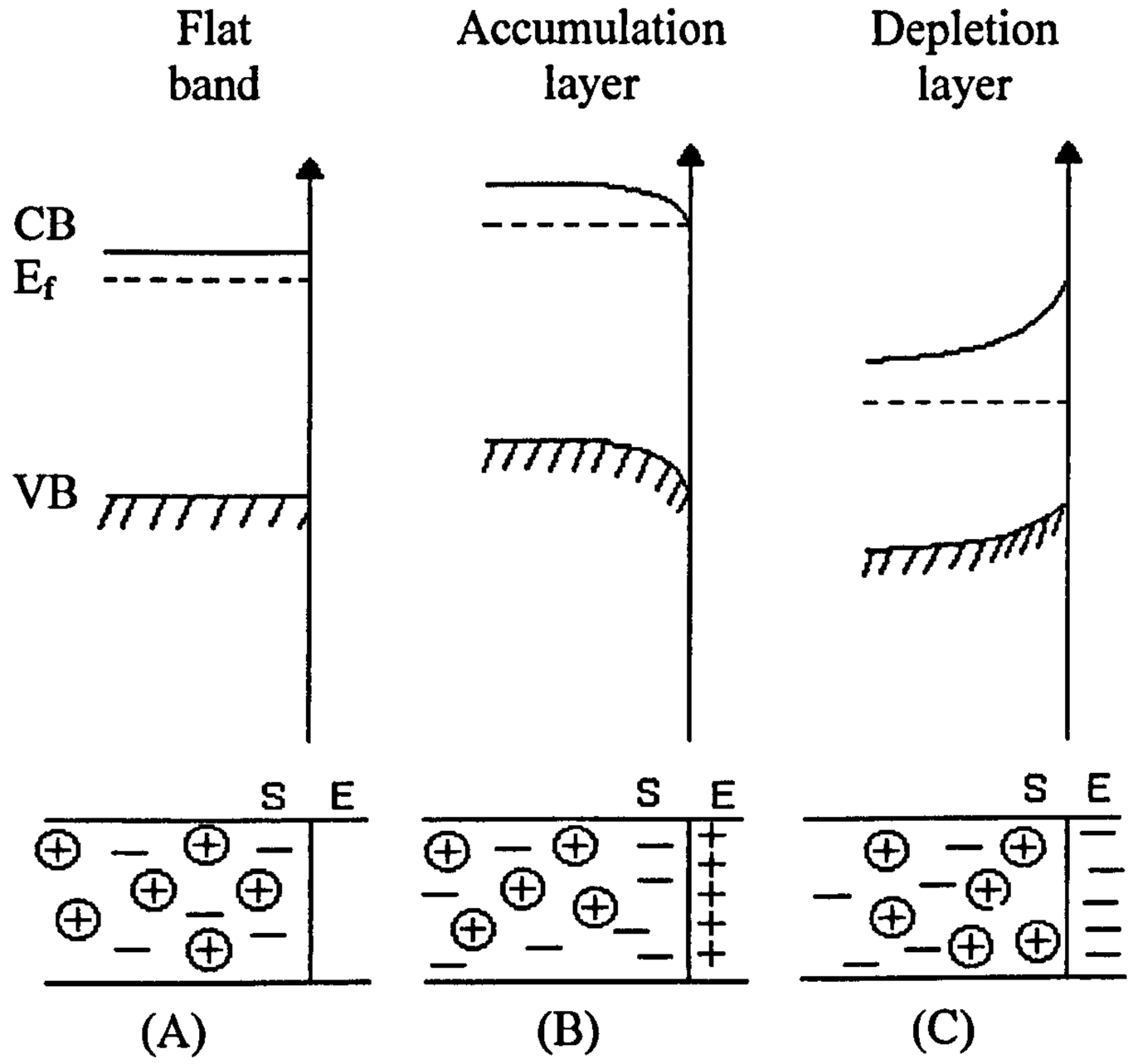


*Figure 2.4. Space charge layer formation at an n-type semiconductor-solution interface. (adapted from Linsebigler[12]).*

The space charge layer that is formed at semiconductor-metal interfaces (known specifically as a Schottky barrier) can be of particular importance in semiconductor photocatalysis as it can serve as an efficient trapping site for photoexcited electrons (or photogenerated holes, depending on the nature of the two materials in contact). Figure 2.5 illustrates the formation of a Schottky barrier for an n-type semiconductor in contact with a metal of higher work function ($\phi_m > \phi_s$). When separated, the positions of Fermi levels for the metal and the n-type semiconductor are different; when they are in electrical contact, electrons migrate from the semiconductor to the metal of higher work function until the two Fermi levels align, causing a depletion of electrons and excess positive charge at the

semiconductor surface. The valence and conduction bands of the semiconductor bend upwards in energy towards the interface to maintain electrical neutrality, and the layer is said to be depleted. Although it is possible that the formation of a Schottky barrier can result in more efficient electron-hole separation, yielding increased lifetimes of the photoexcited states and ultimately increasing the number of possible surface redox reactions, the barrier formed may also act as an electron-hole recombination centre due to the excess charge in the interface region attracting oppositely charged photoexcited states, thus reducing the number of possible redox reactions. The nature of the Schottky barrier formed is dependant on the type and concentration of the modifying species.[16,17]

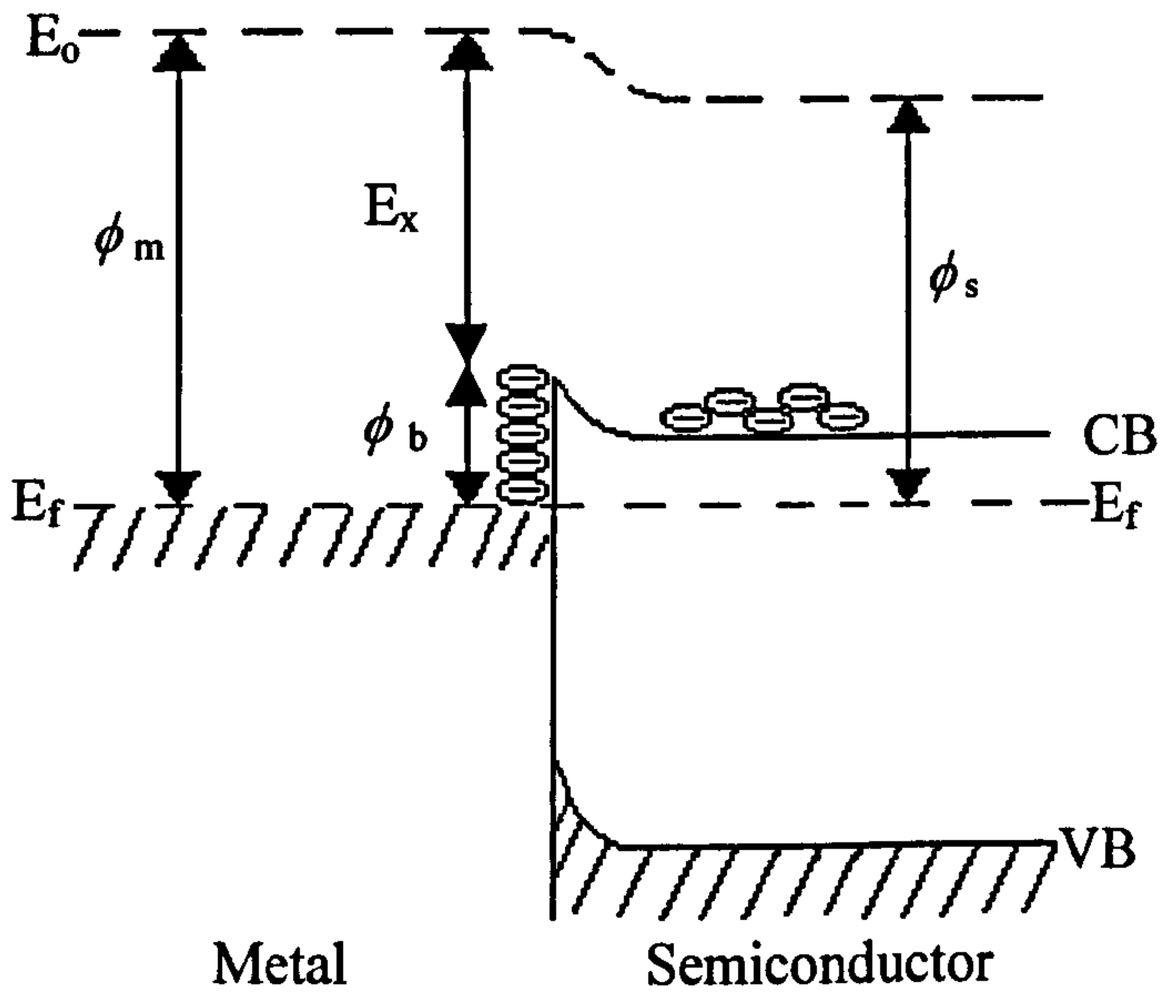


*Figure 2.5. Schematic of a Schottky barrier formed at the interface of a semiconductor-metal system. (adapted from Linsebigler[12]).*

## 2.4 Titanium dioxide photocatalysis

### 2.4.1 Properties of titanium dioxide

The most common semiconductor photocatalyst compound used in both research and commercial applications of photocatalysis is titanium dioxide ($TiO_2$). The $TiO_2$ used usually exists in one of two common crystalline phases, anatase or rutile, although another metastable phase called brookite also exists. Both the anatase and rutile structures are based on tetragonal unit cells, and are built up of octahedra of oxygen ions ($O^{2-}$) with titanium ions ($Ti^{4+}$) at the centre of each octahedron. In the anatase phase each octahedron has 8 neighbours (4 edge sharing and 4 corner sharing, figure 2.6) whilst in rutile phase each octahedron has 10 neighbours (2 edge sharing and 8 corner sharing, figure 2.7). Brookite has a more complicated crystal structure, in which the unit cell is orthorhombic. The band gap energies of the anatase and rutile phases are 3.2 eV and 3.0 eV respectively.

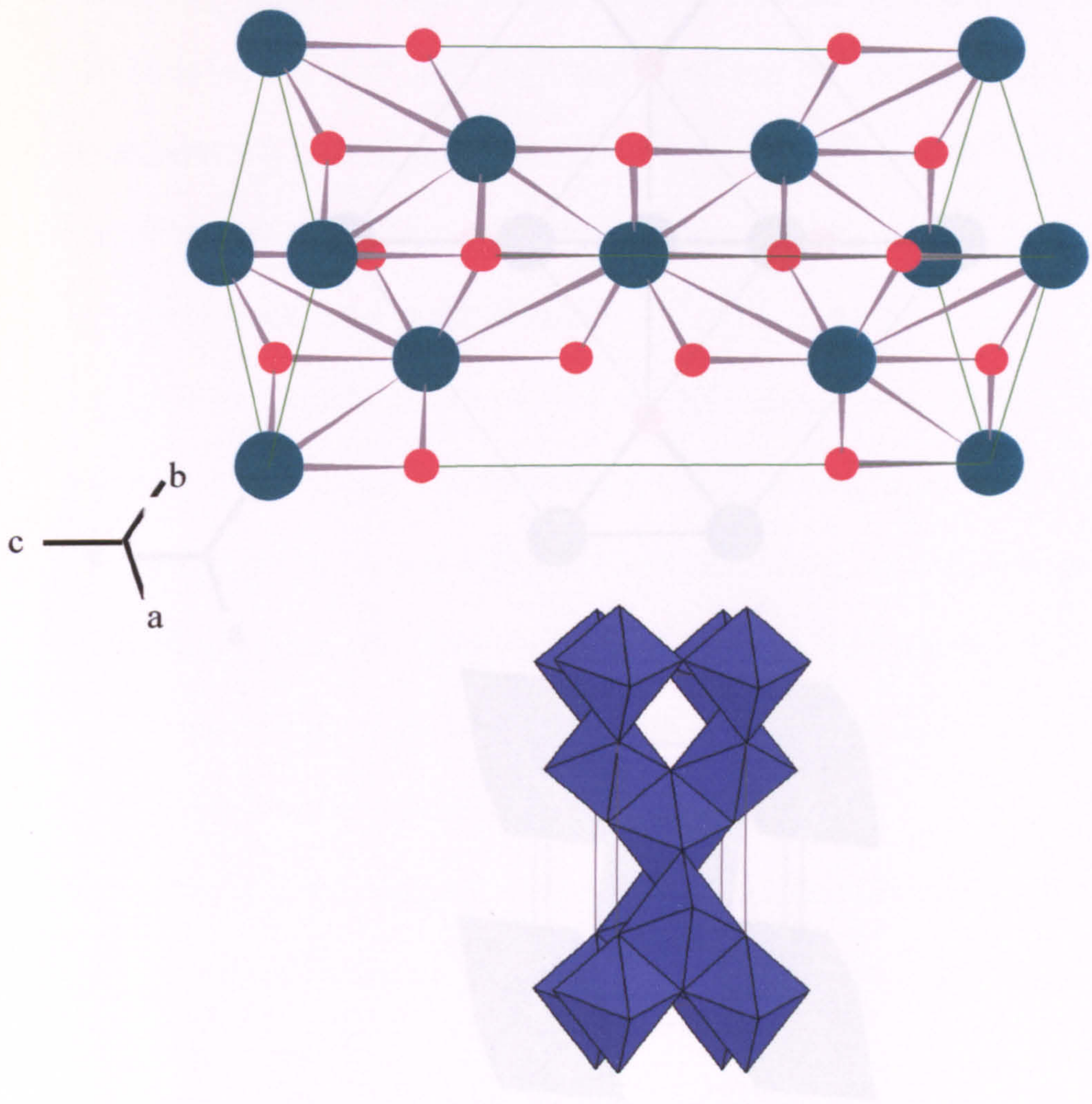


*Figure 2.6. (a) General arrangement of anatase viewed down the (111) zone axis (Green balls= titanium; Red balls= oxygen). (b) Anatase structure showing the corner sharing octahedra.*

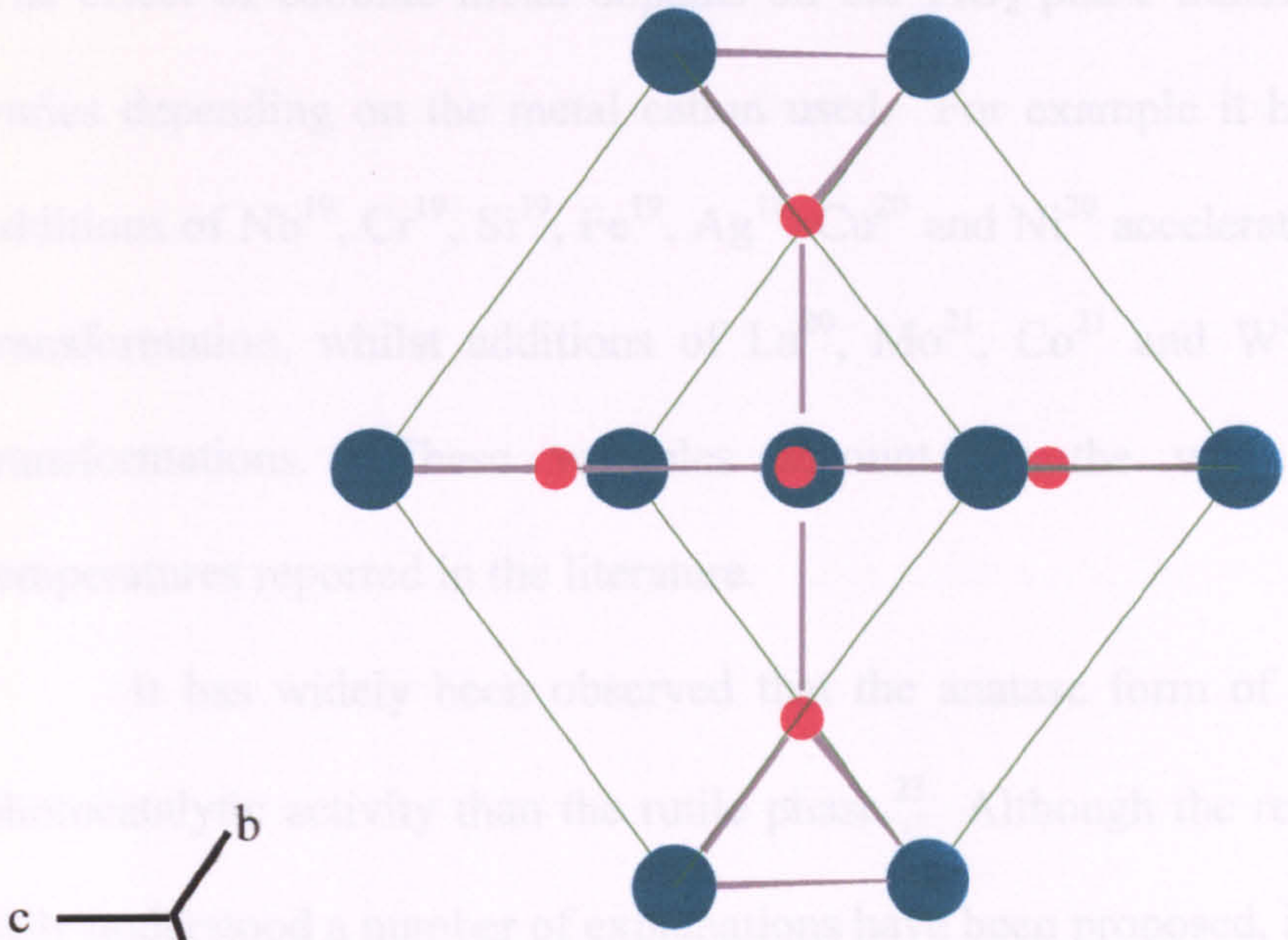


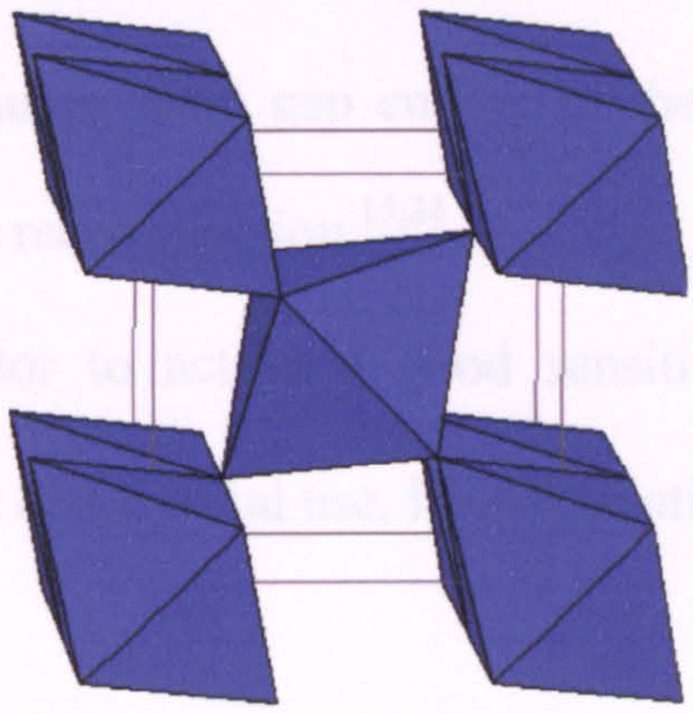

*Figure 2.7. (a) General arrangement of rutile viewed down the (111) zone axis (Green balls= titanium; Red balls= oxygen). (b) Rutile structure showing the edge sharing octahedra.*

Of the three morphological forms of $TiO_2$, rutile is the most thermodynamically stable and both anatase and brookite transform irreversibly to the rutile phase between 500-800 °C. Generally, the precise temperature and rate at which the phase transition occurs depends markedly upon several factors, including the method of preparation, the level of impurities and the surface area of the sample. It is thought that small particles, and consequently large surface areas, favour the transformation process, which is accelerated by the presence of oxygen vacancies.[18]

The effect of cationic metal dopants on the $TiO_2$ phase transformation temperature varies depending on the metal cation used. For example it has been reported that additions of Nb[19], Cr[19], Si[19], Fe[19], Ag[18], Cu[20] and Ni[20] accelerate the anatase-to-rutile transformation, whilst additions of La[20], Mo[21], Co[21] and W[22] inhibit $TiO_2$ phase transformations. These variables account for the wide range of transition temperatures reported in the literature.

It has widely been observed that the anatase form of $TiO_2$ shows a higher photocatalytic activity than the rutile phase.[23] Although the reasons for this are not fully understood a number of explanations have been proposed, including the different mass densities and band structures caused by the differences in lattice structure of the two forms, and also the larger band gap energy of the anatase phase, which helps suppress electron-hole pair recombination.[15,24]

For a semiconductor to act as a good sensitiser of a photoreaction, and therefore be considered for commercial use, it should satisfy the following criteria:

(a) photoactive,

(b) chemically inert,

(c) photostable (i.e. not liable to photoanodic corrosion),

(d) non-toxic,

(e) inexpensive,

(f) able to utilise visible and / or near-UV light.

$TiO_2$ is the one of the few semiconductors that fulfils the above requirements, therefore making it the most widely studied semiconductor photocatalyst. Of particular importance for environmental applications is the ability of $TiO_2$ to utilise visible and/or near-UV irradiation, thus avoiding the use of bio-hazardous UV (< 254 nm) wavelengths and allowing the use of solar as well as artificial sources.

A commercial $TiO_2$ photocatalyst (Degussa P25), is used in many laboratories either in the as received form, as a precursor material (as is the case for the experiments reported in this thesis), or as a reference material. Degussa P25 is produced via high temperature (> 1200 °C) flame hydrolysis of $TiCl_4$ in the presence of hydrogen and oxygen. The by-product of HCl is removed from the $TiO_2$ in a steam treatment. Both the anatase and rutile $TiO_2$ phases are formed (anatase : rutile ratio, 80 : 20) with a overall $TiO_2$ purity of 99.5 %. The particles formed are aggregates of non-porous cubic shaped (with rounded edges) primary particles with an average diameter of 21 nm and an aggregate size of 0.1 μm.[25,26] The BET surface area of P25 powder is 50 ± 15 $m^2 g^{-1}$.[25] The sol-gel route (both inorganic and alkoxide routes) is also commonly reported to yield highly photocatalytically active $TiO_2$ compounds, and there are many reports stating the sol-gel titanias have a higher activity than Degussa P25.[27-29]

### 2.4.2 Supported $TiO_2$ photocatalysts- Effect of film thickness

It has been shown by Jacoby *et al.*[30] that as the photocatalyst loading (film thickness) increases, the rate of the photoreaction increased linearly with loading until an optimum thickness was reached (*ca.* 30 μm) when the rate is reported in units of moles of reactant converted per second per $cm^2$ of catalyst film. Increasing the loading further had no effect on the reaction rate. From these results it was concluded that if the catalyst coating is greater than the critical thickness then it is more accurate to report photoreaction rates using units of μmol $h^{-1}$ $cm^{-2}$ rather than the more traditional unit of μmol $h^{-1}$ $g^{-1}$ as not all the photocatalyst participates in the reaction.

## 2.5 Effect of transition metal modification on photocatalytic behaviour

As mentioned previously, modification of semiconductor materials with transition metals (or metal ions) is of importance in the field of heterogeneous photocatalysis, as it can help in suppressing the energy wasting electron-hole pair recombination reactions and in some cases can beneficially alter the band-gap energy of the semiconductor (see below). Because of the significance in photocatalysis, there have been many reports concerning the effects of deposited transition metals on semiconductors, especially $TiO_2$. In most cases though, the role of the additive is purely in increasing the efficiency of photoreactions by the enhanced charge separation properties of the modified photocatalyst, although the transition metals themselves may also be catalytically active and offer alternative active sites on which reactions may proceed, thus opening new reaction pathways.

The types of metals and metal ions that have been deposited on $TiO_2$ include Cu, Fe, Ag, Cr, Pt, Pd and Rh (a more comprehensive list can be obtained by the reviews by Litter[31] and Howe[32]). The resulting efficiency of the modified photocatalyst depends on the preparation method and on the physicochemical properties of the materials. The most commonly reported methods for semiconductor modification are impregnation with a metal salt followed by thermal decomposition[33] or hydrogen reduction[34,35] or photodeposition.[10,36,37] Photodeposition involves the reduction of metal ions by photogenerated electrons, and in most studies oxidisable additives (e.g. alcohols[38]) are used as hole scavengers, with the aim of increasing the deposition rate.

Throughout the numerous studies there is widespread conflict as to whether certain transition metals have a positive or negative effect on the activity of reactions.

For example it has been reported that the presence of $Cr^{3+}$ ions are detrimental for the photoreduction of $N_2$ with $H_2O$ producing $NH_3$[39] (a gas-solid system), whilst they have no effect on phenol degradation (a liquid-solid system).[40] However, when $Cr^{3+}$ ions are present on $TiO_2$ the sustainability for the photodissociation of water was improved compared to unmodified $TiO_2$ (a liquid-solid system).[41] These differences in the photocatalytic reactivities of the above reactions has been attributed by the authors to the inherent differences in the gas-liquid and liquid-solid interfaces, rather than to differences induced by the metal doping.[40] In contrast to these results, the presence of $Fe^{3+}$ ions on $TiO_2$ enhanced the photoreduction of $N_2$ (a gas-solid system).[42] This latter result shows that the effect of transition metal addition on photocatalyst activity is not solely dependant on the nature of the system (e.g. gas-solid vs. liquid-solid), but also depends on the type of modifying metal (or metal ions used) and the individual reaction being photocatalysed.

In a study of the oxidation of benzene in air over $TiO_2$ (Degussa P25 type) and a $Rh/TiO_2$ photocatalyst, using a flow style reactor, it was found that the presence of rhodium not only altered the activity of the reaction, but also the deactivation properties of the photocatalyst.[43] The authors reported that under stationary conversion conditions the $Rh/TiO_2$ catalyst was about three time more active, compared to unmodified $TiO_2$ (*ca.* 40 % conversion for $Rh/TiO_2$ compared to 13 % conversion for $TiO_2$). The selectivity for $CO_2$ formation was similar for both the $TiO_2$ and $Rh/TiO_2$ photocatalysts, at *ca.* 90 %. [44]

Deactivation studies by the same authors[43] showed that over $TiO_2$, the initial benzene conversion (70 %) rapidly decreased with reaction time, and reached steady state conditions with a 13 % conversion after only 180 min. The time period for steady state conditions (at 40 % conversion) to be achieved over the $Rh/TiO_2$

photocatalyst was *ca.* 10 h. The deactivation was ascribed to the formation of carbon deposits on the $TiO_2$ surface, which changed from white to a brownish colour during the course of the reaction. The initial activity (and white colour) of the catalysts could be restored by illumination in humid air without benzene; with the carbon deposits being oxidised to $CO_2$ and CO. It was estimated that the mass of carbon deposited was approximately 0.5 times less for the Rh containing catalyst. It was concluded that the presence of Rh inhibited the formation of carbon deposits and accelerated their decomposition, thus improving the lifetime of the $TiO_2$ catalyst for the photocatalytic oxidation of benzene.

Yamashita *et al.*[45,46] prepared $Cr^+/TiO_2$ photocatalysts using an ion-implanter consisting of a metal ion source, high voltage ion accelerator (150 keV) and a vacuum pump. It was found that these materials were able to absorb visible light. Figure 2.8 shows the shift in the absorption edge for samples implanted with increasing concentrations of Cr ions. It was thus expected that photocatalytic reactions would be observed under visible light. Under UV illumination, the photocatalytic activity of the ion implanted catalysts for NO decomposition was similar to the $TiO_2$ photocatalyst, therefore indicating that the implanted ions did not act as electron-hole recombination centres. When the same reactions were performed using a visible light source only the ion-implanted catalyst showed any activity, the NO being decomposed into $N_2$, $O_2$ and $N_2O$. Hence it was concluded that the implantation of the ions was the determining factor in the ability to utilise a visible light source.

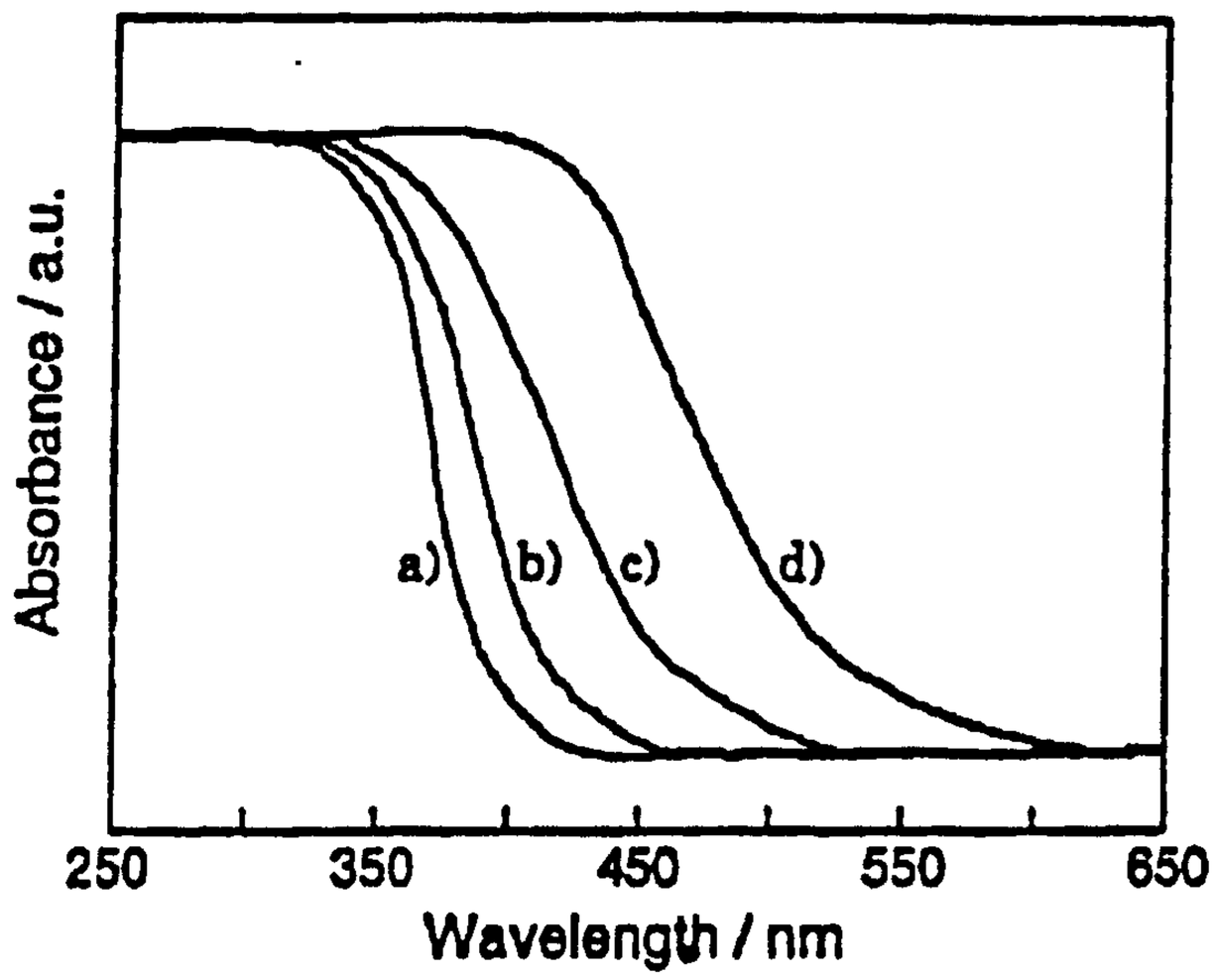


*Figure 2.8. UV-VIS spectra of a) $TiO_2$ and the $TiO_2$ implanted with Cr ions (b-d). Amount of Cr ion implanted: (in mol $g^{-1}(TiO_2)$) b) $2.2 \times 10^{-7}$, c) $6.6 \times 10^{-7}$, d) $1.3 \times 10^{-6}$. (Adapted from Yamashita[46]).*

The concentration of the dopant is another factor that can affect the activity of transition metal modified photocatalysts.[17,47] Chao *et al.*[17] investigated the photocatalytic degradation of methylene blue over sol-gel prepared $TiO_2$ doped with varying amounts of silver, and it was found when 2-4 mol. % Ag (2.7 - 5.4 wt. %) was used the photocatalytic activity was nearly double that of unmodified $TiO_2$. However, increasing the silver content to 6 mol. % (8.1 wt. %) yielded a photocatalyst with an activity similar to that of $TiO_2$. Increasing the amount of silver used resulted in further reductions in photocatalytic activity.

The enhanced activity at low Ag loadings was attributed to two separate effects. Firstly the presence of small amounts of silver inhibited grain growth, thereby yielding photocatalysts with increased surface areas. Secondly, the small metallic silver particles helped in suppressing the energy wasting electron-hole recombination reactions. Jointly these two effects resulted in an overall increase in the rate of $TiO_2$ photocatalysis in the presence of a low concentration of silver.

The detrimental effect on activity at higher silver loadings was also attributed to two effects. Firstly, $TiO_2$ grain growth was no longer inhibited, but rather grain growth was observed due the higher density of defects and anion vacancies at the surface of the $TiO_2$ grains which promote grain growth.[18] As a result, photocatalysts which had lower specific surface areas and hence fewer active adsorption sites were produced. Also, larger Ag clusters were formed, which served as efficient electron-hole recombination centres rather than suppressing electron-hole recombination.

From these results it is apparent that there is no hard and fast rule for predicting what effects transition metal modification of semiconductor photocatalysts will have upon the behaviour of a catalysed photoreaction. The overall effect depends on several factors including; reaction type, preparation method, nature and concentration of the additive.

## 2.6 Environmental applications of semiconductor photocatalysis

### 2.6.1 Photocatalytic degradation of organic pollutants

The first systematic studies on the implementation of $TiO_2$ photocatalysis for the destruction of organic pollutants were conducted by Ollis and coworkers[48,49] when they demonstrated the photomineralisation of various chlorinated hydrocarbons dissolved in aqueous solution (e.g. trichloroethylene, dichloromethane, chloroform and carbon tetra chloride). Initially it was thought that this method for the removal of organic pollutants could only be applied to non-aromatic compounds, however this was proved to be incorrect when in 1985 Okamoto demonstrated the photomineralisation of dissolved phenol using $TiO_2$ as a photocatalyst.[50] The process

of oxidation of organic pollutants via $TiO_2$ photocatalysis can be summarised by the general reaction equation

$$\text{Organic pollutant} + O_2 \xrightarrow[h\nu]{TiO_2} CO_2 + H_2O + \text{mineral acids}$$

Since the initial studies, the photocatalytic oxidation of many different organic compounds (over 200 to date) has been demonstrated. Examples of the types of classes of compounds studied include; simple alkanes and alkenes, halogenated alkanes and alkenes, alcohols, carboxylic acids, aromatic compounds (including halogenated compounds), polymers, organic surfactants and dyes such as methylene blue. As the focus of this literature review is not reactions at liquid-solid interfaces (but rather reactions at gas-solid interfaces) the reader is directed to the review article by Hoffmann *et al.*[51] for a more exhaustive list.

Gas-phase heterogeneous photooxidation of organics over $TiO_2$ surfaces was first reported by Teichner and Djeghri in 1980[52] in their studies of the oxidation of 2-methylbutane. The reaction was an unselective partial oxidation producing a mixture of ketones (58 %), aldehydes (26 %), carbon dioxide (15 %) and some other minor products, with only a 2-methylbutane conversion of 2 %. It wasn't until the 1990's that studies of the gas-phase photooxidation of organic compounds over illuminated $TiO_2$ surfaces began in earnest, and it has now been demonstrated that $TiO_2$ based photocatalysts have the ability to mineralise many different types of organic compounds.[53] The different types of organic compounds studied in the field of gas-phase $TiO_2$ photocatalysis can be classified in one of the following groups:

1. oxidation of alkanes and alkenes
2. oxidation of alcohols and ketones and aldehydes

3. oxidation of aromatics
4. organic acid decarboxylation (photo-Kolbe reaction)
5. oxidation of heteratom (e.g. N, S) organic compounds
6. oxidation of trichloroethylene (TCE)

The oxidation of TCE is grouped separately from the oxidation of alkenes due to the numerous studies involving this species following the initial discovery by Dibble and Raupp of the ability to $TiO_2$ to photocatalytically degrade TCE to $CO_2$, $H_2O$ and HCl.[54,55] Only the oxidation of alkanes, alkenes and alcohols, all of which are closely related (see below), will be reviewed here because the fundamental mechanisms for these semiconductor-assisted photocatalytic reactions are similar to those for the NO decomposition and reduction reactions reported in this thesis.

Calculations of the formal quantum efficiencies (FQE) have shown that the values are generally more than an order of magnitude higher for the photomineralisation of organics in gas-solid systems, compared to the photodestruction of the same organic compounds dissolved in aqueous medium.[56-58] For example the reported FQE values for TCE photomineralisation in aqueous solution and the gas phase are 0.01 and 0.5-0.9 respectively. The discovery of these high efficiencies for gaseous photooxidation reactions has resulted in a dramatic increase in the number of studies of $TiO_2$ photocatalysis as a method for purifying air in the last 10 years. Potential commercial applications of such systems are:[26]

1. remediation of contaminated soils and water through air stripping, coupled with a semiconductor photocatalytic air purification process
2. purification of industrial gaseous emissions
3. purification of indoor or closed air systems
4. reduction of atmospheric pollution levels

The latter two applications potentially open up a very important market, as the general public are becoming increasingly concerned about the effect of the quality of air on their general health.

#### 2.6.1.1 Water and oxygen adsorption on $TiO_2$ surfaces

For all 6 groups of organic compounds listed previously it is agreed that both UV induced surface bound activated oxygen (atomic and molecular) and hydroxyl radical ($OH^{\bullet}$) species play an important role in the oxidation process, although questions still remain as to the precise mechanisms of the reactions.[51,59] The adsorption of oxygen and water (resulting in the formation of surface OH groups[60]) are therefore fundamentally important processes.

Bickley[61] found that in the presence of UV irradiation, the $O_2$ photoadsorption rate followed a parabolic form (i.e. a plot of $O_2$ photoadsorption vs. time$^{1/2}$ was linear). In the same study, it was also shown that no $O_2$ photoadsorption occurred on $TiO_2$ powders that had been dehydroxylated by heating at 800 °C under vacuum. After exposure of the dry powder to water vapour, the activity for $O_2$ adsorption was partially restored. There have been numerous studies on the adsorption of $H_2O$ on $TiO_2$ surfaces, and it is agreed that the resulting surfaces contain molecular water, hydrogen bonded OH groups and free OH groups.[62,63] The OH groups may be formed by reaction of $H_2O$ molecules with bridging O atoms.[60] Suda[62] and Tanaka[63] have both reported that adsorbed molecular water is removed from the surface of $TiO_2$ powders by heating to 150 °C and that the concentration of surface bound OH groups decrease linearly with increasing outgassing temperature.

In the FTIR studies by Suda[62] it was reported that four absorption bands were observed at 3660, 3520, ~3400, and 1625cm$^{-1}$ for titanias that had been exposed to

water vapour at room temperature and then degassed at 25°C. The bands were assigned to the OH stretching vibrations of free OH groups, hydrogen-bonded OH groups, surface adsorbed molecular water and to the bending vibration of the molecular water respectively. After increasing the degassing temperature to 100°C the bands due to molecular water were still present, but somewhat reduced in intensity. Whilst at 150°C the band at 1625cm$^{-1}$ disappeared completely indicating the removal of molecular water from the rutile surface. With increasing temperature the intensity of the band at 3400cm$^{-1}$ decreased at the same rate as the band at 1625cm$^{-1}$, although a weak absorption band at 3370cm$^{-1}$ was seen after degassing at temperatures above 150°C. This band was assigned to the presence of the hydrogen bonded OH groups. The intensity of the band at 3660cm$^{-1}$ did not decrease until degassing at temperatures above 150°C. Increasing the treatment temperature caused a further reduction in the intensity of the band, until reaching 600°C, where no absorption bands were seen for any surface bound hydroxyls or molecular water species.

Surface bound OH groups can act as trapping sites for the photogenerated holes, forming hydroxyl radicals ($OH^{\bullet}$), thus leaving the photoexcited electron to interact with weakly held molecular oxygen. Decreasing the density of surface OH groups via outgassing at higher temperatures resulted in lower $O_2$ photoadsorption rates. These results have been confirmed in the work of Munera *et al.*,[64-66] in which it was shown that $O_2$ photoadsorption was favoured on highly hydroxylated $TiO_2$ surfaces and that the presence of $H_2O$ vapour helped sustain the process.

In a simultaneous study of photoconductivity and photocatalytic activity of $TiO_2$ for isobutene oxidation, it was found that none of the carbonaceous compounds taking part in the reaction (either as reactants or products), influenced the photoconductivity of the $TiO_2$.[67] Hence, interaction between the photogenerated holes

and the reaction compounds was not the rate determining step, so the origin of the activity for photocatalytic oxidation must have arisen from the $O_2$-$TiO_2$-UV system, i.e. activated oxygen species or surface bound OH radicals.

The following reactions may be used to describe the formation of the activated surface species:[68,69]

$$OH^-_{(ads)} + h^+ \rightarrow OH^\bullet \quad (2.1)$$

$$O_{2(ads)} + e^- \rightarrow O_2^-{}_{(ads)} \quad (2.2)$$

$$OH^\bullet + O_2^-{}_{(ads)} \rightarrow HO_2^\bullet + O^-_{(ads)} \quad (2.3)$$

$$O^{2-}_{(lat)} + h^+ \rightarrow O^- \quad (2.4)$$

$$O^- + h^+ \rightarrow O \quad (2.5)$$

$$O^-_{(ads)} + h^+ \rightarrow O \quad (2.6)$$

where the subscript (ads) represents that the species is adsorbed on the surface and $O^{2-}_{(lat)}$ represents lattice oxygen species. It is well documented that the dissociated atomic species formed via reactions 2.5 and 2.6 are able to attack the chemical bonds of organic compounds adsorbed onto the surface of $TiO_2$, and that the $OH^\bullet$ radicals are powerful oxidising agents capable of mineralising most organic pollutants.[70]

### 2.6.1.2 Oxidation of alkanes and alkenes

One of the first systematic studies of the gas-phase photooxidation of both alkanes and alkenes containing up to 8 carbon atoms over a non-porous $TiO_2$ photocatalyst were conducted by Teichner and colleagues.[52,71-74] The studies involved the oxidation of both linear and branched molecules in a fixed bed flow reactor using a total flow rate of 20 sccm, which corresponded to a contact time of 0.6 s. The composition of the gas mixture was usually 37.5 % $O_2$, 37.5 % hydrocarbon and 25 %

helium, although other compositions were investigated. It was found that small alkanes (methane and ethane) and alkenes containing 4 or less carbons were mineralised, forming $CO_2$ and $H_2O$. Longer chain alkanes and alkenes were only partially oxidised unselectively forming a mixture of ketones, aldehydes and $CO_2$ (see table 2.2). The amount of total oxidation that occurred varied only slightly for the different compounds, with on average 20 % of the converted compound (which was usually less than 10 % of the initial amount of compound) forming $CO_2$ and $H_2O$.

| Alkane | Product Selectivity / % | | |
|---|---|---|---|
| | Ketones | Aldehydes | Carbon Dioxide |
| Methane | 0 | 0 | 100 |
| Ethane | 0 | 18 | 82 |
| Propane | 57 | 11 | 32 |
| Butane | 49 | 19 | 32 |
| 2-Methylpropane | 61 | 7 | 32 |
| Pentane | 54 | 22 | 24 |
| 2-Methylbutane | 54 | 26 | 20 |
| 2,2-Dimethylpropane | 42 | 8 | 50 |
| Hexane | 73 | 14 | 13 |
| 2-Methylpentane | 53 | 29 | 18 |
| 3-Methylpentane | 53 | 20 | 27 |
| 2,2-Dimethylpentane | 44 | 19 | 37 |
| 2,3-Dimethylpentane | 78 | 12 | 10 |
| Heptane | 49 | 33 | 18 |
| 2-Methylhexane | 65 | 17 | 18 |
| Octane | 52 | 22 | 26 |

*Table 2.2. Table of selectivities for the photocatalytic oxidation of various alkanes. Gas composition was 37.5 % $O_2$, 37.5 % hydrocarbon and 25 % helium. Data was obtained from the work of Teichner.*[73]

Figure 2.9 shows a simple schematic of the oxidation products for alkanes containing primary, secondary, tertiary and quaternary carbon atoms. It should be noted that although it would be possible for primary alcohols, formed in the oxidation of a primary carbon atom, to undergo a dehydration reaction, thus forming alkenes and then ketones, no evidence for this was reported by the authors. It was proposed

that the aldehydes and ketones formed were intermediates in the complete oxidation process, and hence it was oxidation of the intermediates that resulted in the small amounts of $CO_2$ and $H_2O$ produced. From the intermediate compounds that were formed, it was shown that the carbon atom with the highest probability of being initially attacked by oxygen was the one with the highest electron density and the lowest steric hindrance, although any of the carbon atoms may be attacked, hence the reactions were all unselective. In general, the reactivity of the different types of carbons atoms followed the order $C_{tert} > C_{quat} > C_{sec} > C_{prim}$.

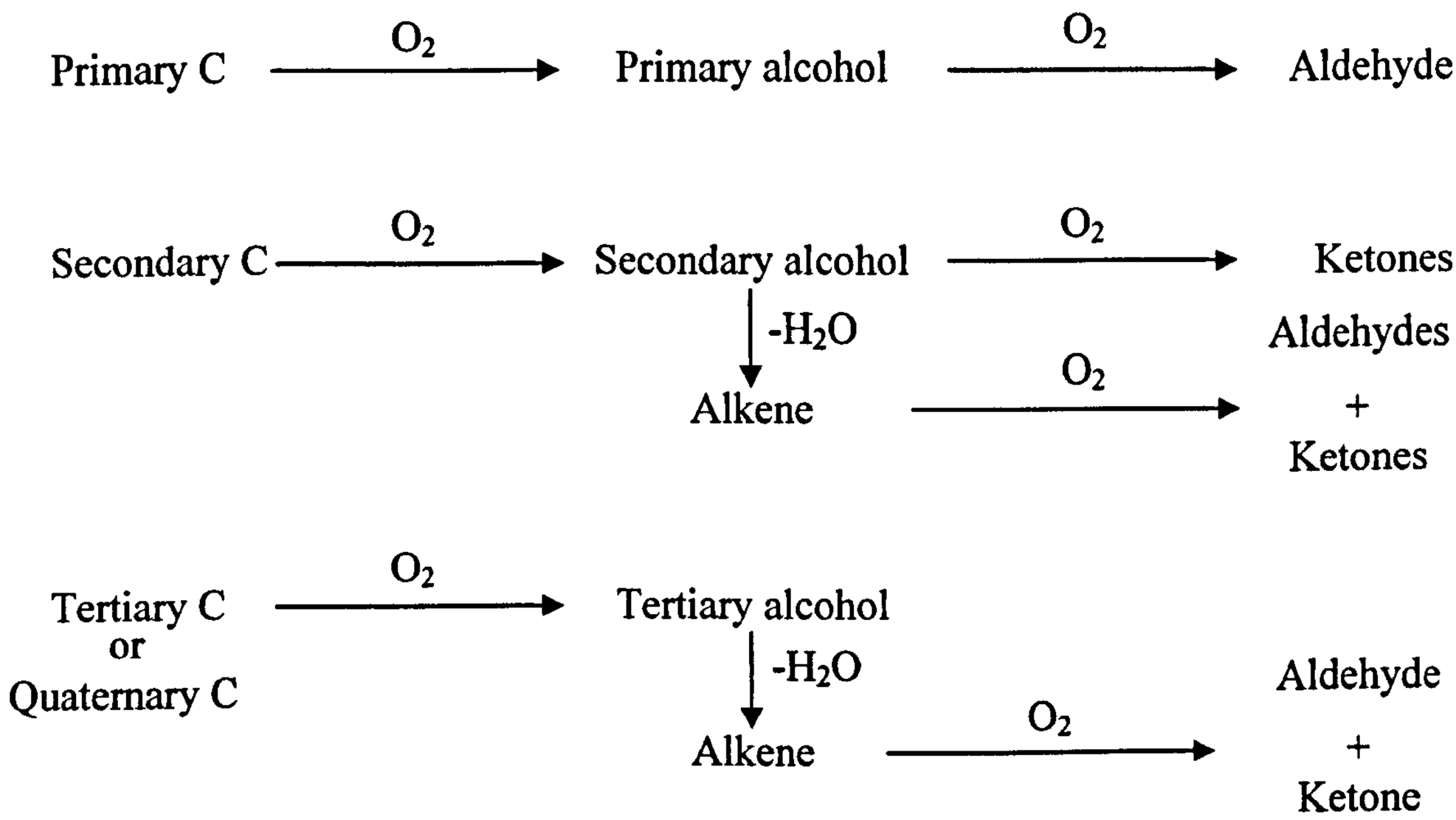


*Figure 2.9. Schematic of the oxidation products of alkanes as a function of their structure.*[26]

The same authors proposed an oxidation mechanism that involved single oxygen atoms rather than $O_2$ molecules, thus forming an alcohol intermediate that was then oxidised further to a ketone or an aldehyde. When secondary and tertiary carbon atoms are attacked by oxygen, it is thought that the alcohol intermediate formed may be firstly dehydrated to an alkene, which is finally oxidised directly to an aldehyde,

ketone or $CO_2$ and $H_2O$. For example, the proposed general reaction schemes for the oxidation of 2-methylbutane to its various products is:[52]

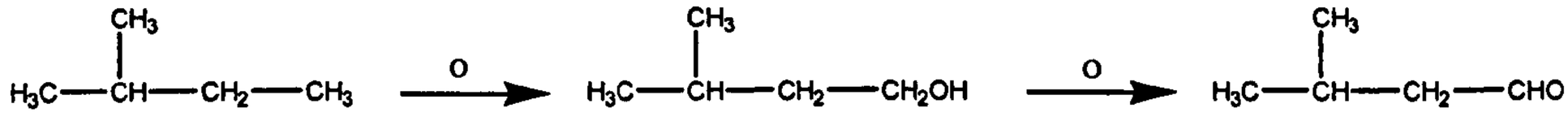


3-Methylbutanal

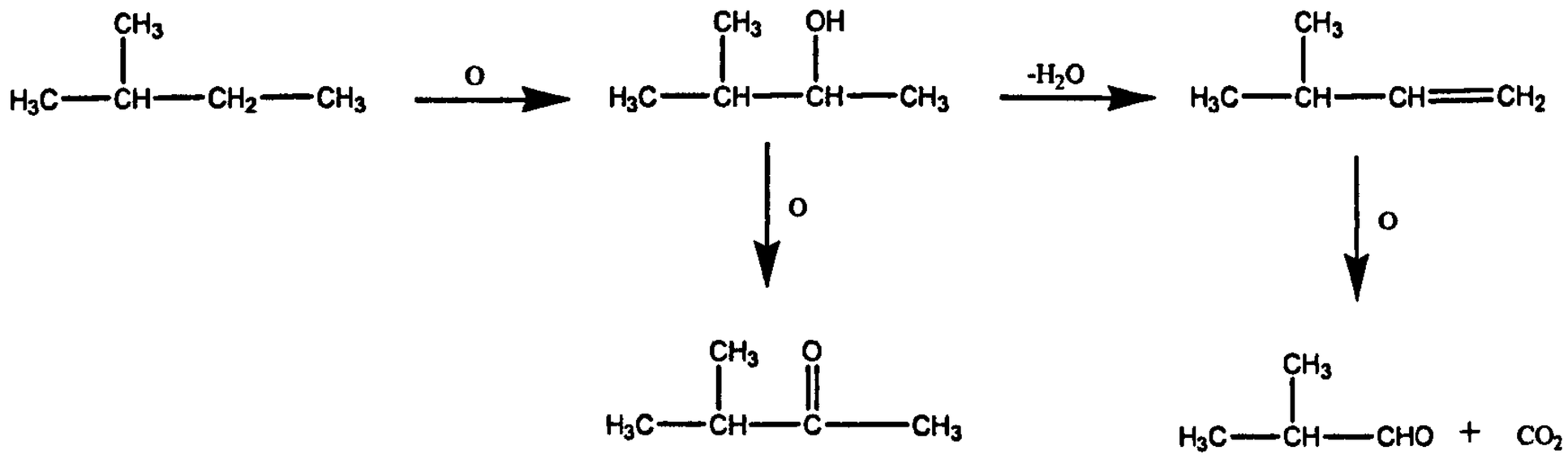


3-Methylbutanone

2-Methylpropanal

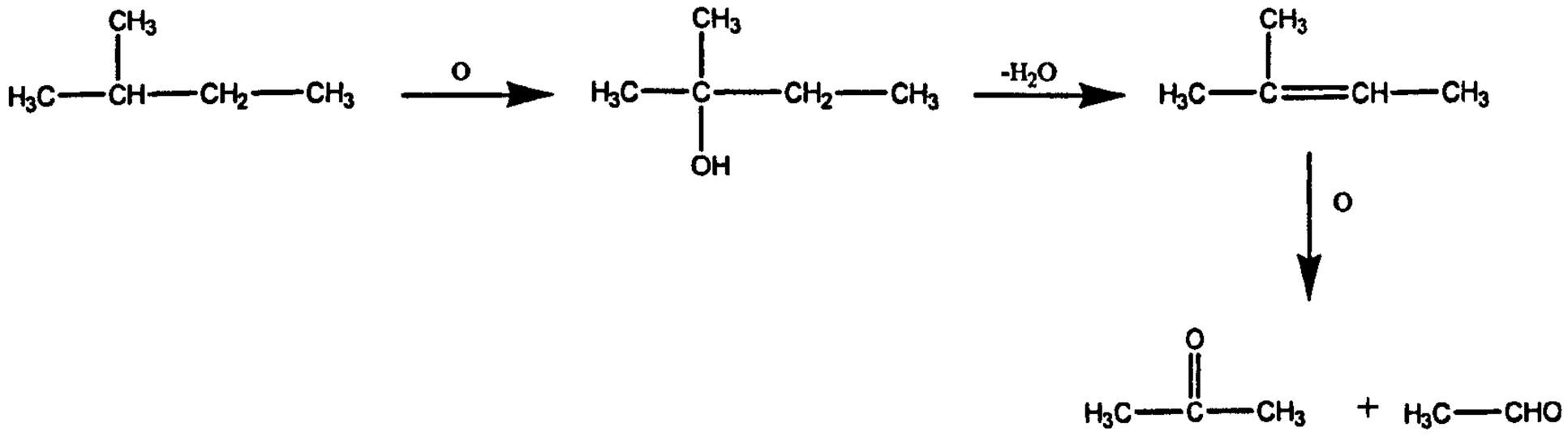


Acetone and ethanal


Butanone

In experiments conducted by the same authors with varying gas compositions, it was shown that the selectivity for $CO_2$ formation depended on the ratio of oxygen/hydrocarbon in the reaction stream. Unsurprisingly, it was found that increasing the oxygen content resulted in a higher selectivity for $CO_2$ formation, with fewer partial oxidation products in the exhaust gas.[73]

There are many more reports in the literature investigating the photocatalytic oxidation of alkanes and alkenes and most of the more recent reports focus on the oxidation of previously studied compounds with varying reaction conditions or looking at the mechanisms in more detail.[27,53,60,75-77] Examples of the types of reaction parameters investigated include; oxygen/organic ratios, contact times, concentration of reactants, effect of water vapour, type of illumination source (i.e. wavelength, intensities) and the effect of $TiO_2$ preparation method used. Although there are conflicting arguments as to the actual mechanisms of the oxidation and partial oxidation pathways (i.e. the roles of the active oxygen species, $O^{-}$, $O_2^{-}$ and $O_3^{-}$, and OH radicals (see below)), it is accepted that the complete oxidation of alkanes to $CO_2$ and $H_2O$ occurs via the formation of intermediate species (namely ketones, aldehydes, alcohols and alkenes). For this reason mechanistic studies of the photocatalytic oxidation of alkanes are usually broken down into the individual steps of alcohol oxidation to ketones and aldehydes, and then the oxidation of ketones and aldehydes to $CO_2$ and $H_2O$. It is apparent from the reports that sustained high conversions coupled with complete oxidation are favoured by:

1. presence of excess of oxygen
2. long gas-catalyst contact times
3. presence of some $H_2O$ in the gas phase
4. low concentration of organic being mineralised.

For example, Alberici and Jardim[53] have reported that it is possible to oxidise isooctane completely, forming only $CO_2$ and $H_2O$ when appropriate reaction conditions are used. The conditions for complete oxidation and > 95 % conversion involved a contact time of 6 s (decreasing this resulted in the formation of intermediates) for a reaction gas of synthetic air ( 21 % oxygen (*ca.* 210, 000 ppm) and 23 % relative humidity) containing 400 ppm of isooctane. The authors do not report the results from experiments with varying isooctane and humidity levels, however it has been shown by Teichner *et al.* that the oxidation of isooctane over a $TiO_2$ photocatalyst with a reaction gas composition of 37.5 % $O_2$, 37.5 % isooctane and 25 % helium results in the formation of a mixture of aldehyde and ketone intermediates with only a low selectivity for $CO_2$ formation.[73] These results show that intermediate formation is dependant on the experimental conditions used. It was also demonstrated by Alberici and Jardim that the type of UV (e.g. black light vs. germicidal lamp) source used had no effect on the reaction pathway.

### 2.6.1.3 Oxidation of alcohols

As it has been proposed that alcohols are intermediates formed in the production of aldehydes and ketones from alkanes (see above), most of the studies involving the gas-phase photocatalytic oxidation of alcohols focus on the possible reaction mechanisms rather than studies into the different types of alcohols. Two mechanisms have been reported for the photocatalytic oxidation of alcohols over $TiO_2$ (and ZnO) photocatalysts. Oxidation can occur via dehydrogenation reactions ($-H_2$) forming ketones directly or via dehydration reactions ($-H_2O$) forming alkenes.

Among the alcohols investigated the photocatalytic oxidation of 2-propanol (IPA) over illuminated $TiO_2$ photocatalysts has been the most extensively studied, and

it is accepted that acetone is the major product formed. This finding adds evidence to substantiate that the oxidation of alkanes to ketones (and aldehydes) occurs via the formation of an alcohol intermediate as the major partial oxidation product in propane oxidations was acetone. Hence it seems reasonable that this should occur via the formation of IPA as an intermediate compound.

One of the first mechanistic studies of IPA photooxidation was conducted by Bickley *et al.*, using a unique photoreactor consisting of a rotating tubular reaction chamber containing powdered $TiO_2$ (rutile) along with the reaction gases (IPA and $O_2$).[78] Illumination along the whole length of the chamber was achieved using a 500 W mercury arc lamp. Two different reaction conditions were studied, one with a preadsorbed IPA layer and no IPA in the gas phase, the other with both a preadsorbed layer and IPA in the gas phase. Oxygen was present in at least tenfold excess. The results showed that IPA was quickly oxidised to acetone and $H_2O$. Acetone appeared in the gas phase as it was displaced from the surface by $H_2O$. Oxidation of adsorbed acetone to $CO_2$ and $H_2O$ was only observed on samples that had been outgassed at high temperatures prior to IPA adsorption. When lower pretreatment temperatures were used, it was suggested that acetone was oxidised to a strongly adsorbed intermediate. The same authors also investigated $O_2$ photoadsorption, as a function of IPA surface coverage and pretreatment outgassing temperature. It was shown that $O_2$ photoadsorption increased as the IPA surface coverage increased, and that adsorption was greater for $TiO_2$ samples that had been outgassed at lower temperatures. It was suggested that the greater density of surface OH was responsible for the increase in $O_2$ photoadsorption rates. In another study by the same author TPD was used to detect the products that remained on the $TiO_2$ surfaces after the photocatalytic oxidation

reactions.[79] The results showed the presence of acetone, water, formic acid and trace amounts of acetic acid.

Larson and Widegren[80] conducted experiments of IPA photooxidation that were similar to those discussed above, but they used a more conventional annular reactor and a Degussa P25 photocatalyst. The results of the experiments were in agreement to those reported by Bickley,[78] however, in addition it was proposed that activated oxygen species (i.e. $O^-$, $O_2^-$, $O_3^-$) were involved in the production of acetone as its rate of formation was independent of $O_2$ concentration. In contrast, the complete mineralisation of acetone to $CO_2$ and $H_2O$ followed first order kinetics at low $O_2$ concentrations and zero order at high concentrations. These results can be explained by considering the amount of oxygen required for each reaction. Oxidation of acetone to $CO_2$ and $H_2O$ requires much more $O_2$ than oxidation of IPA to acetone. Thus, as the $O_2$ concentration decreases, the rate of acetone formation does not change, but the rate of acetone oxidation decreases, so acetone accumulates on the photocatalyst surface. Temperature programme desorption studies confirmed increasing amounts of acetone on the surface of used photocatalysts that had been tested with decreasing concentrations of $O_2$. These results clearly indicate that acetone is an intermediate in photocatalytic mineralisation of IPA.

Hager[81] performed the photocatalytic oxidation of IPA with excess oxygen and varying humidity levels. The results showed that percentage IPA conversion decreased with increasing $H_2O$ levels, but the percentage of IPA converted to acetone increased. It was suggested that competitive adsorption between acetone and $H_2O$ molecules for active sites was the cause of decreased mineralisation of acetone. This is in good agreement with the ideas put forward by Bickley.[78]

Investigation of the conversion of secondary alcohols in the presence of excess $O_2$ again resulted in the formation of a mixture of aldehydes and ketones.[82] It was shown that a photoassisted dehydrogenation reaction produced aldehydes, whilst ketones were formed by photoassisted $C_\alpha$-$C_\beta$ bond cleavages. Trace levels of alkenes, produced by photoassisted dehydration reactions, were also detected.

Walker *et al.*[83] studied the oxidation of primary (3-methyl-1-butanol), secondary (3-methyl-2-butanol) and tertiary (3-methyl-2-butanol) methylbutanols using a similar differential photoreactor to that used by Teichner for his studies of the oxidation of alkanes.[73] The reactions carried out in the presence of excess oxygen gave similar results to other reported alcohol oxidation reactions. The order of reactivity of the three different alcohols followed the sequence $C_{sec} > C_{tert} > C_{prim}$, which is different from that obtained for the oxidation of alkanes (see above). The oxidation of alkanes involves the extra step of oxygen insertion to form an alcohol. The ease of insertion for different types of carbon atoms may be different from the ease of oxidation of alcohols. The main product for the primary alcohol was 3-methyl-1-butanal, which was formed via direct oxidation of the initial molecule, whilst for secondary and tertiary alcohols a mixture of aldehydes and ketones were produced. The presence of water vapour did not effect the photoreactions.

## 2.6.2 Photocatalytic elimination of nitric oxide

### 2.6.2.1 Introduction

The potential to utilise heterogeneous photocatalysts for the elimination of NO was first realised in 1981, and initial studies conducted by Yoneyama[84] showed that it was possible to simultaneously photoreduce and photooxidise NO. In the experiment,

NO was bubbled through a 1 M $HClO_4$ solution containing either rutile $TiO_2$ or $Pt/TiO_2$ (*ca.* 2 wt. % Pt) particles. Over both unmodified titania and Pt modified titania, the reactions were unselective and the products of both NO oxidation ($NO_3^-$ and $NO_2$) and reduction reactions ($NH_3$, $N_2$ and $N_2H_4$) were detected (table 2.3), although the major products were nitrates and ammonia. However, the presence of Pt suppressed the formation of nitrate species (i.e. the oxidative reaction) and enhanced the production of $NH_3$ (i.e. increased the rate of the reduction reaction). As a solution is involved in the reaction (as a source of hydrogen atoms) the system is not self sufficient, which would be preferred for a catalyst system that is to eliminate NO from ambient air.

| Catalyst | Specific surface area / $m^2 g^{-1}$ | Rate of formation / $\mu mol\ h^{-1}\ g^{-1}$ | |
|---|---|---|---|
| | | $NO_3^-$ | $NH_3$ |
| $TiO_2$ (rutile) | 14.2 | 14.6 | 2.1 |
| 2 wt. % Pt-$TiO_2$ | 16.0 | 2.7 | 3.1 |

*Table 2.3. Results of the photocatalytic reaction of NO over $TiO_2$ and $Pt/TiO_2$ suspended in a 1 molar $HClO_4$ solution.*

It was in 1982 that the first report of gas-phase photocatalytic elimination of NO was published,[85] however it was not until the mid-1990s that a significant number of laboratories started publishing their findings of gas-phase NO elimination reactions. It should be noted that there are significantly fewer reports concerning $NO_x$ elimination compared to those investigating the removal of organic pollutants. It is apparent from the literature (and the initial studies by Yoneyama) that there are two possible pathways for the elimination of NO. Firstly, it can be oxidised in the presence of $O_2$, in which case there is agreement that the main reaction products are $NO_2$ and $NO_3^-$.[86-88] Secondly it can be decomposed or reduced (normally in the

absence of $O_2$) to $N_2$ and $N_2O$.[11,89,90] Examples of common reducing agents are CO, $NH_3$ and small chain alkenes.

### 2.6.2.2 NO photooxidation reactions.

A number of studies have reported the photocatalytic oxidation of NO to $NO_2$ and $NO_3^-$ in the presence of $O_2$ over $TiO_2$ photocatalysts.[86,87,91-94] The rapid oxidation of sub-ppm levels of NO to $NO_2$ was shown to readily occur over $TiO_2$ (anatase) powders in the presence of excess $O_2$.[95] Desorption of $NO_2$ into the gas phase has to be suppressed as it is also a regulated pollutant. As a result, the effects of modifications to $TiO_2$ have been investigated for NO oxidation reactions. Suppressing $NO_2$ desorption results in the formation of $HNO_3$ on the surface of the catalyst. Transient studies have shown that a complex equilibrium is formed, and that formation of $HNO_3$ involves a series of oxidation steps by photogenerated surface $OH^{-\bullet}$ radicals:[96]

$$NO + OH^{-\bullet} \rightleftharpoons HNO_2 + OH^{-\bullet} \rightleftharpoons NO_2 + H_2O \quad (2.5)$$

$$NO_2 + OH^{-\bullet} \rightleftharpoons HNO_3 \quad (2.6)$$

The density of surface hydroxyls and the amount of adsorbed water play a key role in these reactions, hence the catalyst preparation method is a crucial factor in determining the photocatalytic behaviour.

Hashimoto *et al.*[86] investigated the NO photooxidation properties of $TiO_2$ photocatalysts prepared by high temperature hydrolysis of titanium butoxide in toluene followed by heat treatment in air. The reactions were analysed in a fixed bed continuous flow photoreactor, using air containing 10 ppm NO at a flow of 110 sccm

as the reaction gas. It was found that titania calcined at 300°C (Hycom type) was highly active for the oxidation of NO, compared to Degussa P25, although the production of $NO_2$ was still observed. The increased activity was attributed to the larger surface area of Hycom titania. ESR measurements revealed that the number of $O_2^-$ radicals produced during illumination was proportional to the photocatalytic activity and the authors concluded that $O_2^-$ radicals react easily with NO, forming $NO_3^-$ and $NO_2$ species. No deactivation studies were conducted in these experiments.

Negishi *et al.*[92,93] have also studied the activity of sol-gel prepared $TiO_2$ for the photocatalytic oxidation of NO using a flow type photoreactor. The $TiO_2$ was prepared by hydrolysis of titanium isopropoxide in ethanol with the addition of polyethylene glycol (PEG) of varying average molecular weights. The resulting sols were coated on to glass slides and heat treated at 450°C in air, to remove the polymer particles, forming modified photocatalyst coatings (up to 1μm thick). The role of the polymer additive was in altering the surface structure of the $TiO_2$ coating by changing the size of the $TiO_2$ aggregates formed. Increasing the PEG molecular weight resulted in larger more separated $TiO_2$ polycrystals. Percentage NO conversions over the modified films were higher than those achieved over Degussa P25 $TiO_2$ (the same weight of catalyst was used) and increased from 65 % to 81 % when the average molecular weight of the PEG used was increased from 600 to 1000 amu respectively. The increase in activity was attributed to the increase in the specific surface area of the $TiO_2$ with increasing average molecular weight of the PEG. It was also shown that the film thickness had a dramatic effect on photocatalytic properties. Activity for NO conversion increased with increasing film thickness, which was most probably due to more efficient photon adsorption.[30] More importantly, the amount of $NO_2$ formed by the most active film (1 μm) was lower than that for the thinner coatings.

The larger surface area of the 1 μm film would lead to more adsorbed water which forms additional surface OH groups during illumination (discussed in section 2.5.1.1.). Therefore the $NO_2$ could easily be oxidised to $HNO_3$, according to equation 2.6, before desorption occurred.

Prolonged experiments (over 20 h) by the same authors showed that the activity of the photocatalysts for NO conversion decreased linearly during the first 5 h of illumination, after which time NO conversion reached a steady state. It was proposed that the $HNO_3$ formed and retained on the catalyst surface blocked the active sites and thus deactivated the photocatalyst.

The problem of $NO_2$ desorption from titania surfaces has also been tackled by preparing titania based composite catalysts. The effects of activated carbon[94] and zeolite[97] additions to titania have been reported. In both cases it was shown that desorption of $NO_2$ into the gas phase was suppressed whilst the yield of $HNO_3$ increased. It was reported that the additives have high adsorptive activities for $NO_2$ and thus act as $NO_2$ traps. This then allows the $TiO_2$ enough time to re-photooxidise $NO_2$ to $NO^-_3$. Figure 2.10 shows a simple schematic of the surface reaction over an activated carbon-$TiO_2$ catalyst. In both cases, the additives were inert towards the photocatalytic oxidation reactions. As with the studies conducted by Negishi, it was reported that the activity of the activated carbon-$TiO_2$ catalyst decreased during the course of the reaction. However, it was also noted that the original activity was regenerated after washing the catalysts in purified water. Analysis of the spent water revealed the presence of nitrate groups, thus confirming deactivation by residual nitric acid on the catalyst surface.

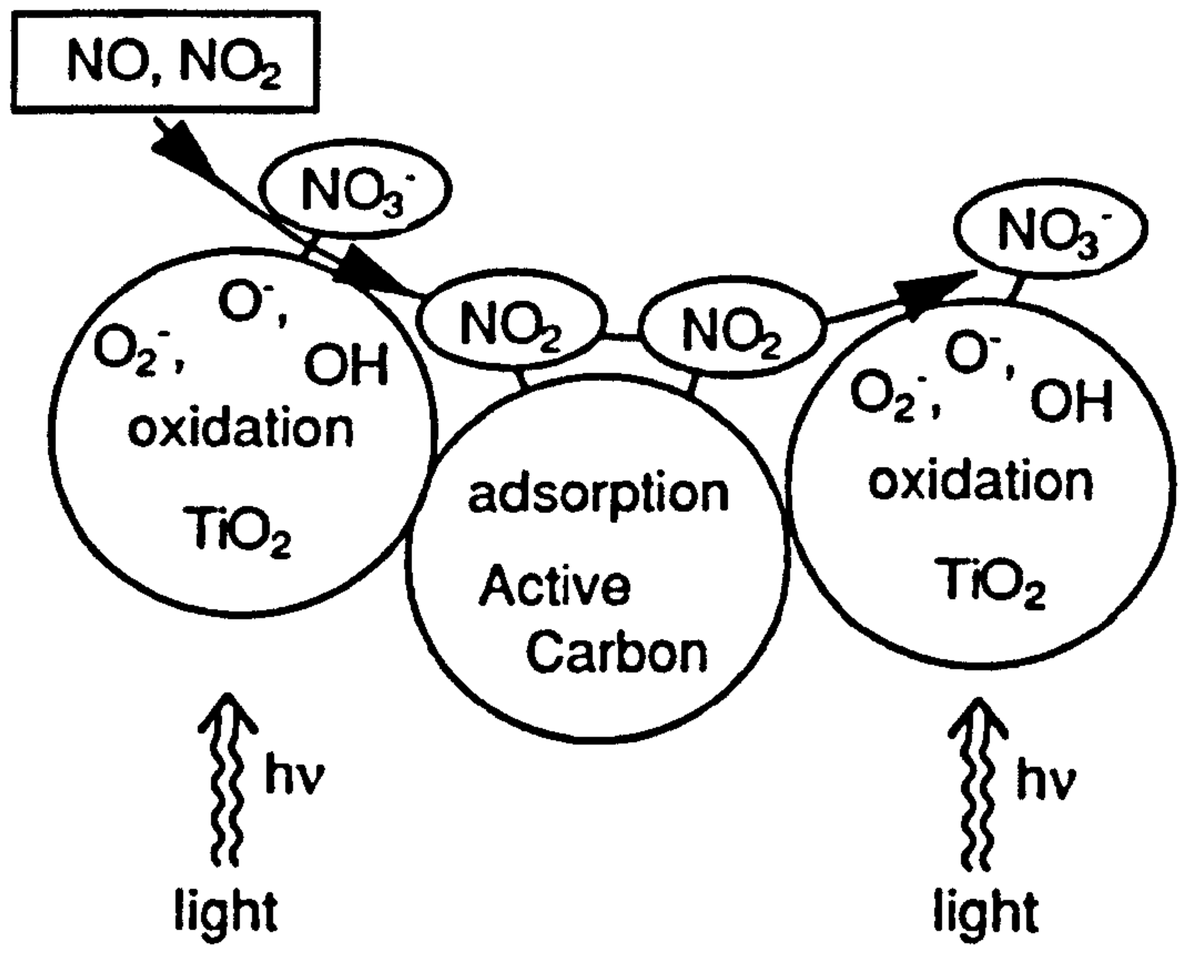


*Figure 2.10. Reaction scheme of $NO_x$ (NO and $NO_2$) removal by an activated carbon-$TiO_2$ catalyst. (Adapted from Ibusuki[94]).*

A novel preparation method for $TiO_2$, which was active for NO oxidation under visible light irradiation, has been reported by Nakamura and colleagues.[98,99] It was shown that a commercial $TiO_2$ photocatalyst (ST-01) treated in a hydrogen plasma (13.56 MHz, 500 W) was active in the visible light region up to 600 nm and was more active than unmodified $TiO_2$ for NO decomposition in the UV region. Consistent with the other reports of NO elimination in an oxidative atmosphere, the NO was removed as nitrate species which accumulated on the catalysts surface. XRD and BET analysis revealed neither the crystal structure nor specific surface area changed after the plasma treatment. ESR of the plasma $TiO_2$ showed the appearance of visible light activity was due to a new photoexcitation process that involved the formation of an oxygen vacancy state located between the valence and conduction bands (figure 2.11).

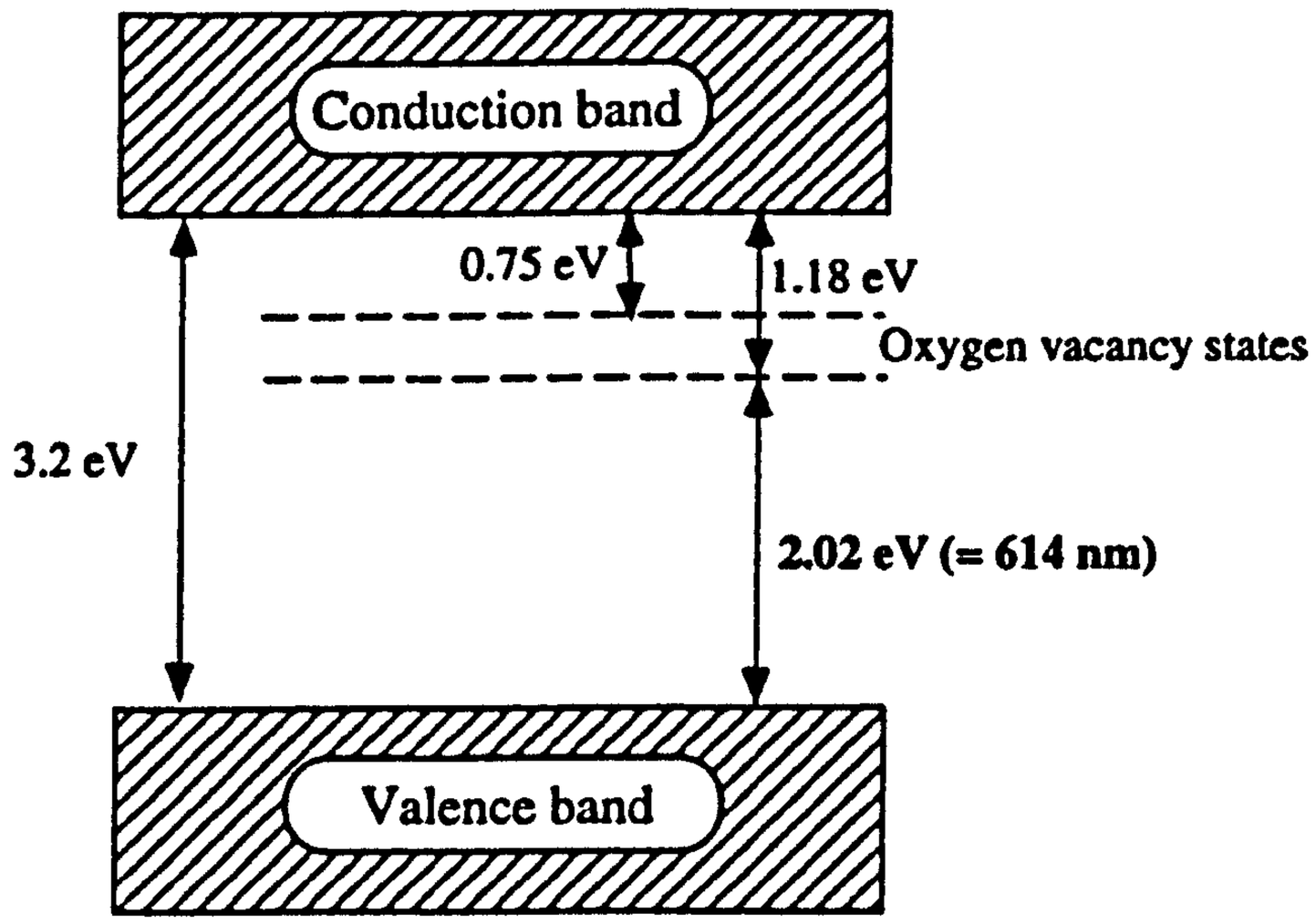


*Figure 2.11. A proposed band structure model for the anatase $TiO_2$ with oxygen vacancies, formed during a hydrogen plasma treatment. (Adapted from Nakamura[98]).*

Current commercial photocatalytic technologies for removal of NO over titania based photocatalysts utilise oxidation reactions, of the type discussed above, where NO is oxidised to nitrate species which are bonded to the catalyst surface. Many researchers have also reported the ability of titania to photocatalytically oxidise other atmospheric pollutants including hydrocarbons and CO [53] to $CO_2$ and water. Therefore, at present $TiO_2$ could be used for air pollution control, by oxidising all pollutants according to the following reaction:

$$NO + zCO + C_xH_{2y} \xrightarrow[h\nu]{TiO_2,\ O_2} HNO_3 + (x+y)CO_2 + yH_2O \qquad (2.7)$$

It would clearly be more desirable to have a catalyst system that, whilst oxidising CO and hydrocarbons, selectively reduced NO to $N_2$ gas, thus avoiding the deactivation of the catalyst by $HNO_3$, which can take place when reaction 2.7 occurs.

### 2.6.2.3 NO decomposition reactions

Along with titanium dioxide based photocatalysts, metals ions supported on zeolites and silver species supported on alumina have also proved to be effective for the photocatalytic decomposition NO in $N_2$ and $N_2O$.

Courbon and Pichat[11] reported the decomposition of NO, in an oxygen free environment, over $TiO_2$ (Degussa P25) samples, which had been pre-oxidised or pre-reduced The reactions were carried out in a batch style reactor in which the catalyst was spread in a thin layer a horizontal optical window, using a 125 W UV lamp to irradiate the catalyst. The significant role of surface bound $O^-$ species was highlighted by the use of isotopically substituted $N^{18}O$ molecules. Mass spectroscopic analysis of gas inside the reactor after a period of illumination, revealed that oxygen isotopic exchange between the oxygen of NO molecules and surface oxygens had occurred as both $N^{18}O$ and $N^{16}O$ were detected. Further mass spectra recorded with several ionisation energies, indicated the formation of $N_2$, $N_2{}^{18}O$ and $N_2{}^{16}O$, with $N_2$ formation favourable only on the pre-reduced catalysts during the early stages of reaction. No $NO_2$ formation was detected. The authors suggested that the production of $N_2$ from NO, which yields two oxygen atoms, is more favourable for the oxygen deficient reduced surface than $N_2O$ production, which produces only one oxygen atom.

It was hypothesised that photo-generated $O^-$ species are directly involved in the decomposition of NO according to the reaction equation:

$$NO^-_{(ads)} + O^-_{(lat)} \longrightarrow N_{(ads)} + O_{(ads)} + O^{2-}_{(lat)} \qquad (2.8)$$

Where $NO^-_{ads}$ and $O^-$ species are formed by the reaction of electron-hole pairs generated in the $TiO_2$ during illumination. The products $N_{(ads)}$ and $O_{(ads)}$ are then able

to react with other surface species to yield the products described earlier. Although these results show a decomposition route for NO, the $N_2O$ formed is also an air pollutant which would need to be eliminated.

Zhang *et al.*[100] carried out a systematic study of the NO decomposition reaction over a series of commercially available $TiO_2$ samples that had been pretreated in an $O_2$/Ar mixture at different temperatures. The 5 types of $TiO_2$ used were supplied by Catalysis Society of Japan and contained samples with various phase compositions, surface areas and degree of surface hydroxylation. For all the catalysts and pretreatment temperatures used only $N_2$ and $N_2O$ were detected as products. The most efficient photocatalyst had an anatase structure, relatively large surface area and a high density of surface hydroxyl groups and the optimal pretreatment temperature was 300 °C. Higher temperatures resulted in a decrease in activity, which was attributed to the removal of surface OH groups, thus it was confirmed that they play an important role in the decomposition of NO in a flow style system. It was found that the activity was not proportional to the intensity of UV photons when relatively high intensities were used. As a result, the FQEs were higher with lower intensities of UV photons. Similar findings have also been reported by Lim.[9]

Although it is agreed that the products of NO decomposition over photoactivated $TiO_2$ are $N_2$ and $N_2O$, none of the above reports gave the selectivities for formation of the two products. This is most probably due to limitations with the analysis methods employed, making quantification difficult. One group that has published values for the selectivity of the reaction products for NO decomposition reactions over $TiO_2$ is that of Anpo and Yamashita,[101] with selectivities of 25 % and 75 % for $N_2$ and $N_2O$, respectively.

Significant work on copper ions, silver ions and $TiO_2$ species anchored with ZSM-5 zeolite frameworks for` photocatalytic decomposition of NO has been carried out by a number of researchers.[45,102-109] The zeolite framework, with its shape selective porous structure provides a unique environment for photocatalytic reactions that cannot be achieved with normal bulk catalysts. Incorporation of transition metal ions within zeolite pores can induce photocatalytic capabilities due to ion-exchange between the zeolite and the metal ion. Whilst incorporation of $TiO_2$ particles into the zeolite framework results in electronic modification of the photocatalyst due to the size quantization effect.[110] The reported preparation method used to produce highly dispersed metal ions within a zeolite framework is that of ion-exchange using aqueous solutions of an appropriate metal salt. For the preparation of $Ag^+$/ZSM-5 and $Cu^{2+}$/ZSM-5 photocatalysts aqueous solutions of $Ag(NH_3)_2^+$ and $Cu(NH_3)_4^{2+}$ were used, respectively.[104,107] Prior to photocatalytic activity testing, the samples were degassed at 20°C, heated in $O_2$ at 400°C for 1 h, followed by evacuation at 200°C. $Ag^0$-ZSM-5 catalysts were prepared by reducing the $Ag^+$/ZSM-5 in an $H_2/H_2O$ atmosphere. $Cu^0$/ZSM-5 catalysts were prepared following the same procedures. All of the reported NO decomposition experiments by Anpo *et al.*, over zeolite supported photocatalysts, were carried out in a batch reactor using a 100 W high pressure mercury UV light source.

From the photocatalytic reactor studies using Ag and Cu modified ZSM-5 catalysts it was found that systems in which the metal ions were highly dispersed exhibited a high activity for NO photo-decomposition. Whereas, systems with aggregated metallic components showed very little photocatalytic activity towards NO decomposition. Silver(I) catalysts showed a high activity towards NO decomposition, however, some $N_2O$ and $NO_2$ was also formed.[107] Copper(I)

ion-exchanged zeolites fully reduced NO to $N_2$ and $O_2$, without the formation of by-products, but a problem that would be faced with these catalysts is that in the presence of oxygen the active copper(I) species would be photooxidised to inactive copper(II) species. Hence these copper(I) ion exchanged zeolites are not a viable option for the photocatalytic elimination of NO from air.

It was proposed by Anpo *et al.*[104] that the main mechanism of reduction over both types of catalyst was via electron transfer from the photo-induced electronic excited states ($3d^94s^1$ and $4d^95s^1$ states for Cu(I) and Ag(I) respectively) to the π-antibonding orbital of NO, and the simultaneous electron transfer from the π-bonding orbital of another NO, to the vacant electron state of the metal ion centre ($3d^94s^0$ and $4d^95s^0$ states for Cu(I) and Ag(I) respectively) resulting in the selective formation of $N_2$ and $O_2$. However, the mechanism involving two relatively close metal centres is also a possibility.[104] A further drawback for both the copper(I) and silver(I) exchange catalysts is that they require short wavelength UV radiation for excitation, due to the large band gap between the ground and excited states thus prohibiting the use of solar energy.

Courbon and Pichat's early work on $TiO_2$ powders was combined with the ZSM-5 research, leading to studies involving NO photodecomposition on $TiO_2$ anchored within zeolite cavities.[101,110,111] These investigations highlight the importance of the catalyst preparation method and the state of the $TiO_2$ species on the final photocatalytic properties of the materials produced. In these studies, the same style of photoreactor as used for the Ag/ZSM-5 work was employed using similar reaction conditions.

$TiO_2$/ZSM-5 catalysts prepared by an ion-exchange method yielded highly dispersed isolated tetrahedral titanium dioxide species which were highly selective for

the formation of $N_2$ from the photocatalytic decomposition of NO. Whilst those prepared by impregnation of the zeolite produced aggregated octahedrally coordinated titanium dioxide species which led to the formation of $N_2O$ from NO. Table 2.4 shows the product yields and selectivities for NO decomposition reactions over $TiO_2$/ ZSM-5. On the isolated titanium dioxide species, under UV irradiation, it was proposed that excited complexes, ($Ti^{3+}$-$O^-$) were formed. Electron transfer from the electron trapped centre ($Ti^{3+}$) into the π-antibonding orbital of NO takes place and simultaneously the electron transfer from the π-bonding of another NO into the hole trapped centre ($O^-$) occurs. These electron transfer reactions lead to the direct decomposition of two molecules of NO to form $N_2$ and $O_2$. For the aggregated catalysts, the photo-formed electron-hole pairs separate rapidly from each other. These large separations prevent the simultaneous activation of two NO molecules on the same active site and result instead in the formation of $N_{(ads)}$ and $O_{(ads)}$ which can then react with other $NO_{(ads)}$ molecules, forming $N_2O$ and $NO_2$ rather than $N_2$ and $O_2$. Although the highly dispersed tetrahedral $TiO_2$ species appear to be good photocatalysts for the reduction of NO into $N_2$, they were only partially successful as they do not fully reduce all the NO, but some $N_2O$ was also produced.[101]

| Catalyst | Yields / μmol $h^{-1}$ $g^{-1}$ ($TiO_2$) | | | Selectivity / % | |
|---|---|---|---|---|---|
| | $N_2$ | $N_2O$ | Total | $N_2$ | $N_2O$ |
| Ion-exchange | 14 | 1 | 15 | 91 | 9 |
| Impregnated | 7 | 10 | 17 | 41 | 59 |
| P25 | 2 | 6 | 8 | 25 | 75 |

*Table 2.4. Comparison of yields of $N_2$ and $N_2O$ and their selectivities in the photocatalytic decomposition over various $TiO_2$ photocatalysts.*[101]

### 2.6.2.4 NO reduction reactions

The third option for the elimination of nitric oxide is through photocatalytic reduction, which, like the decomposition reaction, has been attempted with a variety of catalysts and reducing agents. Cole and Cant[89] investigated the photocatalytic reduction of nitric oxide with ammonia over $TiO_2$ wafers using a static reactor system. The wafers were prepared by pressing a commercial $TiO_2$ powder that had a phase composition of 85 % anatase and 15 % rutile. The reaction gas used consisted of 10 Torr of $NH_3$ and 10 Torr of NO. For comparison, a decomposition experiment with only NO present was run. It was found that in the presence of ammonia, the NO conversion rate was approximately five times greater and the ratio of the products ($N_2/N_2O$) also increased compared to the corresponding decomposition reaction (table 2.5). When isotopically labelled reactants were used ($^{14}NO$ and $^{15}NH_3$), $^{14}N^{15}N$ and $^{14}N_2O$ were almost exclusively formed. From these observations, the following scheme was proposed for the $NO + NH_3$ reaction:

$$^{14}NO^{-}_{(ads)} + O^{-}_{(lat)} \longrightarrow {}^{14}N_{(ads)} + O_{(ads)} + O^{2-}_{(lat)} \quad (2.9)$$

$$^{14}N_{(ads)} + {}^{14}NO_{(ads)} \longrightarrow {}^{14}N_2O_{(ads)} \longrightarrow {}^{14}N_2O_{(gas)} \quad (2.10)$$

$$O_{(ads)} + {}^{15}NH_{3(ads)} \longrightarrow {}^{15}NH_{2(ads)} + OH_{(ads)} \quad (2.11)$$

$$OH_{(ads)} + {}^{15}NH_{3(ads)} \longrightarrow {}^{15}NH_{2(ads)} + H_2O_{(ads)} \quad (2.12)$$

$$^{15}NH_{2(ads)} + {}^{14}NO_{(ads)} \longrightarrow {}^{14}N^{15}N_{(ads)} + H_2O_{(ads)} \quad (2.13)$$

| Initial pressures / Torr | | $N_2$ produced / μmol $h^{-1}$ | $N_2O$ produced / μmol $h^{-1}$ | $N_2/N_2O$ | Rate of NO conversion / μmol $h^{-1}$ |
|---|---|---|---|---|---|
| $NH_3$ | NO | | | | |
| 0 | 10.3 | 0.5 | 1.20 | 0.4 | 1.7 |
| 10.2 | 9.8 | 5.95 | 2.68 | 2.2 | 8.63 |

*Table 2.5. Comparison of NO decomposition and NO + $NH_3$ reactions over $TiO_2$ wafers. Illumination time was 2 h for each experiment. Data from Cole et al.[99]*

Recently very similar results have been report by Teramura *et al.*[112,113] over powdered $TiO_2$ photocatalysts (JRC-TIO-4, Japan Catalysis Society). In addition they also studied the photocatalytic reduction of NO with $NH_3$ in the presence of $O_2$ and found that the reaction was 100 % selective for $N_2$ formation, i.e. no $N_2O$ was produced. The stoichiometric reaction is:

$$4NO + 4NH_3 + O_2 \longrightarrow 4N_2 + 6H_2O \qquad (2.14)$$

From IR data collected during the experiments it was proposed that the active site on the $TiO_2$ surface was a $Ti^{4+}$ Lewis acid site to which $NH_3$ could be easily adsorbed. Gas phase NO then attacks adsorbed $NH_3$ species and $N_2$ and $H_2O$ are generated via a nitrosamide intermediate. The reduced $Ti^{3+}$ site that is consequently formed is then reoxidised to the $Ti^{4+}$ species by oxygen. In the absence of $O_2$, NO reoxidises the $Ti^{3+}$ species and $N_2O$ is produced.

More recently, the use of hollandite type ($K_2Ga_2Sn_6O_{16}$, KGSO) catalysts for the photocatalytic reductive decomposition of NO in the presence of ethane ($C_2H_6$) as a reducing agent have been reported.[114,115] The reactions were carried out using a batch style reactor containing 4000 ppm NO and 2000 ppm $C_2H_6$ in an oxygen free environment. When the gases were brought into contact with the photocatalyst during irradiation NO was fully reduced to $N_2$ gas, but the ethane was only partially oxidised to $CH_3CHO$ according to the reaction:

$$2NO + C_2H_6 \xrightarrow[h\nu]{KGSO} N_2 + CH_3CHO + H_2O \qquad (2.15)$$

IR studies of the catalyst surface during the course of the reactions revealed the formation of isocyanate (-NCO) intermediates on surface $K^+$ sites, although no

explanation was put forward as to the role of isocyanate groups in the formation of $N_2$.

The aldehyde partial oxidation product is a very important industrial reagent but to utilise this by-product it would need extracting from the other gas phase products which would be expensive and add further complications to any potential system. It would clearly be more desirable to have a system which, whilst selectively reduced NO to $N_2$, fully oxidised hydrocarbons to $CO_2$ and water. A further drawback to this system is the position of the absorption edge of KGSO (*ca.* 280 nm,[115] *cf.* 380 nm for $TiO_2$,[59] which requires short wavelength UV for excitation).

Silver and silver chloride catalysts supported on alumina have also shown high activity for NO reduction in the presence of $O_2$ and ethane.[116] A flow-type photoreactor was used with a gas composition of 10 ppm NO, 10 % (or zero) $O_2$, 5 ppm (or zero) $C_2H_6$, and $N_2$ as the balance. The total flow rate of the system was 620 sccm. The wavelength of photons required for photoexcitation to occur was around 250 nm, but depended on the specific catalyst used. It was found that NO conversion was higher over the AgCl catalysts for all the reaction conditions used. The presence of both $O_2$ and $C_2H_8$ in the reaction gas enhanced the NO conversion rates. The authors report that the main product was $N_2O$ for all the reactions, but do not include any data showing the selectivity values of the reactions. It was suggested that the increased activity of the AgCl catalysts in the presence of $O_2$ was due to stabilisation of AgCl particles, thus suppressing the formation of less active $Ag^0$ atoms and clusters. The proposed role of hydrocarbon species was to react with the photogenerated holes, suppressing recombination reactions with the excited electrons

which are then involved in charge transfer to the π–antibonding molecular orbital of adsorbed NO molecules.

Current technologies for the removal of atmospheric NO operate via selective catalytic reduction (SCR) of NO with CO at elevated temperatures.[34] Most of the catalysts used consist of noble metals dispersed on an oxide support of high specific surface area. Noble metals show good adsorption properties for both NO and CO, thus making them an ideal choice as catalysts for the removal of NO and CO pollutants.[117,118] It is apparent from the literature that there are similarities in the mechanisms of NO decomposition over thermal and photo-activated catalysts.

For example it has been found that NO adsorbed on rhodium, a well known NO SCR catalyst, is susceptible to reduction because the rhodium pushes electron density into the $\pi$-antibonding orbital of adsorbed NO species.[119] It has also been shown that highly dispersed supported rhodium particles have high selectivity for $N_2$ production from NO, but when it becomes aggregated on the surface the main reduction product was $N_2O$.[34] These observations are remarkably similar to those observed for the zeolite supported photocatalysts.[104,107,111] In light of these similarities, it is surprising to find that there has been only one laboratory that has studied the photocatalytic properties of $TiO_2$ supported noble metals for the elimination of NO in the presence of CO.[120]

Ru, Rh/Ru and Cu/Ru modified $TiO_2$ (Degussa P25 type) were prepared using standard impregnation and reduction techniques and their photocatalytic behaviour for NO reduction in the presence of CO was investigated using a batch type photoreactor.[120] Over $Ru/TiO_2$ catalysts NO was reduced to $N_2O$, producing only a small amount of $N_2$ during the first 5 hours of illumination. Continued illumination resulted in the reduction of $N_2O$ to $N_2$ and after 25 h all of the $N_2O$ was consumed.

Whilst, over co-modified Cu/Ru and Rh/Ru modified $TiO_2$, the $N_2O$ concentration increased during the first 1 h of illumination and was then slowly consumed. After 8 h all of the $N_2O$ produced was converted to $N_2$, indicating the increased activity in the presence of Rh and Cu. It should be noted that Rh additions were more effective than Cu for accelerating the $N_2O$ reduction reaction.

It was proposed that the mechanism for the decomposition of $N_2O$ was via the formation of an isocyanate species on the metal particles by reaction of adsorbed an N atom with a CO molecule. From the observed results, it was thought that formation of isocyanate species occurred more readily on Rh particles than on Ru and Cu particles, hence explaining the increased $N_2O$ reduction rate in the presence of Rh. Figure 2.12 shows a schematic of the proposed mechanism. The formation of isocyanate species over illuminated $Rh/TiO_2$ in the presence of NO and CO has been confirmed by FTIR studies conducted by Rasko.[121]

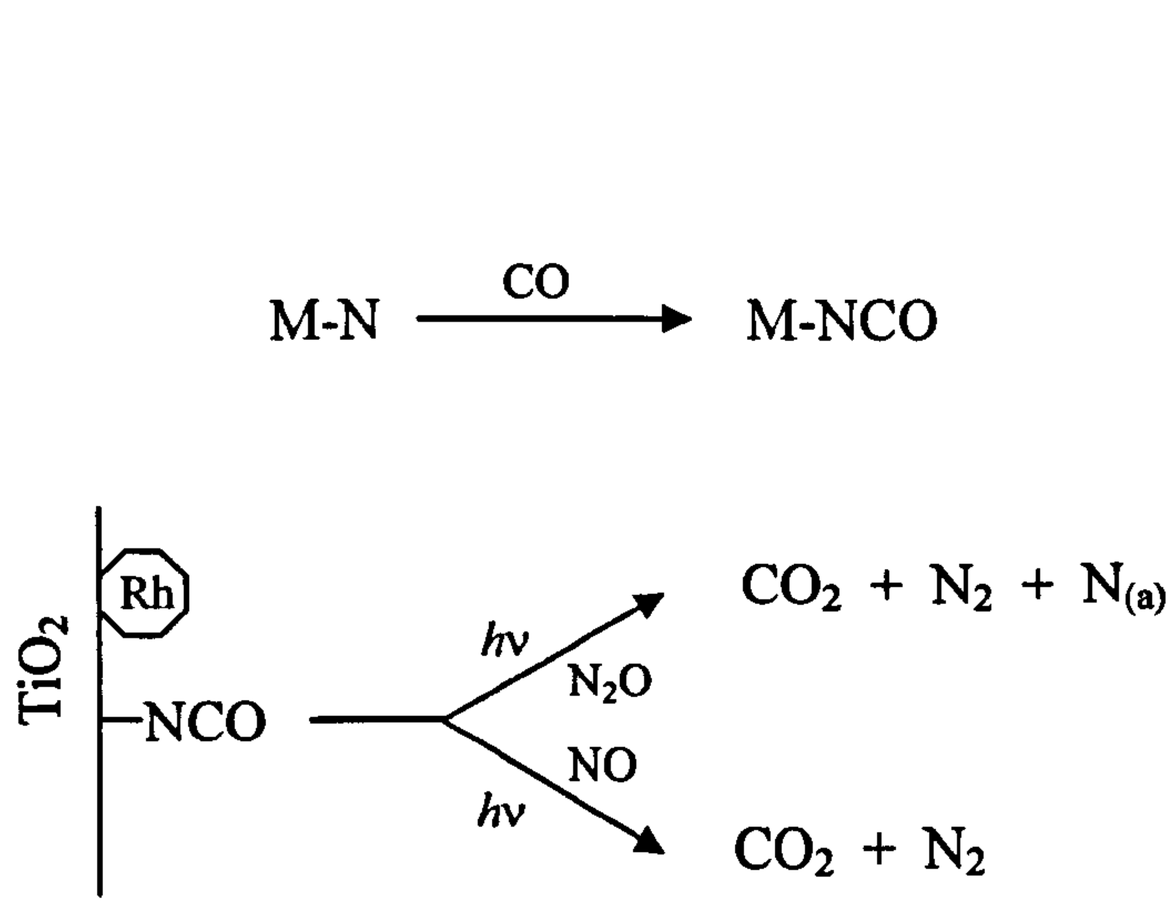


*Figure 2.12. Proposed reaction mechanism for the removal of $N_2O$ over supported noble metal particles. (Adapted from Thampi[120]).*

A novel silica-supported molybdenum oxide catalyst containing 2.5 wt. % of $Mo^{6+}$ has also been reported to be an active catalyst for the reduction of NO in the

presence of CO.[122-124] The catalyst was prepared by impregnation of a silica gel with an aqueous solution of $(NH_4)_6Mo_7O_{24}$ which was then dried in air at 80°C. The catalyst was pretreated in $O_2$ at 800°C in the photoreactor which was then evacuated and cooled before the introduction of the reactant gas. The photoreactor was a circulating batch type reactor in which the catalyst (1 g) was placed on an optically transparent window. Figure 2.13 shows the partial pressures of the reactants and products during the course of the reaction. As soon as the lamp was turned on both NO and CO were consumed whilst $CO_2$ and $N_2O$ were produced. Initially no $N_2$ formation was detected and only after $N_2O$ formation reached a maximum (*ca.* 320 s) that $N_2$ formation occurred. These results indicated that the complete reduction of NO to $N_2$ took place in two stages, which is similar to the mechanism reported by Thampi *et al.*[120] In the first stage NO was reduced to $N_2O$ (equation 2.16) and in the second stage $N_2O$ was further reduced to $N_2$ (equation 2.17). Although it was suggested that this system was similar to those reported by Thampi it should be pointed out that the induction period before $N_2$ formation was much shorter over the $MoO_3/SiO_2$ catalysts (*ca.* 6 min for the $MoO_3/SiO_2$ system compared to *ca.* 60 min. for the $TiO_2$ supported noble metal catalysts).

$$2NO + CO \longrightarrow CO_2 + N_2O \qquad (2.16)$$

$$N_2O + CO \longrightarrow N_2 + CO_2 \qquad (2.17)$$

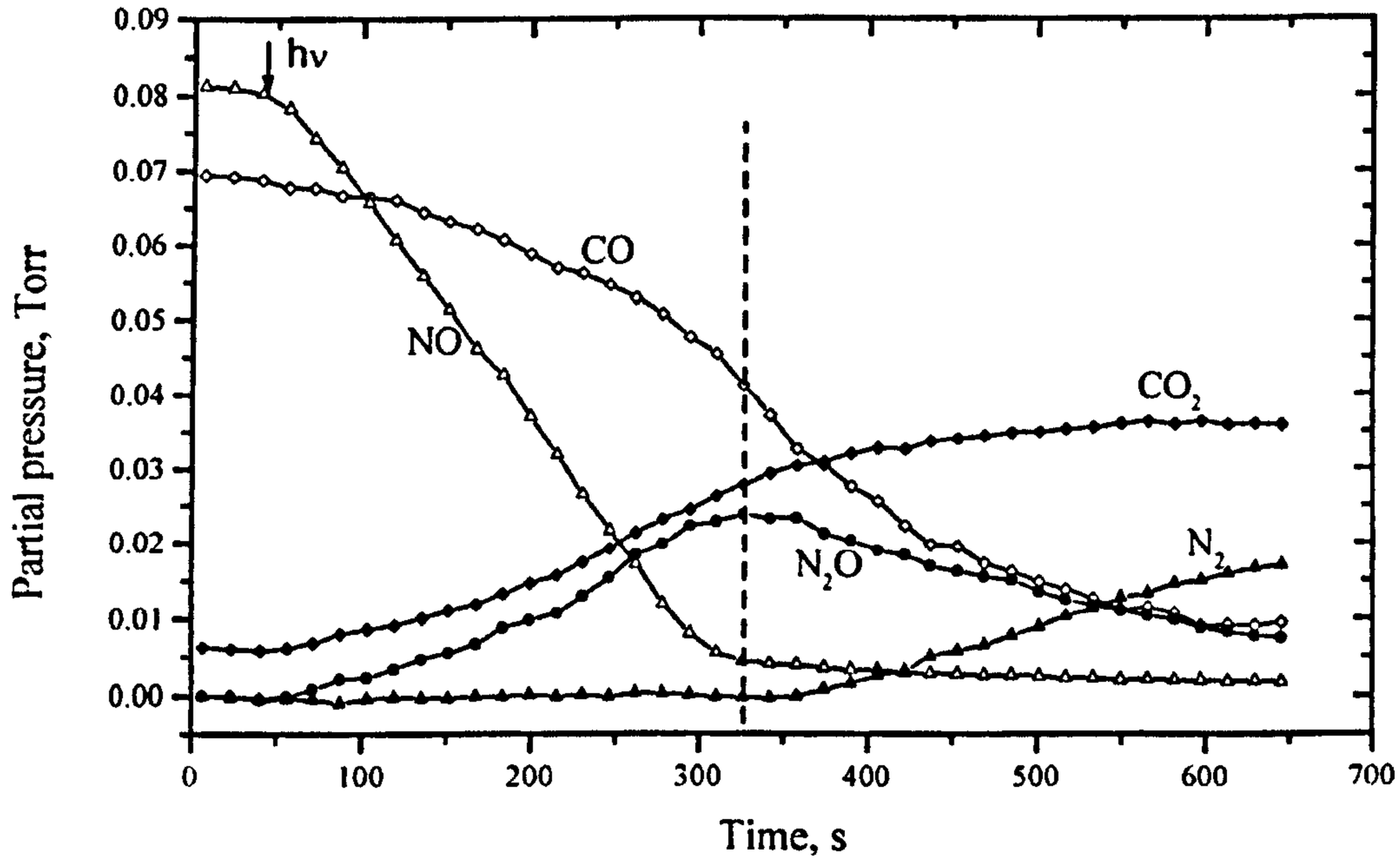


*Figure 2.13. Kinetics of NO + CO reaction on $MoO_3/SiO_2$ upon UV irradiation at 20°C. The vertical dashed line marks the position of the $N_2O$ maximum. (Adapted from Shelimov[123]).*

## 2.7 Summary

It is evident that the photooxidation of NO, in the presence of $O_2$, will occur readily over $TiO_2$ photocatalysts. Consistent in all the reports, is the formation of nitrate groups which result in deactivation of the $TiO_2$ surface. Although, the activity can be restored by washing that catalyst with water, this adds an extra undesirable complication to the NO elimination process.

From the studies of NO decomposition over $TiO_2$ photocatalysts, it is apparent that the reaction pathway is unselective, resulting in the formation of $N_2$ and $N_2O$, which is also a regulated pollutant. NO photodecompositions over isolated silver species incorporated into a zeolite framework are highly selective for $N_2$ formation. The high selectivity was attributed to the active sites present on the isolated silver species. A problem though, with these photocatalysts is that they require the use of

biohazardous short wavelength UV irradiation for photoexcitation. Hence, they are not a viable system for the removal of NO from the atmosphere.

The selective photocatalytic reduction of NO has been investigated over a variety of photocatalysts including, KGSO, Ag-$Al_2O_2$, AgCl-$Al_2O_3$, Ru-$TiO_2$, Rh/Ru-$TiO_2$ and Cu/Ru-$TiO_2$ systems. The photoreactions over the $TiO_2$ supported noble metal photocatalysts are the only photocatalytic reactions reported that utilise CO as a reducing agent. It was found that the presence of rhodium on Ru/$TiO_2$ photocatalysts increased the rate of $N_2$ formation. There are no reports of the NO-CO photoreaction over unmodified $TiO_2$ photocatalysts.

Although previous studies have shown that silver species are highly selective NO decomposition photocatalysts, there have been no reports of Ag-$TiO_2$ photocatalysts used for NO decomposition and reduction reactions. Such a system should be able to utilise UV wavelengths and offer the high selectivity of silver active sites. Through the work of Thampi it was shown that the presence of rhodium aided the complete reduction of NO to $N_2$, however, no one has yet reported the properties of Rh/$TiO_2$ photocatalysts for the selective photocatalytic reduction of NO, nor for NO decomposition reactions.

It is evident that further research is still required in order to develop efficient and practical photocatalysts for the elimination of NO from the atmosphere. The work presented in this thesis is furthering the studies previously reported for the photocatalytic elimination of NO.

## 2.8 References


(1) Bond, G. C. *Heterogeneous Catalysis. Principles and Applications*, 2nd ed.; Clarendon Press: Oxford, 1978.
(2) Serpone, N.; Emeline, A. V. *Int. J. Photoenergy* **2002**, *4*, 91.
(3) Palmisano, L.; Sclafani, A. Thermodynamics and Kinetics for Hetergeneous Photocatalytic Processes. In *Hetergeneous Photocatalysis*; Schiavello, M., Ed.; John Wiley and Sons Ltd: Chichester, 1997; Vol. 3; pp 109.
(4) Kalyanasundaram, K.; Gratzel, M.; Pelizzetti, E. *Coord. Chem. Rev.* **1986**, *69*, 57.
(5) Adachi, K.; Ohta, K.; Mizuno, T. *Sol. Energy* **1994**, *53*, 187.
(6) Rao, N. N.; Dube, S.; Manjubala; Natarajan, P. *Appl. Catal. B Environ.* **1994**, *5*, 33.
(7) Chen, J.; Ollis, D. F.; Rulkens, W. H.; Bruning, H. *Water Res.* **1999**, *33*, 661.
(8) Wahl, A.; Ulmann, M.; Carroy, A.; Jermann, B.; Dolata, M.; Kedzierzawski, P.; Chatelain, C.; Monnier, A.; Augustynski, J. *J. Electroanal. Chem.* **1995**, *396*, 41.
(9) Lim, T. H.; Jeong, S. M.; Kim, S. D.; Gyenis, J. *J. Photochem. Photobiol. A Chem.* **2000**, *134*, 209.
(10) Borgarello, E.; Harris, R.; Serpone, N. *Nou. J. De Chim.* **1985**, *9*, 743.
(11) Courbon, H.; Pichat, P. *J. Chem. Soc. Faraday Trans. I* **1984**, *80*, 3175.
(12) Linsebigler, A. L.; Lu, G. Q.; Yates, J. T. *Chem. Rev.* **1995**, *95*, 735.
(13) Martin, S. T.; Herrmann, H.; Choi, W. Y.; Hoffmann, M. R. *J. Chem. Soc. Faraday Trans.* **1994**, *90*, 3315.
(14) Martin, S. T.; Herrmann, H.; Hoffmann, M. R. *J. Chem. Soc. Faraday Trans.* **1994**, *90*, 3323.
(15) Schiavello, M. *Heterogeneous Photocatalysis*, 1st ed.; John Wiley & Sons Ltd.: Chichester, 1997; Vol. 3.
(16) Sclafani, A.; Herrmann, J. M. *J. Photochem. Photobiol. A Chem.* **1998**, *113*, 181.
(17) Chao, H. E.; Yu, Y.; Hu, X. F.; Larbot, A. *Appl. Surf. Sci.* **2002**, *200*, 239.
(18) Chao, H. E.; Yun, Y. U.; Xingfang, H. U.; Larbot, A. *J. European Ceram. Soc.* **2003**, *23*, 1457.
(19) Karvinen, S. *Solid State Sci.* **2003**, *5*, 811.
(20) Nair, J.; Nair, P.; Mizukami, F.; Oosawa, Y.; Okubo, T. *Mater. Res. Bull.* **1999**, *34*, 1275.
(21) Amores, J. M. G.; Escribano, V. S.; Busca, G. *J. Mater. Chem.* **1995**, *5*, 1245.
(22) Eibl, S.; Gates, B. C.; Knozinger, H. *Langmuir* **2001**, *17*, 107.
(23) Tanaka, K.; Hisanaga, T.; Rivera, A. P. Effect of Crystal Form of $TiO_2$ on the Photocatalytic Degradation of Pollutants. In *Photocatalytic Purification and Treatment of Water and Air*; ELSEVIER SCIENCE PUBL B V: Amsterdam, 1993; Vol. 3; pp 169.
(24) Sumita, T.; Yamaki, T.; Yamamoto, S.; Miyashita, A. *Appl. Surf. Sci.* **2002**, *200*, 21.
(25) Nargiello, M.; Herz, T. Physcial-chemical characteristics of P-25 making it extremely suited as the catalyst in photodegradtion of organic compounds. In *Photocatalytic purification and treatment of water and air*; Ollis, D. F., Al-Ekabi, H., Eds.; Elsecier: Amsterdam, 1993.
(26) Mills, A.; LeHunte, S. *J. Photochem. Photobiol. A Chem.* **1997**, *108*, 1.
(27) Cao, L. X.; Huang, A. M.; Spiess, F. J.; Suib, S. L. *J. Catal.* **1999**, *188*, 48.

(28) Blount, M. C.; Kim, D. H.; Falconer, J. L. *Environ. Sci. Technol.* **2001**, *35*, 2988.
(29) Zhang, Z. B.; Wang, C. C.; Zakaria, R.; Ying, J. Y. *J. Phys. Chem. B* **1998**, *102*, 10871.
(30) Jacoby, W. A.; Blake, D. M.; Noble, R. D.; Koval, C. A. *J. Catal.* **1995**, *157*, 87.
(31) Litter, M. I. *Appl. Catal. B Environ.* **1999**, *23*, 89.
(32) Howe, R. F. *Dev. Chem. Eng. Mineral Process.* **1998**, *6*, 55.
(33) Kohno, Y.; Hayashi, H.; Takenaka, S.; Tanaka, T.; Funabiki, T.; Yoshida, S. *J. Photochem. Photobiol. A Chem.* **1999**, *126*, 117.
(34) Castillo, S.; Moran-Pineda, M.; Molina, V.; Gomez, R.; Lopez, T. *Appl. Cat. B Environ.* **1998**, *15*, 203.
(35) Linsmeier, C.; Knozinger, H.; Taglauer, E. *Nucl. Instrum. Methods Phys. Res. Sect. B-Beam Interact. Mater. Atoms* **1996**, *118*, 533.
(36) Clarke, W. C.; Vondjuidis, A. G. *J. Catal.* **1965**, *4*, 691.
(37) Borgarello, E.; Serpone, N.; Emo, G.; Harris, R.; Pelizzetti, E.; Minero, C. *Inorg. Chem.* **1986**, *25*, 4499.
(38) Fernandez, A.; Gonzalezelipe, A. R. *Appl. Surf. Sci.* **1993**, *69*, 285.
(39) Palmisano, L.; Augugliaro, V.; Sclafani, A.; Schiavello, M. *J. Phys. Chem.* **1988**, *92*, 6710.
(40) Peral, J.; Casado, J.; Domenech, J. *J. Photochem. Photobiol. A Chem.* **1988**, *44*, 209.
(41) Borgarello, E.; Kiwi, J.; Gratzel, M.; Pelizzetti, E.; Visca, M. *J. Am. Chem. Soc.* **1982**, *104*, 2996.
(42) Soria, J.; Conesa, J. C.; Augugliaro, V.; Palmisano, L.; Schiavello, M.; Sclafani, A. *J. Phys. Chem.* **1991**, *95*, 274.
(43) Einaga, H.; Futamura, S.; Ibusuki, T. *Chem. Lett.* **2001**, 582.
(44) Einaga, H.; Futamura, S.; Ibusuki, T. *Phys. Chem. Chem. Phys.* **1999**, *1*, 4903.
(45) Yamashita, H.; Honda, M.; Harada, M.; Ichihashi, Y.; Anpo, M.; Hirao, T.; Itoh, N.; Iwamoto, N. *J. Phys. Chem. B* **1998**, *102*, 10707.
(46) Yamashita, H.; Ichihashi, Y.; Takeuchi, M.; Kishiguchi, S.; Anpo, M. *J. Synchrot. Radiat.* **1999**, *6*, 451.
(47) Litter, M. I.; Navio, J. A. *J. Photochem. Photobiol. A Chem.* **1996**, *98*, 171.
(48) Pruden, A. L.; Ollis, D. F. *J. Catal.* **1983**, *82*, 404.
(49) Hsiao, C. Y.; Lee, C. L.; Ollis, D. F. *J. Catal.* **1983**, *82*, 418.
(50) Okamoto, K.; Yamamoto, Y.; Tanaka, H.; Tanaka, M.; Itaya, A. *Bull. Chem. Soc. Jpn.* **1985**, *58*, 2015.
(51) Hoffmann, M. R.; Martin, S. T.; Choi, W. Y.; Bahnemann, D. W. *Chem. Rev.* **1995**, *95*, 69.
(52) Djeghri, N.; Teichner, S. J. *J. Catal.* **1980**, *62*, 99.
(53) Alberici, R. M.; Jardim, W. E. *Appl. Catal. B Environ.* **1997**, *14*, 55.
(54) Dibble, L. A.; Raupp, G. B. *Environ. Sci. Technol.* **1992**, *26*, 492.
(55) Dibble, L. A.; Raupp, G. B. *Catal. Lett.* **1990**, *4*, 345.
(56) Sauer, M. L.; Hale, M. A.; Ollis, D. F. *J. Photochem. Photobiol. A Chem.* **1995**, *88*, 169.
(57) Jacoby, W. A.; Nimlos, M. R.; Blake, D. M.; Noble, R. D.; Koval, C. A. *Environ. Sci. Technol.* **1994**, *28*, 1661.
(58) Nimlos, M. R.; Jacoby, W. A.; Blake, D. M.; Milne, T. A. *Environ. Sci. Technol.* **1993**, *27*, 732.
(59) Fox, M. A.; Dulay, M. T. *Chem. Rev.* **1993**, *93*, 341.

(60) Park, D. R.; Zhang, J. L.; Ikeue, K.; Yamashita, H.; Anpo, M. *J. Catal.* **1999**, *185*, 114.
(61) Bickley, R. I.; Stone, F. S. *J. Catal.* **1973**, *31*, 389.
(62) Suda, Y.; Morimoto, T. *Langmuir* **1987**, *3*, 786.
(63) Tanaka, K.; White, J. M. *J. Phys. Chem.* **1982**, *86*, 4708.
(64) Gonzalez-Elipe, A.; Munuera, G.; Soria, J. *J. Chem. Soc Faraday Trans.* **1979**, *75*, 748.
(65) Gonzalez-Elipe, A.; Munuera, G.; Soria, J. *J. Chem. Soc. Faraday Trans.* **1980**, *76*, 1535.
(66) Munuera, G.; Rives-Arau, V.; Saucedo, A. *J. Chem. Soc. Faraday Trans.* **1979**, *75*, 369.
(67) Herrmann, J. M.; Disdier, J.; Pichat, P. *J. Catal.* **1979**, *60*, 369.
(68) Peral, J.; Domenech, X.; Ollis, D. F. *J. Chem. Technol. Biotechnol.* **1997**, *70*, 117.
(69) Yu, J. C.; Lin, J.; Kwok, R. W. M. *J. Phys. Chem. B* **1998**, *102*, 5094.
(70) Ollis, D. F.; Al-Ekabi, H. *Photocatalytic purification and treatment of water and air*; Elsecier: Amsterdam, 1993.
(71) Formenti, M.; Juillet, F.; Meriaudeau, P.; Teichner, S. J. *Chem. Technol.* **1971**, *1*, 680.
(72) Granvelle, P.; Juillet, F.; Meriaudeau, P.; Teichner, S. J. J. *Chem. Soc. Faraday Dis.* **1971**, *52*, 140.
(73) Teichner, S. J.; Formenti, M. Hetergeneous Photocatalysis. In *Photoelectrochemistry, Photocatalysis and photoreactors.*; Schiavello, M., 1st Ed.; Reidel Publishing Company: Dordrecht, 1985; pp 457.
(74) Djeghri, N.; Formenti, M.; Juillet, F.; Teichner, S. J. *J. Chem. Soc. Faraday Dis.* **1974**, *62*, 182.
(75) Maira, A. J.; Yeung, K. L.; Soria, J.; Coronado, J. M.; Belver, C.; Lee, C. Y. *Appl. Catal. B-Environ.* **2001**, *29*, 327.
(76) Pelizzetti, E.; Minero, C. *Colloid Surf. A-Physicochem. Eng. Asp.* **1999**, *151*, 321.
(77) Sahle-Demessie, E.; Gonzalez, M.; Wang, Z. M.; Biswas, P. *Ind. Eng. Chem. Res.* **1999**, *38*, 3276.
(78) Bickley, R. I.; Munuera, G.; Stone, F. S. *J. Catal.* **1973**, *31*, 398.
(79) Bickley, R. I.; Jayanty, R. K. M. *J. Chem. Soc. Faraday Dis.* **1974**, *58*, 194.
(80) Larson, S. A.; Widegren, J. A.; Falconer, J. L. *J. Catal.* **1995**, *157*, 611.
(81) Hager, S.; Bauer, R. *Chemosphere* **1999**, *38*, 1549.
(82) Cunningham, J.; Hodnett, B. K. *J. Chem. Soc. Faraday Trans.I* **1981**, *77*, 2777.
(83) Walker, A.; Formenti, M.; Meriaudeau, P.; Teichner, S. J. *J. Catal.* **1977**, *50*, 237.
(84) Yoneyama, H.; Shiota, H.; Tamura, H. *Bull. Chem. Soc. Jpn.* **1981**, *54*, 1308.
(85) Pichat, P.; Herrmann, J. M.; Courbon, H.; Disdier, J.; Mozzanega, M. N. *Can. J. Chem. Eng.* **1982**, *60*, 27.
(86) Hashimoto, K.; Wasada, K.; Toukai, N.; Kominami, H.; Kera, Y. *J. Photochem. Photobiol. A Chem.* **2000**, *136*, 103.
(87) Hori, Y.; Fujimoto, K.; Suzuki, S. *Chem. Lett.* **1986**, 1845.
(88) Negishi, N.; Takeuchi, K. *Mater. Lett.* **1999**, *38*, 150.
(89) Cant, N. W.; Cole, J. R. *J. Catal.* **1992**, *134*, 317.
(90) Rusu, C. N.; Yates, J. T. *J. Phys. Chem. B* **2000**, *104*, 1729.
(91) Ao, C. H.; Lee, S. C.; Yu, J. C. *J. Photochem. Photobiol. A Chem.* **2003**, *156*, 171.

(92) Negishi, N.; Takeuchi, K.; Ibusuki, T. *J. Sol-Gel Sci. Technol.* **1998**, *13*, 691.
(93) Negishi, N.; Takeuchi, K.; Ibusuki, T. *J. Mater. Sci.* **1998**, *33*, 5789.
(94) Ibusuki, T.; Takeuchi, K. *J. Mol. Catal.* **1994**, *88*, 93.
(95) Ibusuki, T.; Kutsuna, S.; Takeuchi, E. Removal of low concentration air pollutants through photoassisted heterogeneous catalysis. In *Photocatalytic purification of water and air*; Ollis, D. F., Al-Ekabi, H., Eds.; Elsevier Science Publishers B. V.: Amsterdam, 1993.
(96) Devahasdin, S.; Fan, C.; Li, K. Y.; Chen, D. H. *J. Photochem.Photobio. A Chem.* **2003**, *156*, 161.
(97) Hashimoto, K.; Wasada, K.; Osaki, M.; Shono, E.; Adachi, K.; Toukai, N.; Kominami, H.; Kera, Y. *Appl. Catal. B Environ.* **2001**, *30*, 429.
(98) Nakamura, I.; Negishi, N.; Kutsuna, S.; Ihara, T.; Sugihara, S.; Takeuchi, E. *J. Mol. Catal. A Chem.* **2000**, *161*, 205.
(99) Takeuchi, K.; Nakamura, I.; Matsumoto, O.; Sugihara, S.; Ando, M.; Ihara, T. *Chem. Lett.* **2000**, 1354.
(100) Zhang, J. L.; Ayusawa, T.; Minagawa, M.; Kinugawa, K.; Yamashita, H.; Matsuoka, M.; Anpo, M. *J. Catal.* **2001**, *198*, 1.
(101) Yamashita, H.; Ichihashi, Y.; Zhang, S. G.; Matsumura, Y.; Souma, Y.; Tatsumi, T.; Anpo, M. *Appl. Surf. Sci.* **1997**, *121*, 305.
(102) Anpo, M.; Nomura, T.; Kitao, T.; Giamello, E.; Che, M.; Fox, M. A. *Chem. Lett.* **1991**, 889.
(103) Anpo, M.; Matsuoka, M.; Hanou, K.; Mishima, H.; Yamashita, H.; Patterson, H. H. *Coord. Chem. Rev.* **1998**, *171*, 175.
(104) Anpo, M.; Matsuoka, M.; Shioya, Y.; Yamashita, H.; Giamello, E.; Morterra, C.; Che, M.; Patterson, H. H.; Webber, S.; Ouellette, S.; Fox, M. A. *J. Phys. Chem.* **1994**, *98*, 5744.
(105) Giamello, E.; Murphy, D.; Magnacca, G.; Morterra, C.; Shioya, Y.; Nomura, T.; Anpo, M. *J. Catal.* **1992**, *136*, 510.
(106) Huang, Y. J.; Wang, H. P.; Lee, J. F. *Chemosphere* **1999**, *39*, 1347.
(107) Matsuoka, M.; Matsuda, E.; Tsuji, K.; Yamashita, H.; Anpo, M. *Chem. Lett.* **1995**, 375.
(108) Matsuoka, M.; Matsuda, E.; Tsuji, K.; Yamashita, H.; Anpo, M. *J. Mol. Catal. A Chem.* **1996**, *107*, 399.
(109) Kanan, S. M.; Omary, M. A.; Patterson, H. H.; Matsuoka, M.; Anpo, M. *J. Phys. Chem. B* **2000**, *104*, 3507.
(110) Anpo, M.; Yamashita, H.; Matsuoka, M.; Park, D. R.; Shul, Y. G.; Park, S. E. *J. Ind. Eng. Chem.* **2000**, *6*, 59.
(111) Yamashita, H.; Ichihashi, Y.; Anpo, M.; Hashimoto, M.; Louis, C.; Che, M. *J. Phys. Chem.* **1996**, *100*, 16041.
(112) Teramura, K.; Tanaka, T.; Funabiki, T. *Langmuir* **2003**, *19*, 1209.
(113) Tanaka, T.; Teramura, K.; Yamamoto, T.; Takenaka, S.; Yoshida, S.; Funabiki, T. *J. Photochem. Photobiol. A Chem.* **2002**, *148*, 277.
(114) Suzuki, J.; Fujimoto, K.; Mori, T.; Watanabe, M.; Hasegawa, Y. *J. Sol-Gel Sci. Technol.* **2000**, *19*, 775.
(115) Mori, T.; Suzuki, J.; Fujimoto, K.; Watanabe, M.; Hasegawa, Y. "Photocatalytic reductions of nitric oxide in gas phase and nitrate ion in water with reducing agents on hollandite catalyst"; Advanced Catalytic Materials-1998, 1999.
(116) Yamashita, Y.; Aoyama, N.; Takezawa, N.; Yoshida, K. *J. Mol. Catal. A Chem.* **1999**, *150*, 233.
(117) Bustos, V.; Unac, R.; Zaera, F.; Zgrablich, G. *J. Chem. Phys.* **2003**, *118*, 9372.

(118) Chafik, T.; Ouassini, A.; Verykios, X. E. *J. Chim. Phys -Chim. Biol.* **1998**, *95*, 1666.
(119) Ward, T. R.; Alemany, P.; Hoffmann, R. *J. Phys. Chem.* **1993**, *97*, 7691.
(120) Thampi, K. R.; Ruterana, P.; Gratzel, M. *J. Catal.* **1990**, *126*, 572.
(121) Rasko, J.; Szabo, Z.; Bansagi, T.; Solymosi, F. *Phys. Chem. Chem. Phys.* **2001**, *3*, 4437.
(122) Subbotina, I. R.; Shelimov, B. N.; Kazansky, V. B.; Lisachenko, A. A.; Che, M.; Coluccia, S. *J. Catal.* **1999**, *184*, 390.
(123) Shelimov, B.; Dellarocca, V.; Martra, G.; Coluccia, S.; Che, M. *Catal. Lett.* **2003**, *87*, 73.
(124) Lisachenko, A. A.; Chikhachev, K. S.; Zakharov, M. N.; Basov, L. L.; Shelimov, B. N.; Subbotina, I. R.; Che, M.; Coluccia, S. *Top. Catal.* **2002**, *20*, 119.

# 3 Experimental

## 3.1 Introduction

This chapter describes the methods used to prepare the photocatalyst materials studied in this thesis, and the experimental set-up that was utilised to determine the photocatalytic behaviour of the prepared materials. There is also a short discussion of the sample handling and methods of data collection and processing with respect to the characterisation techniques used to gain an understanding of the nature of the prepared photocatalysts.

## 3.2 Preparation of $TiO_2$ and modified $TiO_2$ photocatalysts

For all the experiments discussed in this thesis a commercial $TiO_2$ photocatalyst (Degussa P25) was used and was kindly supplied by Degussa AG. Initially triply deionised water (TDW, 500 $cm^3$) was acidified by 0.05 M $HNO_3$ (6 $cm^3$, prepared from a 70 % $HNO_3$ solution, Aldrich). A partially stabilised dispersion of P25 was prepared by addition of P25 (0.19975 g, 0.0025 mol.) to the acidified TDW (500 $cm^3$). The dispersion was then stirred overnight to yield a partially stabilised P25 dispersion that was white and opaque.

Precursors for rhodium or silver modified P25 photocatalysts were prepared following the same procedure except that appropriate amounts of $Rh(NO_3)_3.2H_2O$ (99.9 % purity, Aldrich) or $AgNO_3$ (99.9 % purity, Aldrich) were dissolved in the acidified TDW prior to addition of P25. Table 3.1 gives the amounts required to produce 0.1, 1, and 5 wt. % modified $TiO_2$ dispersions. The 5Rh-P25 and 1Rh-P25 systems yielded pale yellow coloured opaque dispersions. Whilst the 0.1Rh-P25 and Ag-P25 systems yielded white coloured opaque dispersions. The dispersions were

used as precursors for the photocatalyst powders to be used for characterisation, and for the preparation of the photocatalyst coatings to be tested in the photoreactor. Table 3.1 shows the nomenclature used to identify the photocatalyst samples.

Photocatalyst powders, used in the characterisation methods, were prepared by drying the dispersions at 70°C for 48 h. The colour of the powders depended on the nature and loading of the modifying element. The condition for calcination of the powders was a heating rate of 5°C min.$^{-1}$ and a dwell time of 2 h once the required temperature was attained. The cooling rate used was 10°C min.$^{-1}$. The P25, 0.1Ag-P25 and 0.1Rh-P25 powders remained white irrespective of the calcination temperature used. However, the samples with higher silver loadings became a greyish/white colour after calcination, and darkened further with increasing calcination temperature. The Rh-modified samples with loadings of 1 wt. % and above remained a yellowish/white colour even after calcination at 200°C, the highest calcination temperature used for those samples.

The glass used as substrates for the photocatalyst were cut from Borosilicate glass (Fisher Scientific) with dimensions of 80 mm x 35 mm x 5 mm to fit in the sample holder of the purpose built photoreactor. Prior to photocatalyst deposition they were cleaned and degreased by sonicating in a 5 % Decon90© solution for 5 min. They were then rinsed with TDW and sonicated again in industrial methylated spirits for a further 5 min., after which they were dried at 70°C for at least 12 h. The cleaned slides were kept for a maximum of 24 h before photocatalyst deposition.

The photocatalysts were deposited onto the glass slides by evaporation of 25 cm$^3$ of dispersion at 70°C in a glass petri dish. The mass of P25 deposited was *ca.* 1 mg. Calcination of the films was carried out in an identical manner as the powdered samples using the same final temperatures.

UV and hydrogen reduction of the metal salts deposited onto the P25 was carried out on the coated glass slides. To UV reduce the metal salts, the coated glass slides were suspended in propan-2-ol, in a quartz beaker, and irradiated for 30 min. using a 400 W medium pressure mercury lamp (Photochemical Reactors Ltd.). The slides were then dried at 70°C for 12 h. Hydrogen reduction of the photocatalyst films was carried out in a tube furnace at 450°C. The furnace was heated to 450°C at a rate of 5°C $min.^{-1}$ under argon, then the gas was switched to hydrogen and the temperature maintained for 1 h. The slides were cooled to room temperature under an argon atmosphere.

After the various pretreatments were carried out the photocatalysts were wrapped in foil, so that no photoreactions could occur, and stored in a vacuum desiccator until required.

## 3.3 Estimation of film thickness

The upper and lower limits of the film thickness have been calculated using the density of solid $TiO_2$ assuming a 0.3 void fraction (2.9 g $cm^{-3}$) and the measured density of bulk $TiO_2$ powder (0.09 g $cm^{-3}$) respectively. The values used were those reported by Jacoby *et al.*[1]

Using the above values, and a mass of 1 mg of $TiO_2$ deposited, the upper and lower limits for the film thickness were calculated to be 3.9 and 0.12 μm, respectively. The estimations of upper and lower limits for the film thickness of the photocatalysts prepared for this work were less than the critical thickness reported by Jacoby *et al.*[1] Hence, in accordance with the observations of Jacoby the rates of reactions reported in this thesis will be shown in units of μmol $h^{-1}$ $g^{-1}$.

| Material Studied | Nomenclature | Weight percent ratio ($Ag:Rh:TiO_2$) | Mass of additive used / mg ($AgNO_3$ or $Rh(NO_3)_3.2H_2O$) | μmoles of additive used ($AgNO_3$ or $Rh(NO_3)_3.2H_2O$) |
|---|---|---|---|---|
| P25 | P25 | 0 : 0 : 100 | 0 | 0 |
| 0.1wt. % Ag-P25 | 0.1Ag-P25 | 0.1 : 0 : 99.9 | 0.316 | 1.87 |
| 1wt. % Ag-P25 | 1Ag-P25 | 1 : 0 : 99 | 3.18 | 18.8 |
| 5wt. % Ag-P25 | 5Ag-P25 | 5 : 0 : 95 | 16.5 | 97.5 |
| 0.1wt. % Rh-P25 | 0.1Rh-P25 | 0 : 0.1 : 99.9 | 0.424 | 1.94 |
| 1wt. % Rh-P25 | 1Rh-P25 | 0 : 1 : 99 | 4.29 | 19.6 |
| 5wt. % Rh-P25 | 5Rh-P25 | 0 : 5 : 95 | 22.2 | 101 |

*Table 3.1. Table of the photocatalysts studied and the amount of reactants required for their preparation*

## 3.4 Photoreactor

### 3.4.1 Photoreactor design

A continuous flow style photoreactor was built to enable photocatalytic reactions to be studied using a variety of gases and gas mixtures. A schematic representation of the custom built photoreactor used is shown in figure 3.1. The basic layout of the photoreactor consists of a bank of gases piped into a 1 μm gas filter to ensure effective mixing of the gases, the flow rate of the individual gases being independently regulated by a series of mass flow controllers (MFCs, MKS Instruments).

On leaving the filter the gas flow was passed through the reaction chamber containing the photocatalyst films and then into the exhaust system. The composition of the exhaust gas was measured using a quadruple mass spectrometer (HAL 201 system, Hiden Analytical Ltd.) fitted with a heated rapid capillary inlet system. The reactants and possible products were constantly monitored before, during and after illumination and their corresponding changes in measured partial pressure were used to measure photocatalytic activity. UV illumination of the photocatalyst was through a quartz window using a 400 W medium pressure mercury lamp. A water filter was used to remove the infrared radiation emitted. The relative intensity of the different wavelengths emitted by the UV lamp in the range 185 nm to 900 nm were measured through the quartz window of the reactor using a spectrograph (Verity Instruments) and the intensity of 365 nm radiation at the sample surface was recorded using a RX003 Radiometer with Microprocessor (UVItec). Both the lamp and the reaction chamber were situated in a black polycarbonate box. The temperature inside the reaction chamber was measured during illumination and reached a maximum of 40°C.

### 3.4.2 Reaction chamber

The reaction chamber comprised a circular aluminium back plate that had a 100 mm x 40 mm x 3 mm section milled from the centre. Coated glass slides were fitted into the milled section and held in place using push fitting aluminium pins. The gas inlet and outlet was via two 3 mm diameter channels through the back of the base plate into the top and bottom of the milled section. A quartz window was placed on a nitrile O-ring and was secured in position by an aluminium ring which had another O-ring on the underside to avoid a metal-quartz contact, which could cause the window to crack. The top section was affixed to the base plate using 6 bolts. The reactor volume (i.e. the volume between the milled section and the window) was 12 $cm^3$.

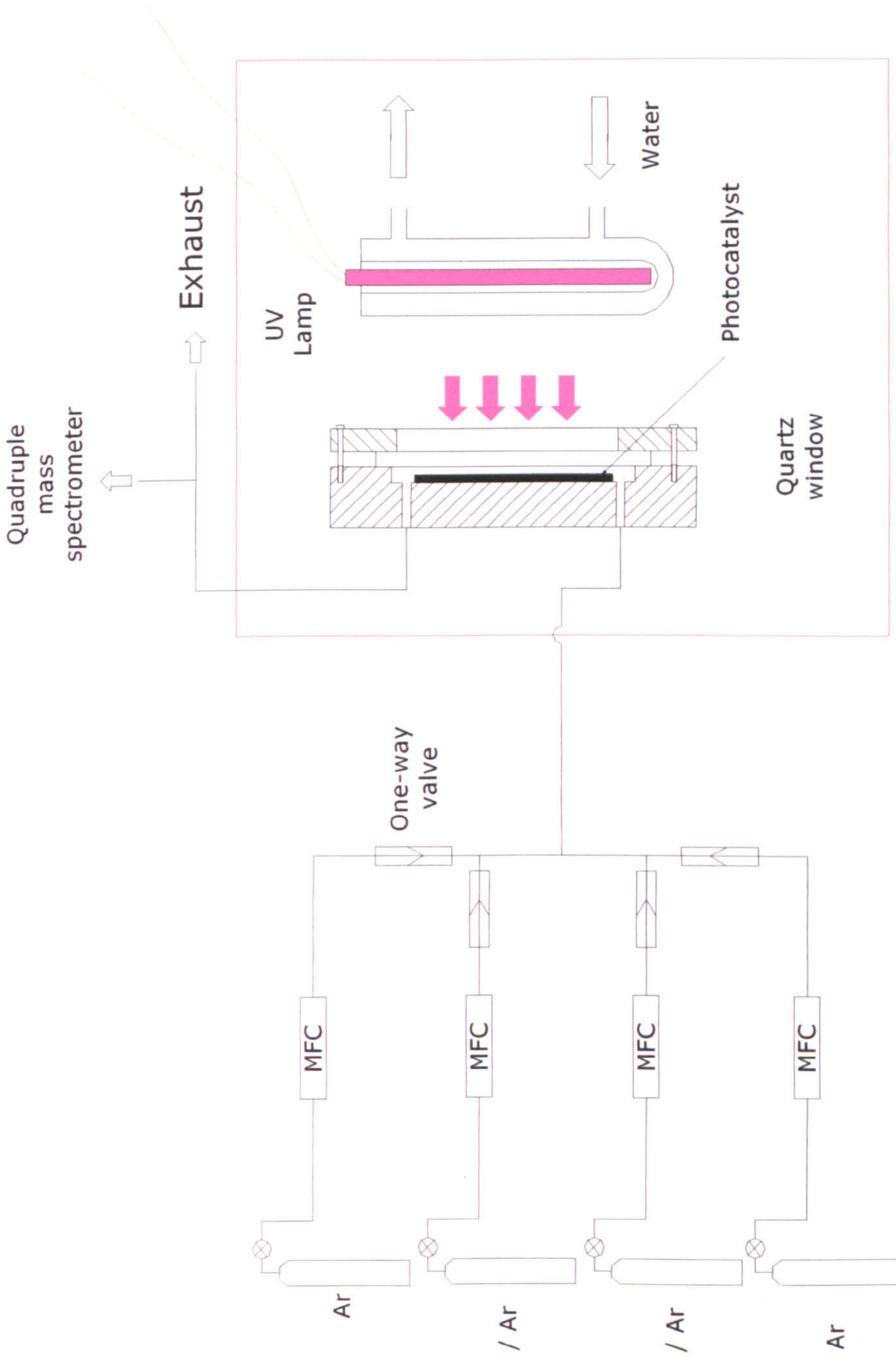


*Figure 3.1. Schematic of the photoreactor used for testing the photocatalytic behaviour of the catalysts prepared.*

### 3.4.3 Photoreactions

For each photocatalyst studied, a standard pre-oxidation to remove surface hydrocarbons, was first carried out. The photocatalyst was put into the reaction chamber, sealed and argon (BOC gases, 99.999 % purity) at 50 sccm was passed through the system until no air could be detected in the exhaust gas using the mass spectrometer (*ca.* 30 min.). The gas inlet was then switched to 20 % oxygen (20,000 ppm in argon (BOC gases 99.999 % purity) with a flow rate of 10 sccm. Once the oxygen concentration was constant (*ca.* 30 min.) the UV lamp was turned on and the photocatalyst was illuminated for 15 min. The mass spectrometer data showed a decrease in the oxygen concentration and the formation of $CO_2$ upon illumination, once the lamp was switched off the concentrations of $O_2$ and $CO_2$ returned to their original values. This procedure was repeated once more after 15 min. Repeating the oxidative treatment a third time resulted in no detectable formation of $CO_2$. After the oxidative pre-treatment, argon was passed through the system at 50 sccm for 2 h, after which time no oxygen could be detected in the exhaust.

Two types of reactions were studied, photodecomposition of NO in an inert atmosphere and photoreduction of NO in the presence of CO. For all the reactions studied isotopically substituted $^{15}NO$ was used, instead of the more abundant $^{14}NO$. The purity of $^{15}NO$ in argon was 99.9995 % (CK Gas Products Ltd.) and the level of isotopic substitution of $^{15}N$ for $^{14}N$ and calibrated volume of $^{15}NO$ were determined by the manufacturers to be > 99.5 %, and 1.00 % respectively. Possible reaction products are $N_2$, $N_2O$, CO and $CO_2$ which have the parent ion peaks of 28, 44, 28 and 44 amu, respectively, therefore making it difficult to discriminate between $N_2$ and CO species and $N_2O$ and $CO_2$ species by mass spectrometry. Using $^{15}NO$ gives the parent ion peaks of $^{15}N_2$ and $^{15}N_2O$ of 30 and 46 amu, respectively, thus making

quantification of the reactions possible by mass spectrometry. From now on in this thesis when referring to nitric oxide (NO) the reader should bear in mind that what is actually being discussed is the isotope $^{15}NO$.

The first reaction type is the photodecomposition of NO in Ar. After the pre-treatment, NO was introduced into the system and the total flow rate was reduced to 5.5 sccm, with an NO concentration of 909 ppm. The gases were allowed to flow over the photocatalyst in the dark. Once a steady state concentration of NO was attained (*ca.* 30 min.) the photocatalyst was irradiated for 30 min. The gases were left flowing for a further 15 min. after the lamp was switched off to ensure the reactant concentrations returned to their original levels. During the reaction period the mass spectrometer continuously monitored the levels of the reactants and products in the exhaust gas mixture. Typical m/z traces for a reactant and product are shown in figure 3.2 (a) and (b) respectively and the m/z values used to detect the reactants and products are shown in table 3.2.

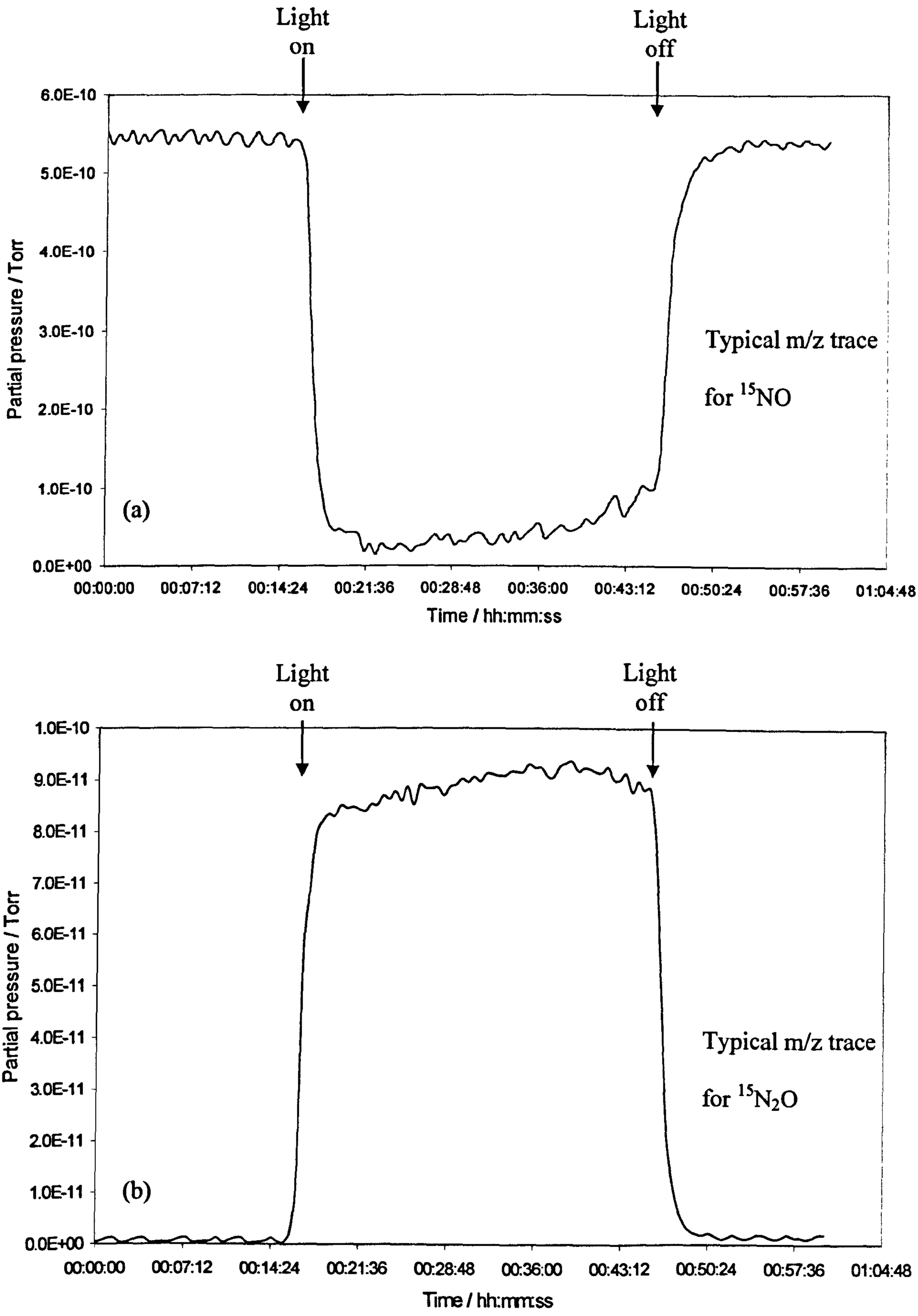


*Figure 3.2. Typical m/z traces for (a) NO (m/z 31) and (b) $N_2O$ (m/z 46) for a reduction reaction.*

Variations on the general decomposition reaction were investigated for selected photocatalysts, by varying the concentration of NO in the feed gas. For all the experiments the total flow rate and illumination period were kept constant at 5.5 sccm and 30 min. respectively. The reaction gas compositions for all the decomposition reactions are given in table 3.3.

| Parent ion | Mass / charge ratio (m/z) |
|---|---|
| $^{12}CO^+$ | 28 |
| $^{15}N_2^+$ | 30 |
| $^{15}NO^+$ | 31 |
| $^{12}CO_2^+$ | 44 |
| $^{15}N_2O^+$ | 46 |

*Table 3.2. Table showing the m/z values for various parent ions.*

| Photocatalytic reaction | Reactant gas composition | Total flow rate / sccm |
|---|---|---|
| General decomposition | 909 ppm NO + Ar balance | 5.5 |
| Effect of NO concentration 1 | 455 ppm NO + Ar balance | 5.5 |
| Effect of NO concentration 2 | 909 ppm NO + Ar balance | 5.5 |
| Effect of NO concentration 3 | 1818 ppm NO + Ar balance | 5.5 |

*Table 3.3. Table of reaction conditions for the NO photodecomposition reactions investigated.*

The second reaction type was the photoreduction of NO by CO with Ar as the balance gas. The concentration of both NO and CO were 919 ppm and 1818 ppm, respectively, and the total flow rate was 5.5 sccm. The m/z values monitored during the reaction are shown in table 3.2.

Variations in the general reduction reaction were investigated over a selection of the photocatalysts. These variations included changing the NO or CO feedstock concentrations. For all the experiments the total flow rate and illumination period were kept constant at 5.5 sccm and 30 min., respectively. The reaction gas compositions for all the reduction reactions are given in table 3.4.

| Photocatalytic reaction | Reactant gas composition | Total flow rate / sccm |
|---|---|---|
| General reduction | 909 ppm NO + 1818 ppm CO + Ar balance | 5.5 |
| Effect of NO concentration 1 | 455 ppm NO + 1818 ppm CO + Ar balance | 5.5 |
| Effect of NO concentration 2 | 909 ppm NO + 1818 ppm CO + Ar balance | 5.5 |
| Effect of NO concentration 3 | 1818 ppm NO + 1818 ppm CO + Ar balance | 5.5 |
| Effect of CO concentration 1 | 909 ppm NO + 0 ppm CO + Ar balance | 5.5 |
| Effect of CO concentration 2 | 909 ppm NO + 364 ppm CO + Ar balance | 5.5 |
| Effect of CO concentration 3 | 909 ppm NO + 909 ppm CO + Ar balance | 5.5 |
| Effect of CO concentration 4 | 909 ppm NO + 1818 ppm CO + Ar balance | 5.5 |

*Table 3.4. Table of reaction conditions for the NO photoreduction reactions investigated.*

### 3.4.4 Quantification of the reaction data

To quantify the changes in concentration of reactants and products seen in the data collected during the reactions it was first necessary to calibrate the mass spectrometer in order to convert the partial pressures recorded into more meaningful units, such as moles or ppm of the reactants or products. In calibrating the spectrometer the relative sensitivities for detection of the different species monitored were calculated.

Fragmentation patterns were determined for all species being monitored so that contributions from different species at the same m/z value could be accounted for. This was carried out using calibrated gas mixtures containing *ca.* 1 % of the individual $^{14}N$ containing species in argon as the same fragmentation could be expected for $^{15}N$ containing species. The gases were purchased from BOC gases with purities of 99.999 %. Table 3.5 shows the fragmentation patterns for all the species monitored. Due to slight day-to-day variations in the results, the values shown are averages of 30 fragmentation patterns collected for each species over the period of one month. Once determined the fragmentation patterns were checked weekly to ensure there were no significant changes as the mass spectrometer detector aged.

| $N_2O$ | | NO | | $N_2$ | | $CO_2$ | | CO | |
|---|---|---|---|---|---|---|---|---|---|
| Ion | R.I. | Ion | R.I. | Ion | R.I. | Ion | R.I. | Ion | R.I. |
| $N_2O^+$ (44) | 100 | $NO^+$ (30) | 100 | $N_2^+$ (28) | 100 | $CO_2^+$ (44) | 100 | $CO^+$ (28) | 100 |
| $NO^+$ (30) | 27.9 | $O^+$ (16) | 1.3 | $N^+$ (14) | 7.8 | $CO^+$ (28) | 9.0 | $O^+$ (16) | 1.7 |
| $N_2^+$ (28) | 18.0 | $N^+$ (14) | 2.4 | - | - | $O^+$ (16) | 9.2 | $C^+$ (12) | 4.7 |
| $O^+$ (16) | 7.1 | - | - | - | - | $C^+$ (12) | 8.7 | - | - |
| $N^+$ (14) | 11.6 | - | - | - | - | - | - | - | - |

*Table 3.5. Table of fragmentation patterns for the different species monitored. Values inside ( ) are the m/z values for the corresponding fragment. R.I. = relative intensity.*

Background levels were subtracted from the corresponding readings to give partial pressure values for the different m/z species. Calibrated gas containing 1 % $^{15}NO$ in argon was used to calibrate the mass spectrometer before each experiment. It should be noted here that the integrated areas for the m/z species were first corrected for contributions from other species.

The integrated area for the NO signal collected over time, t, is proportional to the number of moles of NO passed in the time, t. Therefore,

$$\frac{\int_{t}^{o}[NO signal]}{moles\ of\ NO\ in\ time, t} = CF_{NO} \qquad (3.1)$$

Where $CF_{NO}$ is the NO conversion factor. The percentage conversion of NO during a reaction was then calculated using the equation below.

$$\%NO\ conversion = \frac{moles\ of\ NO\ used}{Total\ number\ of\ moles\ of\ NO} \times 100\% \qquad (3.2)$$

The conversion factors for the products $N_2$ and $N_2O$ were calculated by solving equation 3.3 simultaneously using data from two photoreactions with very different selectivities.

$$\tfrac{1}{2} \times moles\ of\ NO\ used = moles\ of\ N_2O\ produced + moles\ of\ N_2\ produced \qquad (3.3)$$

$$\text{where,} \quad moles\ of\ N_2O\ produced = \frac{[N_2O\ integrated\ area]}{CF_{N_2O}} \qquad (3.4)$$

and,

$$moles\ of\ N_2\ produced = \frac{[N_2\ integrated\ area]}{CF_{N_2}} \qquad (3.5)$$

where

$CF_{N_2}$ = $N_2$ *conversion factor*

$CF_{N_2O}$ = $N_2O$ *conversion factor*

Due to slight day-to-day variations in the mass spectrometer signal, the calculated values of all the conversion factors also varied daily. However, it was not practical to calculate $CF_{N_2}$ and $CF_{N_2O}$ daily and therefore sensitivity factors for $N_2O$ ($SF_{N_2O}$) and $N_2$ ($SF_{N_2}$) relative to $CF_{NO}$ were calculated according to equations 3.6 and 3.7.

$$SF_{N_2O} = \frac{CF_{N_2O}}{CF_{NO}} \tag{3.6}$$

$$SF_{N_2} = \frac{CF_{N_2}}{CF_{NO}} \tag{3.7}$$

Equations 3.3 – 3.7 were solved five times, using different sets of data each time, and the average values were used when quantifying the data recorded in the photoreaction experiments. The average relative sensitivity factors for $N_2O$ and $N_2$ were 0.3985 and 2.0897, respectively. These sensitivity factors were then used to calculate $CF_{N_2}$ and $CF_{N_2O}$ using the measured $CF_{NO}$ for each experiment.

Once the daily conversion factors were calculated, the moles of $N_2$ and $N_2O$ produced could be calculated simply by dividing the corrected integrated areas by the corresponding conversion factor. The conversion factors for $CO_2$ and CO were calculated following similar procedures.

The selectivities for $N_2$ and $N_2O$ formation were calculated using equations 3.8 and 3.9, respectively, and their corresponding rates of formation using equations 3.10 and 3.11, respectively.

$$S_{N_2} = \frac{Moles\ of\ N_2\ produced}{total\ moles\ of\ N_2 + N_2O\ produced} \times 100\% \quad (3.8)$$

$$S_{N_2O} = \frac{Moles\ of\ N_2O\ produced}{total\ moles\ of\ N_2 + N_2O\ produced} \times 100\% \quad (3.9)$$

$S_{N_2}$ = Selectivity for $N_2$ formation

$S_{N_2O}$ = Selectivity for $N_2O$ formation

$$\text{Rate of } N_2 \text{ formation} = S_{N_2} \times \frac{Moles\ of\ NO\ used}{2 \times time \times mass\ of\ photocatalyst} \quad (3.10)$$

$$\text{Rate of } N_2O \text{ formation} = S_{N_2O} \times \frac{Moles\ of\ NO\ used}{2 \times time \times mass\ of\ photocatalyst} \quad (3.11)$$

## 3.5 Characterisation techniques and sample handling

### 3.5.1 X-ray diffraction (XRD)

XRD diffraction patterns were recorded using a Philips PW 3710 XPERT diffractometer, operated at 40 kV and 40 mA utilising a CuK radiation source ($\lambda$ = 0.154 nm). The Philips automatic powder diffraction (PC-APD) software program was used to control the scan. Data was collected in step mode with intervals

of 0.02°, over a 2θ range 20-80° for both powders and the films. A relatively long dwell time of 16 s was used so that a good signal-to-noise ratio was achieved. Powder samples were mounted on a hollowed glass stage and flattened using a microscope slide. The samples coated onto glass slides were mounted directly into the instruments sample holder. For the powdered samples, data was collected using a moving θ-2θ scan whereas for the films, data collection used a fixed θ glancing angle of 3° and a 2θ scan of 20-80°. The diffraction patterns were analysed using Philips PC based software packages. Due to the small amount of sample available, XRD for the rhodium containing photocatalysts were collected using a capillary set-up on a Bruker D8 advance diffractometer.

The Bragg conditions for diffraction become less defined if the sample has a very small particle size (< 500 Å), which causes the diffraction pattern to broaden. By measuring broadening the average particle size can be calculated utilising the Scherrer Equation.

$$D = \frac{0.9\lambda}{B\cos\theta} \qquad (3.12)$$

D = average particle size
λ = wavelength of radiation
θ = the Bragg angle
B = width at half peak height

$$where \;\; B = B_b - B_s \qquad (3.13)$$

$B_b$ = observed half width
$B_s$ = instrument associated half width

Equation 3.14 was utilised to determine the volume percentages of both the anatase and rutile phases: -

$$I = (F)^2 \times p \times LP \times A \times \exp^{(-2M)} \qquad (3.14)$$

I = Area under diffraction reflection
F = Structure Factor
p = multiplicity Factor

$$LP = \left(\frac{1+\cos^2 2\theta}{\sin^2 \theta \cos\theta}\right) \qquad (3.15)$$

LP = Lorentz-Polarisation Factor

$$A = \left(\frac{1}{2\mu}\right) \qquad (3.16)$$

A = Absorption Factor
$\mu$ = Linear absorption coefficient
$\exp^{(-2M)}$ = Temperature Factor

The equation takes into account a variety of factors which contribute to the area under one reflection with that of another and allows a ratio of phase volume percentage to be determined. Within the equation, certain factors were discarded due to the nature and physical state of the materials studied in this work. The area under the reflection (I) was calculated by using the computer package WinFit (Version 1.2.1). The Structure Factor (F) was not taken into account since it considers both the lattice type (anatase and rutile are both tetragonal) and the peak position difference which was negligible (*ca.* 2 °/2θ). The multiplicity factor (p) takes into account the fact that crystals will be orientated so that reflection can occur for example from the (100) planes. Other crystals of different orientation may be in such a position that reflection can occur from their (010) or (001) planes. The relative proportion of planes contributing to the same reflection enters the intensity equation as a quantity p, the *multiplicity factor,* which is defined as the number of different

planes in a form having the same spacing. Multiplicity factors for various lattice types are tabulated in Cullity.[3] The Lorentz-Polarisation (LP) factor physically describes the time it takes a point in the reciprocal lattice to move through the Ewald sphere. The numbers for the anatase (101) and rutile (110) reflections were calculated by combining numbers from Lorentz-Polarisation tables,[3] with the 2θ positions of the observed reflections. The absorption factor (A) does not depend on theta and hence was omitted from the equation. Finally the temperature factor ($exp^{(-2M)}$) was not included in the calculation as the data was not available for titania. However, the temperature factor has a negligible effect on the overall result for anatase (101) and rutile (110) reflections are as they are close together (*ca.* 2 °/2θ).

### 3.5.2 Transmission electron microscopy (TEM)

The TEM analysis was carried out using a JEOL FX III microscope. The samples used were prepared by sonicating a suspension of the bulk material (5-10 mg) in propan-2-ol (10 $cm^3$) for 5 min. to aid dispersion of the powder on the TEM grid. Two or three drops of the solution were then transferred to a 3 mm diameter holey carbon coated copper grid (300 mesh). The solvent was then evaporated off at room temperature.

The same apparatus was also used to attain selected area electron diffraction patterns of the photocatalysts. Figure 3.5 shows the diffraction of the electron beam by a crystalline material. If the sample is amorphous in nature then there will be no distinct maxima in the pattern; a diffuse region of rings around the central spot will be observed. However, with crystalline materials it is possible to extract the lattice spacing parameter *d* from the electron diffraction pattern by applying the Bragg Equation.

$$n\lambda = 2dsin\theta \qquad 3.17$$

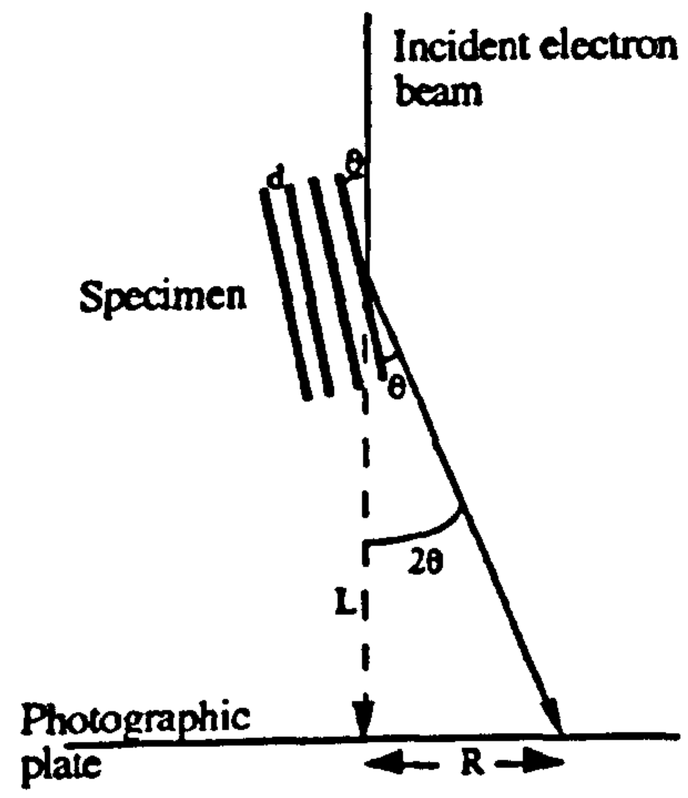


*Figure 3.5. TEM viewed as a diffraction camera.*

The electrons are diffracted through very small angles (1-2°) in TEM, therefore, the distance between the camera and the specimen (L) can be approximated, because $\theta \approx \tan\theta$ at small angles (Equation 3.18. - rearrangement of the Bragg equation)

$$L\lambda = rd \tag{3.18}$$

Since the radius (r) can be measured from the photographic image and both the camera length (L) and incident electrons wavelength ($\lambda$) are known the interplanar spacing *d* can be calculated and compared to known phases.

### 3.5.3 X-ray photoelectron spectroscopy (XPS)

XPS analysis of the P25 and rhodium modified photocatalysts was carried out using a VG Scientific ESCALab X-ray photoelectron spectrometer fitted with a non-monochromated twin Mg/Al X-ray source, and a hemispherical sector analyser that was operated in the constant analyser mode at electron pass energies of 10-50 eV. The electron signal from the spectrometer was amplified by a single channel electron

multiplier. An Al Kα X-ray source was used (5 A and 10 kV). The samples used for the rhodium XPS were coated onto glass slides as the UV reduction pretreatment could not be carried out on the corresponding powders. The slides were adhered to steel stubs using carbon tabs. Entry into the analysis chamber was via a fast entry air lock and a preparation chamber.

A wide scan was run for all the samples from 0-1000 eV using a stepsize of 1 eV and a pass energy of 50 eV to determine the elements were present and which regions high resolution scans were required for. High resolution scans were then run over the appropriate regions using a stepsize of 0.2 eV and a pass energy of 10 eV.

XPS analysis of the P25 photocatalysts containing silver were carried out using a Kratos AXIS ULTRA XPS system fitted with a monochromated Al Kα X-ray source and a hemispherical analyser with eight channeltrons. The source was operated at 10 mA and 15 kV. The powdered samples used were attached to the sample stage using carbon tabs.

A wide scan was run for all the samples from 0-1000 eV using a stepsize of 1 eV and a pass energy of 80 eV to determine the elements present and which regions high resolution scans were required for. High resolution scans were then run over the appropriate regions using a stepsize of 0.1 eV and a pass energy of 40 eV.

Data from both instruments was processed using the CASA XPS data analysis software. The C 1s photoelectron peak was not used for charge correction as the peak shape varied from sample to sample. However, the data from the XPS experiments conducted with the P25 photocatalysts revealed that the Ti $2p_{3/2}$ peak position was the same for all the samples. Therefore the spectra were charge corrected using the Ti $2p_{3/2}$ photoelectron peak at 459.0 eV. A Shirley background type was used to correct the background and the peaks were fitted. Gaussain / Lorentzian contributions

of 30 / 70 were used for the fitted peaks. The relative surface compositions of the photocatalysts samples were calculated semi-quantitatively from the relative intensities of the Ag $3d_{5/2}$, (or Rh $3d_{5/2}$), Ti $2p_{3/2}$ and O 1s peaks by taking the integrated intensities of the high resolution peaks with standard library Scofield sensitivity factors applied. It should be noted that the sensitivity factors were not corrected for either the VG ESCALab or Kratos instruments. For a more detailed discussion of analysis of XPS data the reader is directed to the publication by Briggs and Seah.[4]

### 3.5.4 Differential scanning calorimetry (DSC)

DSC analysis was carried out using a Perkin-Elmer DSC-7 instrument. Data acquisition and processing was done using Perkin-Elmer's Pyris software. A known mass of sample (typically 15-20 mg) was placed in an aluminium pan and heated from 60-500°C at a rate of 20°C $min.^{-1}$ under an argon atmosphere. The samples were then reweighed after the experiment to measure sample weight loss.

## 3.6 References

(1) Jacoby, W. A.; Blake, D. M.; Noble, R. D.; Koval, C. A. *J. Catal.* 1995, *157, 87.*

(2) Lewis, N. S.; Rosenbluth, M.L. *Photocatalysis - Fundamentals and Applications*, 1st ed.; Wiley, Chichester, 1989.

(3) Cullity, B. D.; Stock, S. *Elements of X-ray Diffraction*; Pearson Higher Education, 2001.

(4) Briggs, D.; Seah, M. P. *Practical Surface Analysis: Auger and X-ray Photoelectron Spectroscopy*, 2 ed.; John Wiley and Sons Ltd, 1992.

# 4 Characterisation

## 4.1 Introduction

The activity and selectivity of a photocatalyst are determined by factors such as the crystalline nature and surface properties of the photocatalytically active material as well as the type and chemical nature of any modifying elements along with their corresponding particle sizes and dispersion. This chapter looks in detail at the characterisation of the photocatalysts prepared in order to gain an understanding of the effect different pretreatments had upon both the physical and chemical nature of the materials.

In order to gain a clear understanding of the nature of the photocatalysts studied in chapters 5-7, a number of complementary analytical techniques were used to characterise the three photocatalyst systems that were prepared (unmodified P25, Ag-P25 and Rh-P25). The preparation and pretreatment procedures are detailed in chapter 3. The data reported in this chapter includes results from X-ray diffraction (XRD), transmission electron microscopy (TEM), X-ray photoelectron microscopy (XPS) and differential scanning calorimetry (DSC). Each method of analysis yielded vital information which when combined together gave a more complete picture of the photocatalyst structure.

Although there have already been reports in the literature describing the characterisation results of potential and actual photocatalyst materials of the type $TiO_2$[1-3], Ag-$TiO_2$[4-6] and Rh-$TiO_2$[5,7,8], it has also been shown that even subtle changes in their preparation methodologies can result in materials with very different natures, and ultimately different catalytic properties.[9,10] As the procedures undertaken in

preparing the photocatalytically active materials discussed here have not been reported elsewhere it is important that the materials produced are characterised.

The results from the characterisation of unmodified P25, Ag-P25 and Rh-P25 are presented in sections 4.2, 4.3 and 4.4, respectively with each section presenting the results from XRD, TEM and XPS analysis in order. Also included in section 4.2 are the DSC results from unmodified P25. Section 4.5 includes a discussion of the results presented previously in the chapter and conclusions are drawn in section 4.6.

## 4.2 Results

### 4.2.1 Characterisation of unmodified P25

#### 4.2.1.1 XRD

X-ray diffractograms for the powdered P25 photocatalysts calcined for 2 h at increasing calcination temperatures (70 to 600°C) are shown in figure 4.1. For all the calcination temperatures used, the P25 crystal structure consisted of a mixture of anatase and rutile phases of $TiO_2$ and the reflections attributed to each phase are shown in figure 4.1. The relative intensity of the most intense Bragg reflections for anatase (101) and rutile (110) remained unaltered up to 450°C, indicating that there was no change in the composition of the crystalline phases present and the original composition of 77 vol. % anatase and 23 vol. % rutile was maintained. Increasing the calcination temperature further to 600°C resulted in an increase in the intensity of the rutile reflections relative to anatase reflections therefore indicating an increase in the amount of rutile phase present. Assignment of the reflections observed for P25 dried at 70°C to lattice planes are given in table 4.1. Calculations using the areas of the most

intense reflections showed the composition to be 72 vol. % anatase and 28 vol. % rutile.

The slight broadness of the reflections seen in the diffractograms indicates that P25 was nanocrystalline in nature. Calculation of the crystallite sizes confirmed no change in crystallite size when unmodified P25 was calcined at temperatures up to 450°C; the crystallite sizes for anatase and rutile remained unaltered at *ca.* 28 nm and *ca.* 65 nm respectively. After calcination at 600°C there was a slight increase in both the anatase and rutile crystallite sizes to 30.5 nm and 70 nm, respectively (Table 4.2). Increasing the calcination time at 600°C resulted in the growth of both anatase and rutile crystallites along with further transformation of anatase into rutile.

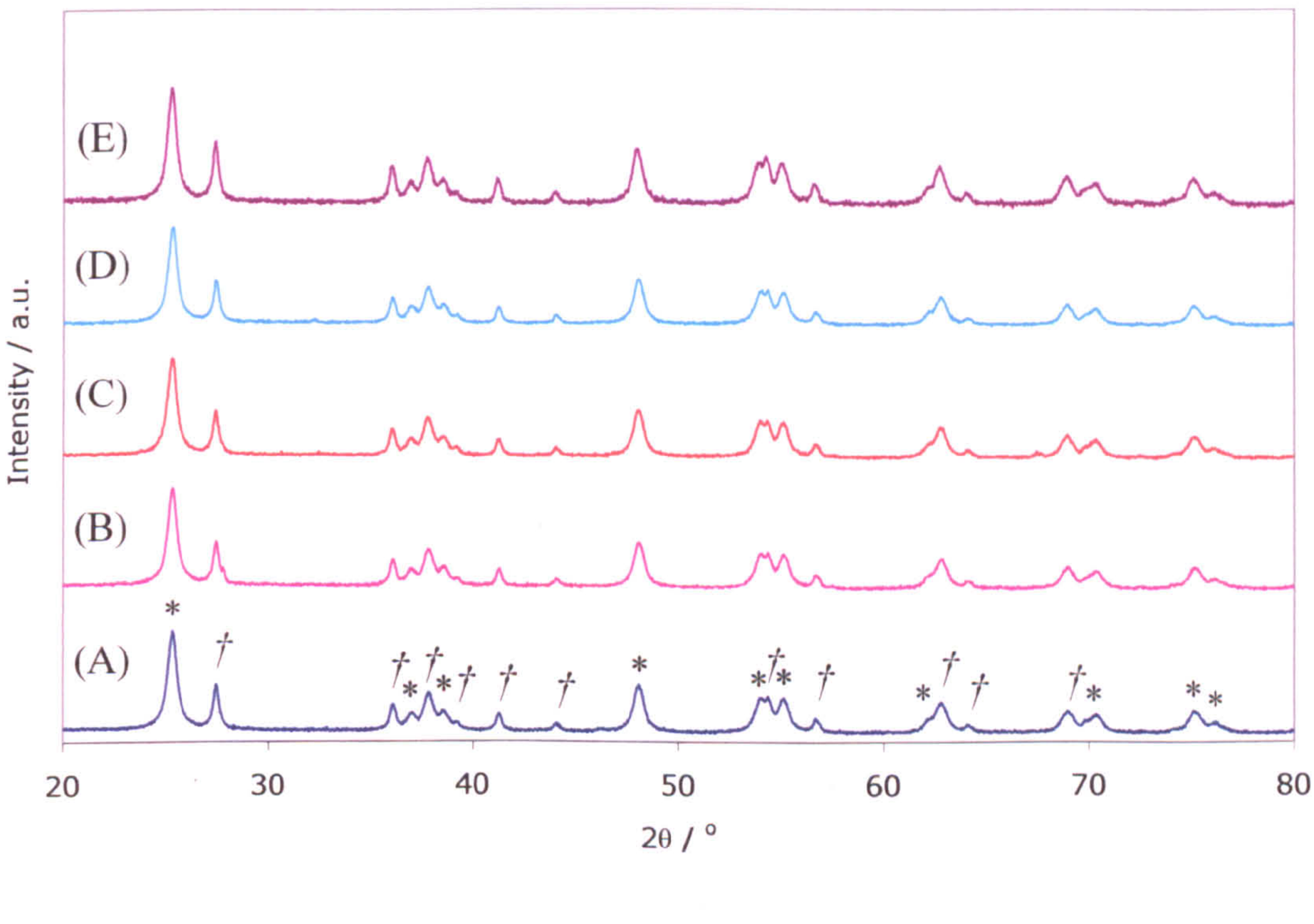


*Figure 4.1. XRD diffractograms for unmodified P25 photocatalysts calcined at temperatures of 70°C (A), 120°C (B), 200°C (C), 450°C (D) and 600°C (E). Reflections due to anatase and rutile are indicated by the symbols * and † respectively.*

Glancing angle XRD diffractograms of P25 coated glass slides, calcined at 70°C and 600°C are shown in figure 4.2. The hump that can be seen over the lower 2θ values was assigned to the amorphous nature of the glass substrate. Assignment of the reflections that were detected, revealed that for both calcination temperatures investigated (70°C and 600°C), the P25 crystal structure consisted of a mixture of anatase and rutile phases. After calcination at 600°C the relative intensity of rutile to anatase reflections appear to be very close to that for the as dried coated slide although actual values could not be used due to the varying background levels.

These results showed similar trends for both the powdered P25 photocatalysts and the coated slides and that there were no significant differences in the XRD pattern for P25 after 2 h calcinations at 600°C. Therefore, characterisation results from investigations of powdered P25 photocatalysts were interpreted as being the same as the photocatalysts deposited onto a glass slide.

| Peak position / 2θ | d / Å | Relative Intensity | Assignment |
|---|---|---|---|
| 25.31 | 3.5161 | 100 | Anatase (101) |
| 27.44 | 3.2478 | 25.1 | Rutile (110) |
| 36.09 | 2.4867 | 10.8 | Rutile (200) |
| 36.98 | 2.4289 | 5.1 | Anatase (103) |
| 37.84 | 2.3757 | 18.8 | Rutile (004) |
| 38.57 | 2.3324 | 5.9 | Anatase (112) |
| 39.20 | 2.2963 | 1.6 | Rutile (200) |
| 41.26 | 2.1863 | 5.6 | Rutile (111) |
| 44.05 | 2.0541 | 1.8 | Rutile (211) |
| 48.04 | 1.8924 | 26.6 | Anatase (200) |
| 53.94 | 1.6985 | 15.6 | Anatase (105) |
| 54.35 | 1.6866 | 14.3 | Rutile (211) |
| 55.06 | 1.6665 | 15.4 | Anatase (213) |
| 56.63 | 1.6240 | 3.9 | Rutile (220) |
| 62.09 | 1.4937 | 2.5 | Anatase (213) |
| 62.73 | 1.4800 | 12.6 | Rutile (002) |
| 64.06 | 1.4524 | 1.6 | Rutile (310) |
| 68.91 | 1.3615 | 7.1 | Rutile (301) |
| 70.07 | 1.3418 | 3.0 | Anatase (220) |
| 70.36 | 1.3370 | 3.3 | Rutile (311) |
| 75.09 | 1.2641 | 7.3 | Anatase (215) |
| 76.10 | 1.2498 | 2.0 | Anatase (301) |

*Table 4.1. Table of peak positions and assignment of the Bragg reflections for unmodified P25 photocatalyst powder dried at 70°C.*

| Calcination temperature / °C | Percentage of Rutile / vol. % | Crystallite size / nm | |
|---|---|---|---|
| | | Anatase | Rutile |
| 70 | 23.0 | 28.0 | 66.3 |
| 120 | 23.2 | 28.8 | 64.8 |
| 200 | 23.0 | 28.2 | 62.7 |
| 450 | 23.0 | 28.3 | 59.6 |
| 600 ( 2 h) | 28.0 | 30.5 | 69.6 |
| 600 (18 h) | 65.0 | 37.2 | 88.9 |

*Table 4.2. Effect of calcination temperature on the composition and crystallite sizes of unmodified P25 photocatalysts.*

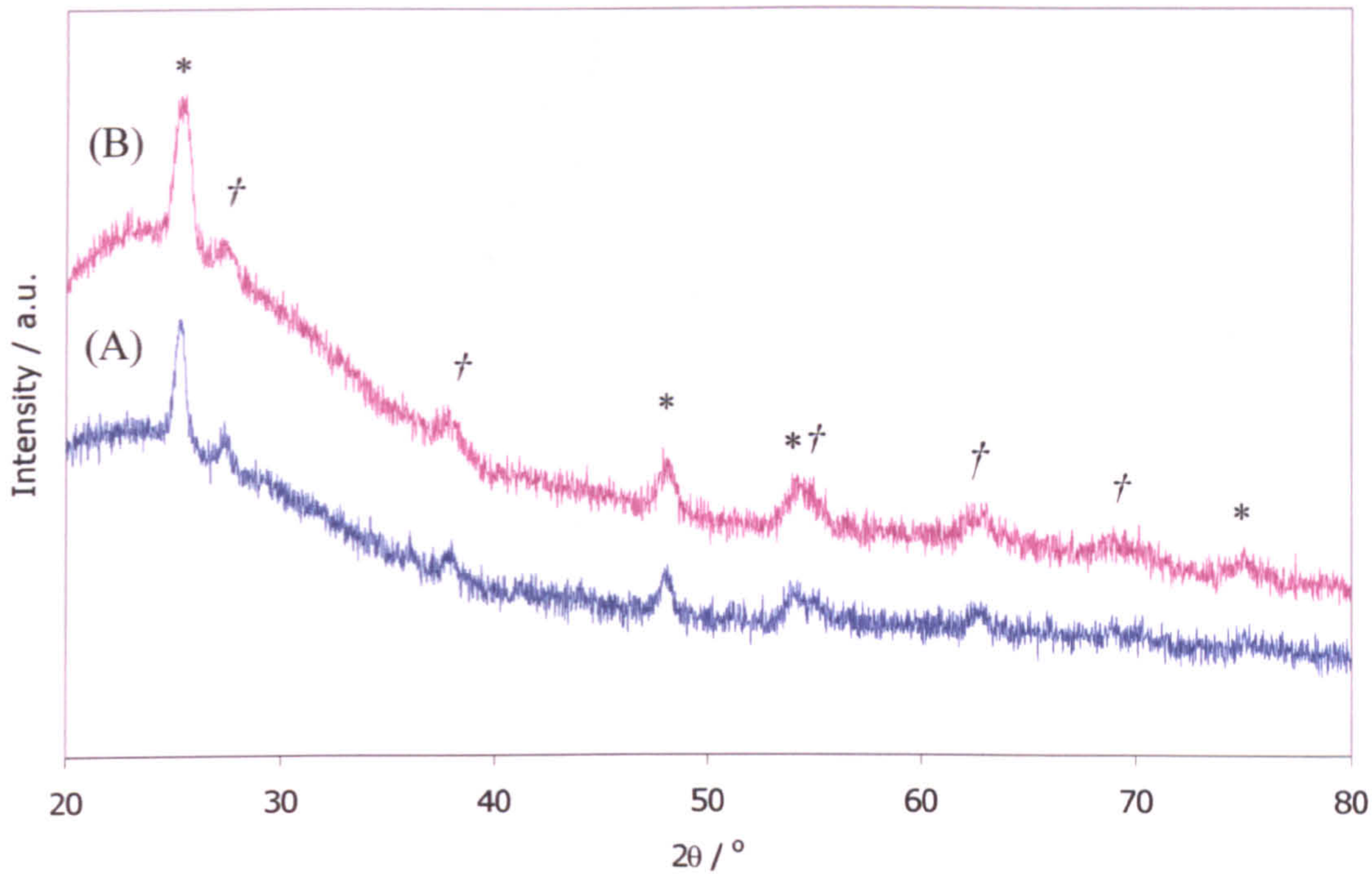


*Figure 4.2. Glancing angle XRD diffractograms of unmodified P25 coated glass slides calcined at 70°C (A) and 600°C (B). Reflections due to anatase and rutile are indicated by the symbols * and † respectively.*

### 4.2.1.2 TEM

TEM analysis of the unmodified P25 photocatalyst powders calcined in the temperature range of 70°C to 450°C confirmed the results observed in the XRD analysis. Measurement of the crystallite sizes from the TEM micrographs showed the average particle size to be *ca.* 20 nm for all the calcination temperatures, which is consistent to the anatase crystallite sizes calculated from the X-ray data. A typical micrograph is shown in figure 4.3 (A). No significant particle growth was observed in the TEM micrograph of P25 sample calcined at 600°C for 2 h (figure 4.3 (B)).

The selected area electron diffraction patterns observed for all the unmodified P25 photocatalysts were diffuse ring patterns, indicating the materials were all nanocrystalline in nature. Calculations of the d-spacings from the diffraction patterns confirmed only the presence of anatase and rutile in each sample (Table 4.3).

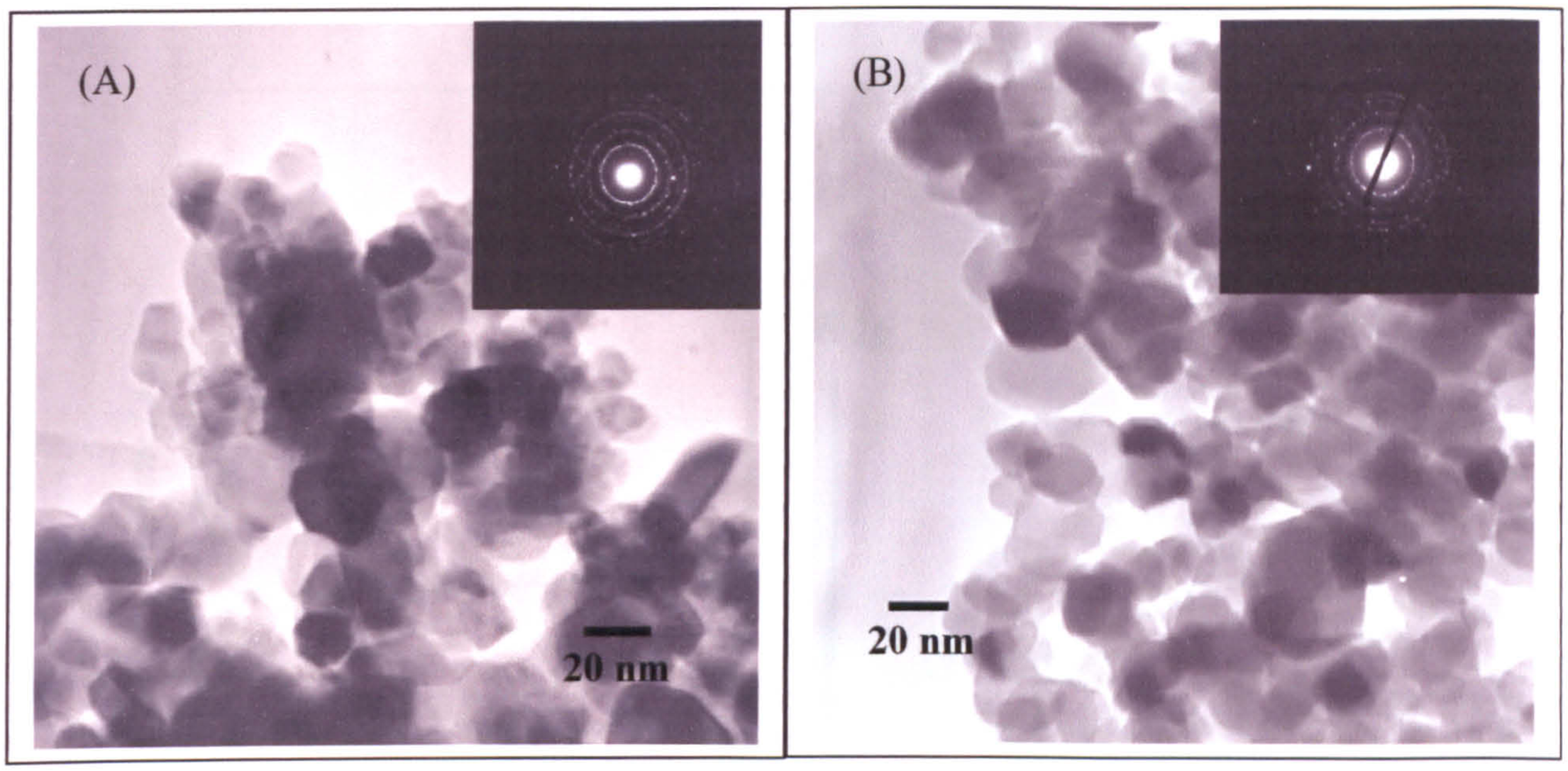


*Figure 4.3. TEM micrographs and their corresponding selected area electron diffraction patterns for unmodified P25 photocatalysts calcined at 450°C (A) and 600°C (B).*

| Ring | d / Å | Assignment |
|---|---|---|
| 1 | 3.55 | Anatase (101) |
| 2 | 3.26 | Rutile (110) |
| 3 | 2.50 | Rutile (101) |
| 4 | 2.35 | Anatase (004) |
| 5 | 2.16 | Rutile (111) |

*Table 4.3. Typical assignment of the d-spacing for unmodified P25 calculated from electron diffraction patterns.*

### 4.2.1.3 XPS

For survey scans of the unmodified P25 photocatalysts calcined at temperatures up to 600°C, the same peaks with similar intensities were observed, a typical XPS wide scan from 0-1000 eV is shown in figure 4.4. All of the XPS photoelectron peaks observed were assigned to either $TiO_2$ or adventitious carbon. Calculations of the weight percentage of oxygen relative to titanium gave a value of *ca.* 41 wt. % oxygen for all of the calcination temperatures used.

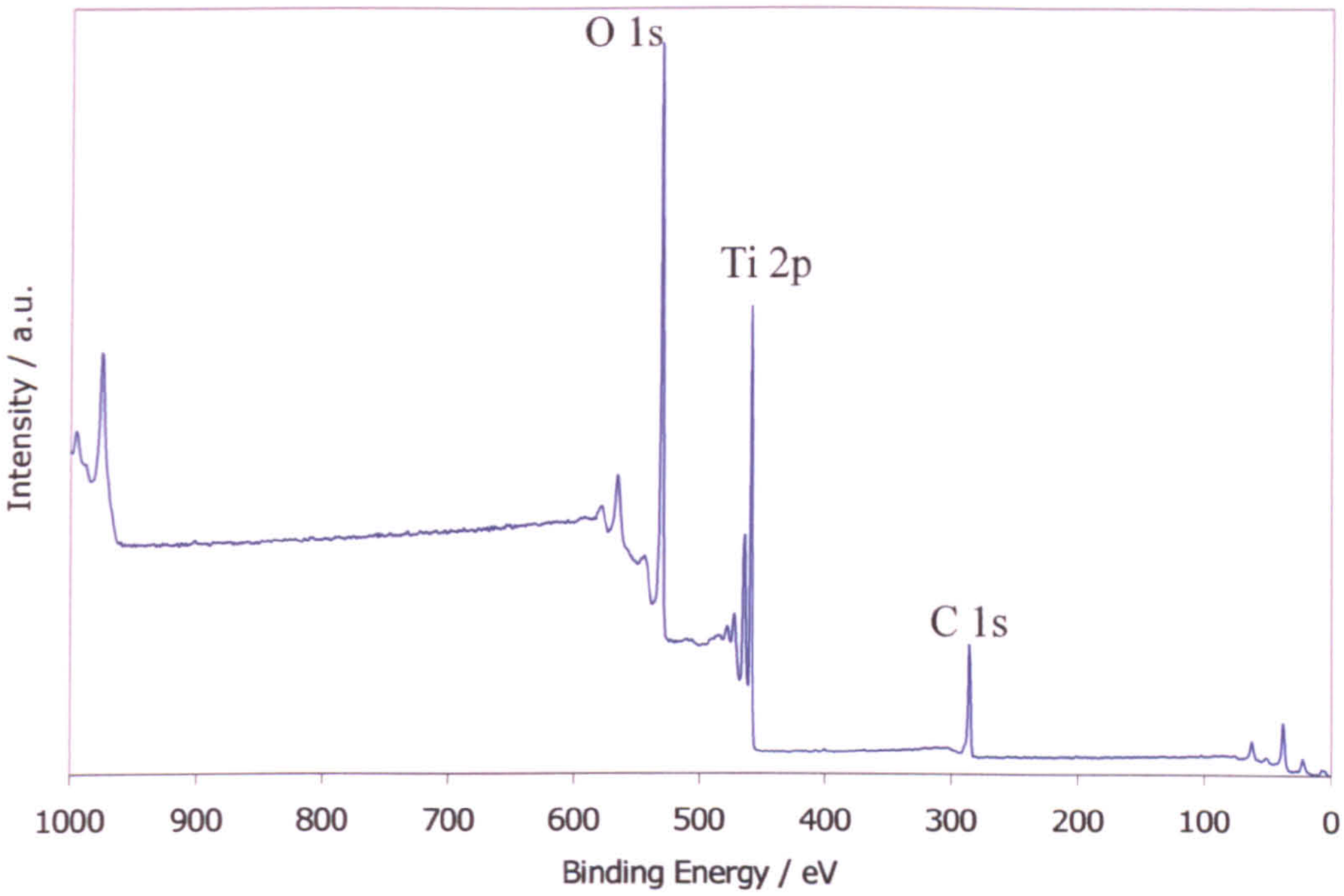


*Figure 4.4. Typical XPS wide scan for an unmodified P25 photocatalyst.*

High resolution scans of the Ti 2p photoelectron peaks from unmodified P25 photocatalysts calcined at temperatures in the range 70°C to 600°C (figure 4.5.) were charge corrected using the carbon 1s photoelectron peak at 285.0 eV. It can be seen that there were no significant changes in either the peak position (459 eV) or peak shape (FWHM was *ca.* 1.0 eV), even after calcination at 600°C where there was a higher percentage of rutile present. One component peak fitted the Ti 2p data well for each of the calcination temperatures used. Typical fitted curve and the peak positions and widths of the Ti $2p_{3/2}$ peaks are presented in figure 4.6 and table 4.4 respectively. The binding energy of the O 1s photoelectron peaks, determined from high resolution scans, was 530.2 eV for all the calcination temperatures investigated.

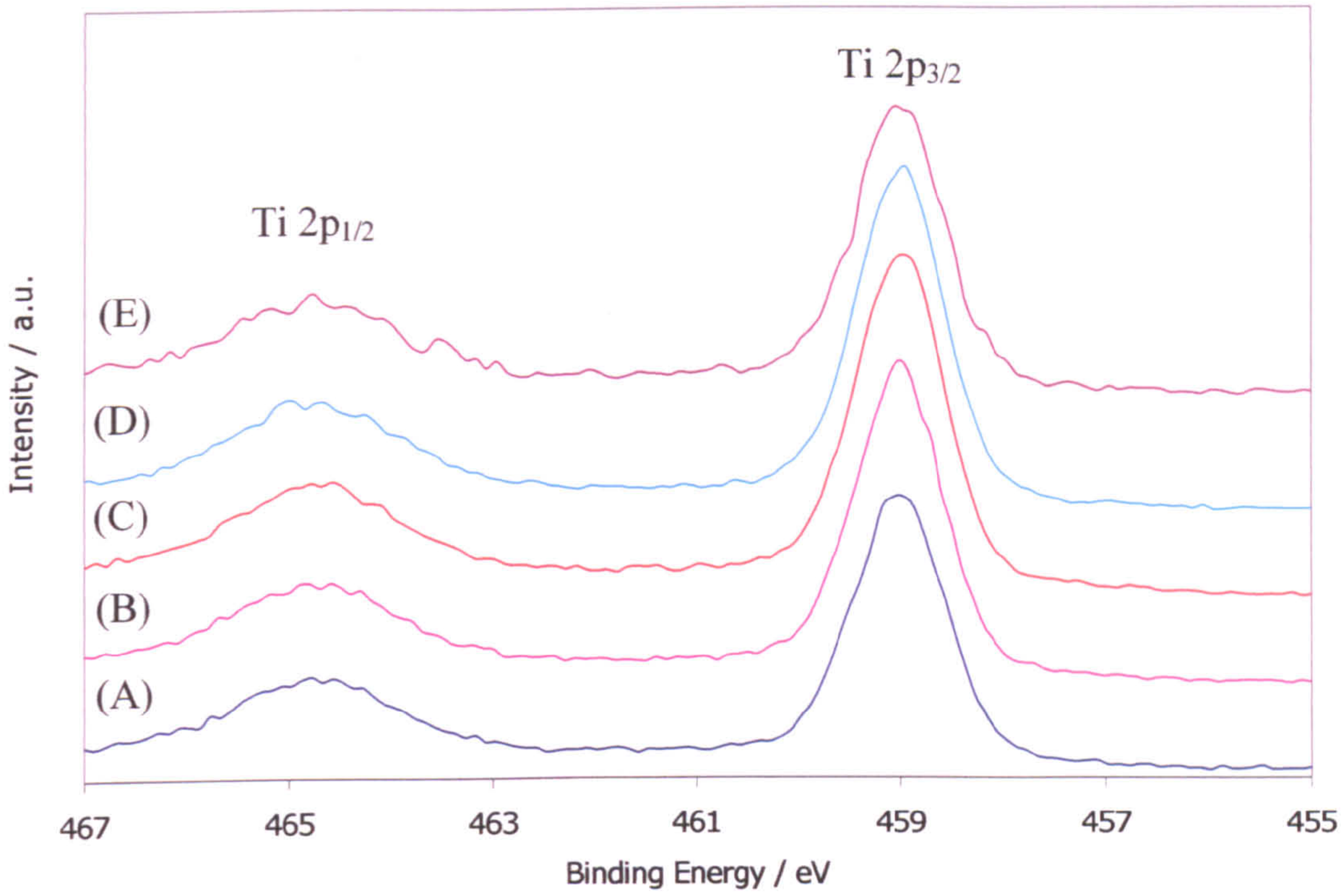


*Figure 4.5. High resolution XPS spectra of the Ti 2p photoelectron peaks for unmodified P25 photocatalysts calcined at temperatures of 70°C (A), 120°C (B), 200°C (C), 450°C (D) and 600°C (E).*

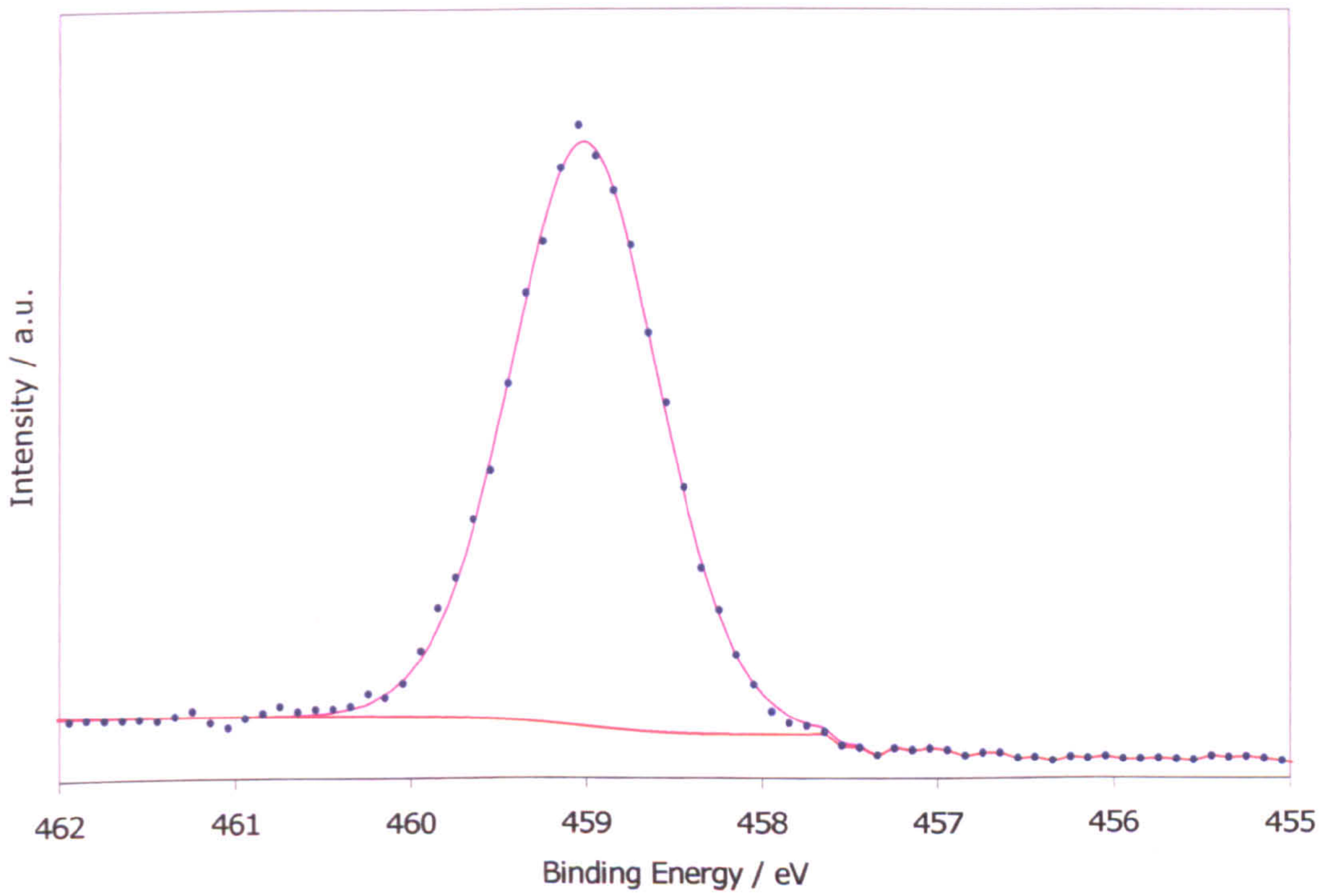


*Figure 4.6. Typical fitted curve for the Ti $2p_{3/2}$ photoelectron peak.*

| Calcination Temperature / °C | Ti $2p_{3/2}$ peak position / eV | Ti $2p_{3/2}$ FWHM / eV |
|---|---|---|
| 70 | 458.97 | 1.07 |
| 120 | 459.00 | 1.01 |
| 200 | 458.98 | 1.02 |
| 450 | 458.96 | 1.01 |
| 600 | 459.02 | 1.02 |

*Table 4.4. Effect of calcination temperature on the Ti $2p_{3/2}$ peak positions and FWHM for unmodified P25 photocatalysts.*

### 4.2.1.4 DSC

DSC analysis was carried out on P25 photocatalysts that had been dispersed in either TDW or acidified TDW (using $HNO_3$) and then dried at 70°C. The resulting DSC traces are shown in figure 4.7. The sharp rise at the start of each trace was not due to the samples but rather the electronics of the equipment. The DSC trace for the P25 that had been dispersed in acidified TDW (A) showed an endothermic reaction in the temperature range of *ca.* 65-125°C and sharp exotherm at 214°C. There also appeared to be an endothermic reaction occurring from 214°C to 410°C. After the sample had been heated to 500°C, it was cooled to room temperature under an argon atmosphere in the sample holder, and the experiment was repeated.

The DSC trace for the re-run sample (B) showed a shallow, broad, endotherm starting at *ca.* 214 °C and ending at 410 °C. The same sample was then redispersed in acidified TDW, dried at 70°C and the experiment repeated, yielding a similar DSC trace (D) as to the original sample (A). This repeatability after redispersion indicated that the changes that occurred were due to reactions of water and / or $HNO_3$ and not any phase change of P25.

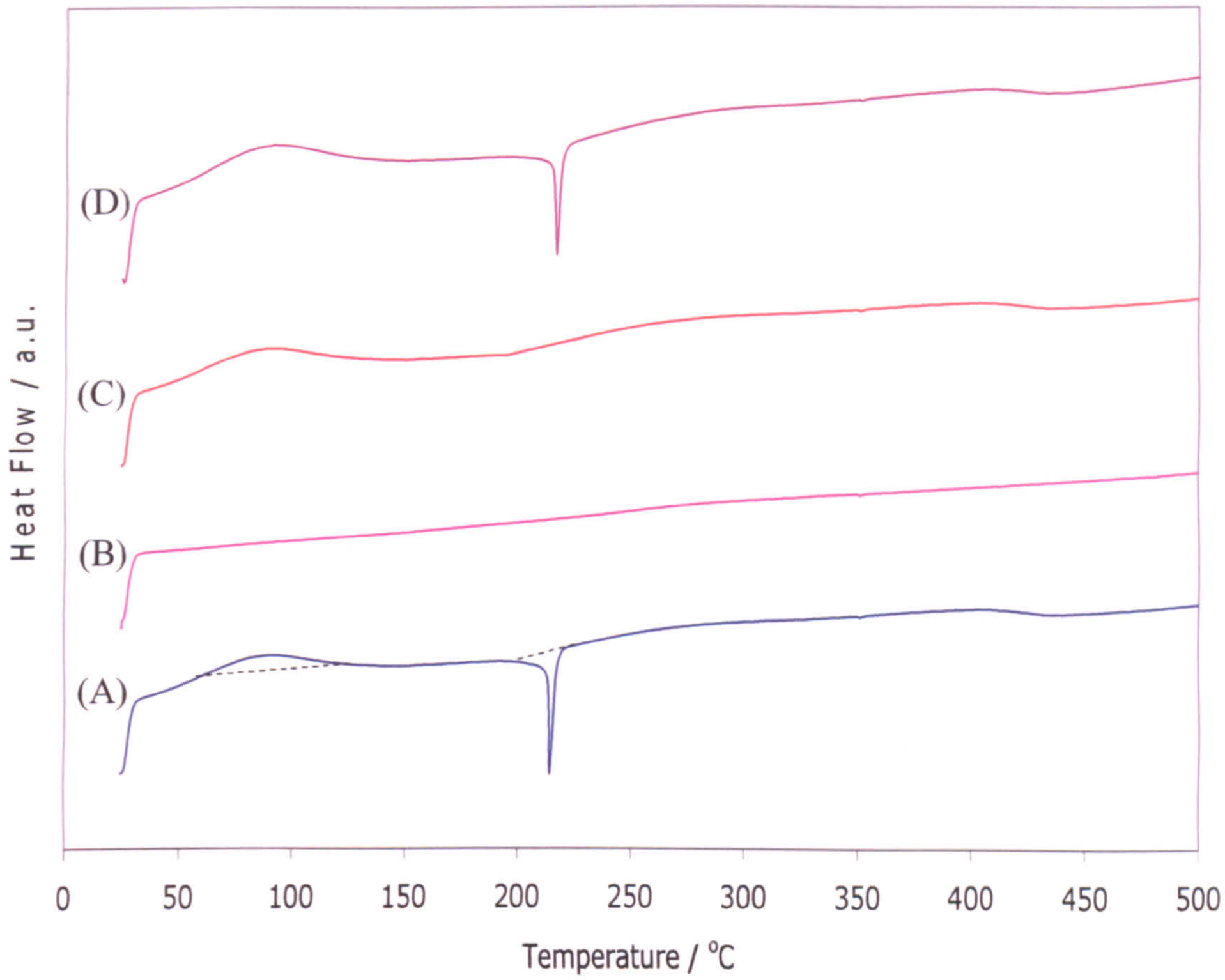


*Figure 4.7. DSC traces for P25 dispersed in acidified TDW (A), rerun of sample (A) after cooling to room temperature (B), P25 dispersed in TDW (C) and sample (A) redispersed in acidified TDW (D).*

To clarify the nature of the endothermic and exothermic reactions, another P25 sample that had been dispersed in TDW with no acid present and dried at 70°C was run (C). The results showed the same endothermic reactions in the temperature ranges 65-125°C and 200-410°C; however, the exothermic reaction at 214°C was absent.

To confirm the removal of the different species from the surface of P25, experiments A and B were repeated using a known mass of sample, but the scan was interrupted when the temperature reached 130°C, 220°C and 500°C and the sample mass was recorded at each interval. At the end of the second run (B) the sample

weight was measured again. Table 4.5 shows that there was a reduction in the mass of the sample with increasing temperature.

| Temperature / °C | Total percentage weight loss / wt. % |
|---|---|
| 130 | 0.80 |
| 220 | 1.10 |
| 500 (1st run) | 1.85 |
| 500 (2nd run) | 2.25 |

*Table 4.5. Table of weight loss for P25 dispersed in acidified TDW then heated in a DSC experiment.*

## 4.2.2 Characterisation of silver modified P25 photocatalysts

### 4.2.2.1 Introduction

Silver modified P25 photocatalysts were prepared by impregnation of P25 with silver nitrate. The experimental procedures are given in chapter 3. The silver loadings investigated were 0.1 wt. %, 1 wt. % and 5 wt. % of silver with respect to $TiO_2$. Powders dried at 70°C were calcined for 2 h at 120°C, 200°C, 450°C, and 600°C. The resulting powders were then used for characterisation of both the P25 support and the silver species present.

P25 coatings with the same silver loadings were prepared and calcined in an identical manner to the powdered samples. The coated slides were used for determining the photocatalytic behaviour of the photocatalyst prepared.

### 4.2.2.2 XRD

The X-ray diffractograms for powdered 0.1Ag-P25 photocatalysts calcined for 2 h at increasing temperatures (70 to 600°C) were comparable to those observed for the unmodified P25 photocatalysts calcined at those temperatures. No reflections due

to any silver containing phases were observed. The composition and crystallite sizes of the P25 phases (anatase and rutile) were similar to the corresponding values for unmodified P25 photocatalysts (table 4.6.).

| Calcination temperature / °C | Percentage of Rutile / vol. % | Crystallite size / nm | |
|---|---|---|---|
| | | Anatase | Rutile |
| 70 | 23.3 | 28.1 | 65.1 |
| 120 | 23.0 | 28.2 | 66.1 |
| 200 | 23.2 | 27.8 | 61.7 |
| 450 | 22.9 | 28.8 | 64.8 |
| 600 | 27.8 | 30.4 | 70.2 |

*Table 4.6. Effect of calcination temperature on the composition and crystallite sizes of 0.1Ag-P25 photocatalysts.*

The X-ray diffractograms for 1Ag-P25 photocatalysts calcined at temperatures up to 450°C were very similar to those observed for the unmodified P25 photocatalysts calcined at the same temperatures. Again no reflections due to any silver containing species were observed. Calculation of the composition and crystallite sizes were consistent with those for the unmodified P25 system (table 4.7).

| Calcination temperature / °C | Percentage of Rutile / vol. % | Crystallite size / nm | |
|---|---|---|---|
| | | Anatase | Rutile |
| 70 | 23.7 | 28.0 | 62.6 |
| 120 | 23.2 | 28.8 | 59.7 |
| 200 | 22.4 | 28.2 | 65.8 |
| 450 | 23.5 | 28.3 | 65.0 |
| 600 | 31.5 | 32.8 | 79.3 |

*Table 4.7. Effect of calcination temperature on the composition and crystallite sizes of 1Ag-P25 photocatalysts.*

After calcination at 600°C for 2 h, the relative intensity of rutile to anatase reflections increased more than was observed for the unmodified P25 photocatalyst calcined using identical conditions (figure 4.8). Calculation of the composition of the

P25 support confirmed that there was 31.5 vol. % of rutile phase present compared to only 28 vol. % for the unmodified P25 calcined at 600°C for 2 h.

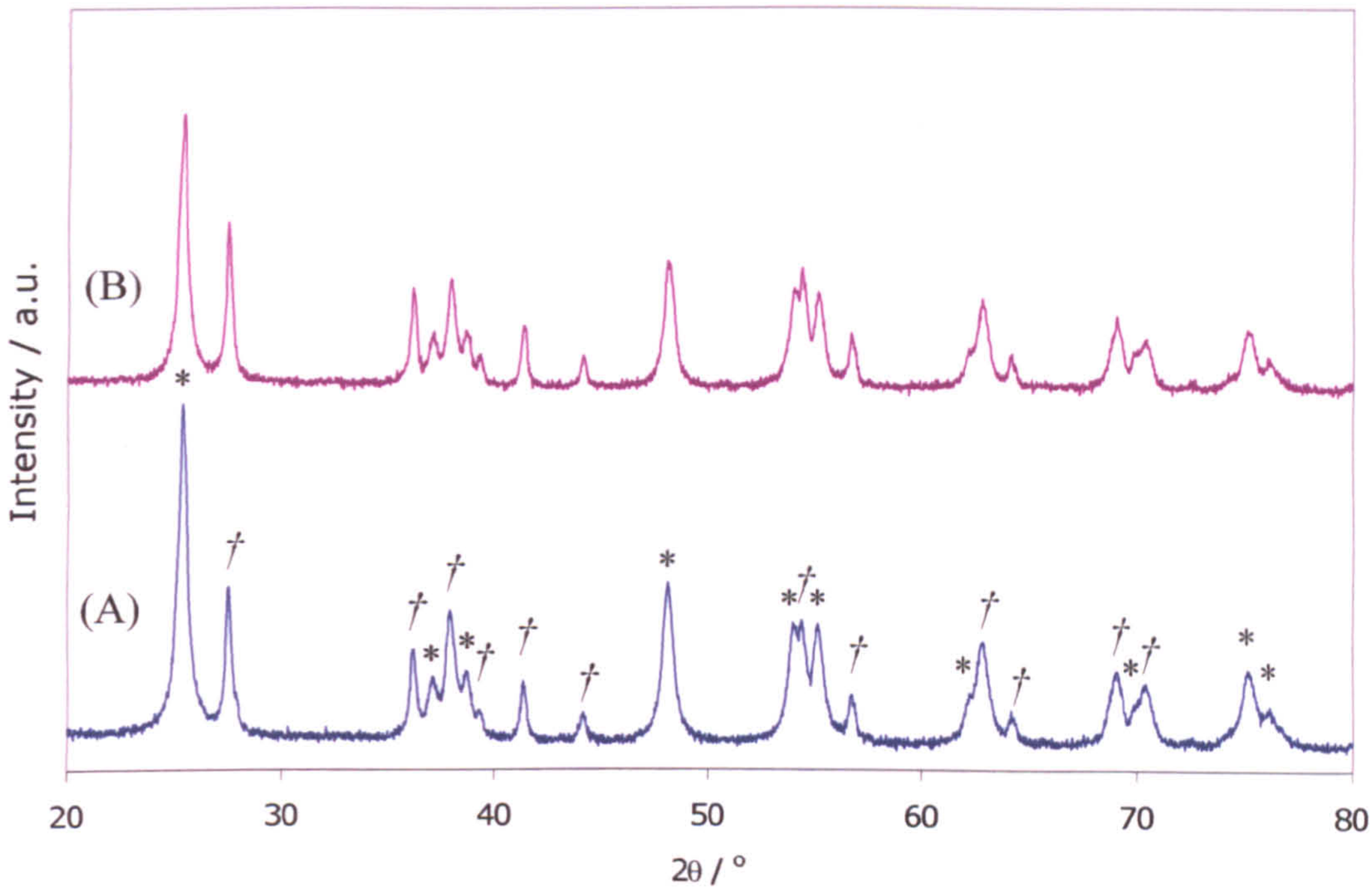


*Figure 4.8. Powder XRD diffractograms for 1Ag-P25 photocatalysts calcined at 450°C (A) and 600°C (B). Reflections due to anatase and rutile are indicated by the symbols * and †, respectively.*

In the X-ray diffractograms for 5Ag-P25 calcined at low temperatures (70-200°C), reflections due to silver nitrate were observed along with the reflections for anatase and rutile (figure 4.9). Assignment of the reflections observed for 5Ag-P25 dried at 70°C to a given lattice plane are shown in table 4.8. As the calcination temperature was increased from 70°C to 200°C the relative intensity of the silver nitrate reflections, with respect to the $TiO_2$ reflections, decreased. After calcination at 450°C no reflections due to any silver containing species were observed, but after calcination at 600°C, reflections assigned to metallic silver were detected (figure 4.9 (b)).

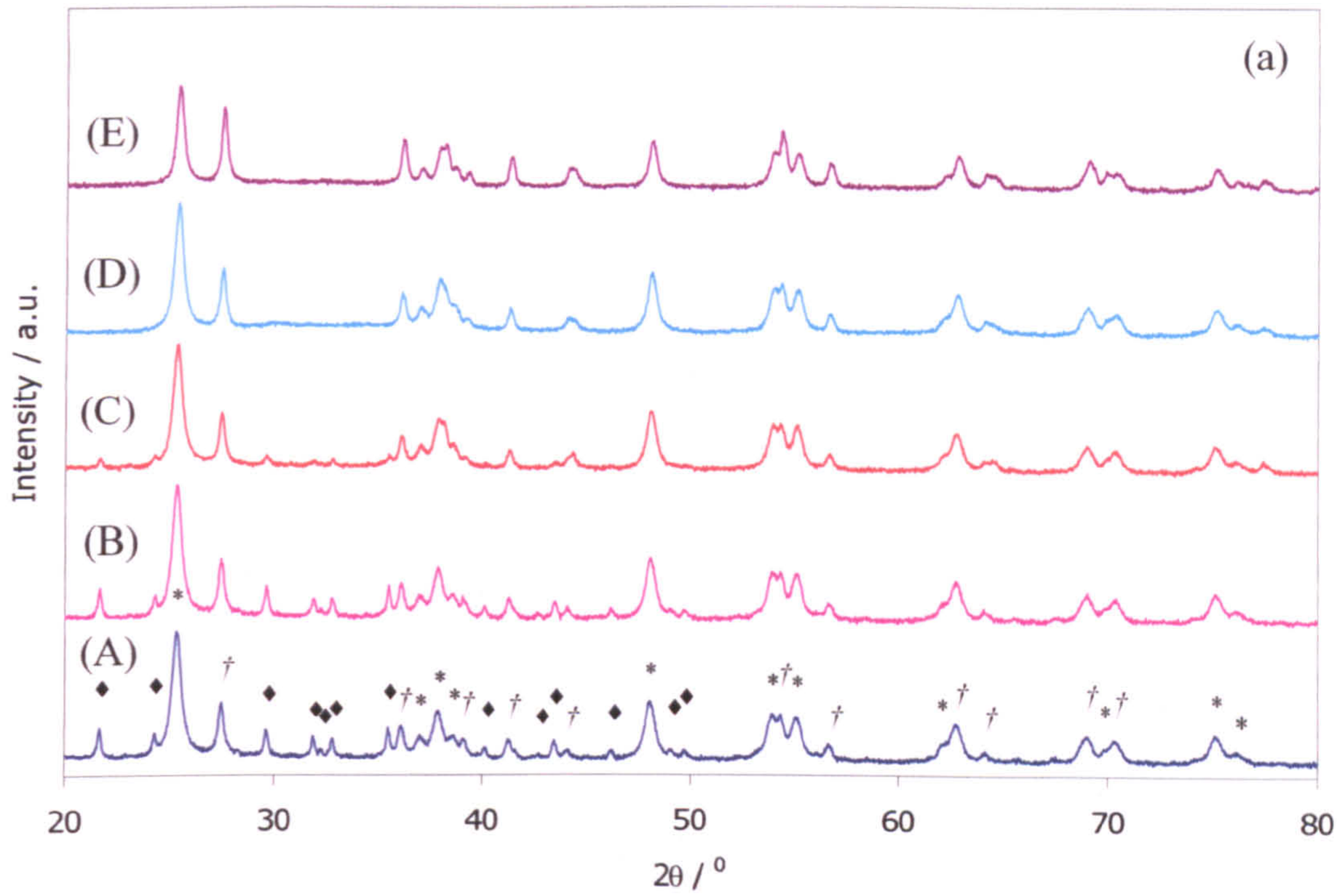


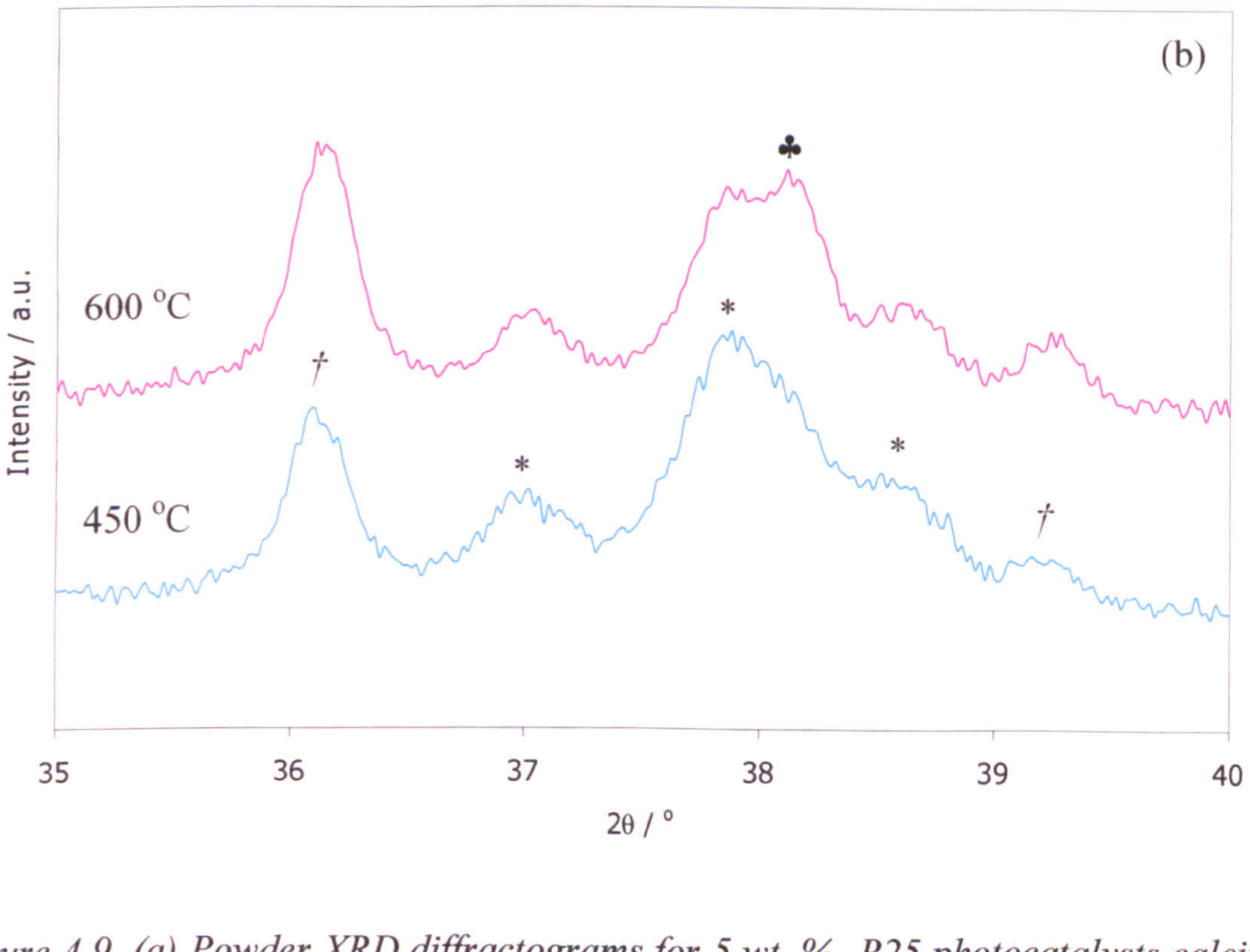


*Figure 4.9. (a) Powder XRD diffractograms for 5 wt. %- P25 photocatalysts calcined at 70°C (A), 120°C (B), 200°C (C), 450°C (D) and 600°C (E). (b) Enlarged section of (a) showing metallic silver diffractions. Reflections due to anatase, rutile, silver nitrate and silver are indicated by the symbols * and †, ♦, and ♣, respectively.*

From the diffractograms it can be seen that the phase transformation behaviour of the P25 substrate was altered when a silver loading of 5 wt. % was used. At temperatures up to 200°C, the structure and composition of the P25 support remained unaltered with *ca.* 23 vol. % rutile present, with a particle size of *ca.* 29 nm, and an anatase particle size of *ca.* 28 nm. However, after calcination at 450°C for 2 h, an increase was measured in both the anatase (31 nm) and rutile (67 nm) crystallite sizes along with an increase in the percentage rutile phase to 25.9 vol. %. For all the other systems investigated no change in the P25 crystallinity was observed after calcination at 450°C for 2 h. Further evidence for an increase in the rate of the anatase-to-rutile phase transformation kinetics came from the sample calcined at 600°C, which showed an increase in the percentage of rutile present up to 47 vol. %, compared to the unmodified P25 system at 600°C which consisted of only 28 vol. % rutile. The crystallite sizes of both anatase and rutile were larger for the sample containing 5 wt. % silver (table 4.9).

| Peak position / 2θ | d / Å | Relative intensity | Assignment |
|---|---|---|---|
| 21.67 | 4.0977 | 9.96 | Silver nitrate (102) |
| 24.28 | 3.6628 | 6.55 | Silver nitrate (020) |
| 25.32 | 3.5147 | 100.00 | Anatase (101) |
| 27.45 | 3.2466 | 24.06 | Rutile (110) |
| 29.62 | 3.0135 | 9.71 | Silver nitrate (211) |
| 31.88 | 2.8049 | 6.68 | Silver nitrate (113) |
| 32.77 | 2.7307 | 5.42 | Silver nitrate (122) |
| 35.47 | 2.5288 | 10.42 | Silver nitrate (220) |
| 36.09 | 2.4867 | 10.96 | Rutile (200) |
| 36.98 | 2.4289 | 5.42 | Anatase (103) |
| 37.83 | 2.3763 | 19.61 | Anatase (004) |
| 38.56 | 2.3329 | 5.80 | Anatase (112) |
| 39.10 | 2.3019 | 4.74 | Rutile (200) |
| 40.08 | 2.2479 | 2.64 | Silver nitrate (131) |
| 41.26 | 2.1863 | 5.68 | Rutile (111) |
| 41.60 | 2.1692 | 1.93 | Silver nitrate (311) |
| 42.67 | 2.1173 | 0.84 | Silver nitrate (302) |
| 43.46 | 2.0806 | 5.55 | Silver nitrate (024) |
| 44.06 | 2.0536 | 1.87 | Rutile (211) |
| 46.20 | 1.9634 | 2.16 | Silver nitrate (231) |
| 48.06 | 1.8916 | 27.35 | Anatase (200) |
| 49.06 | 1.8554 | 1.71 | Silver nitrate (313) |
| 49.71 | 1.8326 | 1.77 | Silver nitrate (322) |
| 53.94 | 1.6985 | 17.48 | Anatase (105) |
| 54.36 | 1.6863 | 14.83 | Rutile (211) |
| 55.06 | 1.6665 | 16.22 | Anatase (213) |
| 56.63 | 1.6240 | 3.81 | Rutile (220) |
| 62.09 | 1.4937 | 3.68 | Anatase (213) |
| 62.74 | 1.4797 | 13.35 | Rutile (002) |
| 64.08 | 1.4520 | 1.61 | Rutile (310) |
| 65.54 | 1.4231 | 0.42 | Silver nitrate (235) |
| 67.42 | 1.3880 | 0.61 | Silver nitrate (342) |
| 68.91 | 1.3615 | 7.67 | Rutile (301) |
| 69.80 | 1.3463 | 2.35 | Anatase (220) |
| 70.30 | 1.3380 | 6.03 | Rutile (311) |
| 75.09 | 1.2641 | 8.55 | Anatase (215) |
| 76.08 | 1.2501 | 1.93 | Anatase (301) |

*Table 4.8. Table of peak positions and assignment of the Bragg reflections for 5Ag-P25 photocatalyst powder dried at 70°C.*

| Calcination temperature / °C | Percentage of Rutile / vol. % | Crystallite size / nm | |
|---|---|---|---|
| | | Anatase | Rutile |
| 70 | 22.7 | 28.4 | 64.3 |
| 120 | 22.9 | 28.9 | 63.2 |
| 200 | 23.1 | 28.6 | 58.4 |
| 450 | 25.9 | 31.0 | 67.4 |
| 600 | 47.0 | 40.3 | 75.2 |

*Table 4.9. Effect of calcination temperature on the composition and crystallite sizes for 5Ag-P25 photocatalysts.*

### 4.2.2.3 TEM

TEM micrographs of both 1Ag-P25 and 5Ag-P25 photocatalysts calcined in the temperature range 70°C to 450°C were very similar to the corresponding micrographs for unmodified P25 calcined at the same temperatures. No silver containing particles could be resolved, although EDX analysis confirmed the existence of silver over all the P25 support. Calculation of the d-spacings, from the selected area diffraction patterns, confirmed only the presence of anatase and rutile.

In the micrographs of both 1Ag-P25 and 5Ag-P25 calcined at 600°C (figure 4.10 (A) and (B) respectively), small spherical particles were observed. EDX analysis of the particles confirmed that they were silver particles. It was also apparent from the micrograph of the 5Ag-P25 sample that the titania particles (the support material) were larger than were observed for the unmodified P25 calcined at 600°C. Further evidence of crystal growth was found from the corresponding electron diffraction pattern which showed obvious speckling, which is indicative of a polycrystalline phase. This result is consistent with the findings from XRD analysis, which showed that the presence of silver increased the rate of the anatase-to-rutile phase transformation.

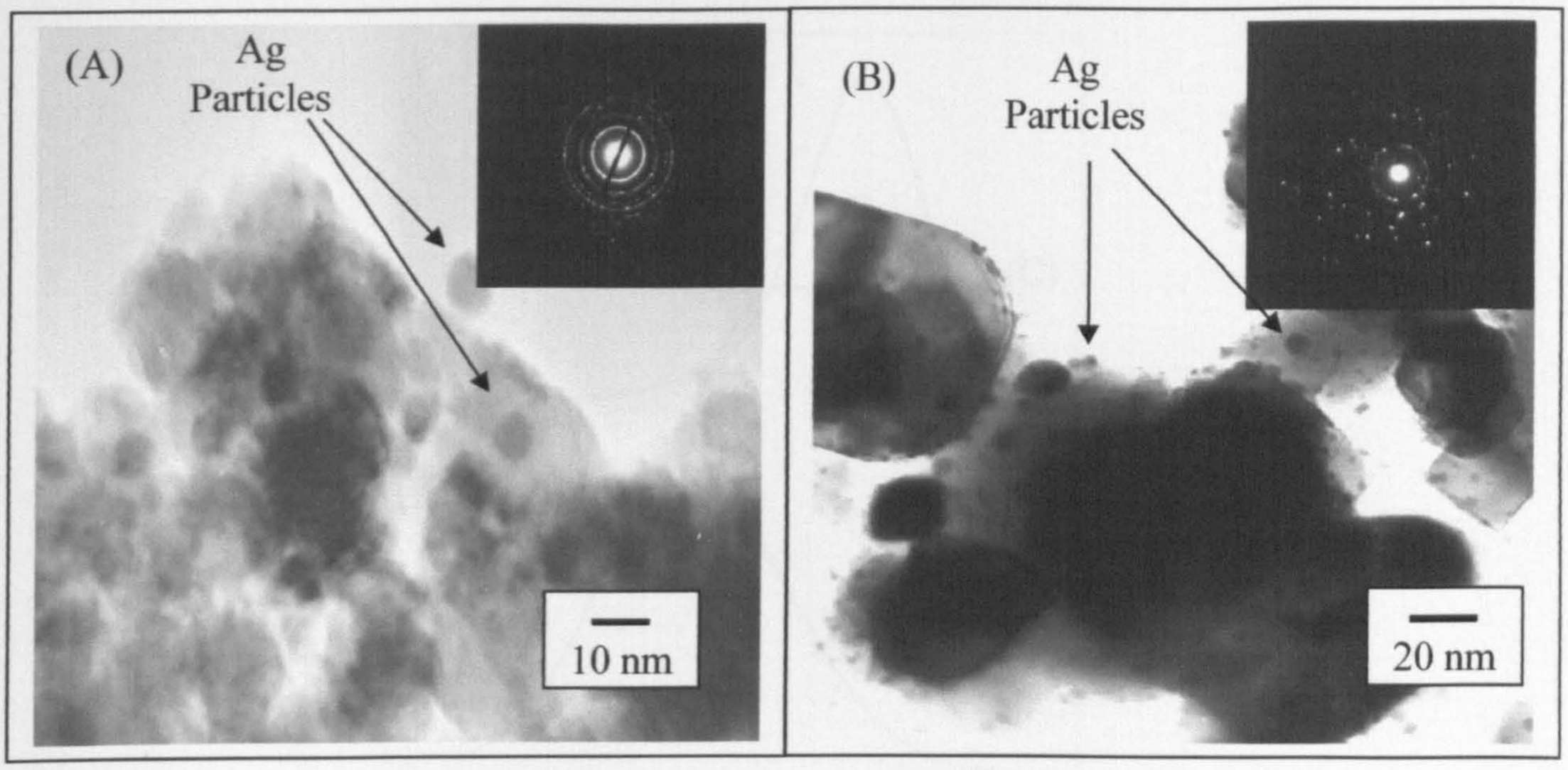


*Figure 4.10. TEM micrographs and their corresponding selected area electron diffraction patterns for 1Ag-P25 (A) and 5Ag-P25 (B) calcined at 600°C.*

### 4.2.2.4 XPS

As the chemical shifts between $Ag^0$ and $Ag^+$ species are less than 1 eV and due to the range of Ag 3d peak position values reported in the literature, XPS analysis of standard silver compounds, $AgNO_3$, $Ag_2O$ and Ag foil, was undertaken. High resolution scans of the Ag $3d_{5/2}$ peaks are presented in figure 4.11. The trend observed was a decrease in the binding energies of the Ag $3d_{5/2}$ photoelectrons from $AgNO_3$ (368.9 eV) to $Ag_2O$ (368.4 eV) and finally to $Ag^0$ (368.1 eV).

For both silver oxide and silver nitrate one peak fitted the data well. The positions and FWHM of the fitted peaks are presented in table 4.10. However, the Ag $3d_{5/2}$ peak for the Ag foil was determined to be the sum of multiple peaks (figure 4.12.), the second being due to a silver oxide layer that had formed on the metal surface.

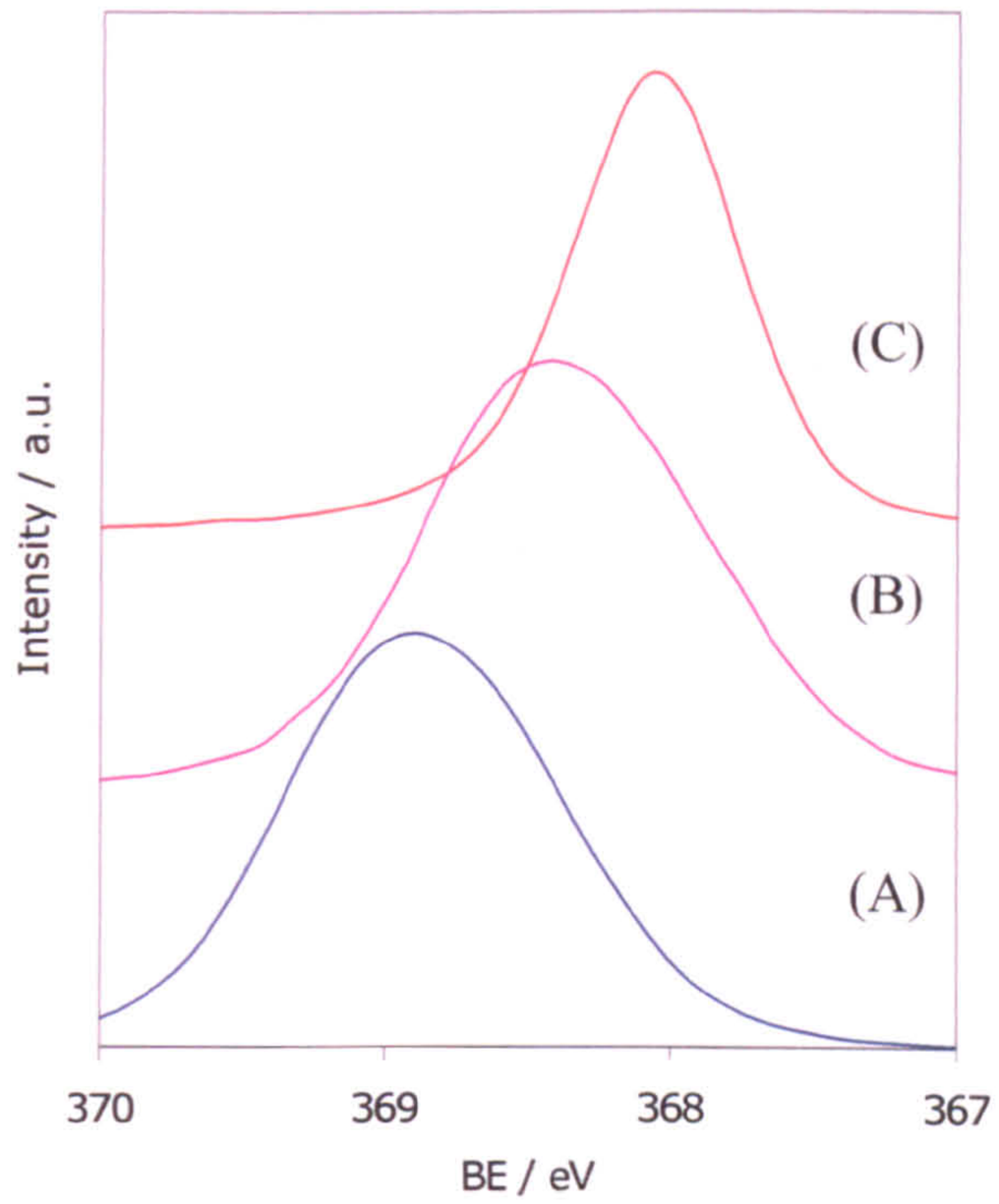


*Figure 4.11. Ag $3d_{5/2}$ spectra for standard silver compounds of $AgNO_3$ (A), $Ag_2O$ (B) and Ag foil (C).*

| Compound | Ag $3d_{5/2}$ | |
|---|---|---|
| | BE / eV | FWHM / eV |
| Silver Nitrate | 368.9 | 1.12 |
| Silver Oxide | 368.4 | 1.15 |
| Silver foil | 368.1 (368.2)* | 0.65 (1.48)* |

*Table 4.10. Ag $3d_{5/2}$ photoelectron peak positions and FWHM for standard silver compounds. * Values for the oxide layer detected on the silver foil.*

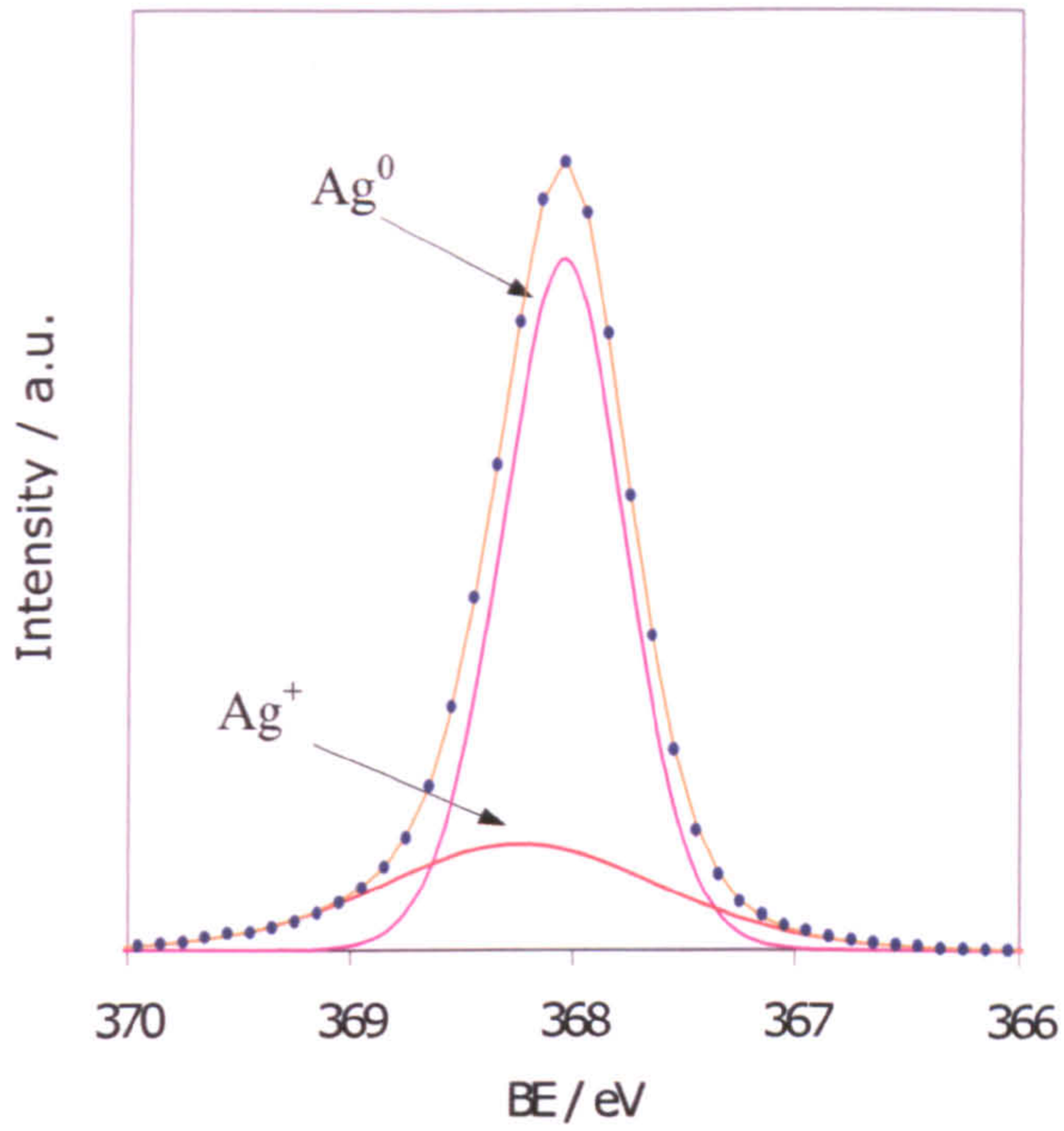


*Figure 4.12. Peak fitting for the Ag $3d_{5/2}$ XPS spectrum for silver foil.*

XPS analysis of the powdered 0.1Ag-P25 photocatalysts did not reveal any peaks arising from silver species as the silver loading was below the detection limits for the spectrometer used. Therefore, the nature of the silver species in these photocatalysts was inferred from the data obtained for the 1Ag-P25 and 5Ag-P25 systems.

Survey scans from 1Ag-P25 photocatalysts calcined at increasing temperatures (70°C to 600°C) all showed identical features that confirmed the presence of silver, titanium, oxygen and adventitious carbon. No nitrogen peak was detected in the survey scan (figure 4.13).

The high resolution scans of the Ag $3d_{5/2}$ peaks (figure 4.14.) were slightly broadened for all of the calcination temperatures, indicating that they were the sum of multiple peaks. Using the data obtained from the silver standards the fitted peaks (A) and (B) (figure 4.12.) were assigned to $Ag^+$ and $Ag^0$ species, respectively.

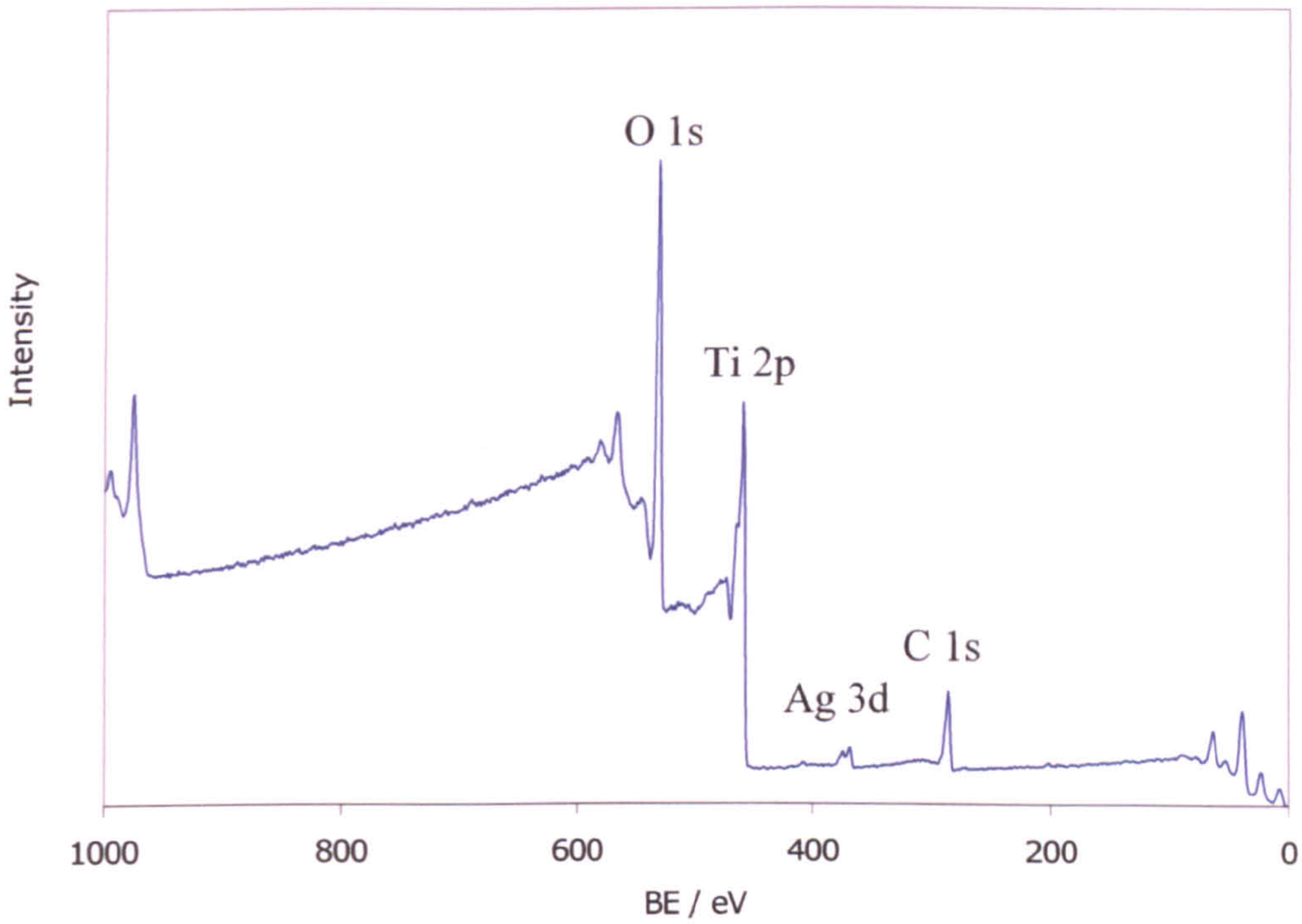


*Figure 4.13. Representative XPS survey scan of a 1Ag-P25 photocatalyst.*

As the calcination temperature was increased from 70°C to 600°C the relative intensity of the $Ag^{+}$ to $Ag^{0}$ decreased. Calculation of the relative atomic percentages of $Ag^{+}$ to $Ag^{0}$ confirmed that increasing amounts of $Ag^{0}$ were present as the calcination temperature increased (table 4.11).

Quantification of the atomic percentage of silver species relative to titanium and oxygen ions was preformed using standard library Scofield sensitivity factors and the results are shown in table 4.12. For all the calcination temperatures investigated, the atomic percentage of silver with respect to $TiO_2$ was *ca.* 1 at. %. However, no real trend was observed with increasing calcination temperature as the signal-to-noise ratio was poor due to the low silver loading, resulting in larger errors when calculating peak areas. Hence, no indication of the dispersion of the silver species on the P25 could be inferred from this data.

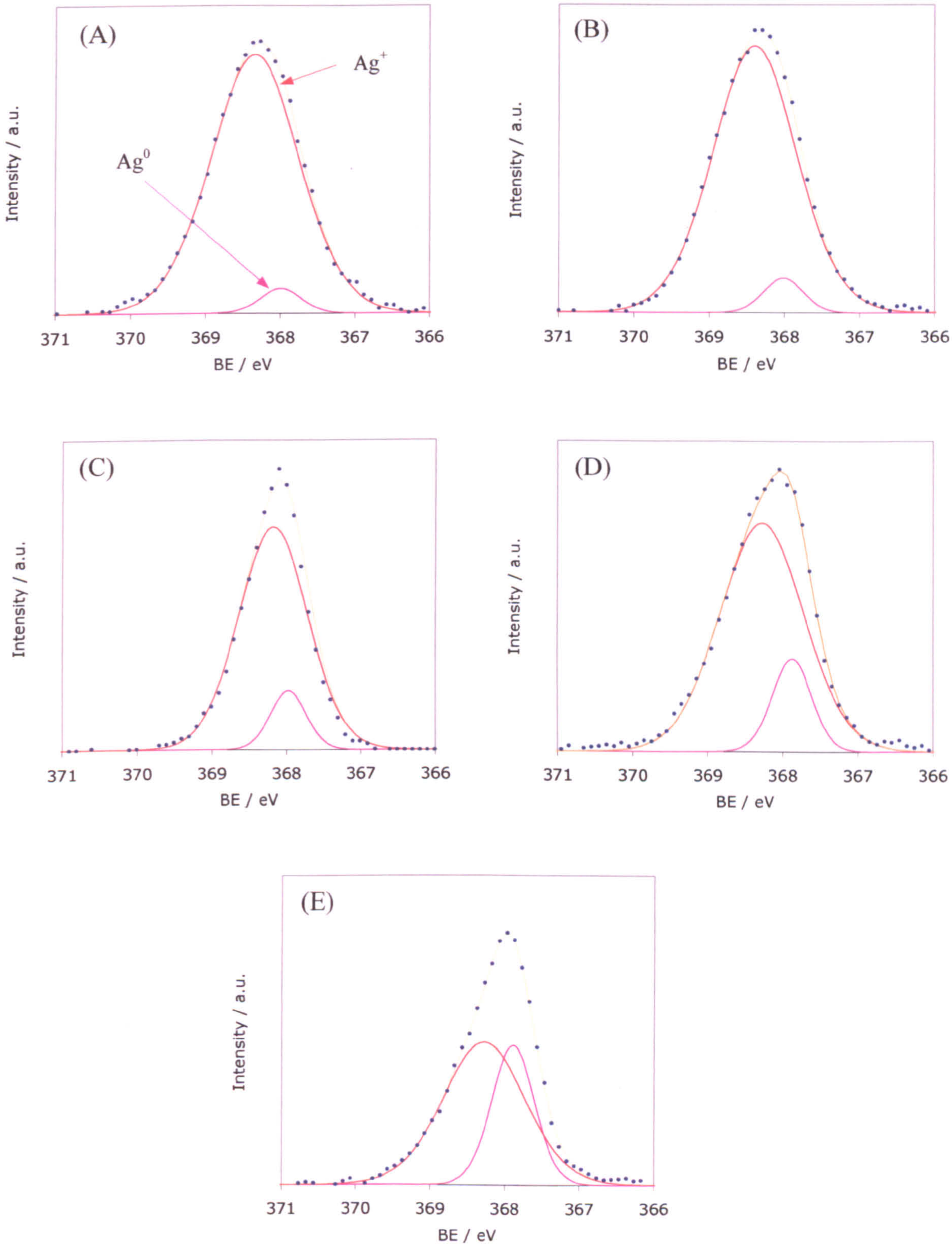


*Figure 4.14. Fitted high resolution XPS spectra of the Ag $3d_{5/2}$ peaks for 1Ag-P25 photocatalysts calcined at 70°C (A), 120°C (B), 200°C (C), 450°C (D) and 600°C (E). The annotation shown in (A) is the same as for the other spectra shown.*

| Calcination temperature / °C | BE / eV | | FWHM / eV | | Silver species ratio / % | |
|---|---|---|---|---|---|---|
| | $Ag^0$ | $Ag^+$ | $Ag^0$ | $Ag^+$ | $Ag^0$ | $Ag^+$ |
| 70 | 368.0 | 368.3 | 0.64 | 1.38 | 4.2 | 95.8 |
| 120 | 368.0 | 368.4 | 0.61 | 1.30 | 5.7 | 94.3 |
| 200 | 368.0 | 368.3 | 0.61 | 1.30 | 9.5 | 90.5 |
| 450 | 367.9 | 368.3 | 0.61 | 1.29 | 15.8 | 84.2 |
| 600 | 367.9 | 368.3 | 0.67 | 1.30 | 33.6 | 66.4 |

*Table 4.11. Table of Ag $3d_{5/2}$ peak positions, FWHM and atomic percent of components for 1Ag-P25 photocatalysts calcined at increasing calcination temperatures.*

| Calcination temperature / °C | Atomic percent of Ag / at. % | Weight percentage of Ag / wt. % |
|---|---|---|
| 70 | 1.01 | 2.50 |
| 120 | 0.84 | 2.08 |
| 200 | 0.82 | 2.03 |
| 450 | 0.70 | 1.73 |
| 600 | 1.00 | 2.48 |

*Table 4.12. Table of XPS derived atomic and weight percentages of Ag species for 1Ag-P25 photocatalysts calcined at increasing calcination temperatures.*

The survey spectra for 5Ag-P25 photocatalysts contained the same peaks as the corresponding spectra from the 1Ag-P25 system, but the relative intensity of the silver 3d peaks was higher due to the higher loading of silver. From the high resolution scans (figure 4.15 and table 4.13) it can be seen that, as with the 1Ag-P25 photocatalysts, the relative abundance of $Ag^0$ species with respect to $Ag^+$ species increased with increasing calcination temperature. It should be noted that the percentage of $Ag^0$ species was greater for all the calcination temperatures for the 5Ag-P25 system, compared to the 1Ag-P25 system.

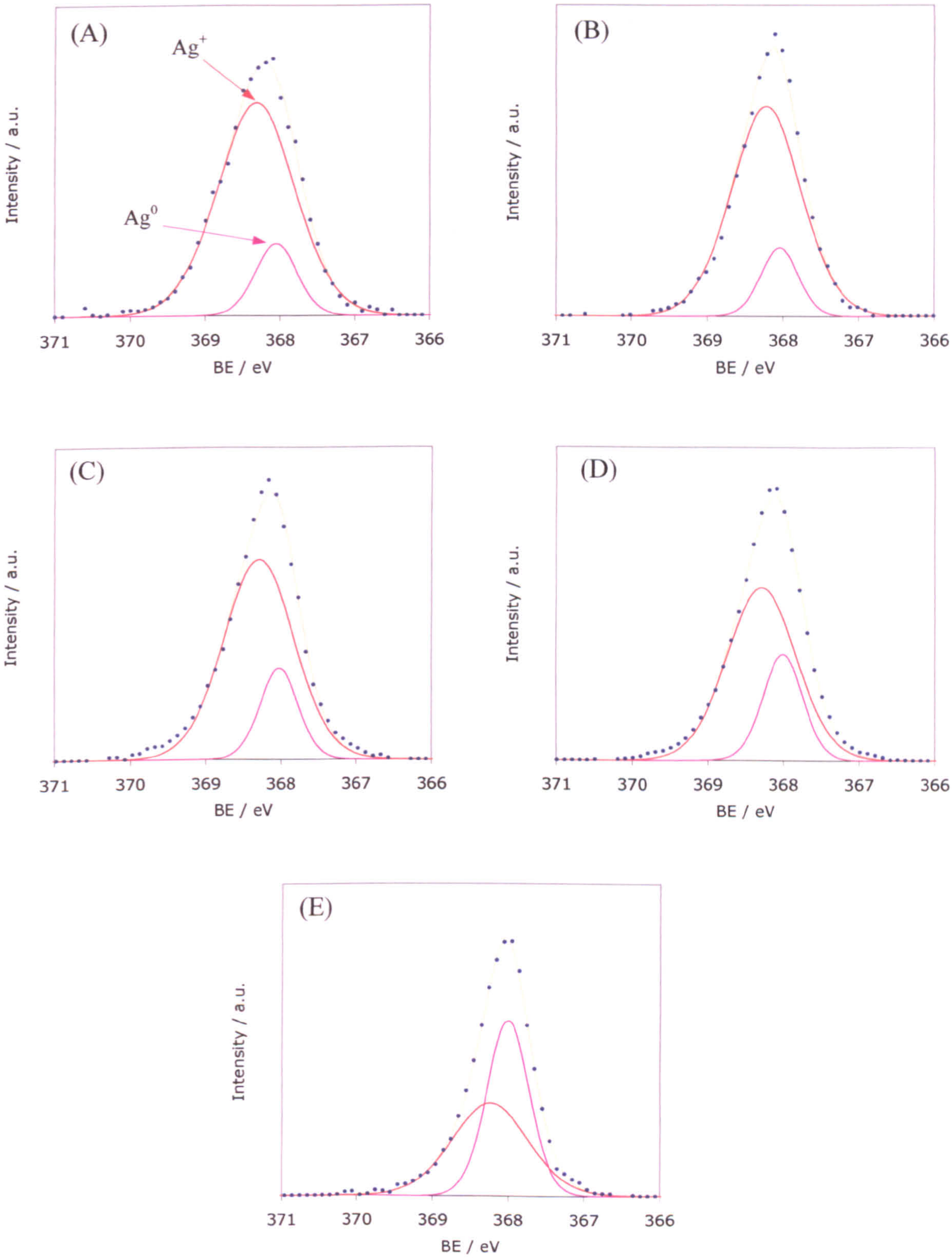


*Figure 4.15. Fitted high resolution XPS spectra of the Ag $3d_{5/2}$ peaks for 5Ag-P25 photocatalysts calcined at 70°C (A), 120°C (B), 200°C (C), 450°C (D) and 600°C (E). The annotation shown in (A) is the same as for the other spectra shown.*

| Calcination temperature / °C | BE / eV | | FWHM / eV | | Silver species ratio / % | |
|---|---|---|---|---|---|---|
| | $Ag^0$ | $Ag^+$ | $Ag^0$ | $Ag^+$ | $Ag^0$ | $Ag^+$ |
| 70 | 368.0 | 368.3 | 0.64 | 1.20 | 7.8 | 92.2 |
| 120 | 368.1 | 368.2 | 0.57 | 1.08 | 10.8 | 89.2 |
| 200 | 368.0 | 368.3 | 0.61 | 1.06 | 25.9 | 74.1 |
| 450 | 368.0 | 368.3 | 0.60 | 1.08 | 29.6 | 70.4 |
| 600 | 368.0 | 368.2 | 0.65 | 1.18 | 63.8 | 36.2 |

*Table 4.13. Table of Ag $3d_{5/2}$ peak positions, FWHM and atomic percentage of the silver components for 5Ag-P25 photocatalysts calcined at increasing calcination temperatures.*

The weight percentage of Ag for the 5Ag-P25 photocatalyst dried at 70°C was 9.5 wt. %, (Table 4.14) which is significantly higher than the theoretical silver loading of 5 wt. % that was used. With increasing calcination temperatures (up to 200°C) there was an increase in the weight percentage of silver (as detected by XPS analysis), indicating that there was an increase in the dispersion of the silver species. At calcination temperatures of 450°C and 600°C a reduction in the percentage of silver was observed, indicating decreased levels of dispersion.

| Calcination temperature / °C | Atomic percentage of Ag / at. % | Weight percentage of Ag / wt. % |
|---|---|---|
| 70 | 3.8 | 9.5 |
| 120 | 5.0 | 12.3 |
| 200 | 8.3 | 20.5 |
| 450 | 7.8 | 19.4 |
| 600 | 7.2 | 17.8 |

*Table 4.14. Table of atomic and weight percentages of Ag with respect to $TiO_2$ for 5Ag-P25 photocatalysts calcined at increasing calcination temperatures.*

## 4.2.3 Characterisation of rhodium modified P25 photocatalysts

### 4.2.3.1 Introduction

Rhodium modified P25 photocatalysts were prepared by impregnation of P25 with rhodium nitrate as described in chapter 3. The rhodium loadings investigated were 0.1 wt. %, 1 wt. % and 5 wt. % of rhodium metal with respect to $TiO_2$. Unlike the unmodified P25 and silver modified photocatalysts the rhodium containing photocatalysts were not simply calcined at increasing temperatures. The preparation treatments used for the rhodium containing systems were mainly reduction processes in the hope of producing metallic rhodium species on the surface of the P25, although one sample calcined at 200 °C was investigated. Both UV and thermal reductions were investigated, which in practice could only be implemented to the photocatalyst coatings and not the powdered samples. Therefore all of the characterisation of the rhodium containing systems was performed either using the coated slides directly or using the small amount of sample which could be removed from the glass slides.

### 4.2.3.2 XRD

Due to the small amount of powdered sample available, a standard powder XRD configuration was not possible for the rhodium containing photocatalysts, therefore a capillary XRD set-up was used to characterise the crystalline nature of the samples. As shown by the X-ray diffractogram of the unmodified P25 coating glancing angle XRD was not a feasible option due to the low intensities recorded (see Figure 4.2.).

For comparison purposes a diffractogram from unmodified P25 dried at 70°C was collected using the capillary configuration (figure 4.16. (A)). Although the signal

to noise ratio from this data was noticeably worse than for the bulk powder X-ray diffractograms, quantification of the data yielded comparable values of crystallite size and phase composition to those calculated using the bulk powder X-ray diffraction data (table 4.15.).

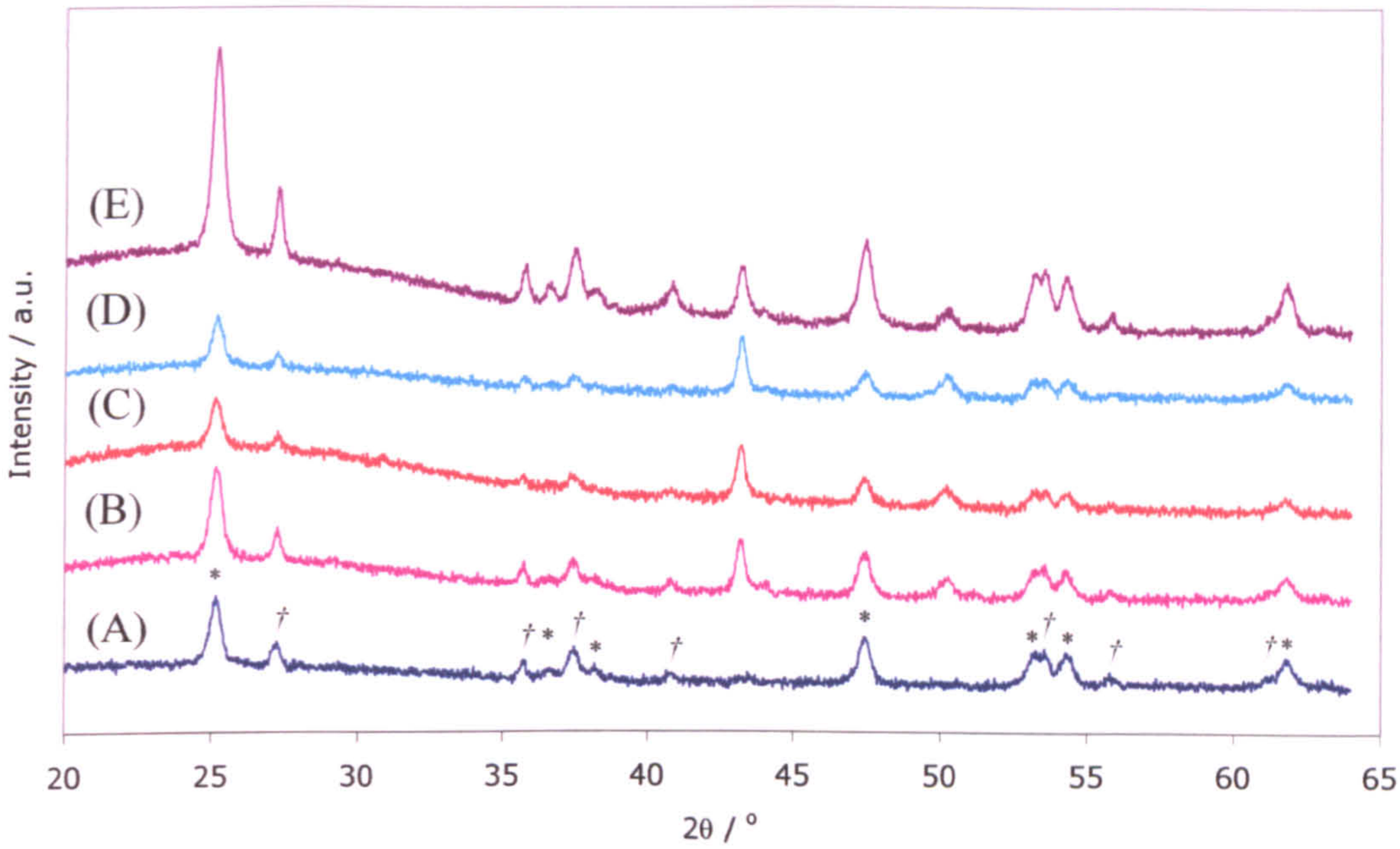


*Figure 4.16. Capillary X-ray diffractograms for P25 (A) and 5Rh-P25 dried at 70°C (B), calcined at 200°C (C), UV reduced (D) and hydrogen reduced(E). Reflections due to anatase and rutile are indicated by the symbols * and † respectively.*

| Photocatalyst | Percentage of Rutile / vol. % | Crystallite size / nm | |
|---|---|---|---|
| | | Anatase | Rutile |
| P25 dried at 70°C | 23.1 | 27.9 | 57.2 |
| 5Rh-P25 dried at 70°C | 22.5 | 26.8 | 62.8 |
| 5Rh-P25 calcined at 200°C | 20.5 | 24.2 | 61.2 |
| 5Rh-P25 / UV reduced | 22.4 | 27.6 | 57.4 |
| 5Rh-P25 / hydrogen reduced | 21.4 | 29.2 | 57.9 |

*Table 4.15. Phase compositions and crystallite sizes for P25 and 5Rh-P25 samples, calculated from capillary XRD data.*

No reflections arising from any rhodium containing species were observed for any of the 5Rh-P25 photocatalysts (figure 4.16. (B-E)). The reflections observed were attributable to either anatase or rutile. However, the two reflections observed at

43.2° and 50.2° in the rhodium modified photocatalysts could not be assigned to any $TiO_2$ phases or any Rh containing species. Standard powder XRD of 5Rh-P25 photocatalyst dried at 70°C did not contain these two peaks observed in the X-ray diffractogram collected using the capillary set-up, it was therefore assumed these two peaks were due to experimental error.

#### 4.2.3.3 TEM

TEM micrographs of both 1Rh-P25 and 5Rh-P25 photocatalysts that had been calcined at 70°C and 200°C were similar to the corresponding micrographs for unmodified P25 calcined at the same temperatures. No rhodium containing particles could be resolved, although EDX analysis confirmed the presence of rhodium species distributed evenly over the P25 support. As with the XRD analysis, no rhodium species could be detected for any of the 0.1Rh-P25 photocatalysts.

Figure 4.17 (A) shows a TEM micrograph of 1Rh-P25 that had been subjected to hydrogen reduction, and although no individual Rh particles were resolved, EDX analysis confirmed the presence of rhodium. The micrographs obtained from 5Rh-P25 that had been subjected to UV and hydrogen reductions showed small spherical particles (figure 4.17 (B) and (C) respectively). The particles formed from the UV reduction treatment were smaller than those formed during the hydrogen reduction at 450°C. Indexing selected area diffraction patterns indicated only the presence of anatase and rutile for all the Rh-P25 systems. This is as expected due to the low volume concentration of rhodium species.

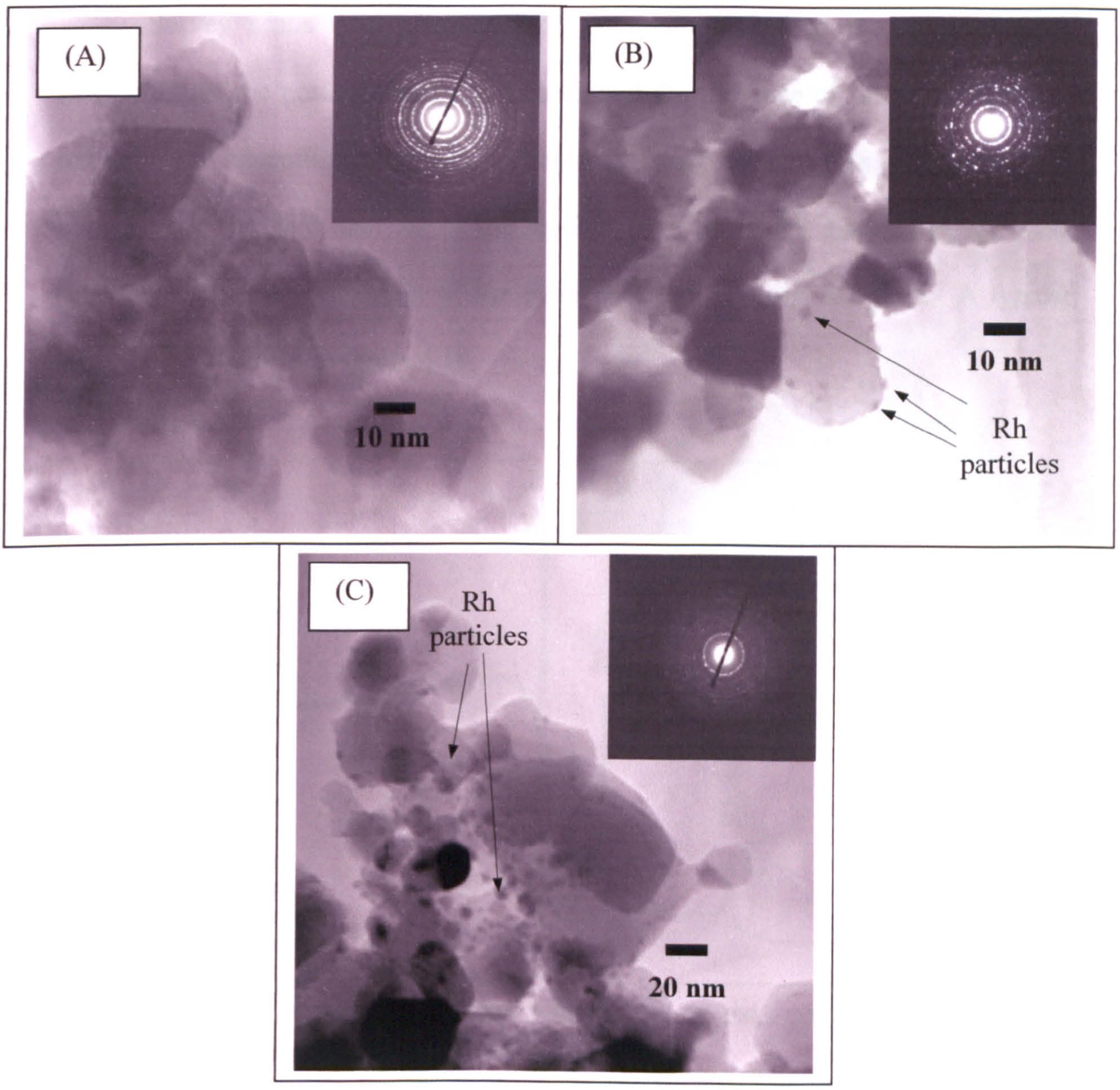


*Figure 4.17. TEM micrographs and their corresponding selected area electron diffraction patterns for 1Rh-P25 hydrogen reduced (A), 5Rh-P25 UV reduced (B) and 5Rh-P25 hydrogen reduced (C).*

### 4.2.3.4 XPS

XPS analysis of the 0.1Rh-P25 coatings did not show any peaks arising from rhodium species, as the rhodium loading was below the detection limits for the spectrometer used. Therefore the nature of the rhodium species in these photocatalysts was inferred from the data obtained for the 1Rh-P25 and 5Rh-P25 systems.

Survey scans from the 1Rh-P25 systems all showed the same features (regardless of the pretreatments), that confirmed the presence of rhodium, titanium, oxygen and adventitious carbon. However, many other peaks were observed compared to the XPS analysis of the Ag-P25 powders. XPS analysis of the glass substrate confirmed the origin of the extra peaks to be from the glass. A typical survey scan is shown in figure 4.18.

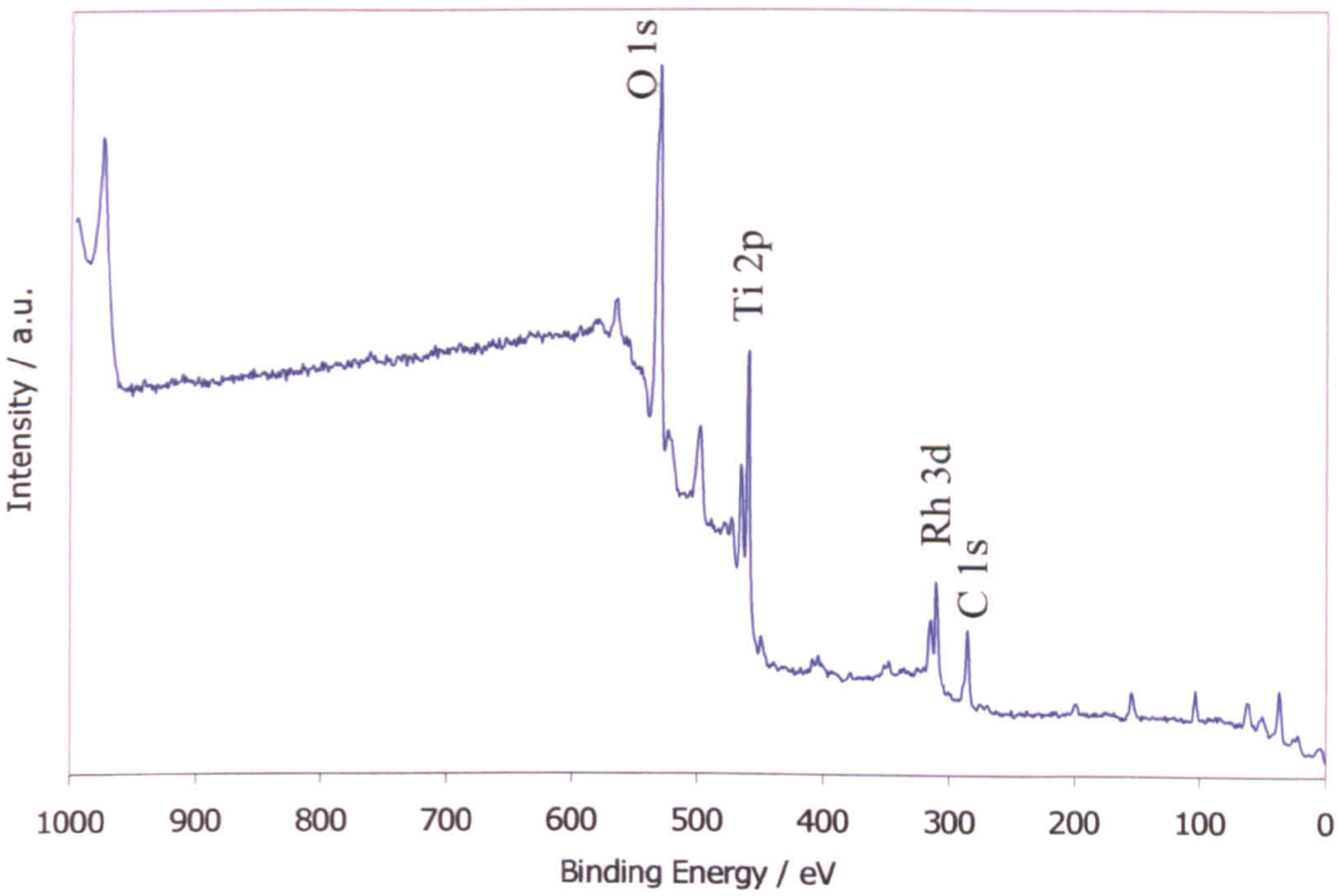


*Figure 4.18. A typical XPS wide scan for a Rh-P25 photocatalyst supported on a glass slide.*

Peak fitted high resolution scans for the Rh 3d peaks from the 1Rh-P25 samples are shown in figure 4.19. The binding energies of the Rh $3d_{5/2}$ photoelectron peaks for 1Rh-P25 photocatalysts that had been calcined at 70°C (A) and 200°C (B) were 309.5 eV and 309.6 eV respectively. Whilst, the binding energies of the Rh $3d_{5/3}$ photoelectrons for the 1Rh-P25 photocatalysts that had been subjected to UV (C) and hydrogen (D) reductions were shifted to 307.3 eV and 307.3 eV respectively, indicating a change in their chemical state. Table 4.16 presents the binding energies of

the Rh $3d_{5/2}$ photoelectrons and the FWHM of the fitted peaks for all of the 1Rh-P25 photocatalysts.

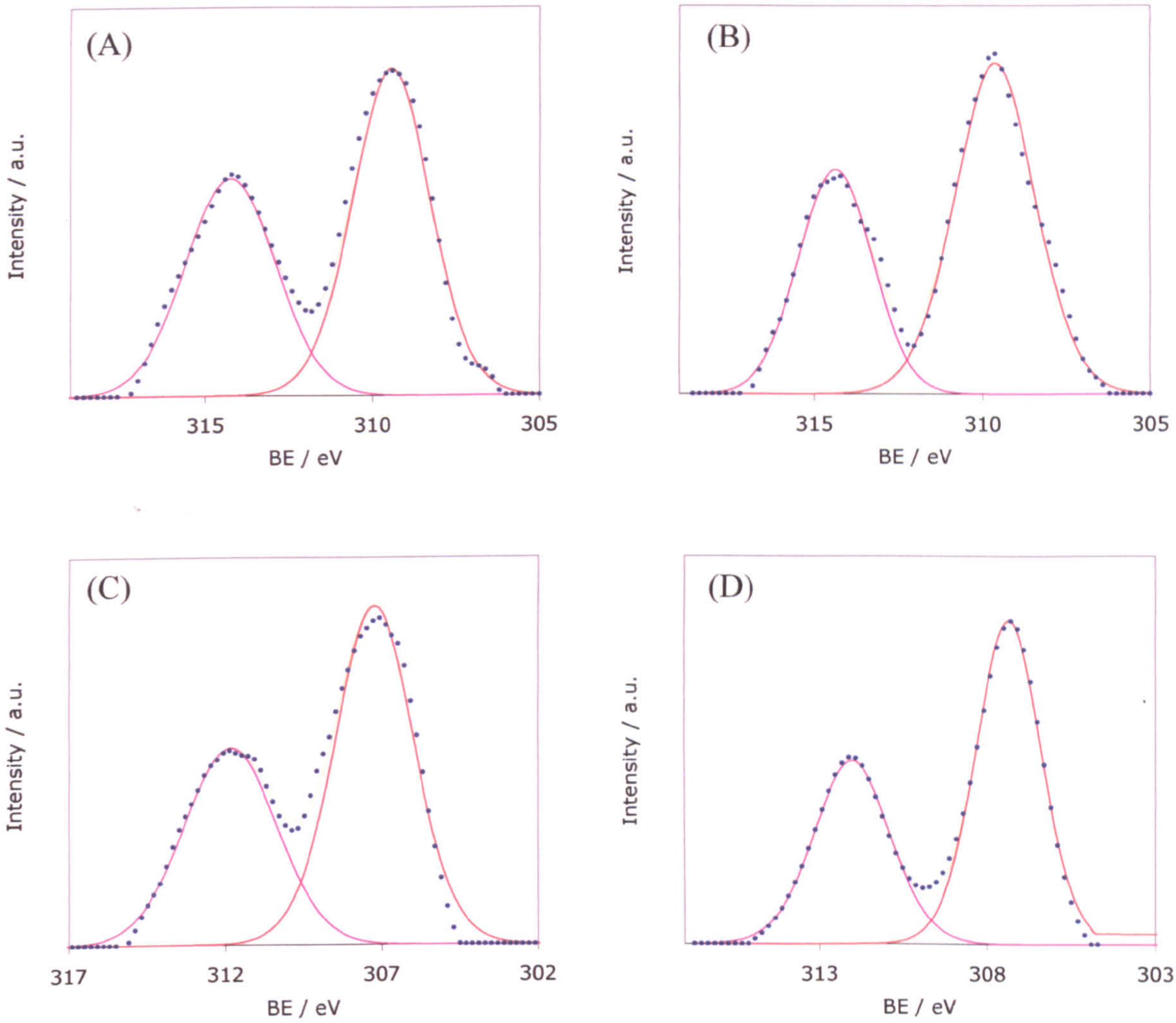


*Figure 4.19. Fitted high resolution XPS spectra of Rh 3d peaks for 1Rh-P25 photocatalysts that had been calcined at 70°C (A), calcined at 200°C (B), UV reduced (C) and hydrogen reduced (D).*

| Pretreatment | Rh $3d_{5/2}$ peak position / eV | Rh $3d_{5/2}$ FWHM / eV |
|---|---|---|
| 1Rh-P25 dried at 70°C | 309.48 | 2.38 |
| 1Rh-P25 calcined at 200°C | 309.59 | 2.15 |
| 1Rh-P25 / UV reduced | 307.25 | 2.44 |
| 1Rh-P25 / hydrogen reduced | 307.34 | 2.08 |

*Table 4.16. Table of Rh $3d_{5/2}$ peak positions and FWHM for 1Rh-P25 photocatalysts.*

Figure 4.20 shows the peak fitted Rh 3d high resolution scans for 5Rh-P25 photocatalysts, which had been prepared using the same procedures used to pre-treat the 1Rh-P25 photocatalysts. It can clearly be seen that the same trend of a decrease in the binding energy of the Rh 3d photoelectrons for the samples that had been subjected to reducing environments, indicating that the rhodium species were reduced. The peak positions (table 4.17) after calcination at 70°C and 200°C correspond to $Rh^{3+}$ species, and after hydrogen and UV treatments the rhodium correspond to $Rh^0$.

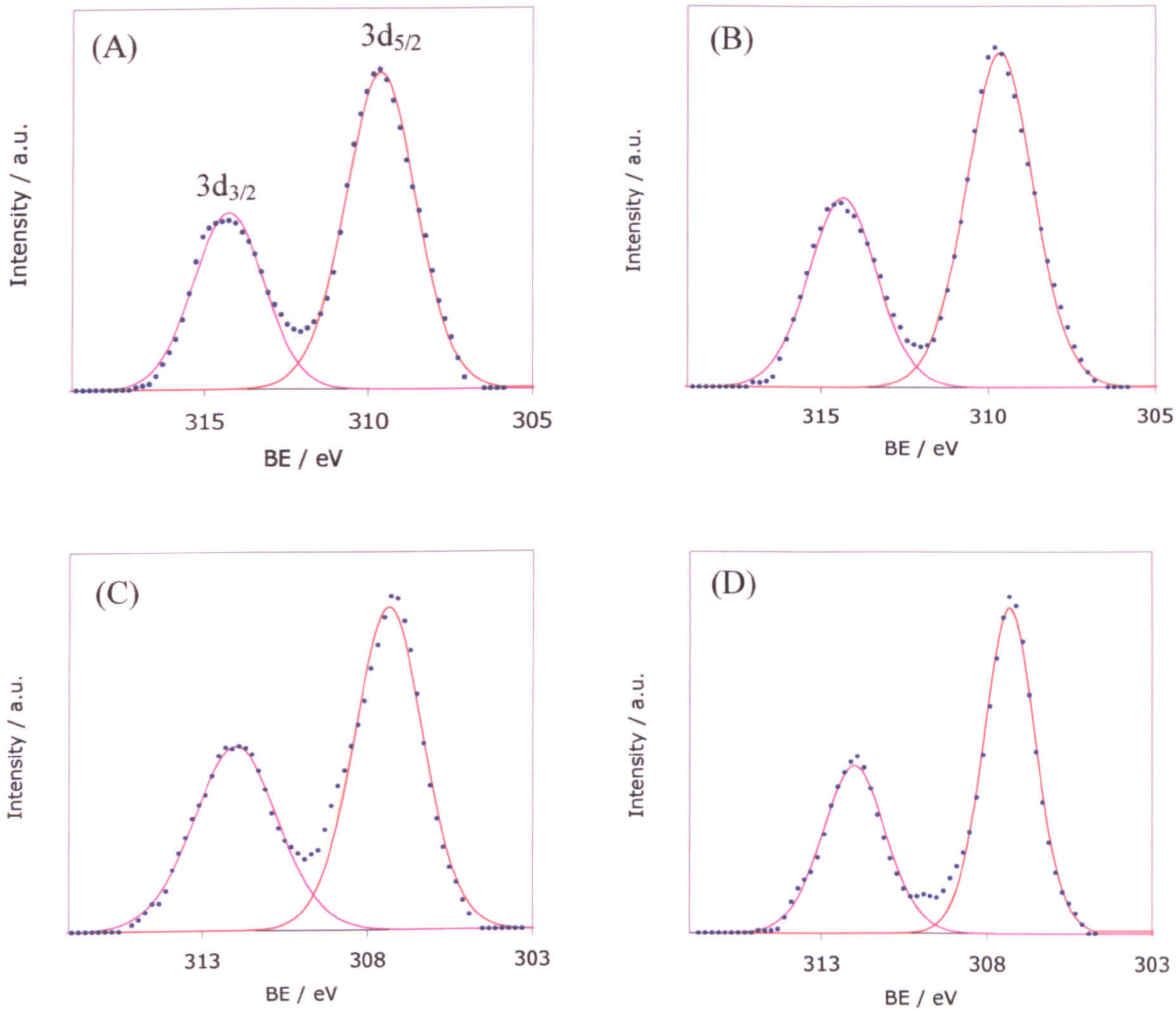


*Figure 4.20. Fitted high resolution XPS spectra of Rh 3d peaks for 5Rh-P25 photocatalysts that had been calcined at 70°C (A), calcined at 200°C (B), UV reduced (C), and hydrogen reduced (D).*

| Pretreatment | Rh $3d_{5/2}$ peak position / eV | Rh $3d_{5/2}$ FWHM / eV |
|---|---|---|
| 5Rh-P25 dried at 70°C | 309.48 | 2.73 |
| 5Rh-P25 calcined at 200°C | 309.62 | 2.77 |
| 5Rh-P25 / UV reduced | 307.28 | 2.96 |
| 5Rh-P25 / hydrogen reduced | 307.29 | 2.58 |

*Table 4.17. Table of Rh $3d_{5/2}$ peak positions and FWHM for 5Rh-P25 photocatalysts.*

## 4.3 Discussion

### 4.3.1 Unmodified P25 photocatalysts

The phase transformation behaviour observed from the XRD analysis of unmodified P25 photocatalysts calcined at temperatures of up to 600°C are in agreement with results published by Zegaoui,[11] in that there was no anatase-to-rutile phase transformation at temperatures up to 600°C. The phase transformation observed at 600°C for P25 in the work reported in this thesis has not been reported elsewhere, however, very similar trends have been reported for P25 calcined at 700°C for increasing time periods.[12] It was shown that as the calcination time increased the percentage rutile present increased from 31 wt. % (29 vol. %) to 51 wt. % (48.8 vol. %) after 3 h and 6 h respectively. After 96 h only a rutile phase was detected.

A conclusion that can be drawn by combining the results presented here and those reported in the literature[11] is that the temperature range for the phase transformation of anatase-to-rutile for P25 was at least over the range 450-700°C. Similar temperature ranges for the anatase-to-rutile phase transformation have been reported for sol-gel prepared titanias.[13,14] Further work investigating the precise values for the phase transformation temperature range is beyond the scope of this thesis as increasing the amount of rutile phase present is not beneficial for photocatalysts.

TEM analysis of the same unmodified P25 samples confirmed the results obtained from XRD analysis, in that the only $TiO_2$ phases detected were anatase and rutile. However, in contradiction to the results from XRD analysis, measurements of the particle sizes from the TEM micrographs did not reveal any significant particle growth for the sample that had been calcined at 600°C for 2 h. This can be explained

by the differing natures of the two techniques, for XRD analysis the calculated crystallite sizes are an average from a relatively large volume of material, whilst TEM analysis utilises a limited amount of sample and may not always give a representative portrayal of the sample.

From the XPS wide scans of the unmodified P25 photocatalysts calcined in the temperature range of 70°C-600°C, the value of the weight percentage of oxygen relative to titanium (41 wt. %) was very close to the theoretical value for stoichiometric $TiO_2$ (40.5 wt. % oxygen), indicating the XPS peaks observed for Ti and O originated entirely from $TiO_2$ and not from other sources.

The stability of the Ti $2p_{3/2}$ peak position after varying calcination temperatures can be explained as the crystal structures of anatase and rutile phases of $TiO_2$ are chemically very similar, therefore it can be expected that no shift in the Ti $2p_{3/2}$ peak position would be detected irrespective of the phase composition. Confirmation of this is found from the XPS studies conducted by Noda *et al.*[15]. It was shown that the Ti $2p_{3/2}$ binding energy was identical in anatase and rutile titanias. Due to the reproducibility of the Ti photoelectron peak positions for P25, the XPS data for the transition metal modified P25 systems were charge corrected using the Ti $2p_{3/2}$ peak at 459.0 eV. For these systems charge correction in this manner was more reliable than using the broad C 1s peaks, as the C 1s peak shape varied from sample to sample.

From the DSC experiments of P25 dispersed in TDW and acidified ($HNO_3$) TDW, it was proposed that the endotherms observed at 65-125°C and 200-410°C were due to the removal of molecular water from the surface of P25 and the removal of surface bound hydroxyl groups respectively, as these features were apparent for both the sample that was dispersed in TDW and the one dispersed in acidified TDW. The

exothermic reaction at 214°C was only observed for the sample that had been dispersed in acidified P25, therefore the reaction involved nitrate groups on the surface of P25 and was most probably due to their decomposition. As could be expected, all of the above processes resulted in a weight loss of the samples (Table 4.5).

During the second DSC cycle of sample (A) (Figure 4.7(B)) the weight loss was attributed to removal of more hydroxyl groups from the surface. It could, therefore, be expected that the surface density of molecular water and hydroxyl groups on the P25 surfaces decreased as the pretreatment temperature was increased.

The assignment of the weight loss in the DSC experiments to the removal of water and hydroxyl groups from the P25 surface was in agreement with FTIR studies conducted by Suda and Morimoto[16] on rutile phase $TiO_2$ that had been exposed to saturated water vapour at room temperature and then degassed *insitu* at various temperatures. After degassing at 25°C, four absorption bands were observed at 3660, 3520, ~3400, and 1625 $cm^{-1}$, and the bands were assigned to the OH stretching vibrations of free OH groups, hydrogen-bonded OH groups, surface adsorbed molecular water and to the bending vibration of the molecular water, respectively. After treatment at 100°C the bands due to molecular water were still present, but somewhat reduced in intensity. Whilst at 150°C the band at 1625 $cm^{-1}$ disappeared completely indicating the complete removal of molecular water from the rutile surface. With increasing temperature the intensity of the band at 3400 $cm^{-1}$ decreased at the same rate as the band at 1625 $cm^{-1}$, although a weak absorption band at 3370 $cm^{-1}$ was seen after degassing at temperatures above 150°C. This band was assigned to the presence of the hydrogen bonded OH groups. The intensity of the band at 3660 $cm^{-1}$ did not decrease until degassing at temperatures above 150°C.

Increasing the treatment temperature caused a further reduction in the intensity of the band, until reaching 600°C, where no absorption bands were seen for any surface bound hydroxyls or molecular water species. Similar studies by Tanaka *et al.*[2] on anatase phase $TiO_2$ showed the same trend of decreasing surface density of free hydroxyl groups as the degassing temperature was increased. However, OH groups bound to anatase surfaces were more stable as weak adsorption bands were still detected even after pretreatment temperatures as high as 800°C. An explanation of the similar trends for both anatase and rutile phases is that the two polymorphs have similar local surface structures.[17]

### 4.3.2 Silver modified P25 photocatalysts.

As shown in figure 4.21, the anatase-to-rutile phase transformation behaviour of P25 was altered when modified with silver loadings of greater than 0.1 wt. %. When a silver loading of 1 wt. % was used there were no significant phase changes below 600°C, but when it was calcined at 600°C for 2 h the percentage of rutile present increased to 31.5 %, compared to 28 % for unmodified P25 calcined at 600°C. This effect became more pronounced when the silver loading was increased to 5 wt. % and the percentage rutile was 47 % at 600°C. The higher silver loading also had the effect of reducing the onset temperature of the anatase-to-rutile phase transformation and an increased rutile percentage (26 %) was observed at 450°C. This showed that the presence of silver at loadings of 1 wt. % or higher increased the rate of the anatase-to-rutile transformation at 600°C, whereas loadings of 0.1 wt. % Ag did not alter the kinetics of the phase transformation at temperatures up to 600°C.

The effect of transition metal dopants on the anatase-to-rutile phase transformation kinetics has been reported in the literature and it is accepted that different dopants have varying effects on the phase transformation. For example it has been reported that additions of Nb[18], Cr[18], Si[18], Fe[18], Ag[4], Cu[1] and Ni[1] accelerate the anatase-to-rutile transformation, whilst additions of La[1], Mo[19], Co[19] and W[10] inhibit the transformation. Chao *et al.*[4] reported that addition of silver promoted the anatase-to-rutile transformation and the higher the concentration of silver, the lower the onset temperature of the phase transformation. This trend is similar to those observed for the Ag-P25 systems studied in this thesis. Chao *et al.* proposed the reason for the promotion of the anatase-to-rutile transformation in the presence of silver was due to the increased number of oxygen vacancies present. The presence of oxygen vacancies aids lattice diffusions, thus lowering the kinetic barrier for phase transformations.

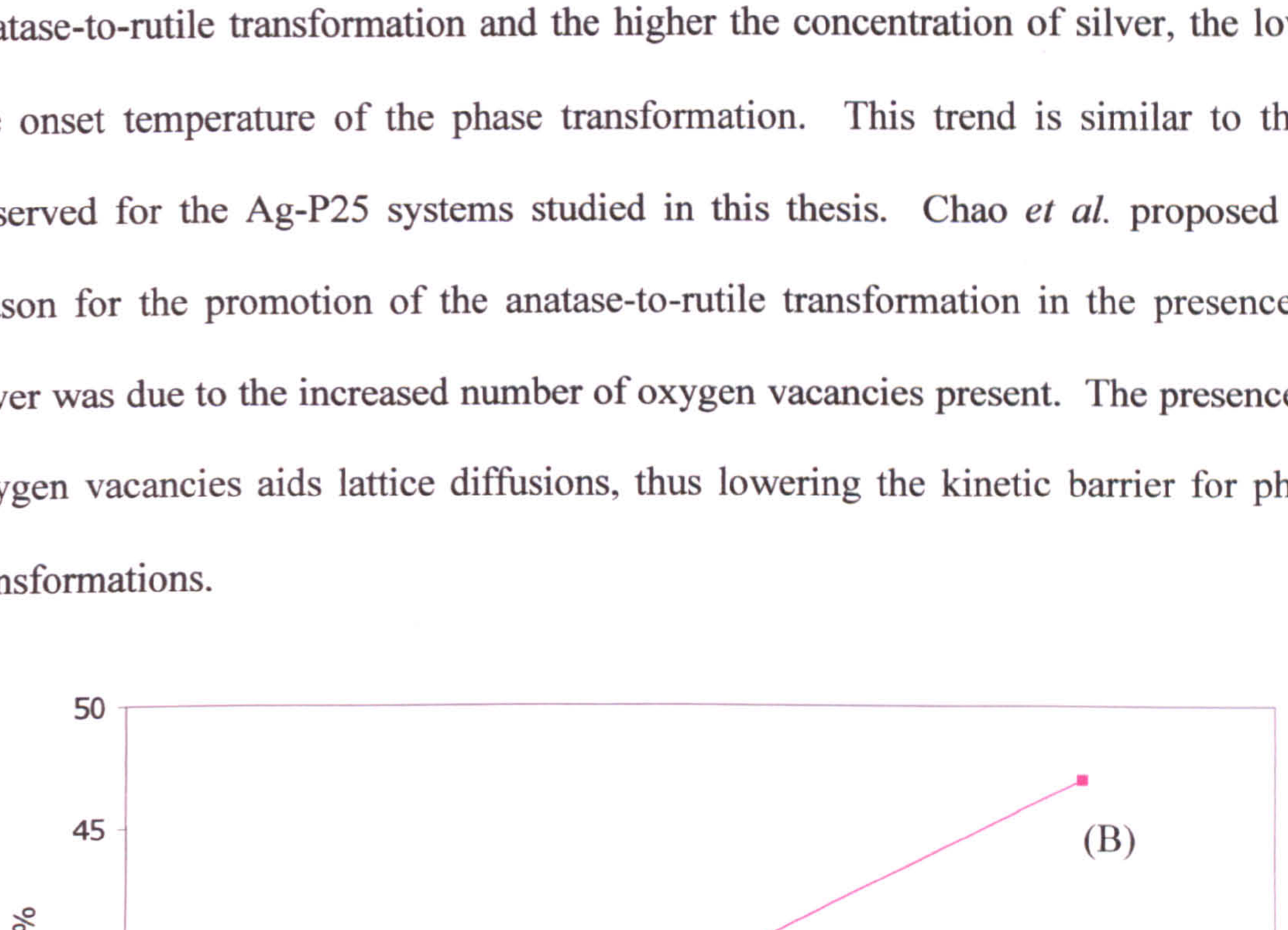


*Figure 4.21. Effect of silver loading on the percentage rutile present for Ag-P25 samples calcined at 450°C (A) and 600°C (B).*

Also apparent from the XRD patterns of the 0.1Ag-P25 and 1Ag-P25 systems was the absence of any reflections from silver containing phases. This was not unexpected as the silver concentration was below the limit for detection in XRD analysis. However a loading of 5 wt. % was sufficiently high so that the silver phases could be analysed using XRD. At low calcination temperature the predominate silver phase was silver nitrate, although the decreasing relative intensity of the reflections indicated that the crystalline silver nitrate decomposed with increasing calcination temperature, until at 450°C no reflections due to any silver phases were detected. Silver was not removed from the P25 as metallic silver reflections were present in the X-ray diffractogram for the sample calcined at 600°C. Therefore, at 450°C, the silver was present as either $Ag^0$, $Ag^+$ species (or both) but the particle sizes were too small to be detected using X-ray diffraction. Increasing the calcination temperature to 600°C would induce the growth of the silver particles and hence they became visible in the X-ray diffraction pattern.

TEM analysis confirmed the P25 grain growth observed in the XRD data for the 5Ag-P25 photocatalyst calcined at 600°C, Figure 4.3 showed larger $TiO_2$ particles and the corresponding selected area diffraction pattern being less diffuse, indicated a more crystalline structure. EDX analysis of the 5Ag-P25 photocatalyst calcined at 450°C confirmed the presence of silver species all over the $TiO_2$ surface, but no silver containing particles were resolved, adding further evidence to the above hypothesis that after calcination at 450°C the silver species present (either $Ag^0$ or $Ag^+$) were very much nanocrystalline (i.e. < 1 nm in diameter). It is thought that the small spherical particles observed in the micrographs of 1Ag-P25 and 5Ag-P25 systems calcined at 600°C were metallic silver (n.b. metallic silver diffractions were observed in the XRD of 5Ag-P25 calcined at 600°C). However, the corresponding selected area diffraction

patterns did not contain any diffractions from silver species, and therefore it cannot be conclusively said that the particles were metallic silver. The absence of any diffractions from silver species was expected due to the low volume concentration of silver.

The XPS analysis of the standard silver compounds showed that binding energies of the Ag $3d_{5/2}$ photoelectrons in $AgNO_3$, $Ag_2O$ and Ag metal were 368.9 eV, 368.4 eV and 368.1 eV, respectively. The increased broadness of the Ag $3d_{5/2}$ photoelectrons peaks for $Ag_2O$ and $AgNO_3$ compared to the metallic Ag sample could be due to a number of factors including the degree of crystallinity, the number of different silver sites in the structure and charging effects which are inherent for all non-metallic materials studied using XPS. It is thought that the charging effect contributes the most to the peak broadening in the $Ag_2O$ and $AgNO_3$ samples. For a more detailed discussion on peak broadening effects the reader is referred to the literature by Briggs and Seah.[20]

The two fitted components for the metallic silver standard at 368.1 eV and 368.2 eV were assigned to photoelectrons from metallic silver and a silver oxide over layer, respectively. The reason for the variation of the peak position and FWHM of the peak arising from the oxide layer compared to standard $Ag_2O$ studied was most probably because it was a less well ordered oxide that formed on the metal surface.

The absence of a nitrogen photoelectron peak from any of the silver containing samples dried at 70°C (XRD analysis showed that silver nitrate was present for the 5Ag-P25 samples) was most probably due to the low sensitivity of N atoms to XPS analysis.[20] Therefore, using the data from the XRD analysis, the Ag $3d_{5/2}$ peak at 368.3 eV, observed for both 1Ag-P25 and 5Ag-P25 samples calcined at temperatures up to 200°C, was tentatively assigned to the photoelectrons emitted from $AgNO_3$

species, even though the binding energy was slightly lower than that for the silver nitrate standard (368.9 eV). The reason for the shift observed was not due to the silver species not existing as silver nitrate, but due to the nature of the Ag-P25 system. When two materials are in contact, equalisation of their Fermi level occurs,[17] which would effect the energy of the photoelectrons emitted. Another possible reason for the shift could be particle size effects. The silver nitrate standard was analysed as bulk material with a large crystallite size, whereas the silver nitrate on the surface of P25 was present as much smaller particles (as shown by TEM imaging), and hence there would be a higher percentage of surface atoms, which have a slightly different chemical environment to the bulk atoms, resulting in a shift in the energy of the photoelectrons emitted.

At the higher calcination temperatures of 450°C and 600°C, there were significant amounts of $Ag^0$ present in both the 1Ag-P25 and 5Ag-P25 systems. It can be expected that $Ag_2O$ was present on the metal surface (as with the metallic silver standard), and this would contribute to $Ag^+$ peaks. Due to the small difference in chemical shift observed for both types of $Ag^+$ species ($AgNO_3$ and $Ag_2O$) it was impossible to resolve the two peaks for the silver modified P25 samples. After calcination of the 5Ag-P25 system at 600°C the silver species present was predominantly metallic, so the $Ag^+$ peak was assigned to be due to a surface oxide layer on the metal clusters, with the possibility of only a minor contribution from silver nitrate species. It should also be noted that no change was observed in the shape of the O 1s peak as the concentration of silver oxide present was insignificant relative to the levels of oxygen detected from $TiO_2$.

The percentage of $Ag^0$ species present relative to $Ag^+$ species was greater for the 5Ag-P25 photocatalysts (compared to the 1Ag-P25 photocatalysts) at all the

calcination temperatures investigated (figure 4.22). An explanation of this effect is based on the mechanism of supported metal particle growth. $Ag^+$ species are more likely to be reduced at $Ag^0$ sites than they are on a titania surface (i.e. grain growth verses cluster nucleation).[5] Therefore, when P25 was modified with higher loadings of silver nitrate, more $Ag^+$ species are available to be reduced at the $Ag^0$ sites, resulting in larger metallic silver particles.

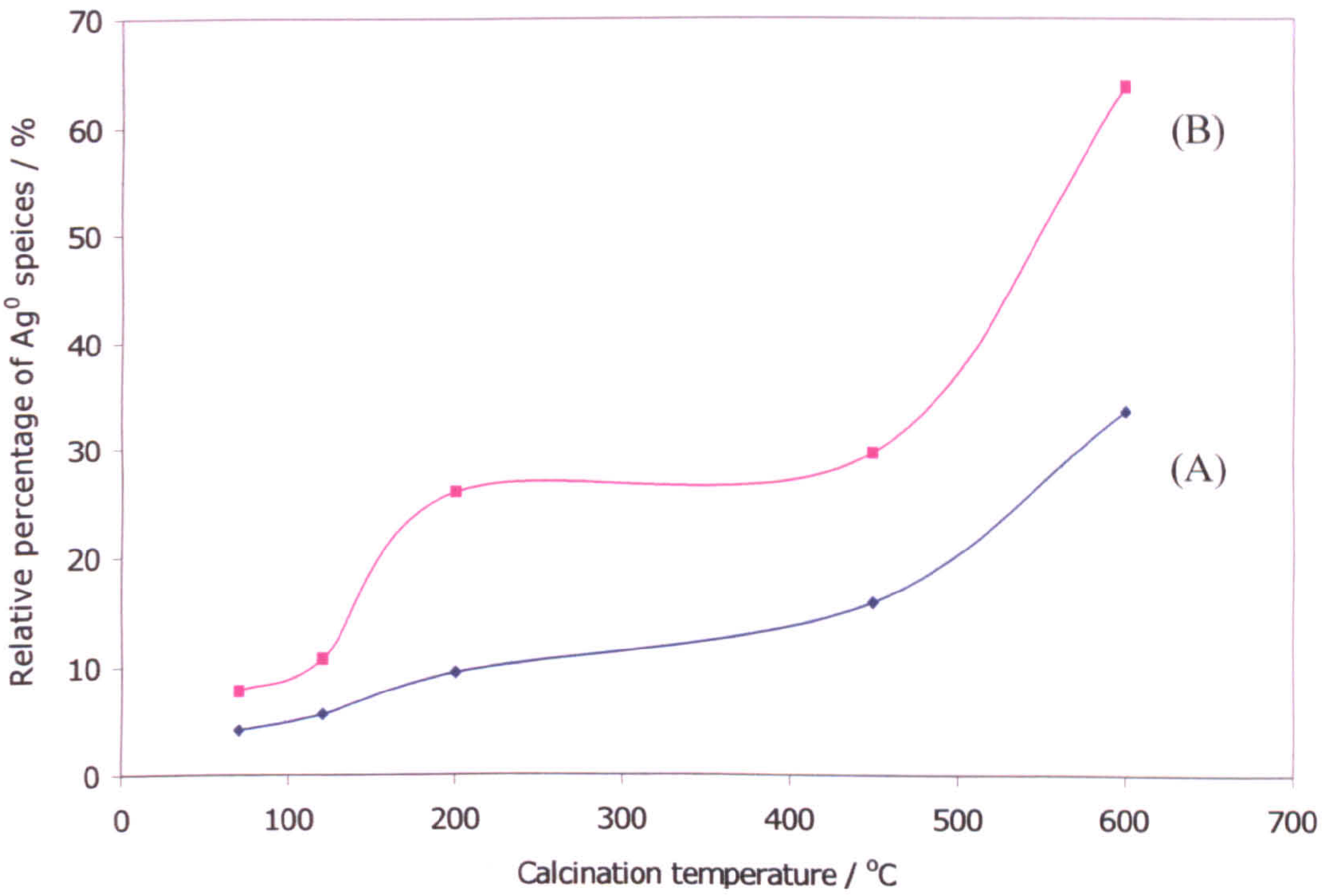


*Figure 4.22. Effect of calcination temperature on the relative percentage of $Ag^0$ species present for 1Ag-P25 photocatalysts (A) and for 5Ag-P25 photocatalysts (B).*

Quantification of the atomic percentage of surface silver species with respect to the amount of $TiO_2$ detected gives an indication of the dispersion of silver species over the P25 support.[20] The weight percent of Ag (as calculated from the XPS data) for the 5Ag-P25 photocatalyst dried at 70°C was 9.5 %, which is significantly higher than the theoretical silver loading of 5 wt. % that was used, indicating that the silver species were situated on the surface of the $TiO_2$ with a high dispersion. This effect is in agreement with the TEM results where no individual silver containing particles

were resolved, but EDX analysis showed silver to be present and evenly distributed over the photocatalyst.

With increasing calcination temperatures (up to 200°C) there was an increase in the weight percentage of silver (as detected by XPS analysis), indicating that there was an increase in the dispersion of the silver species. As shown by the peak fitting of the Ag $3d_{5/2}$ peaks, the amount of $Ag^0$ species increased with increasing calcination temperature due of the thermal reduction of $AgNO_3$. Combining this effect with the increase in percentage silver detected, indicates that the dispersion of the silver species increased upon thermal decomposition of $AgNO_3$, and that small islands of $Ag^0$ were formed with higher dispersions than the original $Ag^+$ species, as the calcination temperature was increased. At calcination temperatures of 450°C and 600°C a reduction in the XPS measured percentage silver was observed, indicating a decreased level of dispersion. This effect was due to sintering/agglomeration of the $Ag^0$ islands, resulting in lower coverage of the P25 surface by silver particles. This result is in agreement with those obtained by TEM analysis. After calcination at 600°C, individual silver containing particles were observed, and EDX analysis showed that silver was no longer present all over the P25 but was only detected from the small spherical particles.

Although XPS analysis of the silver species on the 0.1Ag-P25 photocatalysts could not be undertaken due to the low concentration of silver, the chemical nature of the silver species was inferred from the data obtained from the systems modified with greater amounts of silver. Similar behaviour to that for the 1Ag-P25 and 5Ag-P25 systems was expected to have occurred for the 0.1Ag-P25 photocatalysts, i.e. the thermal reduction of silver nitrate species forming metallic silver particles and clusters, although the level of reduction of silver nitrate would be less than was

observed for the 1Ag-P25 photocatalysts. For example the amount of thermal reduction of $AgNO_3$ would have decreased with decreasing silver loading, as shown in figure 4.22.

### 4.3.3 Rhodium modified P25 photocatalysts

The capillary XRD experiments of the 5Rh-P25 photocatalysts revealed that the addition of rhodium to P25 had no effect of the phase transformation behaviour of the P25 as the composition remained at *ca.* 20 % rutile / 80 % anatase after all of the pretreatments used. However the maximum pretreatment temperature used was only 450°C, and therefore it cannot be said that addition of Rh could not change the phase transformation kinetics of $TiO_2$ as higher pretreatment temperatures would need to be investigated.

The absence of any reflections from rhodium containing phases suggests that they were either amorphous, or the particle sizes were below the detection limit for XRD analysis. XRD of bulk rhodium nitrate showed it to be amorphous, which would explain the absence of any reflections due to Rh phases in the diffractograms from the samples which had been pretreated at 70°C and 200°C in air. It could be expected that rhodium nitrate did not decompose at these temperatures as the samples remained yellow, which is the colour of hydrated rhodium nitrate.

In samples that had been subjected to reduction pretreatments it was expected that the rhodium nitrate would have been reduced, forming metallic rhodium.[5,7] After the reduction pretreatments the colour of the samples became grey, providing evidence for the reduction process. As no reflections due to metallic rhodium particles were observed in the X-ray diffractograms of these samples it was hypothesised that

the crystallite size for the rhodium particles was too small or their concentration was too low to be detected by XRD analysis.

It was concluded that the two un-assigned peaks, apparent in the X-ray diffractograms for all the 5Rh-P25 photocatalysts, were due to instrument contamination as they were absent in the XRD pattern of a 5Rh-P25 photocatalyst dried at 70°C, which was recorded using a standard powder XRD configuration. This conclusion is further substantiated by the regularity of the peaks. Their intensities remained unaltered even though the intensity of the anatase and rutile reflections varied from sample to sample, suggesting the instrument was contaminated.

As no reflections due to rhodium containing species, nor any change to the P25 phases, were observed for the 5Rh-P25 photocatalysts after any of the pretreatments, no differences in the XRD patterns were expected for the P25 photocatalysts modified with only 0.1 and 1 wt. % Rh. Hence X-ray diffraction was not used to characterise them.

TEM analysis of the rhodium containing photocatalysts confirmed the results obtained from XRD analysis, in that no $TiO_2$ particle growth was apparent in any of the micrographs. The presence of small Rh particles (confirmed by EDX) on the surface of the $TiO_2$ particles for the 5Rh-P25 photocatalysts that had been subjected to reducing pretreatments supports the theory that rhodium nitrate was reduced to metallic rhodium. It was thought that the particles formed after hydrogen reduction were larger than those formed during UV reduction because during the hydrogen reduction the temperature was increased to 450°C, resulting in a higher mobility of Rh atoms on the $TiO_2$ surface than for the UV reductions where the temperature was *ca.* 50°C. Therefore, more sintering of the Rh particles could occur during the hydrogen reduction and hence larger particles resulted than for the UV reduction. As

for the Ag-P25 systems, no diffractions were observed from the modifying element (Rh) in the selected area diffraction patterns for any of the Rh-P25 systems. Again, this was due to their low volume concentration.

High resolution XPS spectra of the Rh 3d photoelectron peaks from 1Rh-P25 and 5Rh-P25 systems showed that the peak shapes of the Rh 3d peaks were not symmetrical like the Ag 3d peaks. They were asymmetrically broadened towards higher binding energies. This effect, known as valence band shake-up, is caused by the different arrangement of the electron bands for the elements studied. It is most pronounced for transition metals which have an unpaired electron in the 3d shell. Hence, silver (a $3d^{10}$ system) does not exhibit shake-up losses whilst rhodium (a $3d^{9}$ system) does.[21]

Also apparent from the high resolution scan was that the Rh 3d peaks were broader than those of the silver Ag 3d peaks (table 4.17). There are two reasons for this effect. Firstly the X-ray source used for XPS analysis of the silver containing compounds was monochromatic, whist a non-monochromatic source was used in the analysis of the Rh-P25 photocatalysts. Secondly, the rhodium XPS was carried out on the coated glass slides, resulting in more charging of the sample than was observed for the powdered samples used for the Ag-P25 systems. These two differences combined to give a lower resolution and reduced signal-to-noise ratio. However, the lower energy resolution is not as much of a problem for the Rh-P25 systems as the chemical shift for different rhodium oxidation states is larger than for silver. The binding energies of Rh $3d_{5/2}$ photoelectrons for the different oxidation states of $Rh^{3+}$, $Rh^{+}$ and $Rh^{0}$ are 309.1 eV, 308.0 eV and 307.0 eV respectively.[5]

One component fitted the Rh $3d_{5/2}$ peak well for all of the Rh-P25 photocatalysts investigated, and the peak positions suggested that the rhodium existed

as $Rh^{3+}$ in the samples that had been pretreated at 70°C and 200°C, whilst metallic rhodium was present on the samples which had been subjected to reduction pretreatments (both UV and hydrogen reduction). Due to the poor signal-to-noise ratio, no indication of the amount of dispersion could be attained. However, the TEM results suggest that Rh was present on the surface of $TiO_2$ particles with a fairly high dispersion.

As the XPS analysis showed that the rhodium species present were the same both for the 1Rh-P25 and 5Rh-P25 systems it was expected that the rhodium species would be similar for the 0.1Rh-P25 photocatalysts, although the particle size of the metallic rhodium particle would be smaller than those formed in the 1Rh-P25 system.

## 4.4 Conclusions

XRD and TEM analysis of unmodified P25 showed that 2 h calcinations at temperatures up to 600°C did not result in a significant change in the composition of the $TiO_2$ phases and the original composition of *ca.* 20 % anatase / 80 % rutile was maintained. DSC analysis of P25 powders led to the conclusion that as the calcination temperature was increased, the density of surface bound hydroxyl groups decreased.

XRD and TEM analysis of the Ag-P25 systems showed that the presence of silver reduced the onset temperature and increased the rate of the anatase-to-rutile phase transformation. For the 5Ag-P25 photocatalyst, the percentage of rutile present after calcination at 600°C for 2 h was 47 %. XRD analysis also showed that crystalline silver nitrate was present on the 5Ag-P25 photocatalyst after pretreatment at temperatures of up to 200°C, although the amount decreased with increasing calcination temperature. After calcination at 600°C, reflections were

observed that confirmed the presence of metallic silver, therefore it was concluded that silver nitrate was thermally reduced, forming metallic silver.

XPS analysis of the 1Ag-P25 and 5Ag-P25 photocatalysts showed that for each of the calcination temperatures used both $Ag^+$ and $Ag^0$ were present and that the amount of $Ag^0$ (relative to the amount of $Ag^+$) increased with increasing calcination temperature adding further evidence that silver nitrate was thermally reduced to metallic silver. It was also found that increasing the silver loading resulted in a higher percentage of $Ag^0$ species for each of the calcination temperatures used. Comparison of these results to those obtained from silver standards (Ag, $Ag_2O$ and $AgNO_3$) led to the conclusion that the $Ag^+$ component of the Ag 3d photoelectron peak was actually the sum of contributions from $Ag_2O$ and $AgNO_3$, however, due to the small difference in chemical shift for these compounds deconvolution of the separate components was not possible.

XRD analysis of the 5Rh-P25 photocatalysts did not reveal any reflections due to rhodium containing phases and therefore no information concerning these phases could be obtained from the data. However, it was shown that the presence of rhodium had no effect on the P25 phase transformation kinetics at temperatures up to 450°C. The XPS peak positions of Rh $3d_{5/2}$ indicated that the rhodium existed as $Rh^{3+}$ in the samples that were pretreated at 70°C and 200°C, whilst metallic rhodium was present for the samples which had been subjected to reduction pretreatments (both UV and hydrogen reduction).

## 4.5 References


(1) Nair, J.; Nair, P.; Mizukami, F.; Oosawa, Y.; Okubo, T. *Mater. Res. Bull.* **1999**, *34*, 1275.
(2) Tanaka, K.; White, J. M. *J. Phys. Chem.* **1982**, *86*, 4708.
(3) Negishi, N.; Takeuchi, K. *Mater. Lett.* **1999**, *38*, 150.
(4) Chao, H. E.; Yun, Y. U.; Xingfang, H. U.; Larbot, A. *J. European Ceram. Soc.* **2003**, *23*, 1457.
(5) Fernandez, A.; Gonzalezelipe, A. R. *Appl. Surf. Sci.* **1993**, *69*, 285.
(6) Herrmann, J. M.; Tahiri, H.; AitIchou, Y.; Lassaletta, G.; GonzalezElipe, A. R.; Fernandez, A. *Appl. Catal. B Environ.* **1997**, *13*, 219.
(7) Munoz, A.; Munuera, G.; Malet, P.; Gonzalezelipe, A. R.; Espinos, J. P. *Surf. Interface Anal.* **1988**, *12*, 247.
(8) Borgarello, E.; Serpone, N.; Emo, G.; Harris, R.; Pelizzetti, E.; Minero, C. *Inorg. Chem.* **1986**, *25*, 4499.
(9) Sano, T.; Negishi, N.; Mas, D.; Takeuchi, K. *J. Catal.* **2000**, *194*, 71.
(10) Eibl, S.; Gates, B. C.; Knozinger, H. *Langmuir* **2001**, *17*, 107.
(11) Zegaoui, O.; HoangVan, C.; Karroua, M. *Appl. Catal. B Environ.* **1996**, *9*, 211.
(12) Ding, Z.; Lu, G. Q.; Greenfield, P. F. *J. Phys. Chem. B* **2000**, *104*, 4815.
(13) Wang, C. C.; Ying, J. Y. *Chem. Mat.* **1999**, *11*, 3113.
(14) Allison, F. J. Aqueous sol-gel derived titania and modified titania for biomedical application, University of Nottingham, 2002.
(15) Noda, H.; Oikawa, K.; Ogata, T.; Matsuki, K.; Kamada, H. *Nippon Kagaku Kaishi* **1986**, 1084.
(16) Suda, Y.; Morimoto, T. *Langmuir* **1987**, *3*, 786.
(17) Linsebigler, A. L.; Lu, G. Q.; Yates, J. T. *Chem. Rev.* **1995**, *95*, 735.
(18) Karvinen, S. *Solid State Sci.* **2003**, *5*, 811.
(19) Amores, J. M. G.; Escribano, V. S.; Busca, G. *J. Mater. Chem.* **1995**, *5*, 1245.
(20) Briggs, D.; Seah, M. P. *Practical Surface Analysis: Auger and X-ray Photoelectron Spectroscopy*, 2 ed.; John Wiley and Sons Ltd, 1992.
(21) Neimantsverdriet, J. W. *Spectroscopy in Catalysis*, 1st ed.; VCH,: New York, 1995.

# 5 Photocatalytic reactions over Degussa P25 photocatalysts

## 5.1 Introduction

It has been shown that photocatalysis has the potential to provide an effective method for removal of pollutants such as $NO_x$ from the atmosphere, and its application to environmental problems is attracting much interest.[1,2] Investigations into the photocatalytic activity of various semiconductors (e.g. $ZnO_2$, $TiO_2$,) have shown that the anatase phase of titanium dioxide exhibits the highest activity,[3] although the commercial $TiO_2$ photocatalyst (Degussa P25) with an 80 % anatase 20 % rutile structure also shows high activities. The band-gap of anatase phase $TiO_2$ is 3.2 eV and the oxidation and reduction potentials of the valance and conduction bands are +2.95 V and -0.25 V respectively.[4] The reduction potential of NO to $N_2$ is +3.36 V and the oxidation potential of NO to $NO_3^-$ is -0.934 V,[5] indicating that both photooxidation and photoreduction of NO are feasible reactions over $TiO_2$.

The photocatalytic decomposition of NO over $TiO_2$ has been reported in the literature with the formation of $N_2O$ as the main reaction product.[6-9] Minor reaction products reported are $N_2$, $NO_2$ and $O_2$. The only research group to have reported the selectivity of the NO photodecomposition reaction over $TiO_2$ (JRC-TIO-4 type) is that of Anpo *et al.*[10] In their papers they reported the formation of $N_2O$ and $N_2$ with no other products. Therefore, currently $TiO_2$ is not an ideal catalyst for the removal of NO from the atmosphere as $N_2O$ itself is a regulated pollutant. Tanaka *et al.* have reported that photoassisted selective catalytic reduction (photo-SCR) of NO with ammonia over $TiO_2$ was very selective towards $N_2$ formation, with only relatively

small amounts of $N_2O$ being produced.[11] A problem though with this system is that ammonia is a pollutant, and therefore unused ammonia would need to be eliminated from the exhaust gas, thus increasing the overall costs of a system.

In the area of thermal catalysis for NO reduction, CO has regularly been used as a reducing agent yielding reactions with very high selectivity for $N_2$ formation.[12,13] During the reaction CO is oxidised to $CO_2$. The use of CO as a reducing agent for NO reduction is a logical one as the two gases are both formed during combustion processes and hence are present in polluted atmospheres. The oxidation potential of CO to $CO_2$ is -0.106 V and is therefore a feasible photoreaction over $TiO_2$ as has been reported in the literature.[14] There are no reports in the literature as to the effect of CO on the selectivity of NO photoreductions over unmodified $TiO_2$.

The aim of the work reported in this chapter was to investigate the photocatalytic decomposition and reduction of NO over Degussa P25. The results from the photodecomposition of NO in Ar experiments are compared with those reported by Anpo *et al.* to contrast the activity and selectivity of the two types of $TiO_2$. The effect of photocatalyst pretreatment is also reported. The effect of CO on the activity and selectivity for NO photoreductions over P25 was investigated. Presented in 5.2.1 and 5.2.2 are the results from UV lamp emission and reproducibility experiments, respectively. The reproducible data was used in calculating errors associated with the photocatalytic activity measurements. The effect of the catalyst processing parameters for both the general decomposition and reduction reactions are reported in subsection 5.2.3. The effect of varying the gas compositions is reported in sections 5.2.4 to 5.2.6. Section 5.3 presents a detailed discussion of all the results presented in 5.2, and conclusions from these results are drawn in section 5.4. The results presented are also referred to in Chapters 6 and 7

where the effects of modifying element(s) are compared to the intrinsic photocatalytic behaviour of P25.

## 5.2 Results

### 5.2.1 UV lamp emissions

The relative intensities of the different wavelengths emitted by the UV lamp in the range 185 nm to 900 nm are shown in figure 5.1. The most intense wavelengths were produced in the visible region whilst the most intense UV wavelength was around 365 nm. It is the wavelengths of 365 nm and below that are energetic enough for band-gap excitation of $TiO_2$.[4] No wavelengths in the infrared region were detected. The intensity of 365 nm radiation at the sample surface was measured to be 9.942 mW $cm^{-2}$. Combining the measured intensity of 365 nm radiation and the relative intensities of the other wavelengths it was possible to calculate the total photon intensity at the catalyst surface (137.47 mW $cm^{-2}$) and the intensity for radiation at wavelengths less than or equal to 365 nm (22.23 mW $cm^{-2}$).

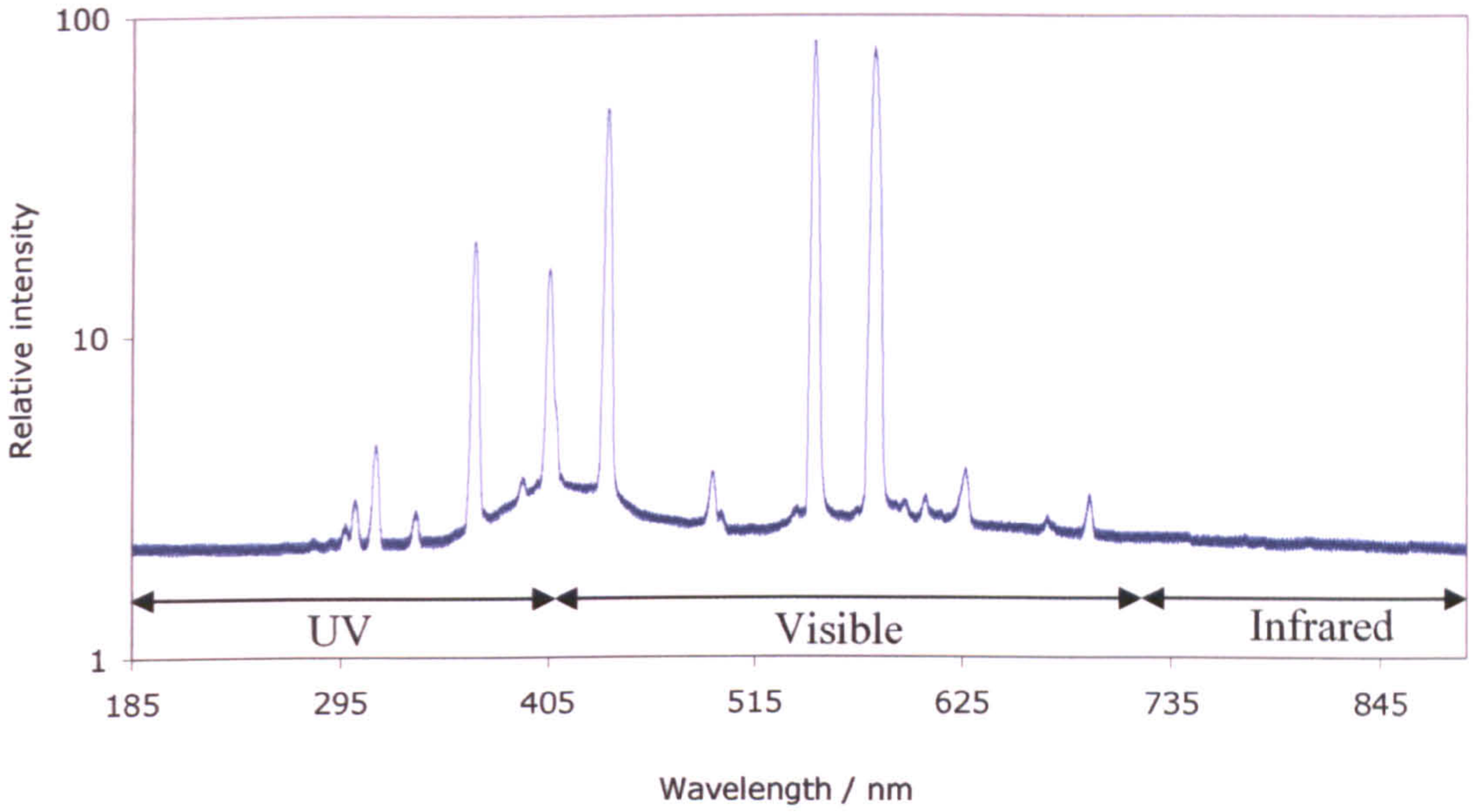


*Figure 5.1. Logarithmic plot of the measured spectral emission from a 400 W medium pressure mercury lamp.*

## 5.2.2 Reproducibility experiments

Unmodified Degussa P25 coatings were prepared and their photocatalytic behaviour was tested according to the procedures described in Chapter 3. Five unmodified P25 photocatalysts were calcined at 200°C for 2 h and their photocatalytic behaviour analysed when irradiated in a continuous gas stream containing both NO and CO. The total flow rate for the reactions was 5.5 sccm and the reactant concentration was 909 ppm and 1818 ppm for NO and CO, respectively.

| Test Number | NO Conversion / % | Rate of NO conversion / μmol $h^{-1}$ $g^{-1}$ | Selectivity for $N_2$ formation / % | Rate of $N_2$ formation / μmol $h^{-1}$ $g^{-1}$ | Rate of $N_2O$ formation / μmol $h^{-1}$ $g^{-1}$ |
|---|---|---|---|---|---|
| 1 | 16.0 | 657 | 46 | 150 | 177 |
| 2 | 15.8 | 647 | 38 | 123 | 200 |
| 3 | 20.1 | 823 | 39 | 160 | 250 |
| 4 | 17.1 | 700 | 36 | 127 | 223 |
| 5 | 18.6 | 760 | 34 | 130 | 250 |

*Table 5.1. Table of results for reproducibility experiments over P25 photocatalysts. Reaction conditions were NO: 909 ppm, CO: 1818 ppm with an Ar balance. The total flow rate was 5.5 sccm.*

The only reaction products detected using the mass spectrometer were that of $N_2$ and $N_2O$. Gaseous oxidation products of $NO_2$ were not detected in the exhaust gas, nor was any production of oxygen measured. Table 5.1 presents the results from these repeated reactions. It should be noted here that only the selectivity for $N_2$ formation is shown as the selectivity for $N_2O$ formation can be calculated simply by using the equation 100-[selectivity for $N_2$]. In the table both the percentage NO conversion and rate of use of NO are shown, as both these values will be used when discussing the results presented later in this thesis. All of the values depicted in table 5.1 show a good degree of reproducibility, indicating that it is possible to compare the results from different reactions. The errors associated with each value reported in this thesis were calculated based on these experiments and the error bars shown represent percentage error of the standard deviation for each set of results shown in table 5.1. Table 5.2 shows the magnitude of the associated errors.

| Parameter | Standard Deviation | Percentage Error / % |
|---|---|---|
| NO Conversion / % | 1.8 | ± 10.4 |
| Rate of NO conversion / μmol $h^{-1}$ $g^{-1}$ | 74 | ± 10.3 |
| Selectivity for $N_2$ formation / % | 4.6 | ± 11.8 |
| Rate of $N_2$ formation / μmol $h^{-1}$ $g^{-1}$ | 16 | ± 11.7 |
| Rate of $N_2O$ formation / μmol $h^{-1}$ $g^{-1}$ | 32 | ± 14.5 |

*Table 5.2. Table of errors associated with each measurement in the photocatalytic activity experiments.*

### 5.2.3 Effect of thermal processing

Unmodified Degussa P25 photocatalysts were calcined in the temperature range of 70°C to 600°C for 2 h and their photocatalytic behaviour was measured under both general decomposition and reduction conditions. The decomposition reactions were carried out under a gas stream at 5.5 sccm containing 909 ppm of NO. The reduction reactions were done under the same conditions but with the addition of CO at 1818 ppm. For both decomposition and reduction conditions the activity of the Degussa P25 photocatalysts decreased significantly with increasing calcination temperature (from 29.6 % to 10.5 % for decomposition reactions and from 16.0 % to 5.8 % for reduction reactions, as the calcination temperature was increased from 70°C to 600°C, table 5.3), with the catalysts showing more activity for NO conversion in the absence of CO at all calcination temperatures.

| Calcination Temperature / °C | Conversion of NO / % | | Rate of NO conversion / μmol $h^{-1}$ $g^{-1}$ | |
|---|---|---|---|---|
| | Decomposition | Reduction | Decomposition | Reduction |
| 70 | 29.6 | 16.0 | 1210 | 657 |
| 120 | 27.1 | 13.7 | 1107 | 560 |
| 200 | 24.0 | 11.4 | 983 | 467 |
| 450 | 13.4 | 6.0 | 550 | 243 |
| 600 | 10.5 | 5.8 | 430 | 240 |

*Table 5.3. Table of NO conversions for the NO decomposition and reduction reactions over P25 photocatalysts calcined at various temperatures. Decomposition conditions: NO: 909 ppm with Ar balance and a total flow rate of 5.5 sccm. Reduction conditions: As for decomposition reactions with the addition of CO at 1818 ppm.*

The selectivities for both the decomposition and reduction reactions are given in table 5.4. The selectivity for $N_2$ formation for the decomposition reactions was approximately the same at 23 % for all the catalysts calcined at temperatures up to 450°C. Increasing the calcination temperature further to 600°C resulted in a slightly

higher selectivity for $N_2$ formation of 30 %. When CO was present, the selectivity for $N_2$ formation increased, e.g. from 21 % (no CO) to 46 % for P25 dried at 70°C. As the pre-treatment temperature increased the selectivity for $N_2$ formation decreased until 450°C, where it gave comparable selectivities to those seen when no CO was present.

Due to the higher activity shown for NO conversion in the absence of CO the rate of formation of both $N_2$ and $N_2O$ was higher at all calcination temperatures for decomposition reactions compared to those performed in the presence of CO. An exception was when the photocatalysts were calcined at 70°C, where the rate of formation of $N_2$ was slightly higher under reduction conditions due to the higher selectivity shown for $N_2$ formation (Table 5.5). For example, for catalysts calcined at 200°C under decomposition conditions the rates of formation of $N_2$ and $N_2O$ were 103 μmol $h^{-1}$ $g^{-1}$ and 387 μmol $h^{-1}$ $g^{-1}$, respectively, compared to 70 μmol $h^{-1}$ $g^{-1}$ and 163 μmol $h^{-1}$ $g^{-1}$ when under reduction conditions with a CO level of 1818 ppm.

| Calcination temperature / °C | Selectivity for decomposition reactions / % | | Selectivity for reduction reactions / % | |
|---|---|---|---|---|
| | $N_2$ | $N_2O$ | $N_2$ | $N_2O$ |
| 70 | 21 | 79 | 46 | 54 |
| 120 | 25 | 75 | 49 | 51 |
| 200 | 21 | 79 | 30 | 70 |
| 450 | 26 | 74 | 26 | 74 |
| 600 | 30 | 70 | 25 | 75 |

*Table 5.4. Table of selectivities for NO decomposition and reduction reactions over P25 photocatalysts calcined at various temperatures. Decomposition conditions: NO: 909 ppm with Ar balance and a total flow rate of 5.5 sccm. Reduction conditions: As for decomposition reactions with the addition of CO at 1818 ppm.*

| Calcination Temperature / °C | Rate of $N_2$ formation / μmol $h^{-1}$ $g^{-1}$ | | Rate of $N_2O$ formation / μmol $h^{-1}$ $g^{-1}$ | |
|---|---|---|---|---|
| | Decomposition | Reduction | Decomposition | Reduction |
| 70 | 127 | 150 | 477 | 177 |
| 120 | 140 | 137 | 413 | 143 |
| 200 | 103 | 70 | 387 | 163 |
| 450 | 73 | 30 | 203 | 90 |
| 600 | 63 | 30 | 150 | 90 |

*Table 5.5. Rates of formation for the products of the photocatalytic reactions over unmodified P25 photocatalysts calcined at various temperatures. Decomposition conditions: NO: 909 ppm with Ar balance and a total flow rate of 5.5 sccm. Reduction conditions: Same as for decomposition reactions with the addition of CO at 1818 ppm.*

### 5.2.4 Effect of Varying NO concentration

To investigate the effect of NO concentration over Degussa P25, unmodified photocatalysts calcined at 200°C were used. The concentration of NO was varied from 455 ppm to 1818 ppm whilst maintaining the same total flow rate of 5.5 sccm. When present, the concentration of CO was kept constant at 1818 ppm. Table 5.6 shows that as the concentration of NO increased the percentage NO conversion decreased from 28.1 % to 21.1 % for the decomposition reactions and from 13.8 % to 7.6 % for the reduction reactions. This trend does not give an accurate portrayal of the catalytic activities when the initial NO concentration is varied (discussed in more detail below). If instead of percentage NO conversion, the rate of NO conversion was used as the measure catalyst activity, then we see a trend that increases with NO concentration for both reaction types (Table 5.6), indicating that more surface reactions occurred as the NO levels increased.

The reason why rate of NO conversion gives a good representation of catalyst activity is that it is a direct measurement of the number of surface reactions per unit mass of catalyst per unit time, and hence can used to compare the number of surface

reactions (i.e. catalytic activity) regardless of reaction conditions. Percentage NO conversion cannot be so readily used as a measure of activity for these reactions as it is dependant on the intial NO concentration. Hence percentage NO conversion can only be used as a measure of photocatalytic activity when comparing catalysts tested under identical reaction conditions as for the other photocatalytic reactions reported in the thesis.

| NO concentration / ppm | NO conversion / % | | Rate of NO conversion / μmol $h^{-1}$ $g^{-1}$ | |
|---|---|---|---|---|
| | Decomposition | Reduction | Decomposition | Reduction |
| 455 | 28.1 | 13.8 | 573 | 280 |
| 909 | 24.0 | 11.4 | 983 | 467 |
| 1818 | 21.1 | 7.6 | 1723 | 620 |

*Table 5.6. NO conversion results for decomposition and reduction reactions with varying NO levels over P25 photocatalysts calcined at 200°C. Decomposition reaction conditions: Total flow rate of 5.5 sccm. Reduction reaction conditions: Same as for decomposition reactions with a constant concentration of CO (1818 ppm).*

Within the errors associated with these results the selectivity for $N_2$ formation under decomposition conditions remained unchanged at all three NO concentrations (Table 5.7). For the reduction reactions, as the NO concentration increased from 455 ppm to 1818 ppm the selectivity to $N_2$ formation decreased from 49 % to 22 %. Under decomposition conditions the rate of $N_2$ formation increased from 83 μmol $h^{-1}$ $g^{-1}$ to 230 μmol $h^{-1}$ $g^{-1}$ as the NO concentration was increased from 455 ppm to 1818 ppm. When CO was present in the reaction gas stream, the rate of formation of $N_2$ remained nearly constant (*ca.* 70 μmol $h^{-1}$ $g^{-1}$) irrespective of the NO concentration (Table 5.8). For both reaction types the rate of formation of $N_2O$ increases with NO concentration, with the decomposition conditions being the most favourable for $N_2O$ production at all NO levels.

| NO concentration / ppm | Selectivity for decomposition reactions / % | | Selectivity for reduction reactions / % | |
|---|---|---|---|---|
| | $N_2$ | $N_2O$ | $N_2$ | $N_2O$ |
| 455 | 29 | 71 | 49 | 51 |
| 909 | 21 | 79 | 30 | 70 |
| 1818 | 27 | 73 | 22 | 78 |

*Table 5.7. Table of selectivities for NO decomposition and reduction reactions with varying NO concentrations over P25 photocatalysts calcined at 200°C. Decomposition reaction conditions: Total flow rate of 5.5 sccm. Reduction reaction conditions: Same as for decomposition reactions with a constant concentration of CO (1818 ppm).*

| NO concentration /ppm | Rate of $N_2$ formation / μmol $h^{-1}$ $g^{-1}$ | | Rate of $N_2O$ formation / μmol $h^{-1}$ $g^{-1}$ | |
|---|---|---|---|---|
| | Decomposition | Reduction | Decomposition | Reduction |
| 455 | 83 | 70 | 203 | 73 |
| 909 | 177 | 70 | 317 | 163 |
| 1818 | 230 | 67 | 630 | 243 |

*Table 5.8. Effect of NO concentration on the rates of formation of $N_2$ and $N_2O$ over P25 photocatalysts calcined at 200°C. Decomposition reaction conditions: Total flow rate of 5.5 sccm. Reduction reaction conditions: Same as for decomposition reactions with a constant concentration of CO (1818 ppm).*

### 5.2.5 Effect of varying CO concentration

The effect of CO concentration was investigated by maintaining a constant concentration of NO of 909 ppm whilst varying the CO levels from zero to 1818 ppm. The total flow rate was kept at 5.5 sccm for each experiment. The catalysts used for these experiments were films of Degussa P25 calcined at 200°C. Table 5.9 illustrates how the percentage conversion of NO decreased from 29.6 % to 8.3 % as the CO concentration increased from 0 to 1818 ppm, whilst table 5.10 shows how the selectivity for $N_2$ formation increased from 21 % when no CO was present to 55 % when the CO concentration was 909 ppm. Any further increase in CO concentration did not significantly affect $N_2$ selectivity.

| CO concentration / ppm | NO conversion / % | Rate of NO conversion / μmol $h^{-1}$ $g^{-1}$ |
|---|---|---|
| 0 | 29.6 | 1210 |
| 364 | 24.3 | 993 |
| 909 | 15.0 | 613 |
| 1818 | 8.3 | 340 |

*Table 5.9. NO conversion results for reduction reactions with varying CO levels over P25 photocatalysts calcined at 200°C. Reaction conditions: NO concentration and total flow rate were kept constant at 909 ppm and 5.5 sccm respectively.*

| CO concentration / ppm | Selectivity / % | |
|---|---|---|
| | $N_2$ | $N_2O$ |
| 0 | 21 | 79 |
| 364 | 30 | 70 |
| 909 | 55 | 45 |
| 1818 | 48 | 52 |

*Table 5.10. Selectivity results for reduction reactions with varying CO levels over P25 photocatalysts calcined at 200°C. Reaction conditions: NO concentration and total flow rate were kept constant at 909 ppm and 5.5 sccm respectively.*

The rate of formation of $N_2$ increased with CO concentration until it reached a maximum of 170 μmol $h^{-1}$ $g^{-1}$ at 909 ppm. Doubling the CO concentration up to 1818 ppm had the effect of reducing the rate of formation of $N_2$ by more than half to 80 μmol $h^{-1}$ $g^{-1}$. The rate of formation of $N_2O$ decreased from 477 μmol $h^{-1}$ $g^{-1}$ at zero CO concentration to 90 μmol $h^{-1}$ $g^{-1}$ at 1818 ppm CO concentration (table 5.11)

| CO concentration / ppm | Rate of $N_2$ formation / μmol $h^{-1}$ $g^{-1}$ | Rate of $N_2O$ formation / μmol $h^{-1}$ $g^{-1}$ |
|---|---|---|
| 0 | 127 | 477 |
| 364 | 150 | 347 |
| 909 | 170 | 137 |
| 1818 | 80 | 90 |

*Table 5.11. Effect of CO concentration on the rates of formation of $N_2$ and $N_2O$ over P25 photocatalysts calcined at 200°C. Reaction conditions: NO concentration and total flow rate were kept constant at 909 ppm and 5.5 sccm respectively.*

## 5.3 Discussion

### 5.3.1 Effect of thermal processing

Figure 5.2 clearly shows how the activities of NO conversion under both decomposition and reduction reactions follow the same trend, in that the NO conversion decreased almost linearly as the calcination temperature was increased from 70°C up to 600°C, with the percentage NO conversion being higher at all pretreatment temperatures for the decomposition reactions. Unfortunately the values for the percentage NO conversion cannot readily be compared to those reported in the relevant literature due to differences in experimental configurations and procedures.

Differences in the amount of sample irradiated and the area irradiated within the photoreactor could be accounted for and the results normalised with respect to these parameters by reporting the values in standard units of either μmol $h^{-1}$ $g^{-1}$ or μmol $h^{-1}$ $m^{-2}$. Other differences, however, are more difficult to rationalise. These include parameters such as; type of photoreactor (batch or continuous flow styles), the UV light intensity at the photocatalyst surface and the type of UV source used to initiate the photoreactions, i.e. the wavelengths used for band-gap illumination and also the thickness of the photocatalysts used as it can affect the efficiency of UV absorption.[15] It has been reported that $TiO_2$ particles absorb short wavelength UV (<300 nm) more strongly than longer wavelength UV (300-450 nm),[16] which results in a lower penetration depth for the photons and the photogenerated electron-hole pairs are formed closer to the particle surface. The migration time to the surface of the particle is therefore less when using shorter wavelength UV, resulting in fewer energy wasting recombination reactions before electron transfer takes place.

Quantification of such processes is extremely complex, making a comparison of results obtained in different laboratories difficult.

XRD and TEM characterisation of the P25 photocatalysts prepared using the same pretreatments as the P25 coating used in the photoreactor (Chapter 4) showed that there was only a small change in the crystalline nature of the $TiO_2$ even after calcination at 600°C for 2 hours. The original phase composition of *ca.* 23 vol. % rutile and 77 vol. % anatase remained largely unchanged with only small amounts of crystallite growth. These results indicate that the change in activity with calcination temperature must be due to surface structure of the photocatalysts as the bulk properties of the materials were largely unaltered by calcination up to 600°C.

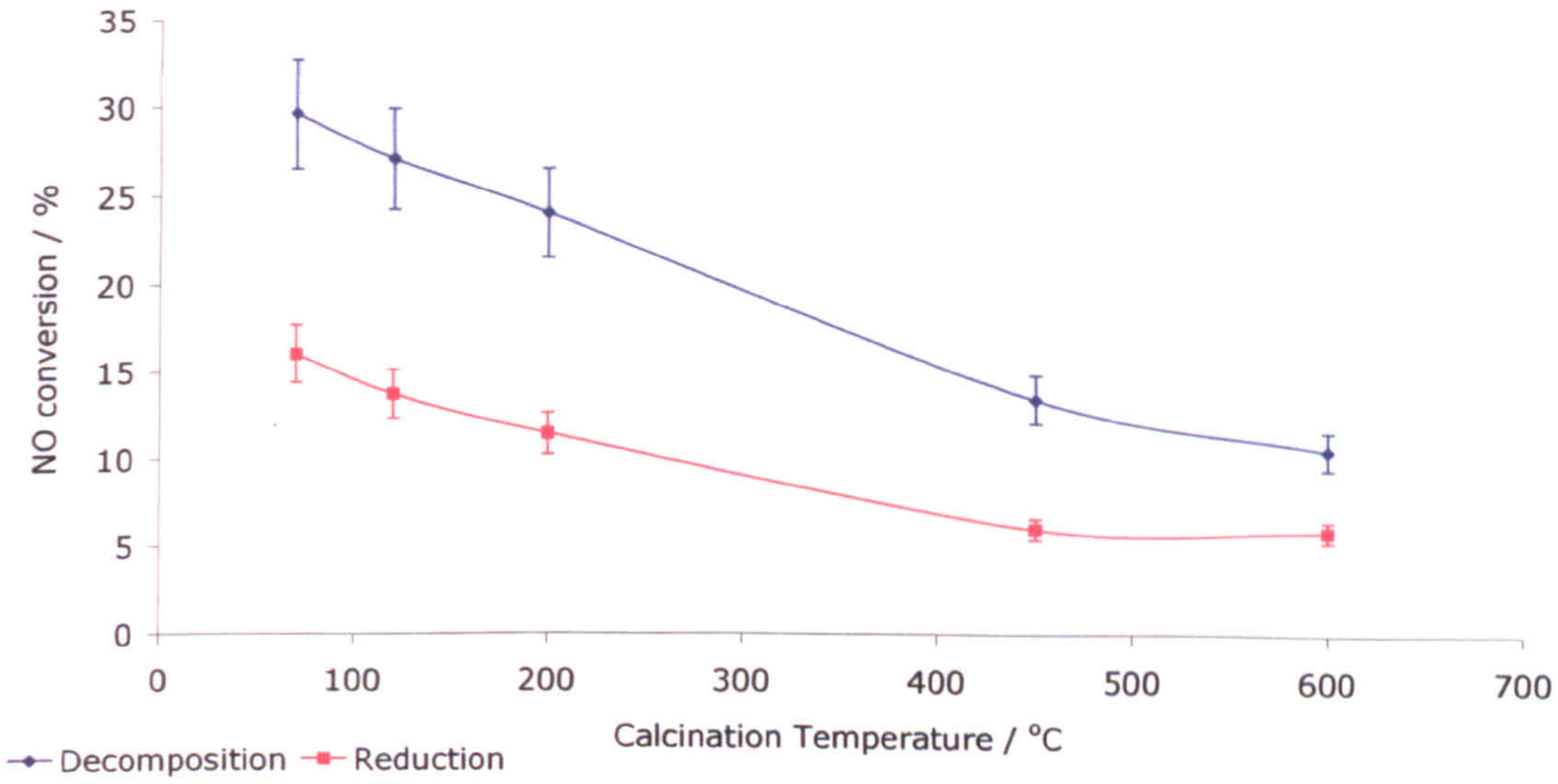


*Figure 5.2. Effect of calcination temperature on percentage conversion of NO over unmodified P25 photocatalysts. Decomposition conditions: NO: 909 ppm with Ar balance and a total flow rate of 5.5 sccm. Reduction conditions: As for decomposition reactions with the addition of CO at 1818 ppm.*

Although molecularly adsorbed water on $TiO_2$ surfaces can cause a decrease in the upwards bending of the conduction band, resulting in more efficient recombination of the photogenerated electron-hole pairs, it can also result in the formation of surface bound OH groups by reaction of $H_2O$ with the bridging oxygen

atoms.[17] It is well documented in the literature that surface bound OH groups play a vital role in a variety of photocatalytic reactions over titanium dioxide[18,19] as they act as efficient trapping sites for the photogenerated holes, thereby suppressing the energy wasting electron-hole recombination process, and yielding an increased lifetime for the photogenerated electron (the mobile charge carrier). The electron is then able to migrate to the surface of the photocatalyst particle and undergo a redox reaction with an adsorbed electron acceptor molecule. The hydroxyl radicals formed under band-gap illumination are powerful oxidants for the mineralisation of organic species in water,[19] and can themselves act as active sites for photocatalysis.

The DSC results reported in chapter 4 showed that molecular water was removed from the Degussa P25 surface in the temperature range of 80°C to 100°C. This was accompanied by a reduction in weight of the sample. On heating the sample further up to 500°C there was a further reduction in the sample mass, which was attributed to the removal of surface bound hydroxyl groups from $TiO_2$ sample. The assignment of the weight loss to the removal of molecularly bound water and surface OH groups is substantiated by FTIR studies of $TiO_2$ surfaces conducted by Suda *et al.*[20] and Tanaka.[21] From these results it was concluded that the surface density of molecular water and hydroxyl groups on the $TiO_2$ photocatalyst surfaces decreased as the pretreatment temperature was increased.

Using the results discussed above it is possible to say that the reason for the decrease in NO conversion rate seen over the Degussa P25 photocatalysts as the calcination increased was due to the decrease in the surface density of molecular water and hydroxyl groups. The decrease in the number of surface hydroxyl groups would have two effects. Firstly, more efficient electron-hole recombination would occur resulting in a decrease in the number of photogenerated electrons available for

reactions with adsorbed NO species. Secondly, OH groups can act as adsorption and/or active sites for NO molecules (although it has also been reported that NO molecules adsorb on reduced $Ti^{3+}$ surface sites[22]), thereby decreasing the number of surface OH groups would result in fewer NO molecules being adsorbed and hence fewer photoreactions. Both of these phenomena have the effect of reducing the NO conversion rate as the calcination temperature is increased. The same arguments are used to explain the decrease in NO conversion rate with increasing calcination temperature for the reactions carried out in the presence of CO. See figure 5.2 for the results of both the decomposition and reduction reactions.

The decrease in the conversion rate when CO was present can be explained in terms of the photoadsorption processes occurring on Degussa P25 during UV illumination. In the reduction experiments, CO was passed over the photocatalyst in the dark before the introduction of NO. Therefore, it might be that there was high levels of CO adsorption on the $TiO_2$ surface, which would inhibit the adsorption of the NO molecules. However, when the reverse experiment was carried out (i.e. NO passed over the catalysts before the introduction of CO), the NO conversion was the same at *ca.* 16 % over the as-dried P25 photocatalyst. Hence, the order in which NO and CO were exposed to the photocatalyst surface did not affect the outcome of the photoreaction. Therefore, it was concluded that the decrease in NO conversion in the presence of CO was due to competitive photoadsorption of CO. As a result, fewer NO molecules would be adsorbed on the $TiO_2$ surface, decreasing the total NO conversion rate.

Figure 5.3 shows that the major reaction product for the NO decomposition reactions at all the tested calcination temperatures was $N_2O$ (~75 %), with $N_2$ (~25 %) being a minor reaction product. Photocatalytic NO decompositions, in the absence of

oxygen, forming $N_2O$ as the major reaction product have been reported in the literature for various commercial $TiO_2$ photocatalysts.[6,16,23] However, the actual selectivities for the reaction products are rarely reported, usually due to limitations of the analysis method, making quantification difficult. One group that has published selectivity values for NO photodecomposition over $TiO_2$ is that of Anpo and Yamashita[24], with selectivities of 25 % and 75 % for $N_2$ and $N_2O$ respectively. These results are in close agreement to the results reported in this thesis, even though a different commercial $TiO_2$ photocatalyst with a different phase composition (100 % anatase) was used (JRC-TIO-4, produced by the Catalysis Society of Japan) and the experiments were conducted in a batch style reactor with a different initial NO concentration. It would, therefore, appear that the selectivity of NO decomposition over predominantly anatase phase $TiO_2$ surfaces will remain constant, as the same type of active sites are still available for decomposition to proceed. The effect of increasing the calcination temperature is not in altering the chemistry of the active sites available, but to reduce the surface density of them, resulting in the similar selectivities but with decreasing activity.

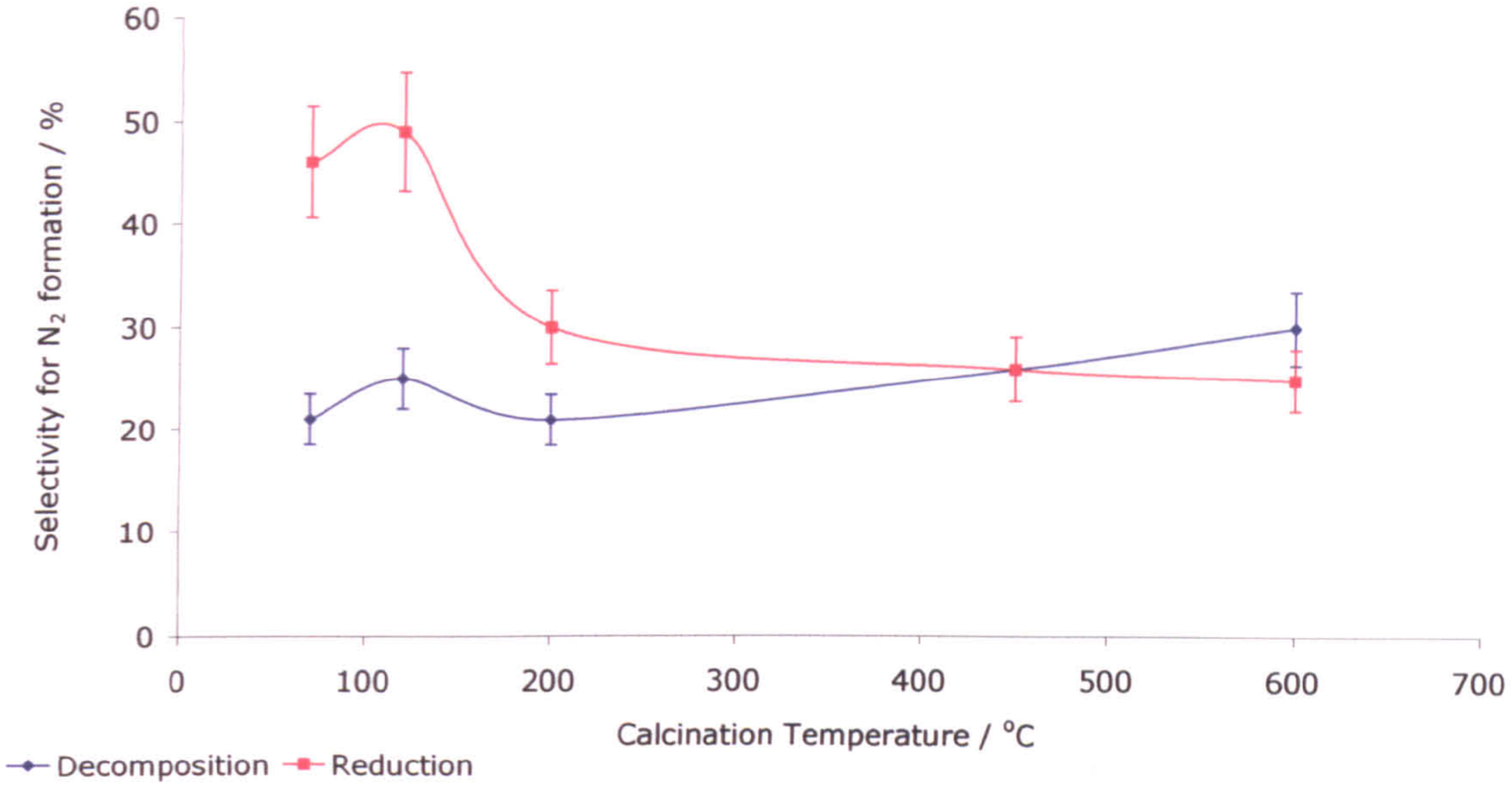


*Figure 5.3. Effect of calcination temperature on the selectivity for $N_2$ formation over unmodified P25 photocatalysts calcined at various temperatures. Decomposition conditions: NO: 909 ppm with Ar balance and a total flow rate of 5.5 sccm. Reduction conditions: As for decomposition reactions with the addition of CO at 1818 ppm.*

Reaction equations 5.1 – 5.9 represent the possible surface processes occurring during the photocatalytic decomposition and reduction of NO on $TiO_2$ surfaces. The first step for any of the reaction steps is the adsorption of NO onto the $TiO_2$ surface (5.1).

$$NO_{(g)} \longrightarrow NO_{(a)} \quad (5.1)$$

$$NO_{(a)} \longrightarrow N_{(a)} + O_{(a)} \quad (5.2)$$

$$NO_{(a)} + N_{(a)} \longrightarrow N_2O_{(a)} \quad (5.3)$$

$$NO_{(a)} + O_{(a)} \longrightarrow NO_{2(a)} \quad (5.4)$$

$$N_2O_{(a)} \longrightarrow N_2O_{(g)} \quad (5.5)$$

$$NO_{2(a)} \longrightarrow NO_{2(g)} \quad (5.6)$$

$$2N_{(a)} \longrightarrow N_{2(g)} \quad (5.7)$$

$$2NO_{(a)} \longrightarrow N_{2(g)} + O_{2(g)} \quad (5.8)$$

$$N_2O_{(a)} \longrightarrow N_{2(g)} + O_{(a)} \quad (5.9)$$

Anpo *et al.* have proposed a mechanism for the photocatalytic decomposition of NO on isolated tetrahedral $TiO_2$ species (formed within zeolites) and bulk $TiO_2$ powders.[25] On isolated tetrahedral $TiO_2$ species, two NO molecules can be adsorbed as weak ligands, which then act as reaction precursors. Absorption of a UV photon induces the formation of charge transfer excited complexes of the type $(Ti^{3+}\text{-}O^{-})^*$. Within the lifetime of the excited state, simultaneous electron transfer from the electron trapped centre ($Ti^{3+}$) into the π-antibonding orbital of NO and from the π-bonding orbital of another NO into the hole trapped centre ($O^{-}$) occurs. These rapid processes lead to the direct decomposition of two NO molecules on one active site, resulting in the formation of $N_2$ and $O_2$. In bulk $TiO_2$ powders, the photogenerated electron-hole pairs are able to migrate away from each other and towards the particle surface, resulting in a relatively large separation between the holes and electrons. This prevents the simultaneous activation of two NO molecules at the same active site, which in turn results in the formation of $N_2O$ and $NO_2$. The adsorbed decomposition products of $N_{(a)}$ and $O_{(a)}$ (5.2) migrate across the surface and react with other NO molecules on different active sites forming $N_2O$ and $NO_2$, respectively (5.3 and 5.4). The $N_2O_{(a)}$ and $NO_{2(a)}$ formed can then desorb from the surface and are released as gas phase products (5.5 and 5.6)

Using ideas developed considering the two mechanisms proposed above it is possible to understand the chemistry that occurs during NO decomposition on

Degussa P25 photocatalysts calcined at various temperatures. However, the mechanism proposed by Anpo *et al.* for the bulk powder $TiO_2$ only considers the possibility of $N_2O$ and $NO_2$ products, whilst clearly the results presented above showed only the formation of $N_2$ and $N_2O$ over P25. As the mechanism suggests that $N_{(a)}$ and $O_{(a)}$ react with $NO_{(a)}$ to form $N_2O$ or $NO_2$, then clearly it would also be possible that $N_{(a)}$ could migrate and react with another $N_{(a)}$ forming $N_2$ (5.7), although this reaction is less likely to occur due to lower concentration of $N_{(a)}$ species, hence $N_2$ is only a minor product of NO decomposition on Degussa P25.

Another possible method of $N_2$ production on powdered $TiO_2$ is via the formation of very shallow electron-hole pairs through the absorption of short wavelength UV photons, as discussed above. This could lead to the formation of localised surface charge transfer excited states, similar to those described for the mechanism on isolated $TiO_2$ species, resulting in the direct decomposition of two NO molecules at one active site, thus yielding $N_2$ and $O_2$ as reaction products (5.8). The latter mechanism described for $N_2$ formation is less likely to occur as the majority of the $TiO_2$ surface would be hydrated, or contain oxygen vacancies formed during the photocatalyst pretreatment. Another possible reaction pathway for the formation of $N_2$ is from the decomposition of $N_2O_{(a)}$ into $N_2$ and $O_{(a)}$ (5.9).[12]

When CO is present on the photocatalyst surface other reactions are possible between the adsorbed CO and NO molecules along with reactions of CO with $N_{(a)}$ and $O_{(a)}$ atoms.

$$O_{(a)} + CO_{(a)} \longrightarrow CO_{2(g)} \quad (5.10)$$

$$2NO_{(a)} + CO_{(a)} \longrightarrow N_2O_{(a)} + CO_{2(a)} \quad (5.11)$$

$$N_2O_{(a)} \longrightarrow N_2O_{(g)} \quad (5.12)$$

$$N_2O_{(a)} + CO_{(a)} \longrightarrow N_{2(g)} + CO_{2(a)} \quad (5.13)$$

$$N_{(a)} + CO \longrightarrow NCO_{(a)} \quad (5.14)$$

The presence of CO in the reaction stream can help with the formation of $N_2O$ (5.11 and 5.12). It can also act as a scavenger for $N_2O$, producing $N_2$ and $CO_2$ (5.13). As discussed earlier, in the presence of CO, NO photoadsorption is reduced and therefore the concentration of $N_{(a)}$ can be assumed to be relativity low. Hence reactions 5.7 and 5.14 would be less likely and reaction 5.13 would be the most likely $N_2$ forming reaction.

FTIR studies of UV illuminated $TiO_2$ powders in the presence of NO and CO have showed that the formation of isocyanate species ($NCO_{(a)}$, 5.14) was negligible at 23°C, but at -70°C the intensity of their IR band increased.[26] This was attributed to increasing amounts of NO adsorption at lower temperatures. This report gives evidence to suggest that the concentration of $N_{(a)}$ was low on illuminated $TiO_2$ surfaces at room temperature, because if the concentration was higher, substantial amounts of $NCO_{(a)}$ would be expected according to reaction 5.14.

It is most likely that all of the reactions shown in 5.1-5.14 occur on the $TiO_2$ surface when both NO and CO are present in the reaction mixture. However, the rate of each reaction may vary with different catalyst pretreatment temperatures, leading to a change in selectivity. For Degussa P25 $TiO_2$ photocatalysts pretreated at low calcination temperatures (70-120°C) the selectivity for $N_2$ formation was higher than for those calcined at the higher temperatures (200-600°C) when CO was present (see figure 5.2 for values). Thus it can be concluded that the rate of reaction 5.13 (the $N_2$ forming reaction) must be faster for P25 calcined at lower temperatures. Hence, decreasing the density of surface hydroxyl groups (i.e. increasing the pretreatment temperature) decreased the rate of $N_2$ forming reactions.

Figure 5.4 shows that the rate of $N_2O$ formation was faster than the rate of $N_2$ formation under both decomposition and reduction conditions, for the calcination

temperatures investigated. However, it is important to note that for both reaction conditions (decomposition and reduction) the rates of $N_2$ formation were similar. However, the rate of $N_2O$ formation was considerably lower when CO was present in the reaction gas. For example, P25 dried at 70°C, the rate of $N_2O$ formation was *ca.* 500 μmol $h^{-1}$ $g^{-1}$ and *ca.* 200 μmol $h^{-1}$ $g^{-1}$ in the absence and presence of CO, respectively. Therefore the presence of CO either hinders the formation of $N_2O$ or accelerates its reduction according to reactions 5.3 and 5.11, respectively.

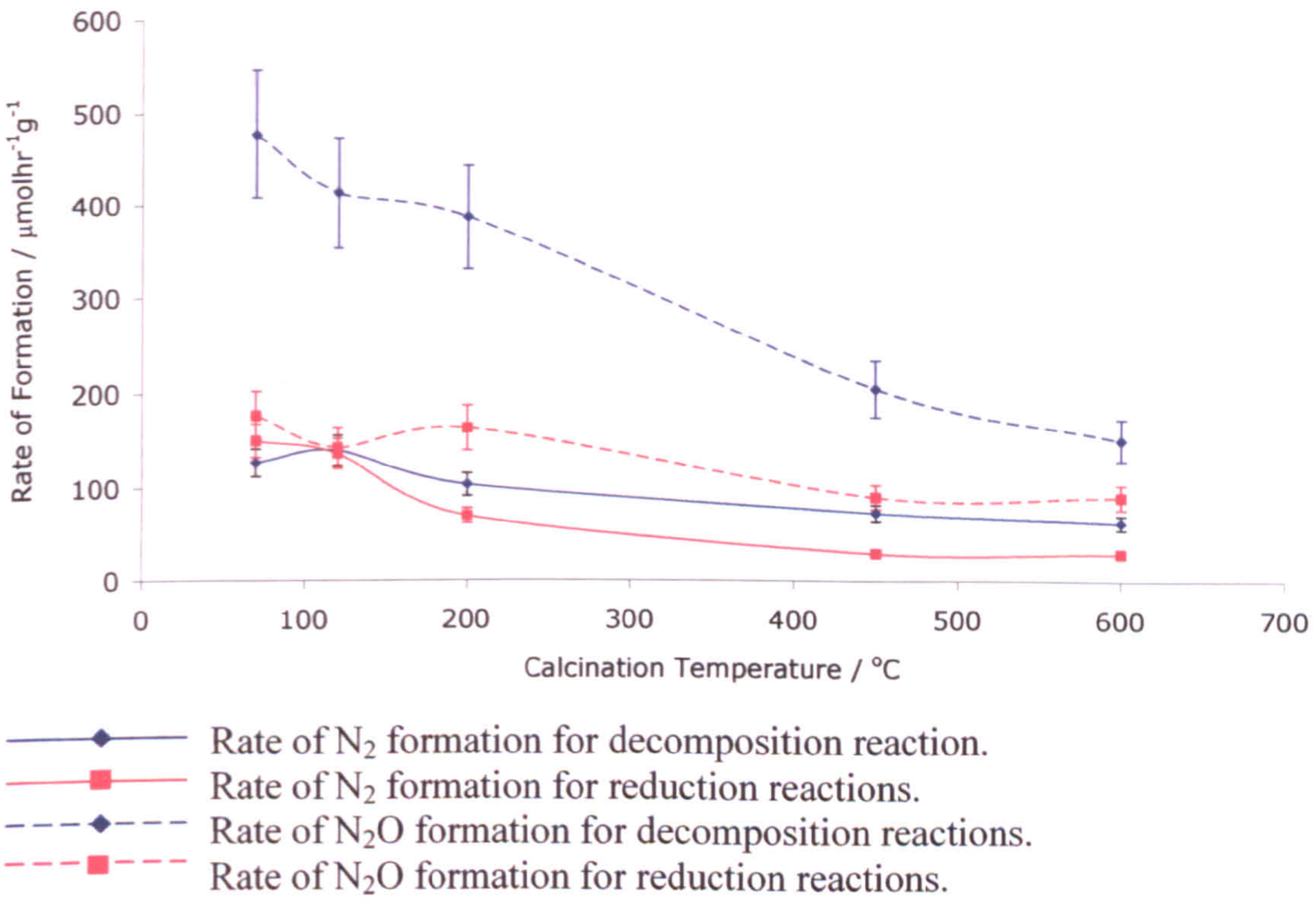


*Figure 5.4. The rates of formation of $N_2$ and $N_2O$ for NO decomposition and reduction reactions over P25 photocatalyst calcined at various temperatures. Decomposition conditions: NO: 909 ppm with Ar balance and a total flow rate of 5.5 sccm. Reduction conditions: As for decomposition reactions with the addition of CO at 1818 ppm.*

### 5.3.2 Effect of varying NO concentration

Figures 5.5 and 5.6 present the percentage NO conversion and the rate of NO conversion, respectively, for both decomposition and reduction reactions with varying NO concentration over P25 photocatalysts calcined at 200°C.

From the values for the percentage NO conversion it appears that the activity of the P25 photocatalysts decreased as the NO concentration increased for both decomposition and reduction conditions. However, this measure of activity does not give a very good representation of catalytic activity when the initial NO concentration is varied. If instead the rate of NO conversion is used, it can be seen that a nearly linear increase in rate with increasing NO concentration was observed for both reaction types as depicted in figure 5.6. It would be expected that the number of NO molecules adsorbed on the catalyst surface would be proportional to the initial concentration of NO in the gas stream until the capacity of the surface for NO adsorption was reached.

Comparison of the activity of P25 photocatalysts under decomposition and reduction conditions with varying NO levels revealed that in the presence of CO the rate of NO conversion was considerably lower than for the direct NO photodecomposition reactions, for all the NO concentration investigated. This is the same result as was observed for the effect of calcination temperature experiments, hence this further supports the argument that the photoadsorption of CO occurs at the expense of NO adsorption. The amount by which the NO conversion rate increased with initial NO concentration in the presence of CO is less than for the decomposition reaction reactions, as the increase in adsorbed NO would be dependant on the NO/CO ratio rather than just the number of NO molecules in the gas stream, as would be the case for the decomposition reactions.

Under decomposition conditions, the selectivity of the photoreaction products remained unaltered irrespective of the NO concentration (figure 5.7). As the P25 photocatalysts used for these experiments were subjected to the same pretreatment temperature, the same number and type of active sites were available for photoreactions to proceed. As a result the same reactions would occur on the surface irrespective of the number of NO molecules adsorbed. The possible reaction mechanisms for the production of $N_2O$ and $N_2$ have been discussed earlier in this chapter (see reaction equations 5.1-5.9).

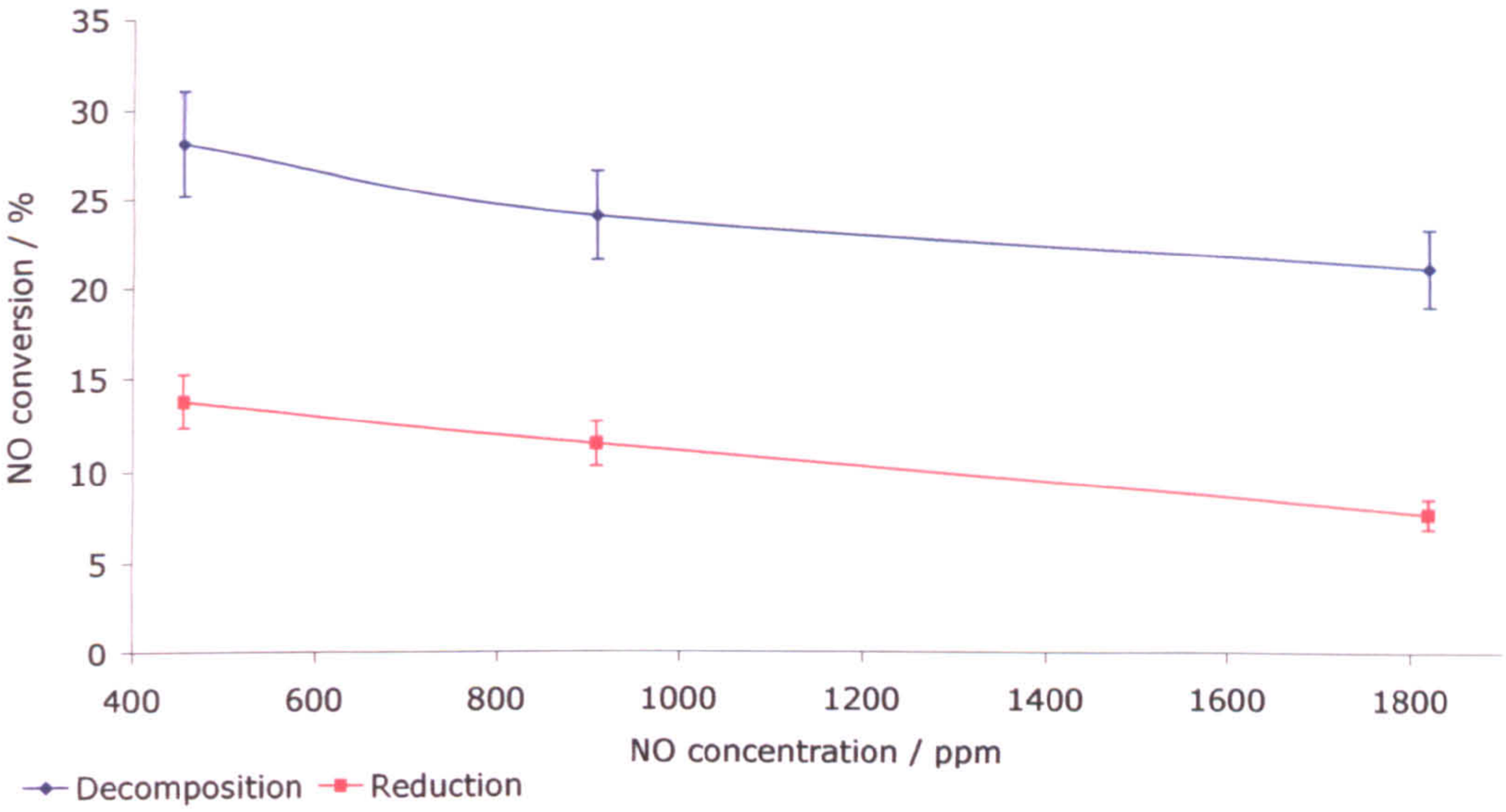


*Figure 5.5. Effect of NO concentration on percentage conversion of NO over P25 photocatalysts calcined at 200°C. Decomposition conditions: Total flow rate of 5.5 sccm. Reduction conditions: Same as for decomposition reactions with a constant concentration of CO (1818 ppm).*

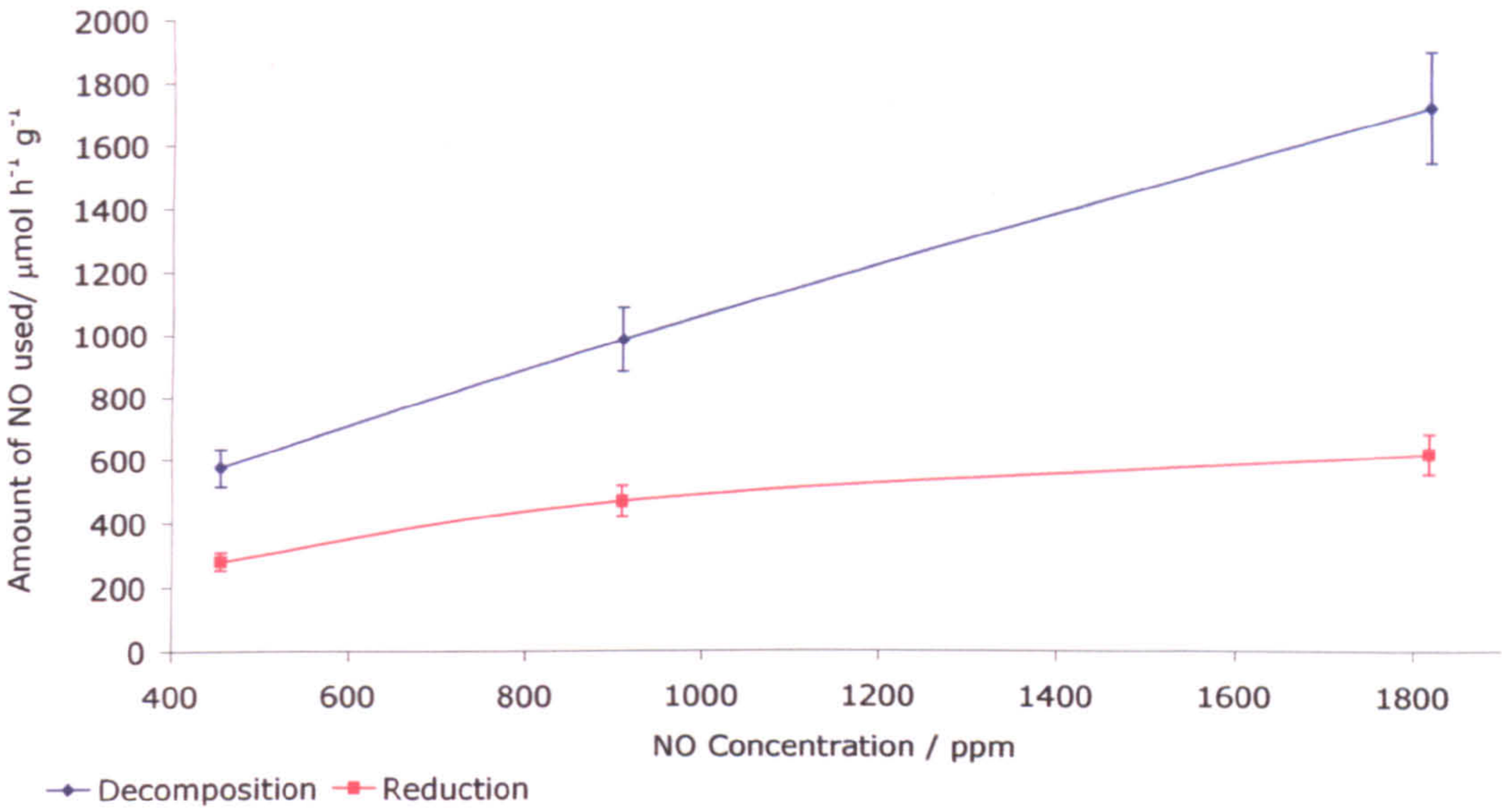


*Figure 5.6. Effect of NO concentration on the moles of NO used over P25 photocatalysts calcined at 200°C. Decomposition conditions: Total flow rate of 5.5 sccm. Reduction conditions: Same as for decomposition reactions with a constant concentration of CO (1818 ppm).*

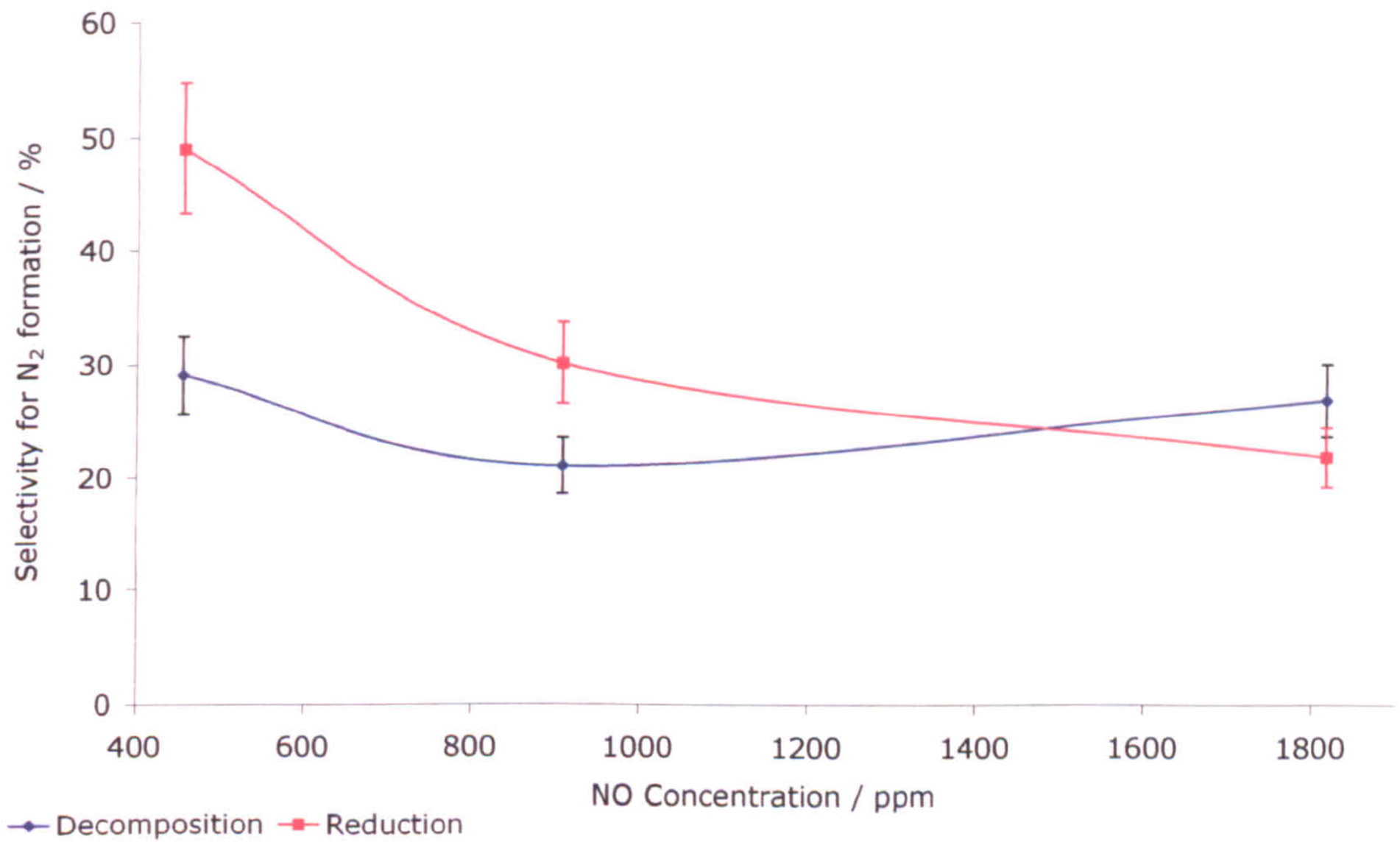


*Figure 5.7. Effect of NO concentration on the selectivity for $N_2$ formation over P25 photocatalysts calcined at 200°C. Decomposition conditions: Total flow rate of 5.5 sccm. Reduction conditions: Same as for decomposition reactions with a constant concentration of CO (1818 ppm).*

Under reduction conditions the selectivity for $N_2$ formation decreased with an increase in the NO/CO ratio, i.e. with increasing NO concentration (figure 5.7). As discussed above, in the presence of CO all 14 of the proposed reaction mechanisms are likely to occur on the photocatalyst, although with varying reaction rates. For this part of the discussion it is more appropriate to refer to absolute reaction rates for the formation of a particular product rather than the relative rates of all the individual reactions (reactions 5.1-5.14). At low NO/CO ratios it could be expected that a large number of the NO molecules will be adsorbed relatively near to CO molecules. Therefore, more NO molecules are likely to react with CO molecules according to reactions 5.10-5.14 and a higher selectivity for $N_2$ production would be seen. As the NO/CO ratio increases fewer NO molecules will adsorb close to CO molecules resulting in fewer NO-CO reactions. As a result more of the NO molecules would react via the reaction schemes shown in equations 5.1-5.9, and it has already been shown that $N_2O$ formation reactions dominate these processes. Hence, as the NO/CO ratio increased, the selectivity for $N_2$ formation decreased as revealed in the results depicted in figure 5.7.

As shown in figure 5.8, under decomposition conditions the rate of formation of both $N_2$ and $N_2O$ increased in a near linear manner with increasing NO concentration. Calculation of the magnitude of the increase of both $N_2$ and $N_2O$ formation rates as the NO concentration was increased from 455 ppm to 1818 ppm showed that both increased by the same factor, *ca.* 3 times the initial rate. This shows that the relative rates of the individual surface reactions did not vary with increasing NO levels, only the total net rate of all the reactions increased. In the presence of a constant concentration of CO (1818 ppm), the rate of $N_2O$ formation increased with increasing NO concentration, whilst the rate of $N_2$ formation remained largely

unchanged. This indicates the net rate of the $N_2O$ forming reactions (5.3, 5.4 and 5.11) increased and the $N_2$ formation was proportional to the concentration of CO.

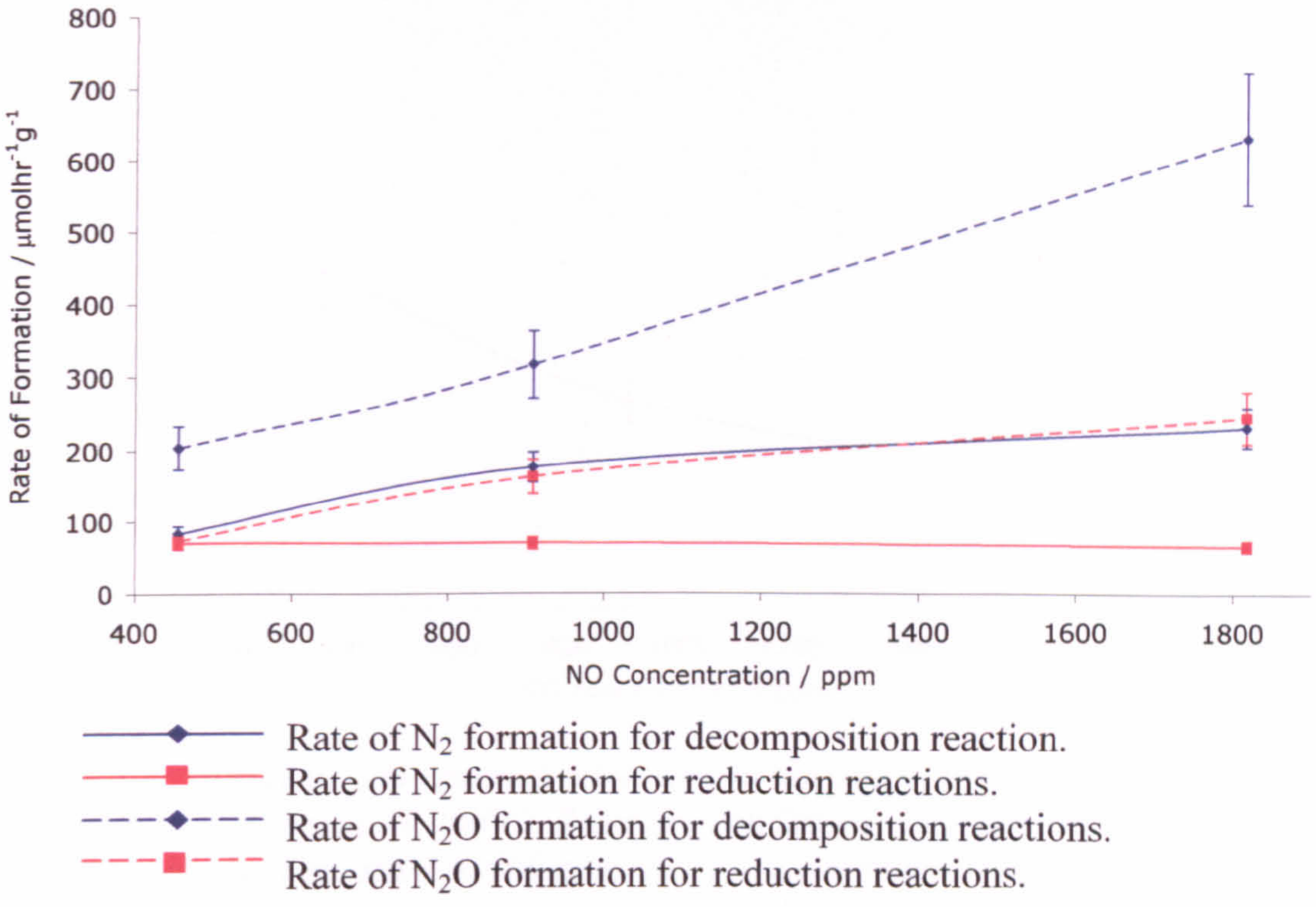


*Figure 5.8. Rates of formation of $N_2$ and $N_2O$ for decomposition and reduction reactions with varying NO levels over P25 photocatalysts calcined at 200°C. Decomposition conditions: Total flow rate of 5.5 sccm. Reduction conditions: Same as for decomposition reactions with a constant concentration of CO (1818 ppm).*

### 5.3.3 Effect of varying CO concentration

The decrease in the NO conversion rates as the CO concentration was increased from 0 to 1818 ppm at constant NO levels (figure 5.9) provides further evidence for CO being adsorbed more strongly than NO, thereby blocking the active sites for NO adsorption. The same theory must apply to CO molecules as that discussed above with respect to the number of NO molecules adsorbed on the P25 surface being proportional to the initial concentration of NO. Therefore, with increasing initial CO levels, a higher number of CO molecules would be adsorbed onto the surface, resulting in fewer adsorption sites for NO and ultimately a lower NO

conversion rate with increasing CO levels. The almost linear relationship between NO conversion and CO concentration provides further evidence to substantiate the above statements.

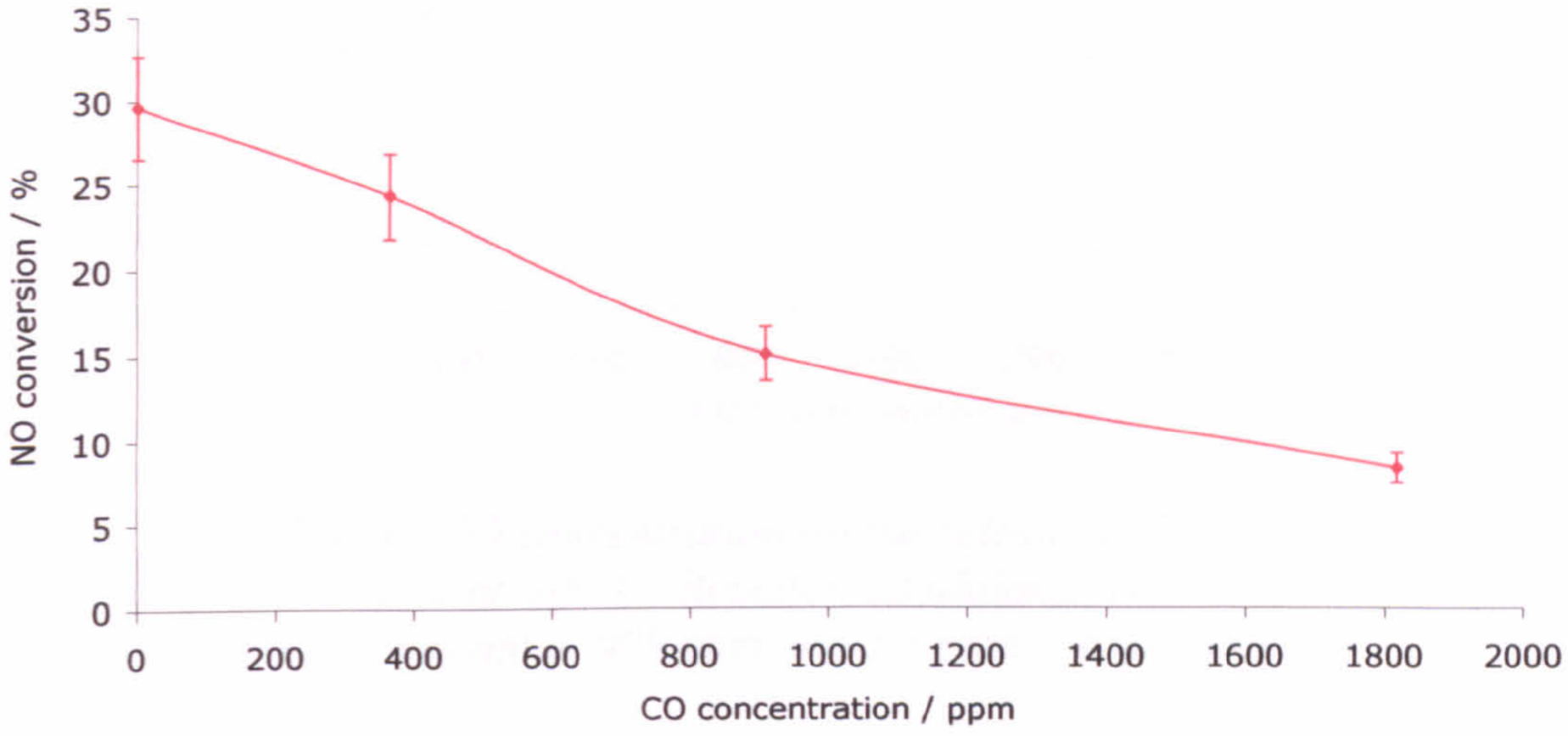


*Figure 5.9. Effect of CO concentration on percentage conversion of NO over P25 photocatalysts calcined at 200°C. Reaction conditions: NO concentration and total flow rate were kept constant at 909 ppm and 5.5 sccm, respectively.*

The increase in selectivity for $N_2$ formation observed with increasing CO concentration at constant NO levels (figure 5.10.) can be explained when you consider the ratio of adsorbed NO and CO molecules together with the possible surface reactions (equations 5.1–5.14). As the concentration of CO is increased, the probability of an NO molecule adsorbing close to a CO molecule increases, resulting in an increase in the number of NO-CO reactions (equations 5.10-5.14) at the expense of NO-NO reactions (equations 5.1-5.9). It has already been shown that $N_2O$ formation reactions dominate NO-NO processes and that $N_2$ is the major product of NO-CO reactions. Hence, decreasing the NO/CO ratio results in a higher selectivity for $N_2$ formation. However, when the CO concentration was increased above 909 ppm, there was no further increase in selectivity for $N_2$ formation.

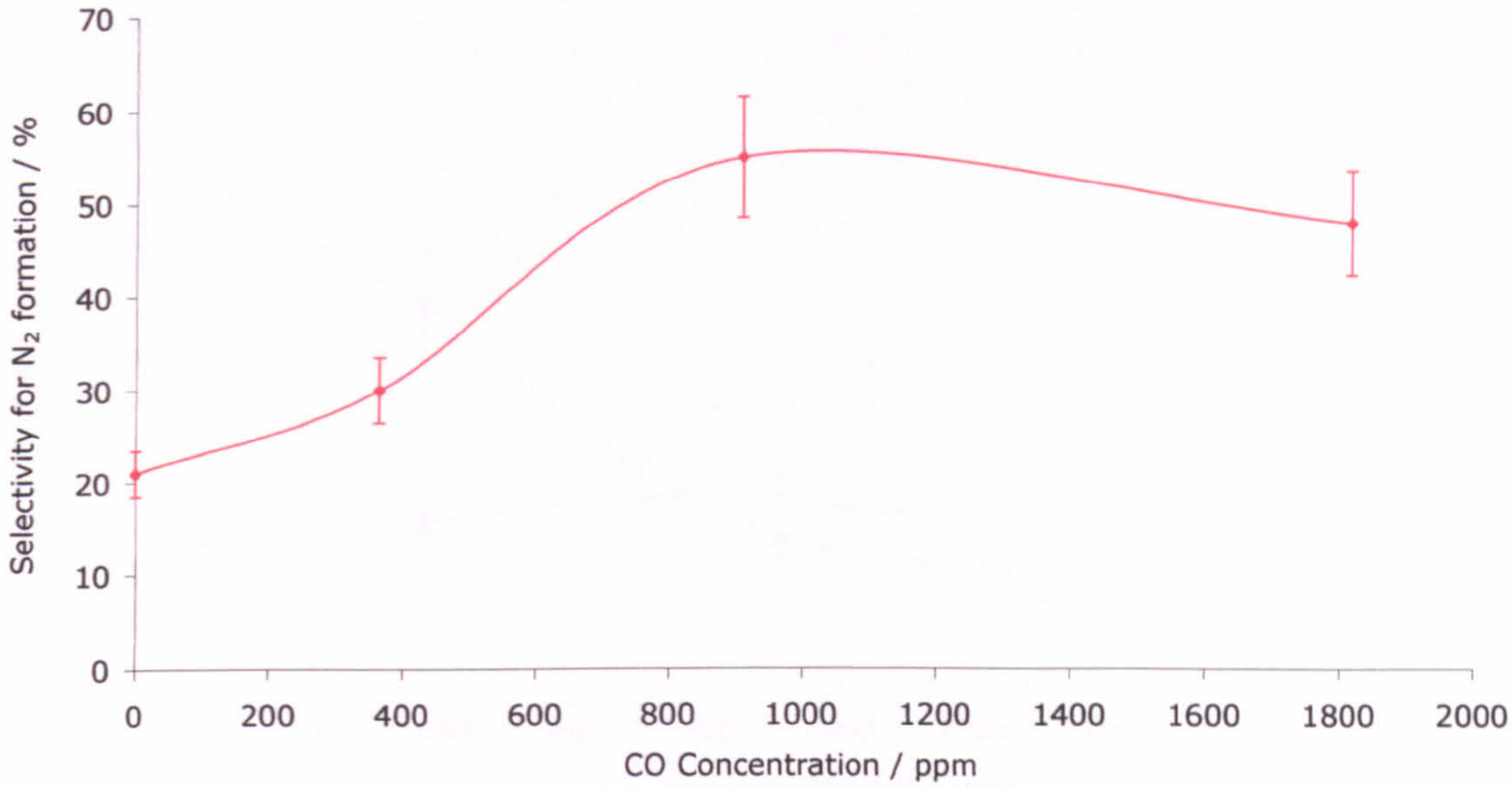


*Figure 5.10. Effect of CO concentration on the selectivity for $N_2$ formation over P25 photocatalysts calcined at 200°C. Reaction conditions: NO concentration and total flow rate were kept constant at 909 ppm and 5.5 sccm, respectively.*

The trends shown in figure 5.11, showing that the rates of $N_2O$ and $N_2$ formation decrease and increase, respectively, help confirm as discussed earlier, that the presence of CO either hinders the formation of $N_2O$ or accelerates its reduction to $N_2$ according to reactions 5.3 and 5.11, respectively. Although as the CO concentration was increased from 909 ppm to 1818 ppm, the effect was much less pronounced compared to the initial change in rates of formation when the CO levels were increased from zero to 909 ppm.

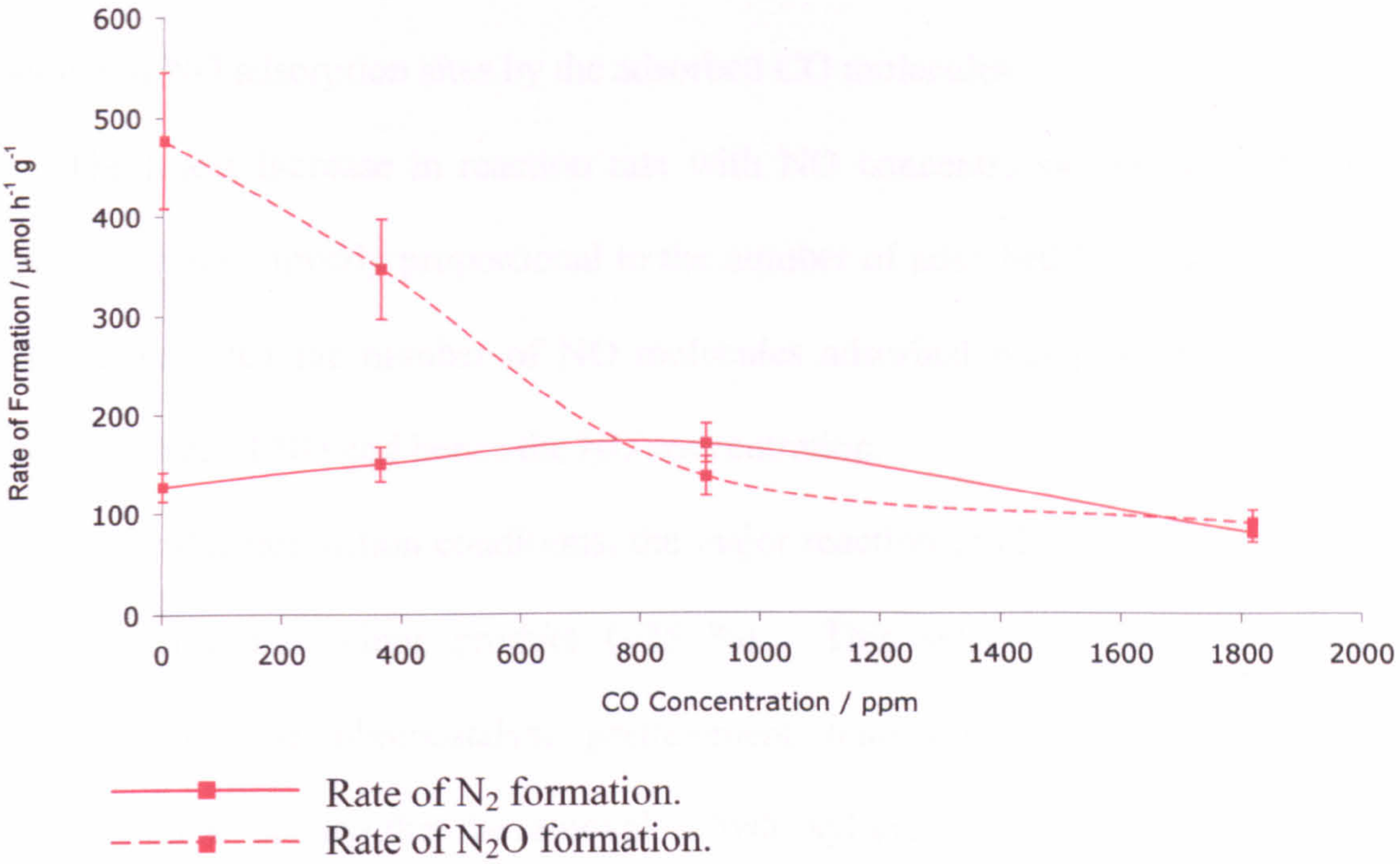


*Figure 5.11. Rates of formation for $N_2$ and $N_2O$ for reduction reactions with varying CO levels over P25 photocatalysts calcined at 200°C. Reaction conditions: NO concentration and total flow rate were kept constant at 909 ppm and 5.5 sccm, respectively.*

## 5.4 Conclusions

The characteristics of photocatalytic decomposition and reduction of NO in the presence of CO have been determined for Degussa P25 $TiO_2$ photocatalysts and it has been shown that over UV irradiated Degussa P25, NO will react to form $N_2$ and $N_2O$ with the selectivity being dependant on the reaction conditions.

Increasing the pretreatment temperature resulted in a decrease in the photocatalytic activity of P25 for both decomposition and reduction reactions even though the crystalline structure remained unchanged for the temperature range used. Therefore, the decrease in activity was due to modifications to the surface chemistry, e.g. removal of molecular water and hydroxyl groups from the surface upon calcination. The activity for NO conversion was less for the reduction reactions

compared to the decomposition reactions for all the conditions tested due to the blocking of NO adsorption sites by the adsorbed CO molecules.

The linear increase in reaction rate with NO concentration indicates that the reaction rate was directly proportional to the number of adsorbed NO molecules as it could be expected the number of NO molecules adsorbed was proportional to the partial pressure of NO and hence the NO concentration.

Under decomposition conditions, the major reaction product was $N_2O$ (~75 %) with $N_2$ being the minor product (~25 %). This selectivity was maintained irrespective of the photocatalyst pretreatment temperature or the initial NO concentration, indicating that the removal of hydroxyl groups from the surface did not affect the nature of the active sites available for photodecompositions. Under reduction conditions, the selectivity for $N_2$ (~48 %) formation increased when pretreatment temperatures of 70°C and 120°C were used. However, when higher pretreatment temperatures were used the selectivity became similar to that achieved in the absence of CO. This indicates that the surface NO-CO $N_2$ forming reaction was more favourable in the presence of many surface hydroxyls and therefore the number of reactions decreased with increasing calcination temperature.

## 5.5 References

(1) Hoffmann, M. R.; Martin, S. T.; Choi, W. Y.; Bahnemann, D. W. *Chem. Rev.* **1995**, *95*, 69.
(2) Peral, J.; Domenech, X.; Ollis, D. F. *J. Chem. Technol. Biotechnol.* **1997**, *70*, 117.
(3) Mills, A.; LeHunte, S. *J. Photochem. Photobiol. A Chem.* **1997**, *108*, 1.
(4) Lewis, N. S.; Rosenbluth, M. L. *Photocatalysis - Fundamentals and Applications*, 1st ed.; Wiley, Chichester, 1989.
(5) Lide, D. R. *CRC Handbook of Chemistry and Physics*, 83 ed.; Interpham / CRC, 2002.
(6) Courbon, H.; Pichat, P. *J. Chem. Soc. Faraday Trans.* **1984**, *80*, 3175.
(7) Negishi, N.; Takeuchi, K.; Ibusuki, T. *J. Sol-Gel Sci. Technol.* **1998**, *13*, 691.

(8) Hashimoto, K.; Wasada, K.; Toukai, N.; Kominami, H.; Kera, Y. *J. Photochem. Photobiol. A Chem.* **2000**, *136*, 103.
(9) Yamashita, H.; Ichihashi, Y.; Anpo, M.; Hashimoto, M.; Louis, C.; Che, M. *J. Phys. Chem.* **1996**, *100*, 16041.
(10) Anpo, M.; Ichihashi, Y.; Takeuchi, M.; Yamashita, H. *Res. Chem. Intermed.* **1998**, *24*, 143.
(11) Tanaka, T.; Teramura, K.; Arakaki, K.; Funabiki, T. *Chem. Comm.* **2002**, 2742.
(12) Thampi, K. R.; Ruterana, P.; Gratzel, M. *J. Catal.* **1990**, *126*, 572.
(13) Chafik, T.; Ouassini, A.; Verykios, X. E. *J. Chim. Phys. Chim. Biol.* **1998**, *95*, 1666.
(14) Vorontsov, A. V.; Savinov, E. N.; Kurkin, E. N.; Torbova, O. D.; Parmon, V. N. *React. Kinet. Catal. Lett.* **1997**, *62*, 83.
(15) Jacoby, W. A.; Blake, D. M.; Noble, R. D.; Koval, C. A. *J. Catal.* **1995**, *157*, 87.
(16) Lim, T. H.; Jeong, S. M.; Kim, S. D.; Gyenis, J. *J. Photochem. Photobiol. A Chem.* **2000**, *134*, 209.
(17) Park, D. R.; Zhang, J. L.; Ikeue, K.; Yamashita, H.; Anpo, M. *J. Catal.* **1999**, *185*, 114.
(18) Fox, M. A.; Dulay, M. T. *Chem. Rev.* **1993**, *93*, 341.
(19) Ding, Z.; Lu, G. Q.; Greenfield, P. F. *J. Phys. Chem. B* **2000**, *104*, 4815.
(20) Suda, Y.; Morimoto, T. *Langmuir* **1987**, *3*, 786.
(21) Tanaka, K.; White, J. M. *J. Phys. Chem.* **1982**, *86*, 4708.
(22) Rusu, C. N.; Yates, J. T. *J. Phys. Chem. B* **2000**, *104*, 1729.
(23) Zhang, J. L.; Ayusawa, T.; Minagawa, M.; Kinugawa, K.; Yamashita, H.; Matsuoka, M.; Anpo, M. *J. Catal.* **2001**, *198*, 1.
(24) Yamashita, H.; Ichihashi, Y.; Zhang, S. G.; Matsumura, Y.; Souma, Y.; Tatsumi, T.; Anpo, M. *Appl. Surf. Sci.* **1997**, *121*, 305.
(25) Anpo, M.; Yamashita, H.; Matsuoka, M.; Park, D. R.; Shul, Y. G.; Park, S. E. *J. Ind. Eng. Chem.* **2000**, *6*, 59.
(26) Rasko, J.; Szabo, Z.; Bansagi, T.; Solymosi, F. *Phys. Chem. Chem. Phys.* **2001**, *3*, 4437.

# 6 Photocatalytic reactions over silver modified Degussa P25 photocatalysts

## 6.1 Introduction

It is widely accepted that the addition of transition metal dopants to photocatalytic materials can have a dramatic effect on the activity and/or selectivity of certain photo-induced reactions, and there have been many examples to this effect reported in the literature[1-5](and references therein). In most cases the role of the dopant is thought to increase the efficiency of the photoreactions via enhanced charge separation properties of the modified photocatalyst,[6] although the dopants themselves may have catalytic properties.[7]

To the best of my knowledge there have been no reports in the literature concerning the photocatalytic decomposition and/or reduction of NO over silver modified $TiO_2$ photocatalysts. However, work by Matsuoka *et al.*[8] showed that UV irradiation of a $Ag^+$/ZSM-5 catalyst in the presence of NO results in the photocatalytic formation of $N_2$, $N_2O$ and $NO_2$, with $N_2$ being the major product. $Ag/Al_2O_3$ and $AgCl/Al_2O_3$ photocatalysts have been reported to be efficient for the photocatalytic decomposition and reduction of NO with propane.[9] In the absence of a reducing agent the main reaction product was $N_2O$. Therefore, this system is not an ideal one for the removal of NO from the atmosphere as $N_2O$ itself is a regulated pollutant. However, these studies show that silver species can offer adsorption sites that are active for NO conversion.

For both the $Al_2O_3$ and ZSM-5 based systems excitation was via direct UV adsorption by the silver species, as the support materials were not semiconductor photocatalysts and therefore required the use of short wavelength UV sources.

However, if silver is supported on a photocatalytically active support such as $TiO_2$, then excitation of the active silver sites via charge transfer from the support would be possible, thereby making use of near UV light sources possible.

In the area of thermal catalysis for NO reduction, it was reported that supported silver catalysts are highly selective for the formation of $N_2$. For example, Bera[10] has reported that $Ag/CeO_2$ catalysts are good SCR for the reduction of NO with CO.

The aim of the work reported in this chapter was to investigate the effects of silver species on Degussa P25 on the photocatalytic activity and the selectivity of NO decomposition reactions, as well as NO reduction reactions in the presence of CO. The results are compared to those obtained for unmodified P25 photocatalysts that are reported in Chapter 5. The effects of photocatalyst processing parameters along with their photocatalytic behaviour under varying reactions conditions were also studied.

This chapter presents the results from the photocatalytic activity tests carried out on Ag-P25 films. The effect of thermal processing parameters for both general decomposition and reduction reactions over 0.1Ag-P25, 1Ag-P25 and 5Ag-P25 are reported in subsections 6.2.1 to 6.2.3. The effect of various gas compositions on the activity and selectivity of the Ag-P25 photocatalysts is reported in sections 6.2.4 and 6.2.5. Section 6.3 presents a detailed discussion of all the results presents in 6.2, and conclusions from these discussions are drawn in section 6.4.

## 6.2 Results

### 6.2.1 0.1Ag-P25 photocatalysts – Effect of calcination temperature

The 0.1Ag-P25 photocatalysts were calcined for 2 h at temperatures in the range of 70°C to 600°C and their photocatalytic behaviour was measured for both NO decomposition and reduction reactions. The decomposition reactions were carried out under a total gas flow of 5.5 sccm containing 909 ppm of NO and the reduction reactions were investigated using the same conditions but with the addition of CO at 1818 ppm. Argon was used as the balance for both reactions.

For both decomposition and reduction conditions the activity of the 0.1Ag-P25 photocatalysts decreased significantly with increasing calcination temperature (from 29.2 % to 0.4 % NO conversion for decomposition reactions and from 18.3 % to 0.1 % NO conversion for reduction reactions as the calcination temperature was increased from 70°C to 600°C, table 6.1), with the catalysts showing more activity for NO conversion in the absence of CO at all the calcination temperatures. The trend observed was similar to that for the unmodified P25 photocatalysts tested under the same reaction conditions, although the activity of the 0.1Ag-P25 was more greatly reduced compared to that of the P25 photocatalysts when the calcination temperature was raised above 200°C.

| Calcination Temperature / °C | Conversion of NO / % | | Rate of NO conversion / μmol $h^{-1}$ $g^{-1}$ | |
|---|---|---|---|---|
| | Decomposition | Reduction | Decomposition | Reduction |
| 70 | 29.2 | 18.3 | 1193 | 750 |
| 120 | 26.9 | 13.6 | 1100 | 557 |
| 200 | 17.0 | 11.9 | 697 | 487 |
| 450 | 4.4 | 3.3 | 180 | 137 |
| 600 | 0.4 | 0.1 | 17 | 3 |

*Table 6.1. Table of NO conversions for the NO decomposition and reduction reactions over 0.1Ag-P25 photocatalysts calcined at various temperatures. Decomposition conditions: NO: 909 ppm with Ar balance and a total flow rate of 5.5 sccm. Reduction conditions: As for decomposition reactions with the addition of CO at 1818 ppm.*

The selectivities for both the decomposition and reduction reactions are presented in table 6.2. The selectivity for $N_2$ formation in the decomposition reactions remained nearly constant at *ca.* 20 % as the calcination temperature was increased from 70°C to 200°C (which was similar to the values observed for the P25 photocatalysts), but when calcined at 450°C and 600°C the selectivity for $N_2$ formation increased to 36 % and 40 % respectively, which was higher than that observed for P25 at the same calcination temperatures. Under reduction conditions the selectivity for $N_2$ formation was higher than for decomposition reactions for all the calcination temperatures investigated, and the trend observed was increasing $N_2$ selectivity with increasing calcination temperature. After calcination at temperatures of 450°C and above, the selectivity for $N_2$ formation reached *ca.* 85 % for the reduction reactions. This is the reverse of the trend observed for the P25 photocatalysts under reduction conditions, in which the selectivity for $N_2$ formation decreased with increased calcination temperature.

| Calcination temperature / °C | Selectivity for decomposition reactions / % | | Selectivity for reduction reactions / % | |
|---|---|---|---|---|
| | $N_2$ | $N_2O$ | $N_2$ | $N_2O$ |
| 70 | 21 | 79 | 30 | 70 |
| 120 | 18 | 82 | 55 | 45 |
| 200 | 25 | 75 | 57 | 43 |
| 450 | 36 | 64 | 88 | 12 |
| 600 | 40 | 60 | 85 | 15 |

*Table 6.2. Table of selectivities for NO decomposition and reduction reactions over 0.1Ag-P25 photocatalysts calcined at various temperatures. Decomposition conditions: NO: 909 ppm with Ar balance and a total flow rate of 5.5 sccm. Reduction conditions: As for decomposition reactions with the addition of CO at 1818 ppm.*

From the results for the rates of formation of $N_2$ and $N_2O$ (table 6.3) it can be seen that the overall trend observed for both products, under both decomposition and reduction conditions, was a decrease in their rates of formation with increasing calcination temperature. These decreases in rates of formation are a result of the significant decreases in NO conversion with increasing calcination temperatures. One result that was an exception to the trend was found as the calcination temperature was increased from 70°C to 120°C, where in the presence of CO, the rate of formation of $N_2$ increased from 113 μmol $h^{-1}$ $g^{-1}$ to 151 μmol $h^{-1}$ $g^{-1}$. This resulted in a significant increase in selectivity for $N_2$ formation for this sample.

| Calcination Temperature / °C | Rate of $N_2$ formation / μmol $h^{-1}$ $g^{-1}$ | | Rate of $N_2O$ formation / μmol $h^{-1}$ $g^{-1}$ | |
|---|---|---|---|---|
| | Decomposition | Reduction | Decomposition | Reduction |
| 70 | 126 | 113 | 471 | 263 |
| 120 | 99 | 151 | 451 | 123 |
| 200 | 88 | 138 | 260 | 103 |
| 450 | 33 | 60 | 57 | 7 |
| 600 | 3 | 1 | 5 | 0.2 |

*Table 6.3. Rates of formation for the products of the photocatalytic reactions over 0.1Ag-P25 photocatalysts calcined at various temperatures. Decomposition conditions: NO: 909 ppm with Ar balance and a total flow rate of 5.5 sccm. Reduction conditions: Same as for decomposition reactions with the addition of CO at 1818 ppm.*

### 6.2.2 1Ag-P25 photocatalysts – Effect of calcination temperature

The 1Ag-P25 photocatalysts were pretreated in the temperature range of 70°C to 600°C for 2 h and their photocatalytic activity for NO decomposition and reduction was measured using identical procedures as for the 0.1Ag-P25 photocatalysts.

For both decomposition and reduction reactions the activity of the 1Ag-P25 photocatalysts decreased with increasing calcination temperature (from 14.3 % to 0.2 % NO conversion for decomposition reactions and from 12 % to 1.2 % NO conversion for reduction reactions as the calcination temperature was increased from 70°C to 600°C, table 6.4). Higher activities were observed under decomposition conditions for the photocatalysts calcined in the temperature range of 70°C to 200°C, whilst for the catalysts that had been subjected to pretreatments of 450°C and above the activity for NO conversion was essentially the same for both decomposition and reductions conditions. For both reaction types, the NO conversion was considerably less than that for the corresponding reactions over unmodified P25 photocatalysts.

| Calcination Temperature / °C | Conversion of NO / % | | Rate of NO conversion / μmol $h^{-1}$ $g^{-1}$ | |
|---|---|---|---|---|
| | Decomposition | Reduction | Decomposition | Reduction |
| 70 | 14.3 | 11.8 | 583 | 483 |
| 120 | 15.0 | 8.6 | 613 | 353 |
| 200 | 12.0 | 8.8 | 489 | 359 |
| 450 | 0.4 | 1.7 | 15 | 68 |
| 600 | 0.2 | 1.2 | 7 | 49 |

*Table 6.4. Table of NO conversions for the NO decomposition and reduction reactions over 1Ag-P25 photocatalysts calcined at various temperatures. Decomposition conditions: NO: 909 ppm with Ar balance and a total flow rate of 5.5 sccm. Reduction conditions: As for decomposition reactions with the addition of CO at 1818 ppm.*

The selectivities for both the decomposition and reduction reactions are presented in table 6.5. The selectivity for $N_2$ formation in the decomposition reactions remained nearly constant at 28 % as the calcination temperature was increased from

70°C to 200°C, but when calcined at 450°C and 600°C the selectivity for $N_2$ formation increased to 45 % and 53 % respectively. Under reduction conditions the selectivity for $N_2$ formation was higher than for decomposition reactions for all the calcination temperatures investigated, and the trend observed was increasing $N_2$ selectivity with increasing calcination temperature. After calcination at temperatures of 450°C and above, no $N_2O$ formation was detected and the reduction reaction became 100 % selective towards $N_2$ formation. The trends observed were similar to those for the 0.1Ag-P25 photocatalysts, but with a higher selectivity for $N_2$ formation at all of the calcination temperatures used.

| Calcination temperature / °C | Selectivity for decomposition reactions / % | | Selectivity for reduction reactions / % | |
|---|---|---|---|---|
| | $N_2$ | $N_2O$ | $N_2$ | $N_2O$ |
| 70 | 29 | 71 | 59 | 41 |
| 120 | 26 | 74 | 88 | 12 |
| 200 | 29 | 71 | 90 | 10 |
| 450 | 45 | 65 | 100 | 0 |
| 600 | 53 | 47 | 100 | 0 |

*Table 6.5. Table of selectivities for NO decomposition and reduction reactions over 1Ag-P25 photocatalysts calcined at various temperatures. Decomposition conditions: NO: 909 ppm with Ar balance and a total flow rate of 5.5 sccm. Reduction conditions: As for decomposition reactions with the addition of CO at 1818 ppm.*

From the results for the rates of formation of $N_2$ and $N_2O$ (table 6.6) it can be seen that the overall trend observed for both products under decomposition and reduction conditions was a decrease in their rates of formation with increasing calcination temperature. For example, under reduction conditions the rate of $N_2$ formation decreased from 142 μmol $h^{-1}$ $g^{-1}$ at 70°C to 25 μmol $h^{-1}$ $g^{-1}$ at 600°C, even though the selectivity for $N_2$ formation increased.

| Calcination Temperature / °C | Rate of $N_2$ formation / μmol $h^{-1}$ $g^{-1}$ | | Rate of $N_2O$ formation / μmol $h^{-1}$ $g^{-1}$ | |
|---|---|---|---|---|
| | Decomposition | Reduction | Decomposition | Reduction |
| 70 | 84 | 142 | 208 | 100 |
| 120 | 78 | 156 | 228 | 20 |
| 200 | 70 | 162 | 174 | 18 |
| 450 | 3 | 34 | 4 | 0 |
| 600 | 2 | 25 | 2 | 0 |

*Table 6.6. Rates of formation for the products of the photocatalytic reactions over 1Ag-P25 photocatalysts calcined at various temperatures. Decomposition conditions: NO: 909 ppm with Ar balance and a total flow rate of 5.5 sccm. Reduction conditions: Same as for decomposition reactions with the addition of CO at 1818 ppm.*

### 6.2.3 5Ag-P25 photocatalysts – Effect of calcination temperature

The 5Ag-P25 photocatalysts were pretreated in the temperature range of 70°C to 600°C for 2 h and their photocatalytic activity for NO decomposition and reduction was measured using identical procedures as for the other silver modified photocatalysts.

Under decomposition conditions the percentage NO conversion remained nearly constant at *ca.* 3 % for the photocatalysts that had been pretreated in the temperature range of 70°C to 200°C and then decreased to 0.4 % when the higher calcination temperatures of 450°C and 600°C were used (table 6.7). For the reduction reactions the percentage NO conversion decreased with every increase in pretreatment temperature. It should also be noted that under reduction conditions the NO conversion rate was higher than for the decomposition reactions for the photocatalysts that had been calcined at low temperature. For all the other systems investigated (P25, 0.1Ag-P25 and 1Ag-P25) the activity of the photocatalyst was always greatest in the absence of CO.

| Calcination Temperature / °C | Conversion of NO / % | | Rate of NO conversion / μmol $h^{-1}$ $g^{-1}$ | |
|---|---|---|---|---|
| | Decomposition | Reduction | Decomposition | Reduction |
| 70 | 2.0 | 7.0 | 83 | 287 |
| 120 | 3.1 | 5.9 | 125 | 243 |
| 200 | 4.0 | 2.6 | 164 | 108 |
| 450 | 0.4 | 0.3 | 15 | 13 |
| 600 | 0.4 | 0.5 | 16 | 20 |

*Table 6.7. Table of NO conversions for the NO decomposition and reduction reactions over 5Ag-P25 photocatalysts calcined at various temperatures. Decomposition conditions: NO: 909 ppm with Ar balance and a total flow rate of 5.5 sccm. Reduction conditions: As for decomposition reactions with the addition of CO at 1818 ppm.*

The selectivities for both the decomposition and reduction reactions are presented in table 6.8. The selectivity for $N_2$ formation in the decomposition reactions remained nearly constant at 75 % for all of the calcination temperatures investigated, whilst for the reduction reactions the selectivity for $N_2$ formation increased from 76 % at 70°C to 100 % at 200°C. When the pretreatment temperature was increased further to 600°C the reduction of NO remained 100 % selective towards $N_2$ formation (within the errors associated with the experiment).

| Calcination temperature / °C | Selectivity for decomposition reactions / % | | Selectivity for reduction reactions / % | |
|---|---|---|---|---|
| | $N_2$ | $N_2O$ | $N_2$ | $N_2O$ |
| 70 | 71 | 29 | 76 | 24 |
| 120 | 75 | 25 | 83 | 17 |
| 200 | 75 | 25 | 100 | 0 |
| 450 | 79 | 21 | 100 | 0 |
| 600 | 77 | 23 | 95 | 5 |

*Table 6.8. Table of selectivities for NO decomposition and reduction reactions over 5Ag-P25 photocatalysts calcined at various temperatures. Decomposition conditions: NO: 909 ppm with Ar balance and a total flow rate of 5.5 sccm. Reduction conditions: As for decomposition reactions with the addition of CO 1818 ppm.*

Due to the higher selectivities of the 5Ag-P25 photocatalysts towards $N_2$ formation under both decomposition and reductions conditions the corresponding

rates of formation of the $N_2O$ product were very low (< 35 μmol $h^{-1}$ $g^{-1}$) at all the calcination temperatures investigated for both reactions types (table 6.9). The rates of formation of $N_2$ were also fairly low due to the low NO conversion levels observed for the 5Ag-P25 photocatalysts. The maximum $N_2$ formation rate was 109 μmol $h^{-1}$ $g^{-1}$ and was observed for the photocatalyst that had been pretreated at 70°C and tested under a reducing atmosphere.

| Calcination Temperature / °C | Rate of $N_2$ formation / μmol $h^{-1}$ $g^{-1}$ | | Rate of $N_2O$ formation / μmol $h^{-1}$ $g^{-1}$ | |
|---|---|---|---|---|
| | Decomposition | Reduction | Decomposition | Reduction |
| 70 | 29 | 109 | 12 | 34 |
| 120 | 47 | 100 | 16 | 21 |
| 200 | 62 | 54 | 21 | 0 |
| 450 | 6 | 6 | 2 | 0 |
| 600 | 6 | 9 | 2 | 1 |

*Table 6.9. Rates of formation for the products of the photocatalytic reactions over 5Ag-P25 photocatalysts calcined at various temperatures. Decomposition conditions: NO: 909 ppm with Ar balance and a total flow rate of 5.5 sccm. Reduction conditions: Same as for decomposition reactions with the addition of CO at 1818 ppm.*

### 6.2.4 Effect of varying NO concentration

To investigate the effect of NO concentration over Ag-P25, a 1Ag-P25 photocatalyst that had been calcined at 200°C was used. The concentration of NO was varied from 455 ppm to 1818 ppm whilst maintaining a constant total flow rate of 5.5 sccm. When present, the concentration of CO was kept constant at 1818 ppm.

Table 6.10 shows that as the concentration of NO increased from 455 ppm to 1818 ppm the percentage NO conversion decreased from 19.1 % to 8.3 % for the decomposition reactions and from 12.2 % to 7.0 % for the reduction reactions. However, if instead of percentage NO conversion, the rate of NO conversion was used as a measure of photocatalytic activity, then we see a trend that increases for

both reaction types (table 6.10), thus indicating that more surface NO reactions occurred as the NO concentration increased.

| NO concentration / ppm | Conversion of NO / % | | Rate of NO conversion / μmol $h^{-1}$ $g^{-1}$ | |
|---|---|---|---|---|
| | Decomposition | Reduction | Decomposition | Reduction |
| 455 | 19.1 | 12.2 | 390 | 249 |
| 909 | 12.0 | 8.8 | 489 | 359 |
| 1818 | 8.3 | 7.0 | 680 | 567 |

*Table 6.10. NO conversion results for decomposition and reduction reactions with varying NO levels over 1Ag-P25 photocatalysts calcined at 200°C. Decomposition reaction conditions: Total flow rate of 5.5 sccm. Reduction reaction conditions: Same as for decomposition reactions with a constant concentration of CO (1818 ppm).*

Within the errors associated with these results the selectivity of the decomposition reactions was very similar (*ca.* 30 % selectivity for $N_2$ formation) for all three NO concentrations (table 6.11). At low NO concentration (455 ppm) in the presence of CO, the selectivity of the reaction for $N_2$ formation was as high as 95 %, but as the concentration of NO was increased the selectivity for $N_2$ formation decreased. When the NO level was 1818 ppm the selectivity for $N_2$ formation had decreased to 65 %. For both decomposition and reduction conditions the rate of $N_2$ formation increased by ca. 161 % when the NO concentration was increased from 455 ppm to 1818 ppm (table 6.12). However, it should be noted that a higher rate of $N_2$ formation was observed in the presence of CO for the NO concentrations investigated. For both reaction types the rate of formation of $N_2O$ increased with NO concentration, with the decomposition conditions being the most favourable for $N_2O$ production at all the NO levels investigated.

| NO concentration / ppm | Selectivity for decomposition reactions / % | | Selectivity for reduction reactions / % | |
|---|---|---|---|---|
| | $N_2$ | $N_2O$ | $N_2$ | $N_2O$ |
| 455 | 36 | 64 | 95 | 5 |
| 909 | 29 | 71 | 90 | 10 |
| 1818 | 34 | 66 | 65 | 35 |

*Table 6.11. Table of selectivities for NO decomposition and reduction reactions with varying NO concentrations over 1Ag-P25 photocatalysts calcined at 200°C. Decomposition reaction conditions: Total flow rate of 5.5 sccm. Reduction reaction conditions: Same as for decomposition reactions with a constant concentration of CO (1818 ppm).*

| NO concentration / ppm | Rate of $N_2$ formation / μmol $h^{-1}$ $g^{-1}$ | | Rate of $N_2O$ formation / μmol $h^{-1}$ $g^{-1}$ | |
|---|---|---|---|---|
| | Decomposition | Reduction | Decomposition | Reduction |
| 455 | 70 | 118 | 123 | 6 |
| 909 | 71 | 163 | 173 | 17 |
| 1818 | 113 | 187 | 227 | 97 |

*Table 6.12. Rates of formation for the products for NO decomposition and reduction reactions with varying NO concentrations over 1Ag-P25 photocatalysts calcined at 200°C. Decomposition reaction conditions: Total flow rate of 5.5 sccm. Reduction reaction conditions: Same as for decomposition reactions with a constant concentration of CO (1818 ppm).*

### 6.2.5 Effect of varying CO concentration

The effect of CO concentration was investigated by maintaining a constant concentration of NO of 909 ppm whilst varying the CO concentration from zero to 1818 ppm. The total flow rate was kept constant at 5.5 sccm for each experiment. The photocatalysts used for these experiments were films of 1Ag-P25 calcined at 200°C. Table 6.13 illustrates how the percentage NO conversion decreased from 12 % to 8.1 % as the CO concentration was increased from 0 to 1242 ppm. Further increasing the CO concentration did not significantly effect the percentage NO conversion.

From the results for the selectivity of the reactions (table 6.14) it can be seen that the addition of even low concentrations of CO (364 ppm) resulted in a dramatic

increase in the selectivity of the reaction towards $N_2$ formation. When no CO was present the selectivity for $N_2$ formation was 29 %, but with 364 ppm of CO in the reaction gases the selectivity for $N_2$ formation nearly doubled to 58 %.

| CO concentration / ppm | NO conversion / % | NO conversion rate / μmol $h^{-1}$ $g^{-1}$ |
|---|---|---|
| 0 | 12.0 | 490 |
| 364 | 10.6 | 431 |
| 909 | 9.7 | 394 |
| 1242 | 8.1 | 333 |
| 1818 | 8.8 | 359 |

*Table 6.13. NO conversion results for reduction reactions with varying CO levels over 1Ag-P25 photocatalysts calcined at 200°C. Reaction conditions: NO concentration and total flow rate were kept constant at 909 ppm and 5.5 sccm respectively.*

| CO concentration / ppm | Selectivity / % | |
|---|---|---|
| | $N_2$ | $N_2O$ |
| 0 | 29 | 71 |
| 364 | 58 | 42 |
| 909 | 86 | 14 |
| 1242 | 82 | 18 |
| 1818 | 90 | 10 |

*Table 6.14. Selectivity results for reduction reactions with varying CO levels over 1Ag-P25 photocatalysts calcined at 200°C. Reaction conditions: NO concentration and total flow rate were kept constant at 909 ppm and 5.5 sccm respectively.*

The rate of formation of $N_2$ increased with CO concentration until it reached a maximum of 169 μmol $h^{-1}$ $g^{-1}$ at 909 ppm (table 6.15). Further increases in the CO concentration resulted in a decrease in the rate of $N_2$ formation. The rate of formation of $N_2O$ decreased from 173 μmol $h^{-1}$ $g^{-1}$ at zero CO concentration to 18 μmol $h^{-1}$ $g^{-1}$ at 1818 ppm of CO.

| CO concentration / ppm | Rate of $N_2$ formation / μmol $h^{-1}$ $g^{-1}$ | Rate of $N_2O$ formation / μmol $h^{-1}$ $g^{-1}$ |
|---|---|---|
| 0 | 71 | 173 |
| 364 | 125 | 91 |
| 909 | 169 | 28 |
| 1242 | 137 | 30 |
| 1818 | 162 | 18 |

*Table 6.15. Effect of CO concentration on the rates of formation of $N_2$ and $N_2O$ over 1Ag-P25 photocatalysts calcined at 200°C. Reaction conditions: NO concentration and total flow rate were kept constant at 909 ppm and 5.5 sccm respectively.*

## 6.3 Discussion

### 6.3.1 Effect of silver species on photocatalytic behaviour

Figures 6.1 and 6.2 show the effect of silver loading for each of the calcination temperatures used on the percentage conversion of NO for decomposition and reduction reactions, respectively. For each of the silver loadings used the rate of NO conversion decreased with increasing calcination temperature, which is the same trend that was observed for the unmodified P25 photocatalysts. As discussed in chapter 5 of this thesis, the reason for the decrease in NO conversion rate as the P25 pretreatment temperature increased was the removal of molecular water and hydroxyl groups from the surface of $TiO_2$. Surface bound OH groups act as both efficient trapping sites for photogenerated holes[4] as well as good adsorption or active sites for NO molecules,[11] thus reducing the surface density of OH groups (by increasing calcination temperatures) has the effect of reducing the NO conversion rate over P25 photocatalysts.

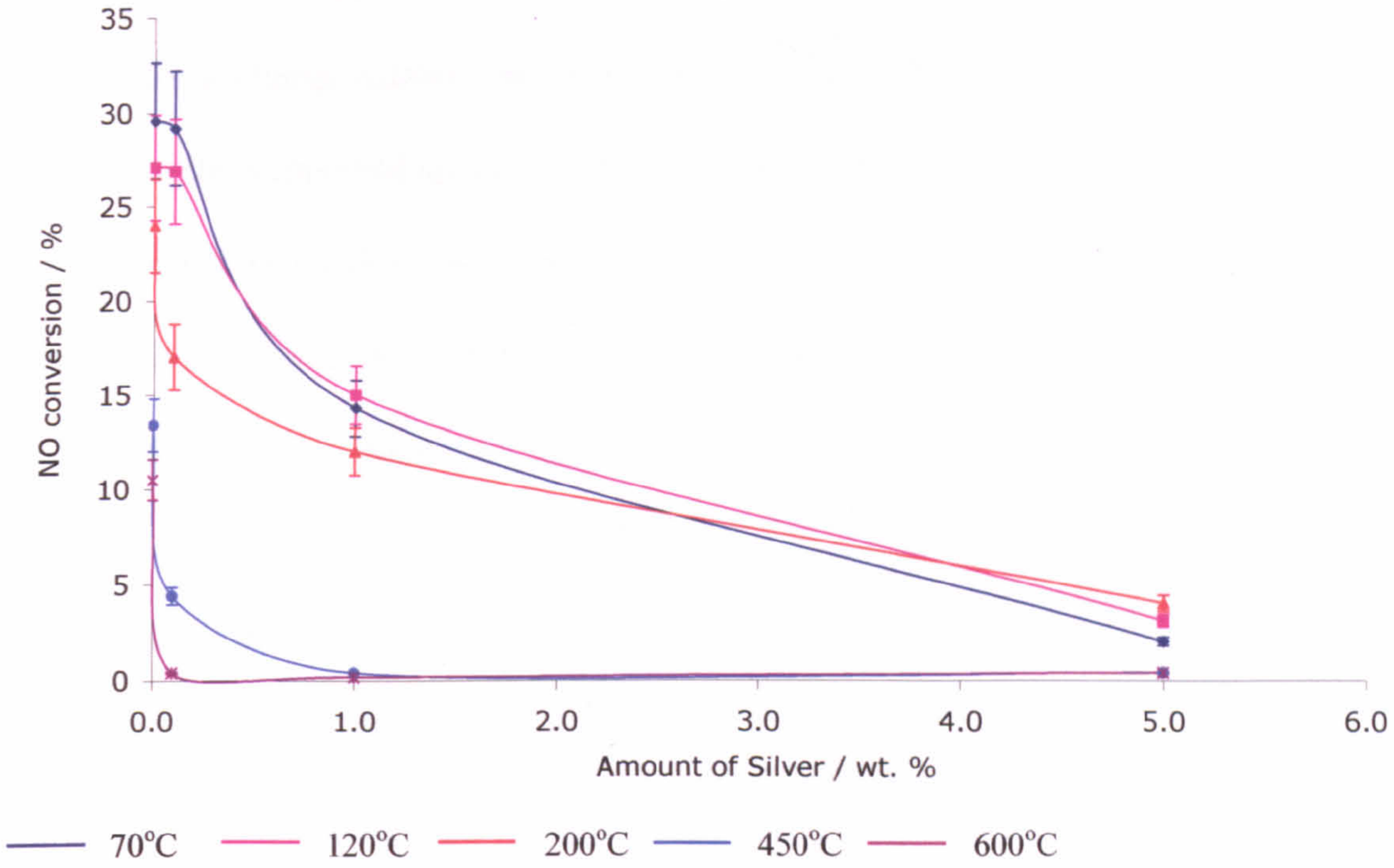


*Figure 6.1. Effect of silver content on the percentage NO conversion for photocatalysts calcined at various temperatures for 2 h. Decomposition conditions: NO concentration was 909 ppm. Total flow rate 5.5 sccm.*

The same rationalisation of decreasing density of surface bound OH groups with increasing calcination temperature can be used to partly explain the decrease in NO conversion observed for all the silver containing photocatalysts under both decomposition and reduction conditions with increasing pretreatment temperature. However, it was also observed that additions of silver to P25 had a detrimental effect on the NO conversion rate, as shown by the decrease in NO conversion observed as the silver loading increased. The trends observed for the percentage NO conversion as the calcination temperature and silver loading vary can be explained by referring to the nature and amount of silver species present on the P25 surface. This result is in agreement with reports in the literature that state that the effect of modifying species on the activity of a photocatalyst are sensitive to their concentration.[4]

The interface that is formed when a photocatalyst and a metal (or metal ion) are in electrical contact can serve as an efficient trap for the photogenerated electrons,

preventing the energy wasting electron-hole recombination reactions. It is also possible for a charge transfer process to occur, in which the photogenerated electron migrates to the supported species. The electron is then able to initiate a redox reaction with adsorbed molecules. Both of these processes can lead to enhanced activity of a photocatalyst. However, it is possible that if the extent of charge transfer from the photocatalysts to the supported species becomes excessive, then the excess negative charge can attract the positively formed photogenerated hole, and the interface acts as a recombination centre, thus reducing the photocatalyst efficiency. The reader is referred back to chapter 2 for a more detailed discussion of the processes occurring.

In characterising the Ag-P25 photocatalysts used for the experiments described in this chapter it was shown that for each of the silver loadings used, the relative amount of metallic silver to silver ions present increased with increasing calcination temperature, with the highest silver loading (5 wt. %) showing the greatest relative percentage of $Ag^0$ at all calcination temperatures (See tables 4.11 and 4.13, Chapter 4). It was also observed that increasing the silver loading resulted in enhanced growth of the anatase particles at lower temperatures and increased the rate of the anatase-to-rutile phase transformation. For example, the phase composition of the 0.1Ag-P25 and 5Ag-P25 photocatalysts calcined at 450°C consisted of *ca.* 22 % and *ca.* 26 % rutile, respectively and the average anatase particle sizes were *ca.* 28 nm and *ca.* 31 nm, respectively. The $TiO_2$ particle sizes and phase composition of all the Ag-P25 photocatalysts were similar after calcination at lower temperatures, but calcination at 600°C resulted in further particle growth and phase changes especially for the systems with higher silver content. As a result of this it would be expected that the surface area of the silver modified P25 catalysts calcined at temperatures above 200°C would decrease with increased silver concentration.

From these observations, it is proposed that the reduction in activity of the Ag-P25 photocatalysts as the silver concentration and pretreatment temperature increase was probably due to two separate effects. Firstly, increasing amounts of metallic silver could result in the metal-$TiO_2$ interface acting as a recombination centre for the photogenerated electrons and holes, rather than helping suppress recombination, thus the number of photoreactions that were able to proceed would decrease as the magnitude of the effect increased. Secondly, the decreasing $TiO_2$ surface area would result in less $TiO_2$ being able to participate in the reactions and also in fewer active adsorption sites, thus reducing the number of possible surface photoreactions.

Similar effects have been observed in the studies by Chao *et al.*[12,13] on the photocatalytic degradation of methylene blue over sol-gel prepared $TiO_2$ modified with varying amounts of silver. It was found that when a suitable amount of Ag was used, the activity of the $TiO_2$ photocatalysts was effectively enhanced. For example, when a 2-4 mol. % (2.7- 5.4 wt. %) Ag was used the photocatalytic activity was increased to more than that of unmodified $TiO_2$. However, increasing the silver content to 6 mol. % (8.1 wt. %) yielded a photocatalyst with an activity similar to that of $TiO_2$. Further increases in the amount of silver used resulted in a further reduction of the photocatalytic activity. XRD, XPS and BET surface area analysis of the photocatalysts also showed similar trends in the composition and particle sizes of the $TiO_2$ support as the silver loading increased as was observed for the silver containing catalysts used for the work presented in this thesis. The authors proposed, in agreement with many other reports in the literature, that the increase in activity at low silver loadings was due to the enhanced electron-hole separation caused by the Schottky barrier formed at the metal-$TiO_2$ interface and that at high silver loadings the

interface served as a recombination centre, thereby reducing the efficiency of the photoreactions.

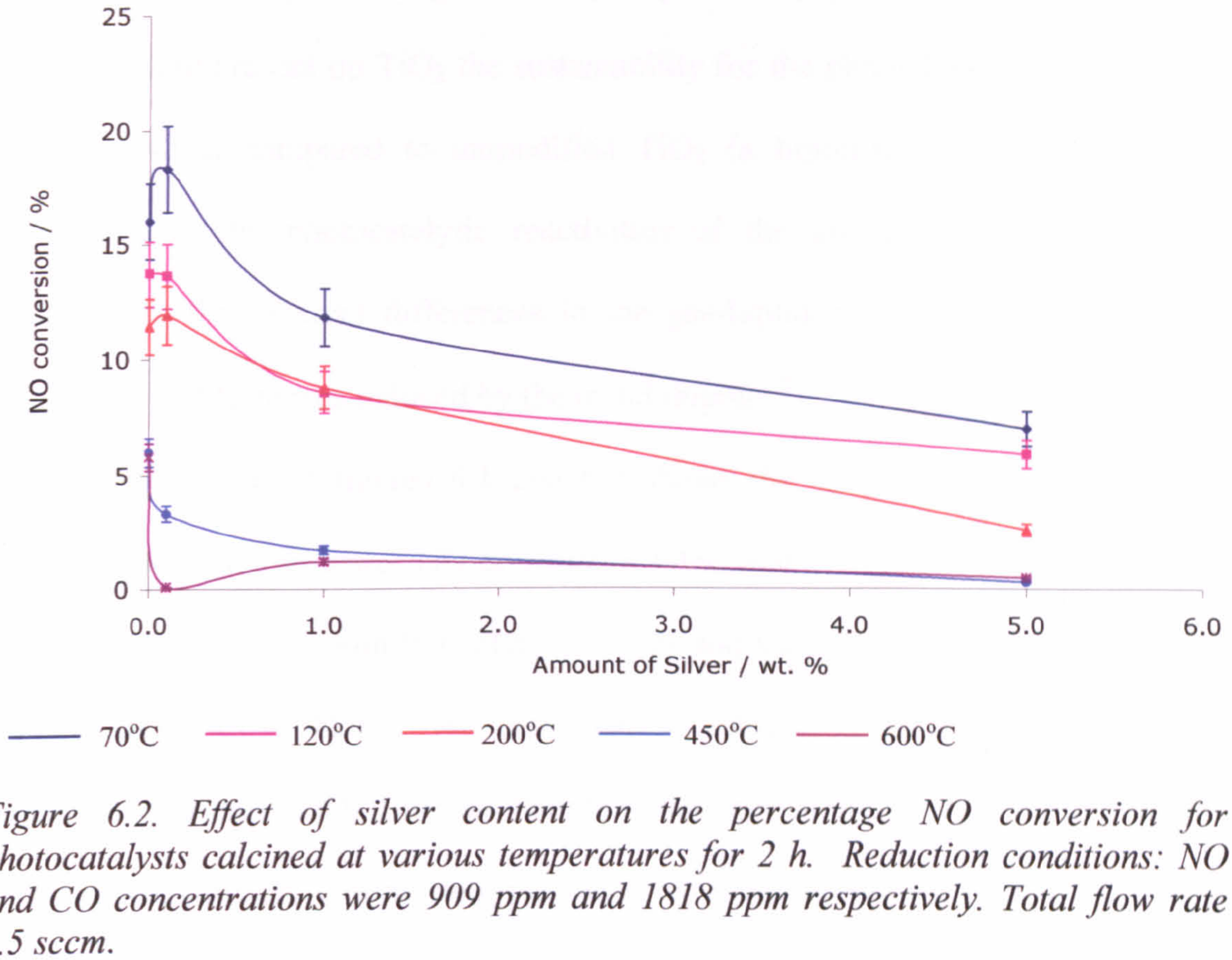


*Figure 6.2. Effect of silver content on the percentage NO conversion for photocatalysts calcined at various temperatures for 2 h. Reduction conditions: NO and CO concentrations were 909 ppm and 1818 ppm respectively. Total flow rate 5.5 sccm.*

As discussed above, the studies by Chao *et al.*[12,13] reported that addition of 4 mol. % (5.4 wt. %) Ag to $TiO_2$ resulted in a higher activity for methylene blue degradation than unmodified $TiO_2$. However, in the results presented in this thesis, the 5Ag-P25 photocatalyst systems were significantly less active for both NO decomposition and reduction than the unmodified P25 photocatalysts (*ca.* 30 % and 2 % NO conversion for unmodified P25 and 5Ag-P25 dried at 70°C, respectively). This indicates that changes in photocatalytic activity observed when silver was present on $TiO_2$ surfaces are not the same for every reaction type, (although similar overall trends are observed) but instead are specific to each reaction and the reaction type (*e.g.* gas-solid or liquid-solid reaction interfaces). Similar trends have been

reported when other transition metals have been used. For example $Cr^{3+}$ ion dopants are detrimental for the photoreduction of $N_2$ to $NH_3$[14] (a gas-solid system), whilst they have no effect on phenol degradation (a liquid-solid system).[15] However, when $Cr^{3+}$ ions were present on $TiO_2$ the sustainability for the photocleavage of water was improved when compared to unmodified $TiO_2$ (a liquid-solid system).[16] These differences in the photocatalytic reactivities of the above reactions have been attributed to the inherent differences in the gas-liquid and liquid-solid interfaces, rather than to differences induced by the metal doping.[15]

Comparison of figures 6.1 and 6.2 shows that the presence of CO in the reaction gas results in lower NO conversion rates, and the effect is more evident in Ag-P25 photocatalysts with low silver loadings and those that have been calcined at temperatures below 450°C. As discussed in chapter 5, CO is competitively photoadsorbed onto $TiO_2$ surfaces thereby reducing the number of NO molecules adsorbed and ultimately decreasing the NO conversion rate. It is proposed that this is the reason for the reduced activity of the Ag-P25 photocatalysts with low silver concentrations. Also apparent from comparison of figures 6.1 and 6.2 is that, over the 5Ag-P25 photocatalysts, the NO conversion in the presence of CO was greater than or equal to the conversion for the NO decomposition reactions. For higher calcination temperatures it is impossible to say which reaction has the higher NO conversion, due to the low NO conversion rates for both. As discussed above, the 5Ag-P25 photocatalysts contained larger amounts of metallic silver species (relative to $Ag^+$ species, see chapter 4) compared to the 1Ag-P25 and 0.1Ag-P25 photocatalysts. It is possible that the presence of metallic silver particles increase the amount of NO that was adsorbed when CO was also present in the reaction gas. Alternatively it is possible that the $Ag^+$ species present in the form of silver nitrate are active for

NO-CO photoreactions, and the effect is enhanced for the lower temperature 5Ag-P25 photocatalysts as more $Ag^+$ species were present. There are reports in the literature that show that both metallic silver and $Ag^+$ compounds are active for the adsorption of NO and CO[10,17-19] (with and without the presence of UV illumination), however there are no reports on the coadsorption properties of silver compounds and hence it is not possible to interpret the data in terms of the competitive adsorption processes occurring during the NO-CO reactions over Ag-P25 photocatalysts reported in this thesis.

Figure 6.3 shows that under decomposition conditions, as the silver loading increased the selectivity for $N_2$ formation also increased for all the calcination temperatures and that, within the errors associated with the measurements, the presence of silver improved the $N_2$ selectivity. As discussed above the calcination temperature and silver loading affects the nature of the silver species present. It could, therefore, be expected that it was the presence of the particular silver species that gave rise to the higher selectivity observed in the presence of silver. From figure 6.3 it can be seen that the selectivity for $N_2$ formation was only slightly increased (compared to unmodified P25) for the decomposition reactions over 0.1Ag-P25 and 1Ag-P25 photocatalysts that had been calcined at temperatures of up to 200°C. In these systems the silver was shown to be present predominantly as silver nitrate, with only small amounts of $Ag^0$. Therefore, silver nitrate had little or no effect on the selectivity of the NO decomposition reaction and the relative rates of the NO surface reactions were comparable to those on unmodified P25 photocatalysts. When the same photocatalysts were calcined at higher temperatures the selectivity for $N_2$ increased, with the highest values (53 % selectivity for $N_2$ formation) observed over the catalyst with the largest relative amount of metallic silver present. From these

observations it can be deduced that metallic silver particles and clusters enhance the number of $N_2$ forming NO-NO reactions relative to the $N_2O$ forming NO-NO reactions. For details of the possible NO surface reactions the reader is referred to reaction equations 5.1-5.9 in the discussion in chapter 5. Further evidence for this hypothesis is seen in the decomposition reactions on 5Ag-P25 catalysts, as much higher selectivity for $N_2$ formation (*ca.* 75 %) was obtained due to the increased number of metallic silver particles and clusters. However, it was shown by XPS analysis of the Ag-P25 photocatalyst systems that the surface of the silver particles and clusters were partially oxidised to $Ag^+$ and it has been reported several times that oxidised silver species are highly selective for $N_2$ formation.[17,20,21]

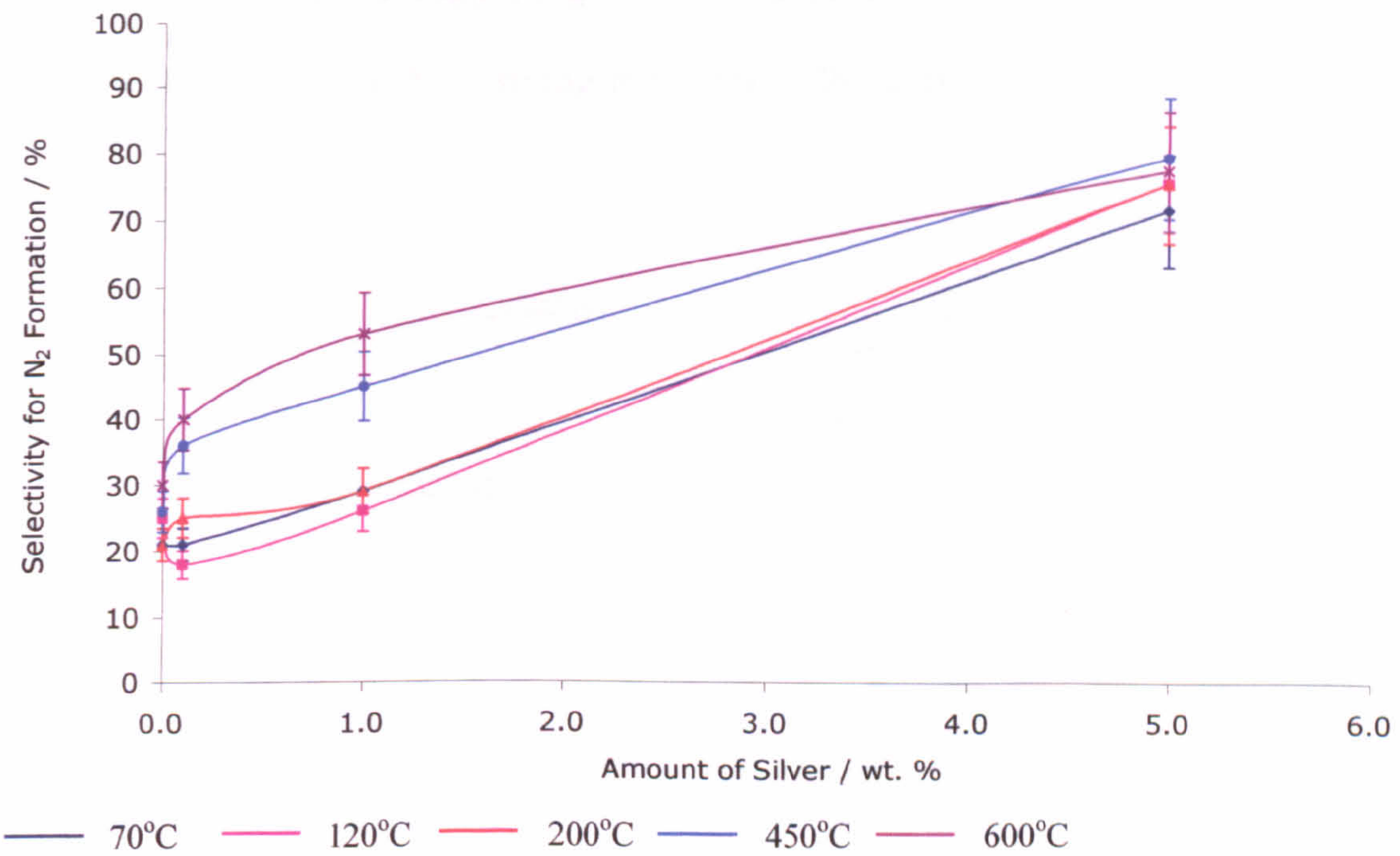


*Figure 6.3. Effect of silver content on the selectivity for $N_2$ formation for photocatalysts calcined at various temperatures for 2 h. Decomposition conditions: NO concentration was 909 ppm. Total flow rate 5.5 sccm.*

Theoretical calculations based on $Ag^+$ monomers and oligomers (figure 6.4 (a) and (b) respectively) have shown that UV initiated NO decomposition reactions forming $N_2$ and $O_2$ via metal-to-ligand charge transfer (MLCT) transitions are feasible reactions as such transitions are favoured due to the symmetry for electric dipole transitions and require low energies which are accessible by UV light sources.[18] It was also suggested that the likelihood for the photoreaction is increased for oligomeric $Ag^+$ species, which is a more realistic model of the surface for the silver clusters present on the photocatalysts used for this thesis.

When CO was present in the reaction gas, the selectivity for $N_2$ formation increased with both increasing temperature and silver loading and the reaction became 100 % selective, again suggesting that the presence of metallic silver particles promotes the rate of the $N_2$ forming reactions at the expense of reactions that yield $N_2O$ (figure 6.5).

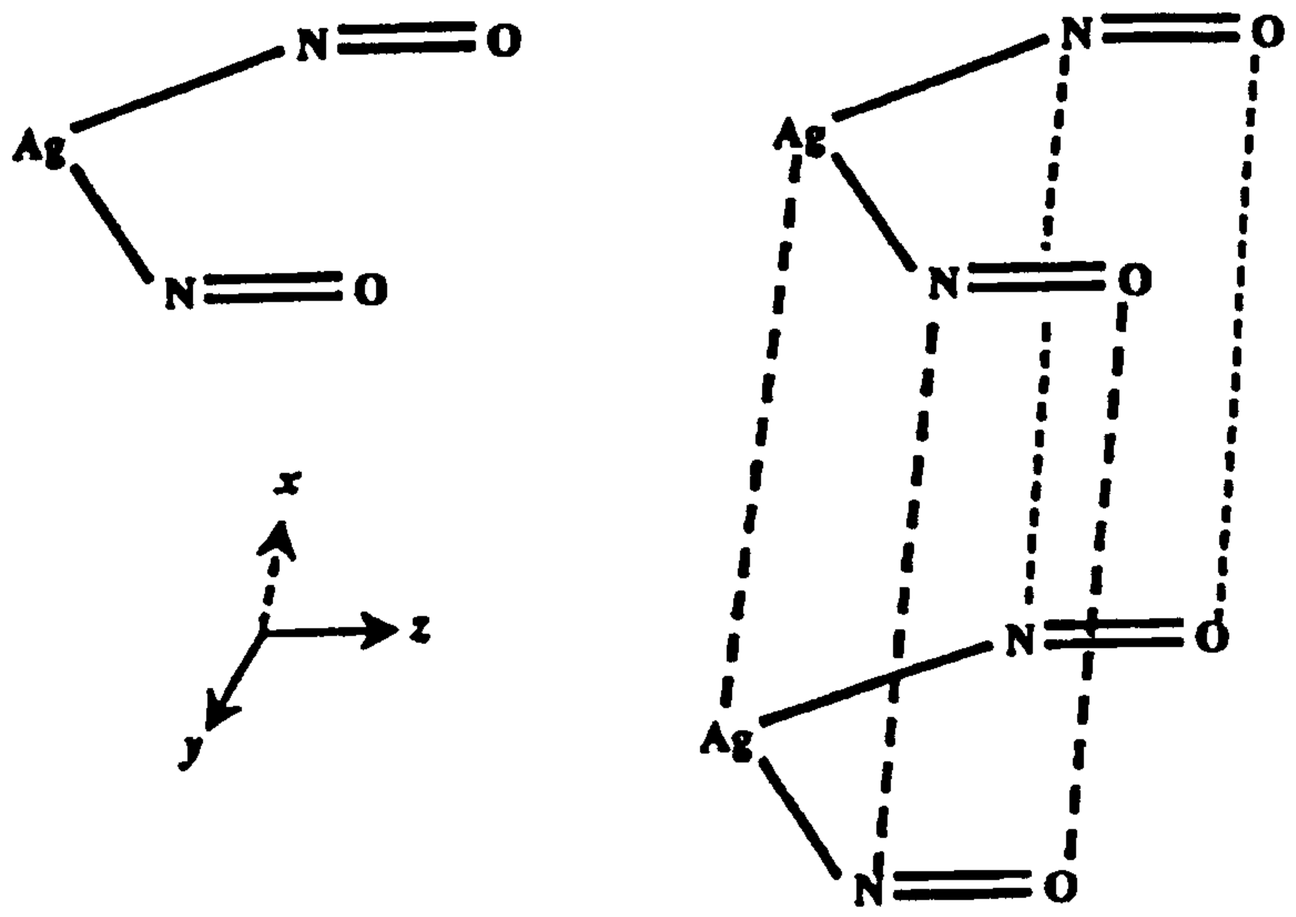


*Figure 6.4. Theoretical models used to calculate the likelihood of NO decompositions reactions occurring on silver species.*[18]

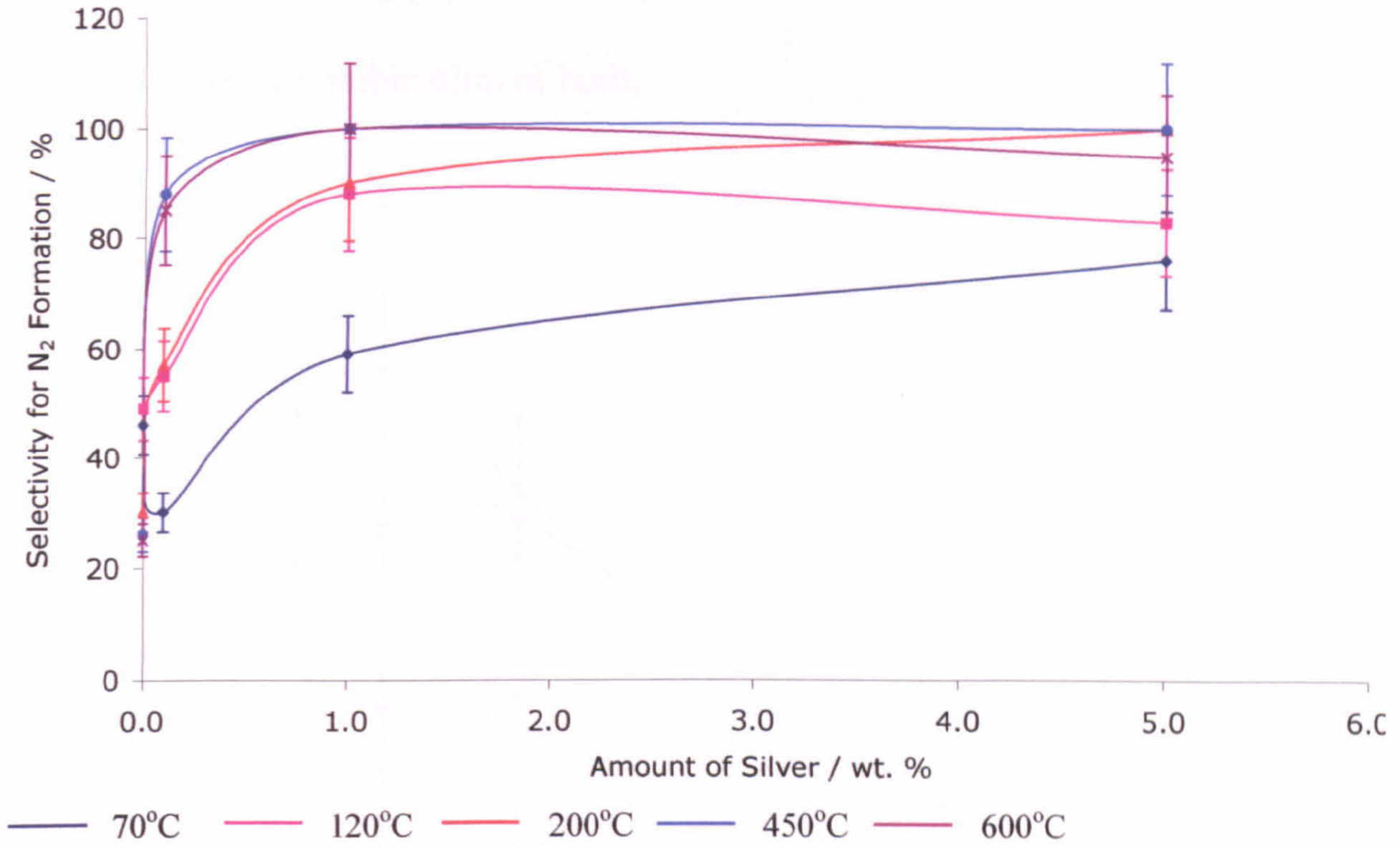


*Figure 6.5. Effect of silver content on the selectivity for $N_2$ formation for photocatalysts calcined at various temperatures for 2 h. Reduction conditions: NO and CO concentrations were 909 ppm and 1818 ppm respectively. Total flow rate 5.5 sccm.*

Comparing the rates of $N_2$ and $N_2O$ formation under decomposition and reduction conditions for the 1Ag-P25 photocatalyst (figure 6.6), it can be seen that both decrease with increasing catalyst pretreatment temperatures. The major factor for the decrease was the reduction in activity of the photocatalyst. More importantly, the rate of $N_2$ formation was higher in the presence of CO, whilst the opposite was observed for the rate of $N_2O$ formation. In fact, in the presence of CO, the rate of $N_2O$ formation was low for all the calcination temperatures (typically $< 30$ μmol $h^{-1}$ $g^{-1}$) and the rate of $N_2$ formation was significantly higher at typically *ca.* 150 μmol $h^{-1}$ $g^{-1}$ (although the rate did drop after calcination at temperatures of 450°C and above). From these observations it is proposed that the decrease in the rate of $N_2O$ formation in the presence of CO was either because of an increase in the rate

of $N_2O$ conversion to $N_2$ (equation 5.13) or a decrease in the rate of formation of $N_2O$ (equation 5.3) or a combination of both.

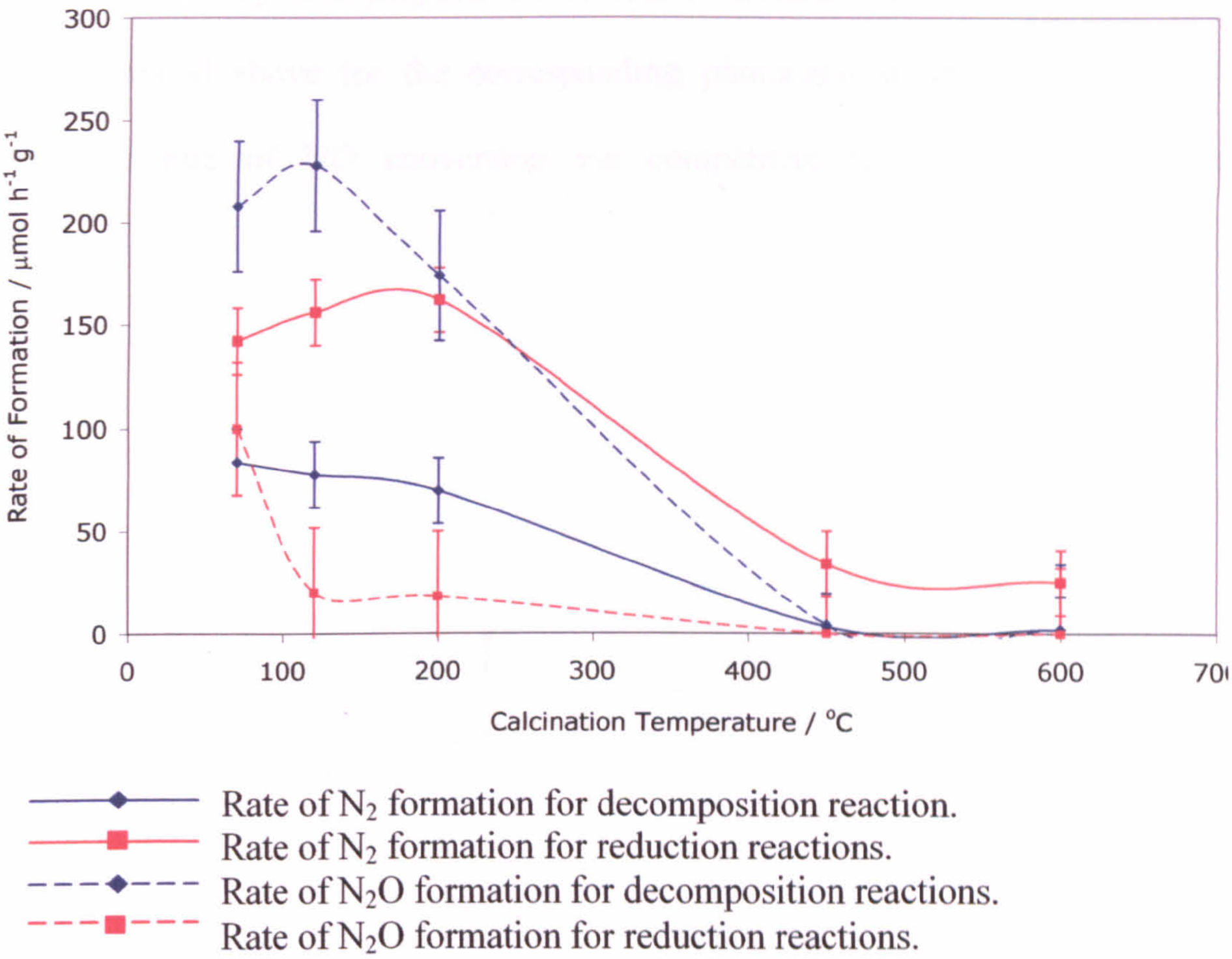


*Figure 6.6. The rates of formation of $N_2$ and $N_2O$ for NO decomposition and reduction reactions over 1Ag-P25 photocatalysts calcined at various temperatures. Decomposition conditions: NO 909 ppm with Ar balance and a total flow rate of 5.5 sccm. Reduction conditions: As for decomposition reactions with the addition of CO at 1818 ppm.*

### 6.3.2 Effect of varying NO concentration

As shown in chapter 5, percentage NO conversion is not a good indication of the activity of photocatalysts when comparing reactions with varying NO concentration and therefore figure 6.7 depicts the trends in NO conversion rate for both decomposition and reductions reactions over 1Ag-P25 photocatalysts calcined at 200°C, with varying NO levels. It is clear that NO conversion rate increased linearly with increasing NO concentration for both reaction types. As shown in figure 6.7, at

constant CO levels the rate of NO conversion was only affected by the initial concentration of NO and not the NO/CO ratio (i.e. as for the decomposition experiments, activity was proportional to NO concentration). Consistent with the results presented above for the corresponding photocatalyst, the presence of CO inhibits the rate of NO conversion via competitive adsorption, as discussed previously.

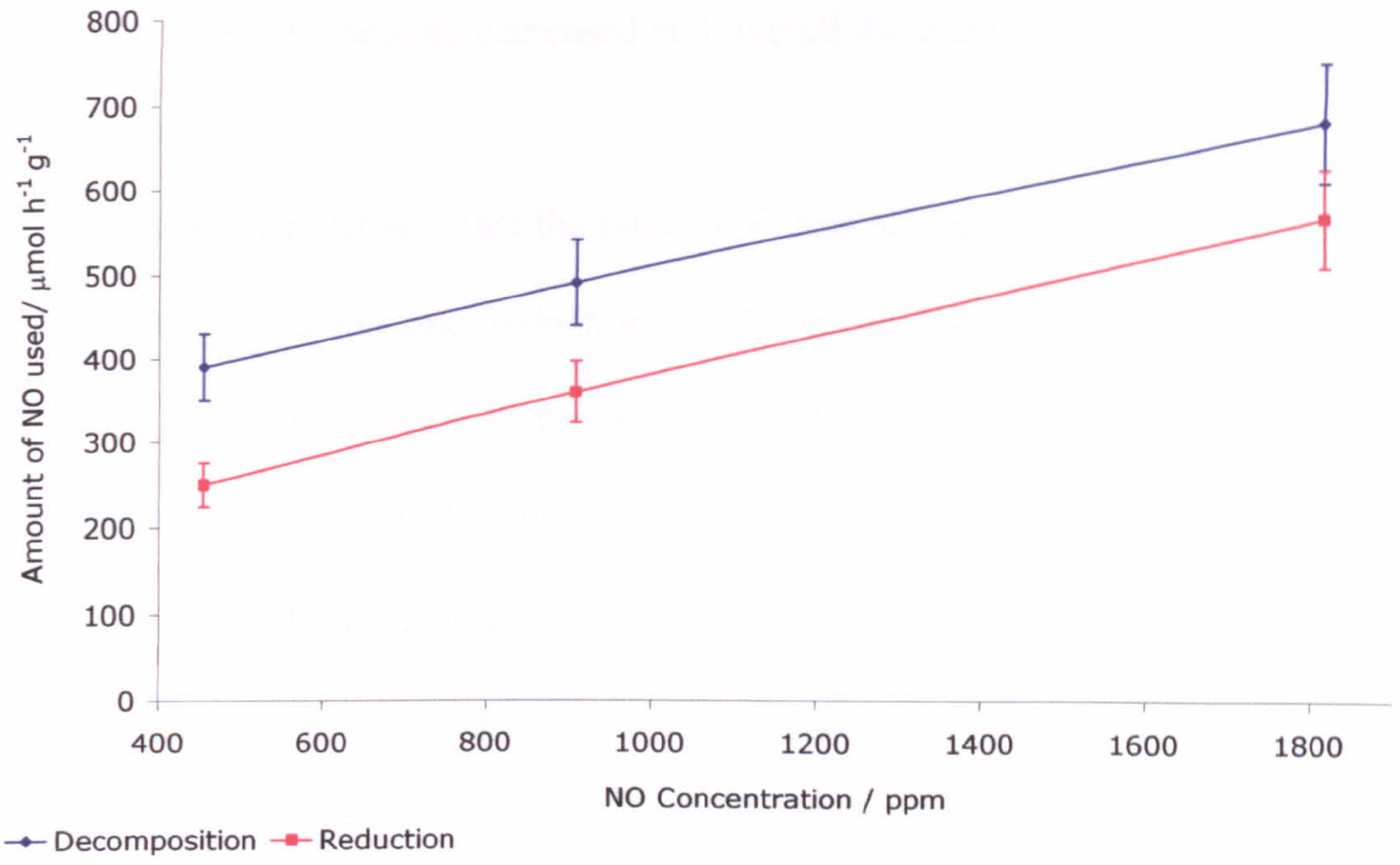


*Figure 6.7. Effect of NO concentration on the moles of NO used over 1Ag-P25 photocatalysts calcined at 200°C. Decomposition reaction conditions: Total flow rate of 5.5 sccm. Reduction reaction conditions: Same as for decomposition reactions with a constant concentration of CO (1818 ppm).*

Under decomposition conditions, the selectivity of the photoreaction products remained unaltered irrespective of the NO concentration (figure 6.8). This is as expected because the relative rate of $N_2$ and $N_2O$ forming reactions would be the same as the same active sites would have been present in each experiment. The overall rate of reactions increased (as indicated by the increase in conversion) due to mass

transport of more NO to the surface of the photocatalyst as the NO concentration increased.

Under reduction conditions the selectivity for $N_2$ formation decreased with an increase in the NO/CO ratio, i.e. with increasing NO concentration (figure 6.8). As discussed above, surface NO-CO reactions over Ag-P25 photocatalysts were very selective for $N_2$ formation, whilst NO-NO reactions were less selective and yielded both $N_2$ and $N_2O$ as products. Obviously as the NO/CO ratio increased the relative number of NO-CO reactions decreased and overall the reaction became less selective for $N_2$ formation.

Figure 6.9 illustrates that the rates of $N_2$ and $N_2O$ formation increased slightly for both decomposition and reduction conditions as the initial NO concentration increased. From comparison of the formation rates it is apparent that the rate of $N_2$ formation in the presence of CO (*ca.* 75 μmol $h^{-1}$ $g^{-1}$ – 100 μmol $h^{-1}$ $g^{-1}$) was higher than the rate of $N_2O$ formation under the same conditions and higher than the rate of $N_2$ formation under decomposition conditions, for all the NO concentrations investigated. Hence, under reduction conditions the 1Ag-P25 photocatalyst was a good catalyst for the production of $N_2$ with minimal $N_2O$ formation for all the NO/CO ratios studied.

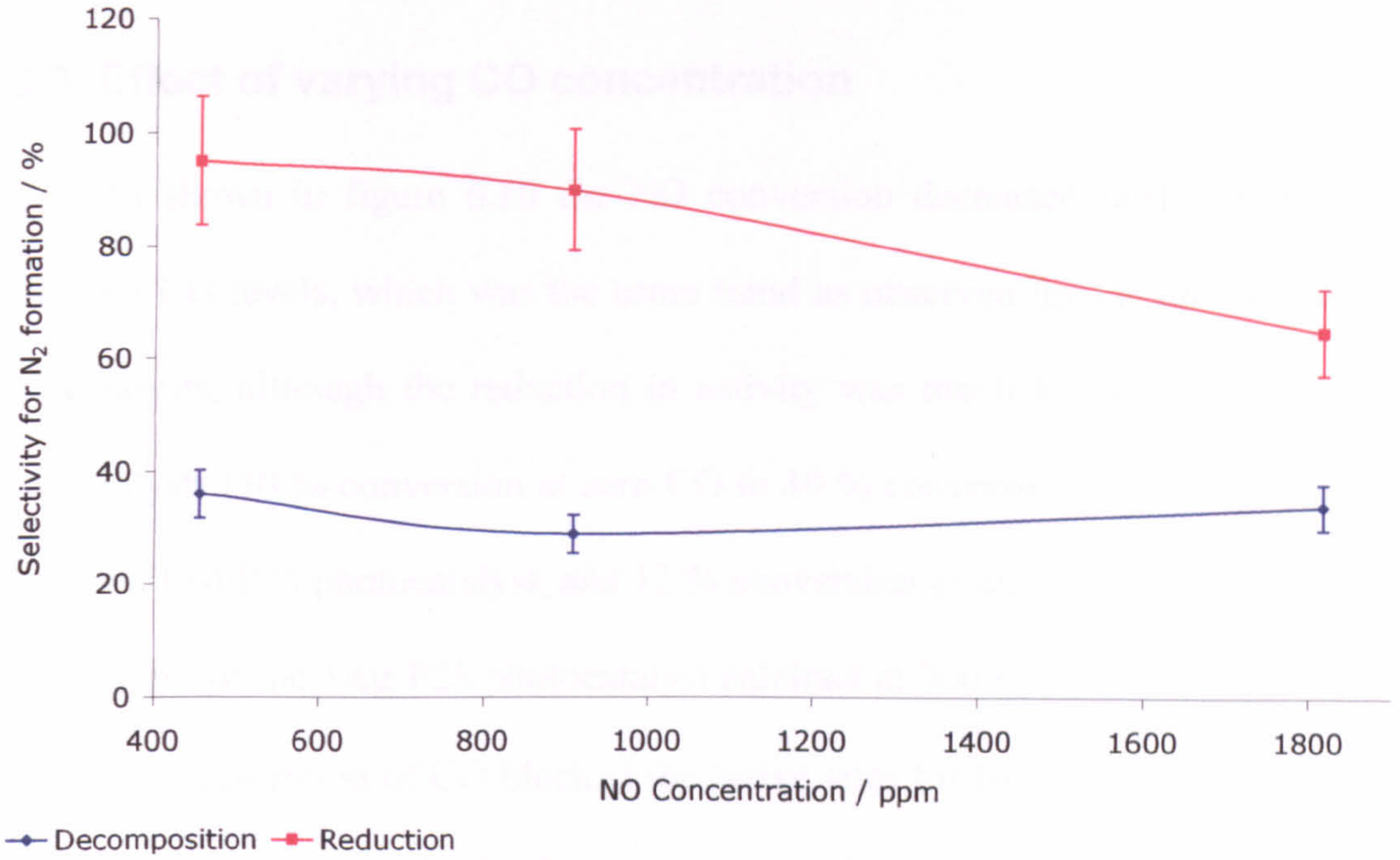


*Figure 6.8. Effect of NO concentration on the selectivity for $N_2$ formation over 1Ag-P25 photocatalysts calcined at 200°C. Decomposition reaction conditions: Total flow rate of 5.5 sccm. Reduction reaction conditions: Same as for decomposition reactions with a constant concentration of CO (1818 ppm).*

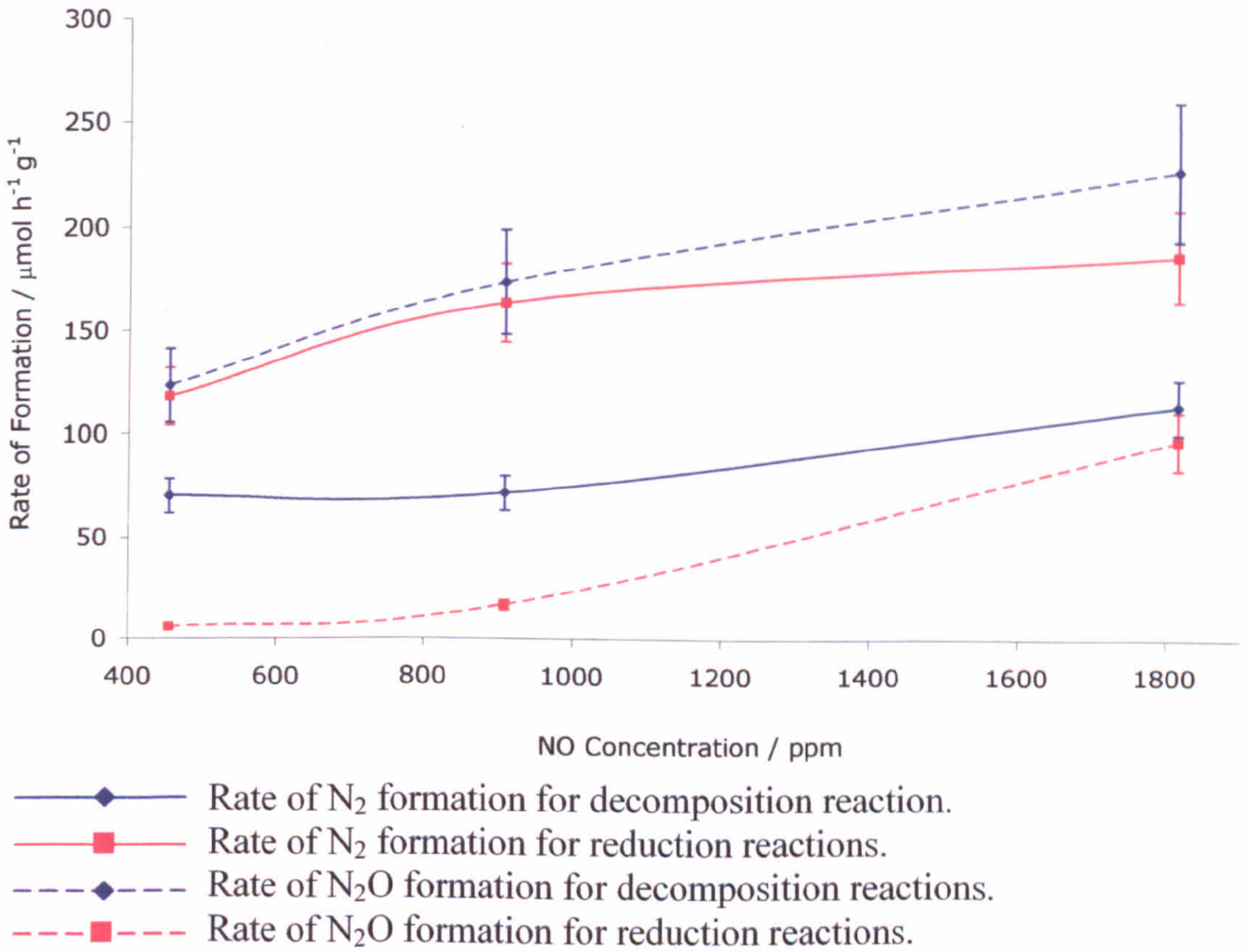


*Figure 6.9. Rates of formation of $N_2$ and $N_2O$ for decomposition and reduction reactions with varying NO levels over 1Ag-P25 photocatalysts calcined at 200°C. Decomposition reaction conditions: Total flow rate of 5.5 sccm. Reduction reaction conditions: Same as for decomposition reactions with a constant concentration of CO (1818 ppm).*

### 6.3.3 Effect of varying CO concentration

As shown in figure 6.10 the NO conversion decreased fairly linearly with increasing CO levels, which was the same trend as observed for the unmodified P25 photocatalysts, although the reduction in activity was much lower for the 1Ag-P25 photocatalysts (30 % conversion at zero CO to 10 % conversion at 1818 ppm CO for the unmodified P25 photocatalyst, and 12 % conversion at zero CO to 8 % conversion at 1818 ppm for the 1Ag-P25 photocatalyst calcined at 200°C). Over unmodified P25 surfaces, the adsorption of CO blocked the active sites for NO adsorption, thus as the CO levels were increased, the NO conversion decreased, as less NO would be adsorbed. Although similar processes would have an effect on the reactions over Ag-P25 photocatalysts, the presence of silver species may offer alternative adsorption and/or additional reaction sites on which NO conversion can proceed even in the presence of CO.

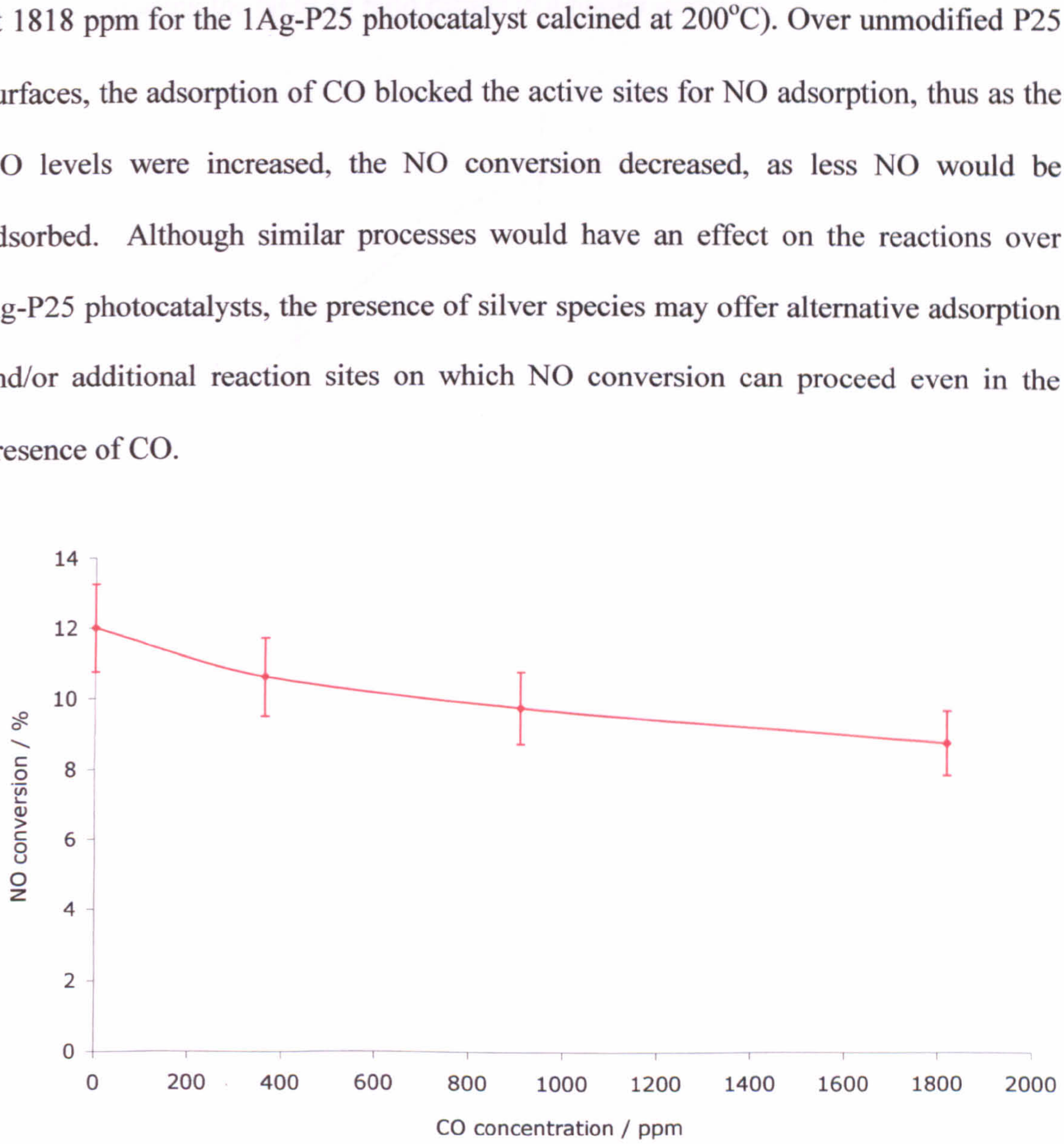


*Figure 6.10. Effect of CO concentration on percentage conversion of NO over 1Ag-P25 photocatalysts calcined at 200°C. Reaction conditions: NO concentration and total flow rate were kept constant at 909 ppm and 5.5 sccm respectively.*

The increase in selectivity for $N_2$ formation observed with increasing CO concentration at constant NO levels (figure 6.11.) can be explained by considering the ratio of adsorbed NO and CO molecules and the possible surface reactions. As the CO concentration was increased, the probability that CO was adsorbed in close proximity to an NO molecule increased, resulting in an increase of the highly selective NO-CO reactions at the expense of the less selective NO-NO reactions. Hence decreasing the NO/CO ratio results in a higher selectivity for $N_2$ formation.

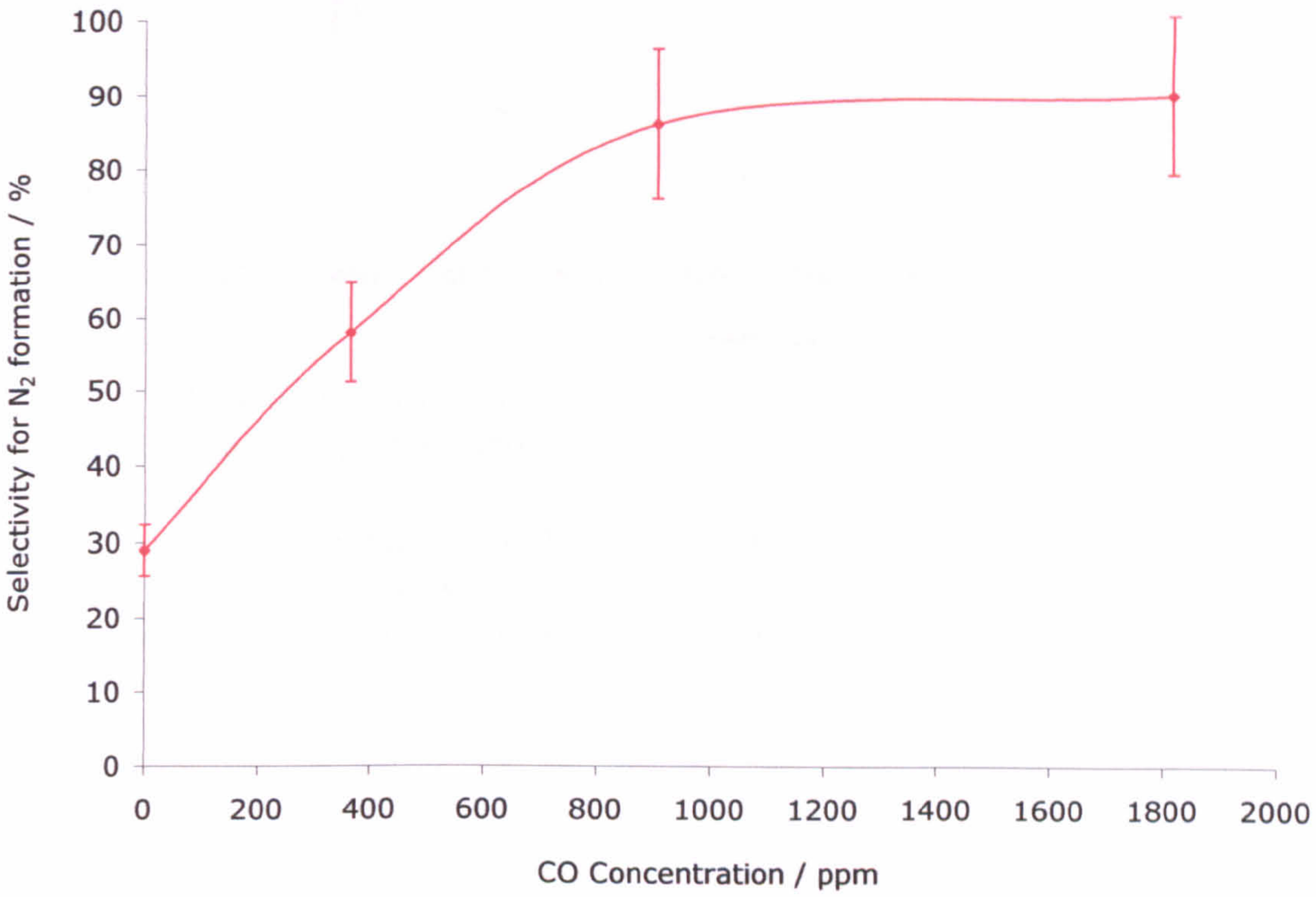


*Figure 6.11. Effect of CO concentration on the selectivity for $N_2$ formation over 1Ag-P25 photocatalysts calcined at 200°C. Reaction conditions: NO concentration and total flow rate were kept constant at 909 ppm and 5.5 sccm respectively.*

The trends shown in figure 6.12 for the rates of formation of $N_2$ and $N_2O$ reflect the fact that although there was a slight decrease in NO conversion with increased CO concentrations, the higher selectivities towards $N_2$ formation resulted in a greater than double increase of the $N_2$ formation rate. The graph also illustrates that

there was little improvement in the rate of $N_2$ formation for CO concentrations greater than 909 ppm.

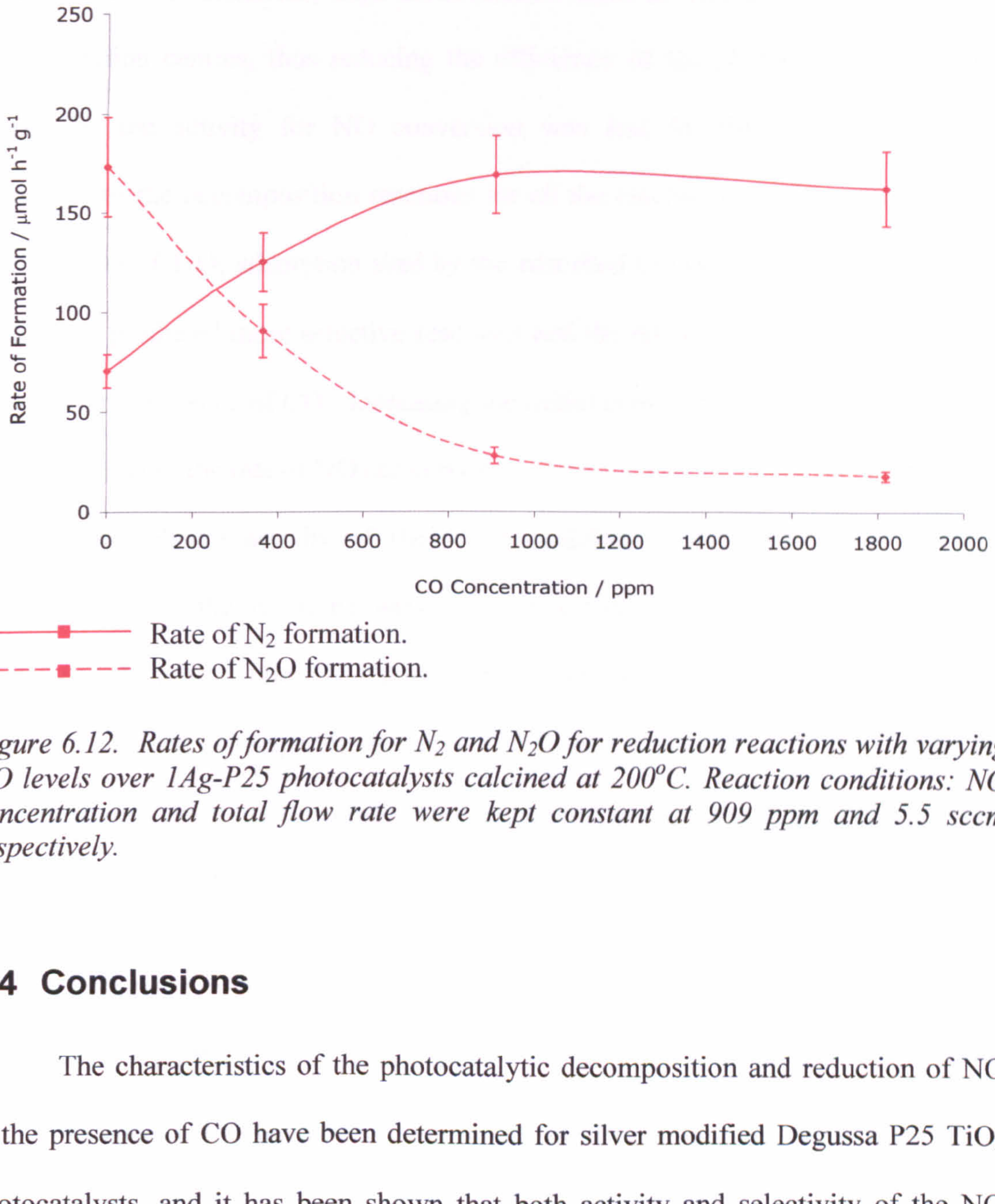


*Figure 6.12. Rates of formation for $N_2$ and $N_2O$ for reduction reactions with varying CO levels over 1Ag-P25 photocatalysts calcined at 200°C. Reaction conditions: NO concentration and total flow rate were kept constant at 909 ppm and 5.5 sccm respectively.*

## 6.4 Conclusions

The characteristics of the photocatalytic decomposition and reduction of NO in the presence of CO have been determined for silver modified Degussa P25 $TiO_2$ photocatalysts, and it has been shown that both activity and selectivity of the NO photoreactions were strongly dependant on the nature of the deposited silver species.

It was found that both increasing the silver loading and increasing the pretreatment temperature had a detrimental effect on the photocatalytic activity of the photocatalysts under both decomposition and reduction conditions. It is believed this was due to the removal of molecular water and hydroxyl groups from the P25 surface

at higher calcination temperatures, thus reducing the number of active sites available. Also, silver nitrate was thermally reduced to form silver particles and clusters which when present in sufficiently high concentration acted as efficient electron-hole pair recombination centres, thus reducing the efficiency of the photocatalytic reactions. Generally, the activity for NO conversion was less for the reduction reactions compared to the decomposition reactions for all the reaction conditions tested due to the blocking of $TiO_2$ adsorption sites by the adsorbed CO molecules. However, these conditions produced more selective reactions and the rate of $N_2$ formation was much higher in the presence of CO. Increasing the initial concentration of NO resulted in a linear increase in the rate of NO conversion.

Although the activity of the silver modified photocatalysts was less than unmodified P25, the reactions were more selective for $N_2$ formation for all the photocatalysts tested. The NO reduction reactions over 1Ag-P25 and 5Ag-P25 that had been calcined at temperatures above 200°C were essentially 100 % selective for $N_2$ formation. Thus, it is concluded that these catalysts were efficient SCR catalysts for the reduction of NO with CO.

## 6.5 References


(1) Yoneyama, H.; Shiota, H.; Tamura, H. *Bull. Chem. Soc. Jpn.* **1981**, *54*, 1308.
(2) Lim, T. H.; Jeong, S. M.; Kim, S. D.; Gyenis, J. *React. Kinet. Catal. Lett.* **2000**, *71*, 223.
(3) Herrmann, J. M.; Tahiri, H.; AitIchou, Y.; Lassaletta, G.; GonzalezElipe, A. R.; Fernandez, A. *Appl. Catal. B Environ.* **1997**, *13*, 219.
(4) Fox, M. A.; Dulay, M. T. *Chem. Rev.* **1993**, *93*, 341.
(5) Hoffmann, M. R.; Martin, S. T.; Choi, W. Y.; Bahnemann, D. W. *Chem. Rev.* **1995**, *95*, 69.
(6) Linsebigler, A. L.; Lu, G. Q.; Yates, J. T. *Chem. Rev.* **1995**, *95*, 735.
(7) Disdier, J.; Herrmann, J. M.; Pichat, P. *J. Chem. Soc. Faraday Trans. I* **1983**, *79*, 651.
(8) Matsuoka, M.; Matsuda, E.; Tsuji, K.; Yamashita, H.; Anpo, M. *J. Mol. Catal. A Chem.* **1996**, *107*, 399.

(9) Yamashita, Y.; Aoyama, N.; Takezawa, N.; Yoshida, K. *J. Mol. Catal. A Chem.* **1999**, *150*, 233.
(10) Bera, P.; Patil, K. C.; Hegde, M. S. *Phys. Chem. Chem. Phys.* **2000**, *2*, 3715.
(11) Ding, Z.; Lu, G. Q.; Greenfield, P. F. *J. Phys. Chem. B* **2000**, *104*, 4815.
(12) Chao, H. E.; Yu, Y.; Hu, X. F.; Larbot, A. *Appl. Surf. Sci.* **2002**, *200*, 239.
(13) Chao, H. E.; Yun, Y. U.; Xingfang, H. U.; Larbot, A. *J. European Ceram. Soc.* **2003**, *23*, 1457.
(14) Palmisano, L.; Augugliaro, V.; Sclafani, A.; Schiavello, M. *J. Phys. Chem.* **1988**, *92*, 6710.
(15) Peral, J.; Casado, J.; Domenech, J. *J. Photochem. Photobiol. A Chem.* **1988**, *44*, 209.
(16) Borgarello, E.; Kiwi, J.; Gratzel, M.; Pelizzetti, E.; Visca, M. *J. Am. Chem. Soc.* **1982**, *104*, 2996.
(17) Bogdanchikova, N.; Meunier, F. C.; Avalos-Borja, M.; Breen, J. P.; Pestryakov, A. *Appl. Catal. B Environ.* **2002**, *36*, 287.
(18) Kanan, S. M.; Omary, M. A.; Patterson, H. H.; Matsuoka, M.; Anpo, M. *J. Phys. Chem. B* **2000**, *104*, 3507.
(19) Akolekar, D. B.; Bhargava, S. K. *J. Mol. Catal. A Chem.* **2000**, *157*, 199.
(20) Haneda, M.; Kintaichi, Y.; Inaba, M.; Hamada, H. *Bull. Chem. Soc. Jpn.* **1997**, *70*, 499.
(21) Furusawa, T.; Seshan, K.; Lercher, J. A.; Lefferts, L.; Aika, K. *Appl. Catal. B Environ.* **2002**, *37*, 205.

# 7 Photocatalytic reactions over rhodium modified Degussa P25 photocatalysts.

## 7.1 Introduction

In the area of thermal catalysis, the reduction of NO with CO (and other reductants) is a rigorously studied topic,[1-10] and supported metals of the type Pt, Pd, Rh, Ru, Cu, etc., have been found to be some of the most active (especially in the realm of three-way automobile exhaust catalysts) when supported on $SiO_2$, $Al_2O_3$, $ZrO_2$, $La_2O_3$ and $CeO_2$.[6] Supported rhodium based catalysts have been intensively studied and in most cases it was reported that NO was selectively reduced to $N_2$ when relatively high reaction temperatures were employed,[7-9] although there have been some reports showing the formation of both $N_2$ and $N_2O$.[5,10]

Although most of the studies of supported rhodium catalysts involved thermally activated processes, it has also been reported that rhodium can be activated by UV photons when a photoactive support such as $TiO_2$ is used.[11,12] For example, Kohno[12] reported that when metallic rhodium particles were supported on $TiO_2$ the rate of conversion and selectivity for benzene mineralisation were enhanced compared to a bare $TiO_2$ photocatalyst. It has been proposed that the activation of Rh sites was via photo-excited electron transfer from the UV irradiated $TiO_2$, to the metallic rhodium centres. Although it has been shown that $Rh^{3+}$ carbonyl complexes are highly active homogeneous photocatalysts, to the best of the author's knowledge there have been no reports in the literature reporting the use of supported $Rh^{3+}$ species for photocatalysed heterogeneous reactions.

The aim of the work presented in this chapter was to investigate the effects of rhodium species supported on Degussa P25, on the photocatalytic activity and the

selectivity of NO decomposition reactions, as well as NO reduction reactions in the presence of CO. Also investigated was the effect of different rhodium loadings along with the effect of different photocatalyst pretreatments, including calcinations in air and both the UV and $H_2$ reduction of the photocatalysts. The results are compared to those obtained for unmodified P25 photocatalysts that were reported in Chapter 5.

This chapter presents the results from the photocatalytic activity tests carried out on rhodium modified Degussa P25 films. The effects of the four different photocatalyst pretreatments used on the NO decomposition and reduction (in the presence of CO) reactions are reported in subsections 7.2.1 to 7.2.4. The effects of varying the concentrations of NO and CO in the reaction gas stream are presented in sections 7.2.5 and 7.2.6. Section 7.3 presents a detailed discussion of all the results presented in 7.2, and conclusions from these discussions are drawn in section 7.4.

## 7.2 Results

### 7.2.1 Rh-P25 photocatalysts – Dried at 70°C

Rh-P25 photocatalysts with Rh loadings of 0.1, 1 and 5 wt. % were prepared by impregnation. Further details of the preparation methodology are described in chapter 3. The resulting dispersions were then dried onto glass slides at 70°C and their photocatalytic behaviour was measured for both NO decomposition and reduction reactions. The decomposition reactions were carried out under a gas stream containing 909 ppm of NO and the reduction reactions were investigated using the same conditions but with the addition of CO at 1818 ppm. The total flow rate was kept constant at 5.5 sccm for all of the reactions.

The activity of the P25 photocatalysts for NO conversion under decomposition conditions, decreased from 30 % to 18 % with the addition of 0.1 wt. % rhodium.

However, increasing the concentration of rhodium had little effect on the conversion rate (table 7.1). The opposite trend was observed when CO was present in the reaction gas, and the NO conversion increased dramatically from 16 % for the as dried P25 photocatalyst to 87 % for all the Rh-P25 photocatalysts. This percentage conversion of NO corresponds to a conversion rate of 3500 μmol $h^{-1}$ $g^{-1}$.

| Rh loading / wt. % | Conversion of NO / % | | Rate of NO conversion / μmol $h^{-1}$ $g^{-1}$ | |
|---|---|---|---|---|
| | Decomposition | Reduction | Decomposition | Reduction |
| 0 | 29.6 | 16.0 | 1211 | 655 |
| 0.1 | 18.0 | 87.4 | 736 | 3576 |
| 1.0 | 17.9 | 87.7 | 731 | 3585 |
| 5.0 | 15.0 | 87.0 | 614 | 3556 |

*Table 7.1. Table of NO conversions for the NO decomposition and reduction reactions for as dried P25 photocatalysts loaded with varying amounts of rhodium. Decomposition conditions: NO 909 ppm with Ar balance and a total flow rate of 5.5 sccm. Reduction conditions: As for decomposition reactions with the addition of CO at 1818 ppm.*

The selectivities for both the decomposition and reduction reactions are presented in table 7.2. Under decomposition conditions the selectivity for $N_2$ formation over the rhodium modified photocatalysts was very similar to the selectivity of an unmodified P25 photocatalyst at 25 % selectivity for $N_2$ formation. The level of rhodium doping had no effect on the selectivity of the decomposition reaction. In the presence of CO, the selectivity for $N_2$ formation was considerably less over the photocatalysts containing rhodium (12 % selectivity for $N_2$ formation) when compared to NO reduction reactions over unmodified P25 photocatalysts (46 % selectivity for $N_2$ formation). Again the level of rhodium doping had no effect on the selectivity of the reaction. For the other photocatalyst systems described in this thesis (P25 and Ag-P25 systems), the selectivity of the reactions for $N_2$ formation was

always greater in the presence of CO when compared to the corresponding NO decomposition reaction.

| Rh loading / wt. % | Selectivity for decomposition reactions / % | | Selectivity for reduction reactions / % | |
|---|---|---|---|---|
| | $N_2$ | $N_2O$ | $N_2$ | $N_2O$ |
| 0 | 21 | 79 | 46 | 54 |
| 0.1 | 26 | 74 | 12 | 88 |
| 1.0 | 24 | 76 | 12 | 88 |
| 5.0 | 25 | 75 | 10 | 90 |

*Table 7.2. Table of selectivities for NO decomposition and reduction reactions over as dried P25 photocatalysts loaded with varying amounts of rhodium. Decomposition conditions: NO 909 ppm with Ar balance and a total flow rate of 5.5 sccm. Reduction conditions: As for decomposition reactions with the addition of CO at 1818 ppm.*

From the results shown in table 7.3 it can be seen that the rates of formation of $N_2$ and $N_2O$ are not affected by the concentration of Rh, but vary depending on the composition of the reaction gas. For decomposition, the rates of formation of $N_2$ and $N_2O$ were *ca.* 90 μmol $h^{-1}$ $g^{-1}$ and *ca.* 270 μmol $h^{-1}$ $g^{-1}$ respectively. When CO was present, both rate of formation of $N_2$ and $N_2O$ were higher at *ca.* 200 μmol $h^{-1}$ $g^{-1}$ and *ca.* 1600 μmol $h^{-1}$ $g^{-1}$, respectively.

| Rh loading / wt. % | Rate of $N_2$ formation / μmol $h^{-1}$ $g^{-1}$ | | Rate of $N_2O$ formation / μmol $h^{-1}$ $g^{-1}$ | |
|---|---|---|---|---|
| | Decomposition | Reduction | Decomposition | Reduction |
| 0 | 127 | 151 | 478 | 177 |
| 0.1 | 96 | 215 | 272 | 1574 |
| 1.0 | 88 | 215 | 278 | 1577 |
| 5.0 | 77 | 178 | 230 | 1600 |

*Table 7.3. Rates of formation for the products of the photocatalytic reactions over as dried P25 photocatalysts loaded with varying amounts of rhodium. Decomposition conditions: NO 909 ppm with Ar balance and a total flow rate of 5.5 sccm. Reduction conditions: As for decomposition reactions with the addition of CO at 1818 ppm.*

### 7.2.2 Rh-P25 photocatalysts – Calcined at 200°C

Rh-P25 photocatalysts with Rh loadings of 0.1, 1 and 5 wt. % were prepared by impregnation. The resulting dispersions were then dried onto glass slides at 70°C and further calcined for 2 h at 200°C. After calcination their photocatalytic behaviour was measured for both NO decomposition and reduction reactions. The decomposition reactions were carried out under a gas stream containing 909 ppm of NO and the reduction reactions were investigated using the same conditions but with the addition of CO at 1818 ppm. The total flow rate was kept constant at 5.5 sccm for all of the reactions.

The activity of the P25 based photocatalysts for NO decomposition decreased from 24 % to 13 % with the addition of 0.1 wt. % Rh, however increasing the concentration of rhodium had little effect on the conversion rate (*ca.* 10 % NO conversion for 5Rh-P25, table 7.4). As with the Rh-P25 photocatalysts tested after drying at 70°C, the rate of NO conversion was higher when CO was present in the reaction stream (*ca.* 25 % conversion for 0.1, 1.0, and 5.0 wt. Rh-P25 photocatalysts). It should be noted that the increase in activity observed over Rh-P25 photocatalysts calcined at 200°C under reduction conditions was significantly less than observed over the Rh-P25 photocatalyst dried at 70°C, where the NO conversion was as high as 88 %.

| Rh loading / wt. % | Conversion of NO / % | | Rate of NO conversion / μmol $h^{-1}$ $g^{-1}$ | |
|---|---|---|---|---|
| | Decomposition | Reduction | Decomposition | Reduction |
| 0 | 24.0 | 11.4 | 982 | 466 |
| 0.1 | 13.0 | 24.3 | 531 | 993 |
| 1.0 | 11.9 | 25.0 | 487 | 1023 |
| 5.0 | 9.7 | 26.1 | 397 | 1067 |

*Table 7.4. Table of NO conversions for the NO decomposition and reduction reactions over P25 photocatalysts loaded with varying amounts of rhodium and calcined at 200°C for 2 h. Decomposition conditions: NO 909 ppm with Ar balance and a total flow rate of 5.5 sccm. Reduction conditions: As for decomposition reactions with the addition of CO at 1818 ppm.*

The selectivities for both the decomposition and reduction reactions are presented in table 7.5. For both reaction types, the selectivity for $N_2$ formation was not affected by the rhodium concentration and remained at 29 % and 15 % for the decomposition and reduction reactions respectively. In the absence of CO the selectivity for $N_2$ formation of the Rh-P25 photocatalysts was slightly higher than the corresponding unmodified P25 photocatalysts, whilst in the presence of CO the selectivity for $N_2$ formation was lower than for the Rh-P25 photocatalysts.

| Rh loading / wt. % | Selectivity for decomposition reactions / % | | Selectivity for reduction reactions / % | |
|---|---|---|---|---|
| | $N_2$ | $N_2O$ | $N_2$ | $N_2O$ |
| 0 | 21 | 79 | 30 | 70 |
| 0.1 | 29 | 71 | 18 | 82 |
| 1.0 | 28 | 72 | 13 | 87 |
| 5.0 | 29 | 71 | 14 | 84 |

*Table 7.5. Table of selectivities for NO decomposition and reduction reactions over P25 photocatalysts loaded with varying amounts of rhodium and calcined at 200°C for 2 h. Decomposition conditions: NO 909 ppm with Ar balance and a total flow rate of 5.5 sccm. Reduction conditions: As for decomposition reactions with the addition of CO at 1818 ppm.*

As was observed with the Rh-P25 photocatalysts dried at 70°C, the rates of formation of $N_2$ and $N_2O$ were not affected by the Rh concentration but varied for the decomposition and reduction reactions (table 7.6). For the decomposition reactions

the rate of formation of $N_2$ and $N_2O$ were *ca.* 70 μmol $h^{-1}$ $g^{-1}$ and *ca.* 80 μmol $h^{-1}$ $g^{-1}$ respectively. In the presence of CO, the rates of formation of both the products were higher at *ca.* 175 μmol $h^{-1}$ $g^{-1}$ and *ca.* 440 μmol $h^{-1}$ $g^{-1}$ for $N_2$ and $N_2O$ respectively.

| Rh loading / wt. % | Rate of $N_2$ formation / μmol $h^{-1}$ $g^{-1}$ | | Rate of $N_2O$ formation / μmol $h^{-1}$ $g^{-1}$ | |
|---|---|---|---|---|
| | Decomposition | Reduction | Decomposition | Reduction |
| 0 | 103 | 70 | 388 | 163 |
| 0.1 | 77 | 89 | 188 | 407 |
| 1.0 | 68 | 67 | 177 | 455 |
| 5.0 | 58 | 75 | 141 | 459 |

*Table 7.6. Rates of formation for the products of the photocatalytic reactions over P25 photocatalysts loaded with varying amounts of rhodium and calcined at 200°C for 2 h. Decomposition conditions: NO 909 ppm with Ar balance and a total flow rate of 5.5 sccm. Reduction conditions: As for decomposition reactions with the addition of CO at 1818 ppm.*

### 7.2.3 Rh-P25 photocatalysts – UV reduced

Rh-P25 photocatalysts with Rh loadings of 0.1, 1 and 5 wt. % were prepared by impregnation. The resulting dispersions were then dried onto glass slides at 70°C and then UV reduced in an IPA solution. After UV reduction their photocatalytic behaviour was measured for both NO decomposition and reduction reactions. The decomposition reactions were carried out under a gas stream containing 909 ppm of NO and the reduction reactions were investigated using the same conditions but with the addition of CO at 1818 ppm. The total flow rate was kept constant at 5.5 sccm for all of the reactions.

The activity of the UV reduced Rh-P25 photocatalysts for NO decomposition was virtually the same, regardless of the Rh concentration, at *ca.* 12 % NO conversion, which was also similar to an unmodified P25 photocatalysts that had also been subjected to UV reduction (table 7.7). However, in the presence of CO the

percentage NO conversion increased from 6.3 % for the UV reduced P25 to 28.4 % for the 0.1Rh-P25. Increasing the rhodium concentration resulted in further increases in NO conversion and at a loading of 5 wt. % Rh the NO conversion was as high as 62.2 %. When Rh was present, the NO conversion was higher for the reduction reactions, however over UV reduced P25 the reverse was observed.

| Rh loading / wt. % | Conversion of NO / % | | Rate of NO conversion / μmol $h^{-1}$ $g^{-1}$ | |
|---|---|---|---|---|
| | Decomposition | Reduction | Decomposition | Reduction |
| 0 | 10.2 | 6.3 | 416 | 256 |
| 0.1 | 11.3 | 28.4 | 463 | 1160 |
| 1.0 | 11.9 | 58.3 | 487 | 2384 |
| 5.0 | 14.7 | 62.2 | 603 | 2544 |

*Table 7.7. Table of NO conversions for the NO decomposition and reduction reactions over UV reduced P25 photocatalysts loaded with varying amounts of rhodium. Decomposition conditions: NO 909 ppm with Ar balance and a total flow rate of 5.5 sccm. Reduction conditions: As for decomposition reactions with the addition of CO at 1818 ppm.*

The selectivities for both the decomposition and reduction reactions are presented in table 7.8. Under decomposition conditions, the same trend was observed as for the NO conversion rate in that the Rh concentration had little effect on the selectivity of the reaction. For both the UV reduced P25 and UV reduced Rh containing systems the selectivity for $N_2$ formation was 35 %, which was higher than the selectivities observed for the as-dried systems and for those that were calcined at 200°C. However, in the presence of CO, the selectivity for $N_2$ formation decreased with increasing Rh concentration. Over UV reduced P25 the selectivity of the reaction for $N_2$ formation was as high as 56 %, but dropped to 21 % for the 0.1Rh-P25 system. Increasing the rhodium concentration resulted in a further decrease in the selectivity for $N_2$ formation, to as low as 10 % for the 5Rh-P25 photocatalyst.

| Rh loading / wt. % | Selectivity for decomposition reactions / % | | Selectivity for reduction reactions / % | |
|---|---|---|---|---|
| | $N_2$ | $N_2O$ | $N_2$ | $N_2O$ |
| 0 | 37 | 90 | 56 | 44 |
| 0.1 | 34 | 89 | 21 | 79 |
| 1.0 | 38 | 88 | 15 | 85 |
| 5.0 | 36 | 85 | 10 | 90 |

*Table 7.8. Table of selectivities for NO decomposition and reduction reactions over UV reduced P25 photocatalysts loaded with varying amounts of rhodium. Decomposition conditions: NO 909 ppm with Ar balance and a total flow rate of 5.5 sccm. Reduction conditions: As for decomposition reactions with the addition of CO at 1818 ppm.*

As shown in table 7.9 under decomposition conditions the rate of formation of both $N_2$ and $N_2O$ increased only slightly with increasing Rh loading ( 77 μmol $h^{-1}$ $g^{-1}$ for zero Rh to 109 μmol $h^{-1}$ $g^{-1}$ for 5 wt. % Rh). In the presence of CO the rate of formation of $N_2O$ increased significantly from 56 μmol $h^{-1}$ $g^{-1}$ over the UV reduced P25 to 1145 μmol $h^{-1}$ $g^{-1}$ over the 5Rh-P25 photocatalyst, whilst the rate of $N_2$ formation varied only slightly.

| Rh loading / wt. % | Rate of $N_2$ formation / μmol $h^{-1}$ $g^{-1}$ | | Rate of $N_2O$ formation / μmol $h^{-1}$ $g^{-1}$ | |
|---|---|---|---|---|
| | Decomposition | Reduction | Decomposition | Reduction |
| 0 | 77 | 72 | 131 | 56 |
| 0.1 | 79 | 122 | 153 | 458 |
| 1.0 | 92 | 179 | 151 | 1013 |
| 5.0 | 109 | 127 | 193 | 1145 |

*Table 7.9. Rates of formation for the products of the photocatalytic reactions over UV reduced P25 photocatalysts loaded with varying amounts of rhodium. Decomposition conditions: NO 909 ppm with Ar balance with a total flow rate of 5.5 sccm. Reduction conditions: As for decomposition reactions with CO at 1818 ppm.*

### 7.2.4 Rh-P25 photocatalysts – Hydrogen reduced

Rh-P25 photocatalysts with Rh loadings of 0.1, 1 and 5 wt. % were prepared by impregnation. The resulting dispersions were then dried onto glass slides at 70°C

and then reduced under $H_2$ at 450°C for 1 h. After hydrogen reduction their photocatalytic behaviour was measured for both NO decomposition and reduction reactions. The decomposition reactions were carried out under a gas stream containing 909 ppm of NO and the reduction reactions were investigated using the same conditions but with the addition of CO at 1818 ppm. The total flow rate was kept constant at 5.5 sccm for all of the reactions.

As shown in table 7.10 the activity of the hydrogen reduced Rh-P25 photocatalysts for NO conversion followed the same trends as was observed for the UV reduced Rh-P25 photocatalysts. For example under decomposition conditions the percentage NO conversion was nearly constant at *ca.* 10 % regardless of the Rh concentration and in the presence of CO the activity increased with Rh concentration (e.g. from *ca.* 6 % conversion for the hydrogen reduced P25 to *ca.* 26 % for hydrogen reduced 5Rh-P25 photocatalyst).

| Rh loading / wt. % | Conversion of NO / % | | Rate of NO conversion / μmol $h^{-1}$ $g^{-1}$ | |
|---|---|---|---|---|
| | Decomposition | Reduction | Decomposition | Reduction |
| 0 | 16.6 | 5.8 | 677 | 237 |
| 0.1 | 10.6 | 6.2 | 435 | 252 |
| 1.0 | 9.7 | 16.4 | 395 | 672 |
| 5.0 | 11.0 | 25.9 | 449 | 1058 |

*Table 7.10. Table of NO conversions for the NO decomposition and reduction reactions over hydrogen reduced P25 photocatalysts loaded with varying amounts of rhodium. Decomposition conditions: NO 909 ppm with Ar balance and a total flow rate of 5.5 sccm. Reduction conditions: As for decomposition reactions with the addition of CO at 1818 ppm.*

The selectivities for both the decomposition and reduction reactions are presented in table 7.11. As was observed for the activity of the hydrogen reduced Rh-P25 photocatalysts, the selectivity for $N_2$ formation was not affected by the Rh concentration and remained at *ca.* 30 % for all three of the Rh loadings used. In the

presence of CO the selectivity for $N_2$ formation again decreased with increasing Rh concentration, although for this system the values were higher than that observed for the corresponding decomposition reactions.

| Rh loading / wt. % | Selectivity for decomposition reactions / % | | Selectivity for reduction reactions / % | |
|---|---|---|---|---|
| | $N_2$ | $N_2O$ | $N_2$ | $N_2O$ |
| 0 | 19 | 81 | 42 | 58 |
| 0.1 | 26 | 74 | 44 | 56 |
| 1.0 | 29 | 71 | 39 | 61 |
| 5.0 | 31 | 69 | 29 | 71 |

*Table 7.11. Table of selectivities for NO decomposition and reduction reactions over hydrogen reduced P25 photocatalysts loaded with varying amounts of rhodium. Decomposition conditions: NO 909 ppm with Ar balance and a total flow rate of 5.5 sccm. Reduction conditions: As for decomposition reactions with the addition of CO at 1818 ppm.*

As the rate of NO conversion and selectivity for the decomposition reactions remained similar for all three rhodium loading used, the rate of formation of both $N_2$ and $N_2O$ also remained similar at *ca.* 60 μmol $h^{-1}$ $g^{-1}$ and *ca.* 150 μmol $h^{-1}$ $g^{-1}$, respectively (table 7.12). In the presence of CO the rate for formation of both products increased with increasing Rh concentration.

| Rh loading / wt. % | Rate of $N_2$ formation / μmol $h^{-1}$ $g^{-1}$ | | Rate of $N_2O$ formation / μmol $h^{-1}$ $g^{-1}$ | |
|---|---|---|---|---|
| | Decomposition | Reduction | Decomposition | Reduction |
| 0 | 64 | 50 | 274 | 69 |
| 0.1 | 57 | 55 | 161 | 70 |
| 1.0 | 57 | 131 | 140 | 205 |
| 5.0 | 70 | 153 | 155 | 376 |

*Table 7.12. Rates of formation for the products of the photocatalytic reactions over hydrogen reduced P25 photocatalysts loaded with varying amounts of rhodium. Decomposition conditions: NO 909 ppm with Ar balance and a total flow rate of 5.5 sccm. Reduction conditions: As for decomposition reactions with the addition of CO at 1818 ppm.*

### 7.2.5 Effect of varying NO concentration

To investigate the effect of NO concentration over rhodium modified P25, an as-dried (70°C) 0.1Rh-P25 photocatalyst was used. The concentration of NO was varied from 455 ppm to 1818 ppm whilst maintaining a constant total flow rate of 5.5 sccm. When present, the concentration of CO was kept constant at 1818 ppm.

Table 7.13 shows that as the concentration of NO increased from 455 ppm to 1818 ppm the percentage NO conversion decreased from 24.2 % to 17.5 % for the decomposition reactions and from as high as 95.5 % to 57.3 % for the reduction reactions. However, if instead of percentage NO conversion, the rate of NO conversion was used as a measure of photocatalyst activity, then we see a trend that increased for both reaction types. Under reduction conditions, with an NO concentration of 1818 ppm the rate of NO conversion was as high as 4689 μmol $h^{-1}$ $g^{-1}$.

| NO concentration / ppm | Conversion of NO / % | | Rate of NO conversion / μmol $h^{-1}$ $g^{-1}$ | |
|---|---|---|---|---|
| | Decomposition | Reduction | Decomposition | Reduction |
| 455 | 24.2 | 94.5 | 495 | 1933 |
| 909 | 18.0 | 87.4 | 736 | 3577 |
| 1818 | 17.5 | 57.3 | 1430 | 4689 |

*Table 7.13. NO conversion results for decomposition and reduction reactions with varying NO levels over 0.1Rh-P25 photocatalysts dried at 70°C. Decomposition reaction conditions: Total flow rate of 5.5 sccm. Reduction reaction conditions: Same as for decomposition reactions with a constant concentration of CO (1818 ppm).*

Within the errors associated with these experiments the selectivity of the decomposition reactions was very similar (*ca.* 27 % selectivity for $N_2$ formation) for all three NO concentrations investigated (table 7.14). In the presence of CO the selectivity for $N_2$ formation was lower than that observed for the corresponding decomposition reactions and decreased with increasing NO concentration. When the

highest concentration of NO was used (1818 ppm) the selectivity for $N_2$ formation was as low at 5 %.

Under decomposition conditions the rates of formation of $N_2$ and $N_2O$ were 69 μmol $h^{-1}$ $g^{-1}$ and 178 μmol $h^{-1}$ $g^{-1}$ respectively when the concentration of NO was 455 ppm, and increased to 197 μmol $h^{-1}$ $g^{-1}$ and 517 μmol $h^{-1}$ $g^{-1}$ when the maximum concentration of NO was used (table 7.15). When CO was present in the reaction gas, the rate of formation of $N_2$ decreased with increasing NO concentration, whilst $N_2O$ was produced at a higher rate. At 1818 ppm NO, the rate of formation of $N_2O$ was 2227 μmol $h^{-1}$ $g^{-1}$.

| NO concentration / ppm | Selectivity for decomposition reactions / % | | Selectivity for reduction reactions / % | |
|---|---|---|---|---|
| | $N_2$ | $N_2O$ | $N_2$ | $N_2O$ |
| 455 | 28 | 72 | 23 | 77 |
| 909 | 26 | 74 | 12 | 88 |
| 1818 | 28 | 72 | 5 | 95 |

*Table 7.14. Table of selectivities for NO decomposition and reduction reactions with varying NO levels over 0.1Rh-P25 photocatalysts dried at 70°C. Decomposition reaction conditions: Total flow rate of 5.5 sccm. Reduction reaction conditions: Same as for decomposition reactions with a constant concentration of CO (1818 ppm).*

| NO concentration / ppm | Rate of $N_2$ formation / μmol $h^{-1}$ $g^{-1}$ | | Rate of $N_2O$ formation / μmol $h^{-1}$ $g^{-1}$ | |
|---|---|---|---|---|
| | Decomposition | Reduction | Decomposition | Reduction |
| 455 | 69 | 227 | 178 | 740 |
| 909 | 97 | 213 | 270 | 1573 |
| 1818 | 197 | 117 | 517 | 2227 |

*Table 7.15. Rates of formation of the products for the photocatalytic reactions with varying NO levels over 0.1Rh-P25 photocatalysts dried at 70°C. Decomposition reaction conditions: Total flow rate of 5.5 sccm. Reduction reaction conditions: Same as for decomposition reactions with a constant concentration of CO (1818 ppm).*

### 7.2.6 Effect of varying CO concentration

The effect of CO concentration was investigated by maintaining a constant concentration of NO (909 ppm) whilst varying the CO concentration from zero to 1818 ppm. The total flow rate was kept constant at 5.5 sccm for each experiment. The photocatalysts used for these experiments were films of 0.1Rh-P25 photocatalysts that had been dried at 70°C. No further pretreatment was used.

Table 7.16 illustrates that as the CO concentration was increased from zero to 909 ppm the activity of 0.1Rh-P25 photocatalysts for conversion of NO increased from 18 % to 87.4 % respectively. Any further increases in CO concentration had no effect on conversion rate. From the results of the selectivity of the reactions (table 7.17) it can be seen that the addition of CO to the reaction gas resulted in a decrease in the selectivity for $N_2$ formation (26 % selectivity for $N_2$ formation with zero CO and 10 % in the presence of CO).

| CO concentration / ppm | NO conversion / % | NO conversion rate / μmol $h^{-1}$ $g^{-1}$ |
|---|---|---|
| 0 | 18.0 | 737 |
| 364 | 54.5 | 2230 |
| 909 | 88.7 | 3627 |
| 1818 | 87.4 | 3577 |

*Table 7.16. NO conversion results for reduction reactions with varying CO levels over 0.1Rh-P25 photocatalysts dried at 70°C. Reaction conditions: NO concentration and total flow rate were kept constant at 909 ppm and 5.5 sccm respectively.*

| CO concentration / ppm | Selectivity / % | |
|---|---|---|
| | $N_2$ | $N_2O$ |
| 0 | 26 | 74 |
| 364 | 13 | 87 |
| 909 | 8 | 92 |
| 1818 | 9 | 91 |

*Table 7.17. Selectivity results for reduction reactions with varying CO levels over 0.1Rh-P25 photocatalysts dried at 70°C. Reaction conditions: NO concentration and total flow rate were kept constant at 909 ppm and 5.5 sccm respectively.*

From table 7.18 it can be seen that the rate of $N_2$ formation was similar for all the CO concentrations used, whilst the rate of formation of $N_2O$ increased from 270 μmol $h^{-1}$ $g^{-1}$ to 1628 μmol $h^{-1}$ $g^{-1}$ as the CO concentration was increased from zero to 1818 ppm.

| CO concentration / ppm | Rate of $N_2$ formation / μmol $h^{-1}$ $g^{-1}$ | Rate of $N_2O$ formation / μmol $h^{-1}$ $g^{-1}$ |
|---|---|---|
| 0 | 97 | 270 |
| 364 | 147 | 967 |
| 909 | 145 | 1668 |
| 1818 | 161 | 1628 |

*Table 7.18. Effect of CO concentration on the rates of formation of $N_2$ and $N_2O$ over 0.1Rh-P25 photocatalysts dried at 70°C. Reaction conditions: NO concentration and total flow rate were kept constant at 909 ppm and 5.5 sccm respectively.*

## 7.3 Discussion

### 7.3.1 Effect of Rhodium

Figures 7.1 and 7.2 show the effect of rhodium loading for each of the pretreatments undertaken (calcination at 70°C, calcination at 200°C, UV reduction and $H_2$ reduction) on the percentage conversion of NO for decomposition and reduction reactions, respectively. Under decomposition conditions it can clearly be seen that increasing the Rh loading from 0.1 wt. % to 5 wt. % had little effect on the percentage NO conversion for any of the photocatalysts prepared, which is in contradiction to reports in the literature.[13] However, it was observed that addition of Rh to P25 generally resulted in less active NO decomposition catalysts than the unmodified P25 photocatalyst pretreated under the same conditions. This result is surprising since Rh has very good adsorption properties for NO, and so it would be expected that for the same concentrations of NO in the gas stream, more NO would be adsorbed onto the

surfaces of the Rh containing photocatalysts, and hence a greater NO conversion would be expected. It is possible that this reduction in NO conversion rate over the Rh-P25 photocatalysts is due to the inability to form the reactive intermediate Rh-N species in the absence of CO (as proposed in the reaction mechanisms reported by Thampi *et al.* [14] A more detailed discussion of the possible reaction intermediates is given later).

The order of the activity for NO decomposition over the 0.1Rh-P25 photocatalysts was 70°C > 200°C > UV reduced ≈ $H_2$ reduced. In chapter 4 it was shown that the rhodium was present as $Rh^{3+}$ on both the as-dried and calcined at 200°C photocatalysts, therefore, as discussed in chapter 5, the reason for the decrease in NO conversion rate as the calcination temperature increased from 70°C to 200°C for the Rh-P25 photocatalysts was most probably due to the removal of water and hydroxyl groups from the surface of $TiO_2$. It could be expected that the density of molecular water and hydroxyl groups on the catalyst surface would be lower for the reduced samples compared to the Rh-P25 photocatalyst calcined at 70°C, due to the reduction of the $TiO_2$ surface.[15] When $TiO_2$ is heated under $H_2$, the surface is dehydrated and dehydroxylated resulting in the reduction of $Ti^{4+}$ sites to $Ti^{3+}$ sites. Similarly when $TiO_2$ is subjected to band-gap illumination in the presence of an electron donor such as IPA, surface hydroxyl groups (the main trapping sites for photogenerated holes) are involved in the oxidation of IPA,[16] thus during illumination the density of hydroxyl groups decreases, resulting in the formation of $Ti^{3+}$ sites. Also during illumination, adsorbed water molecules are dissociated by reaction with bridging oxygen atoms, leading to more surface hydroxyl groups,[17] which may then be involved in oxidation reactions. A more detailed discussion of this process is given

in chapter 4. Hence the activity for NO conversion was decreased for the two reduced Rh-P25 systems.

Another factor that may also contribute to the decrease in NO conversion for the reduced catalysts is that the Rh-$TiO_2$ interface formed could act as a recombination centre for the photogenerated electron-hole pairs, thus reducing the number of active species available to participate in surface reactions. However, as shown in the studies of Ag-P25 photocatalysts (reported in chapter 6) and in the studies of Chao,[18] the magnitude of this effect on the photocatalytic activity would be expected to change with the metal loading. As there was no significant change in the NO conversion with increasing Rh loadings, it is proposed that the major reason for the decreased activity of the reduced catalysts was the lower density of surface hydroxyl groups compared to the catalysts pretreated in air.

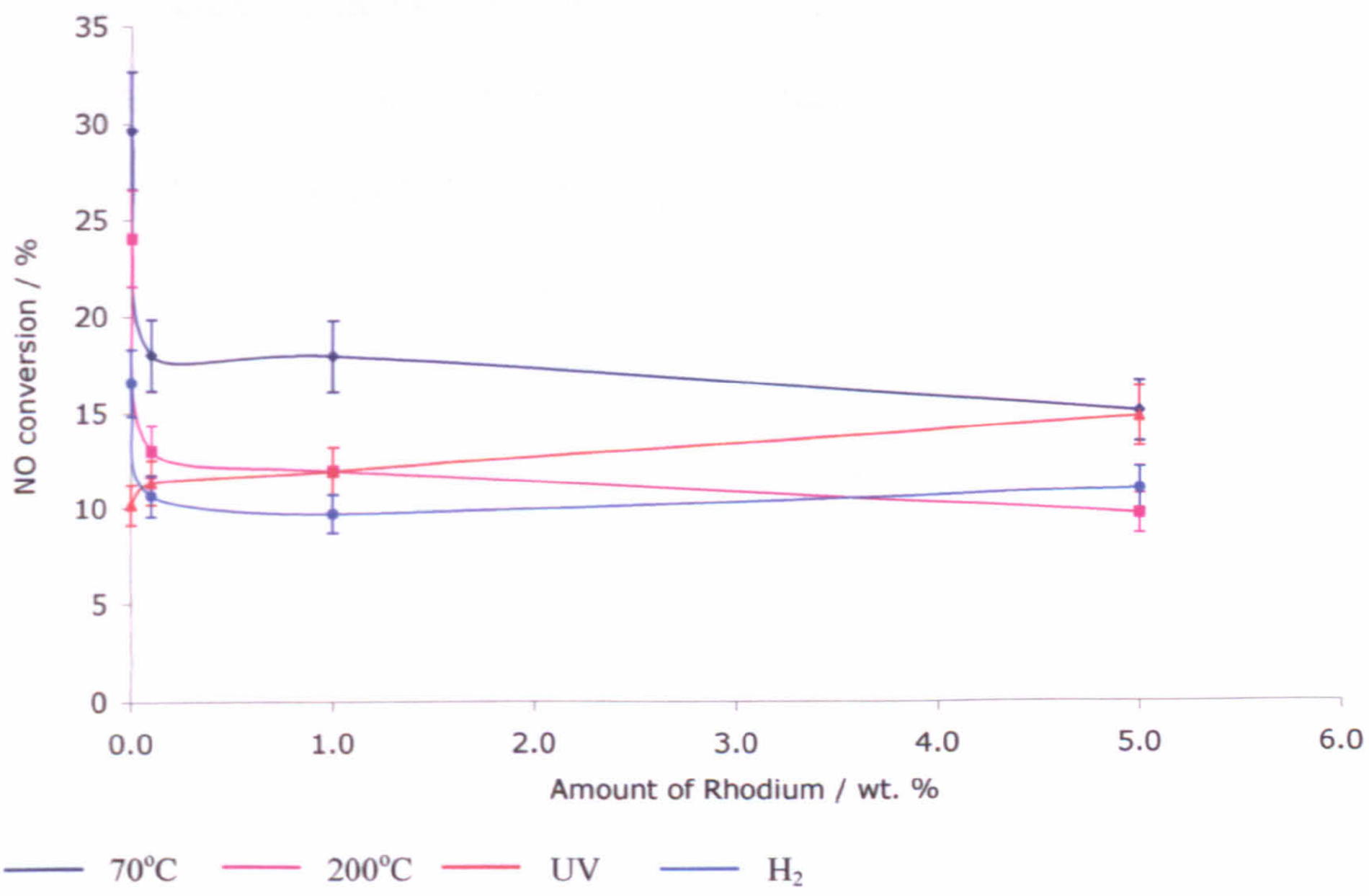


*Figure 7.1. Effect of Rh loadings on percentage NO conversion for a series of differently pretreated Rh-P25 photocatalysts. Decomposition conditions: NO 909 ppm with Ar balance with a total flow rate of 5.5 sccm.*

The same rationale may be used to partially explain the trend in activity for NO conversion observed for the same series of Rh-P25 photocatalysts tested in the presence of NO-CO mixtures (figure 7.2). However, in the presence of CO, the rhodium loading had an effect on the NO conversion for the two reduced photocatalysts, where the rate of NO conversion increased with increasing Rh loading. As the results from the decomposition reactions showed little variation in activity with increasing rhodium concentrations and considering the possible mechanisms for the NO-CO reaction (discussed later) it was thought that the effect was most likely due to the varying Rh particle sizes and dispersion (as shown in chapter 4), rather than alterations in charge transfer properties as the Rh concentration was increased. For Rh concentrations of 0.1 wt. % and 1 wt. % the Rh particle size (as determined by TEM analysis) was < 1 nm for both the thermally and UV reduced catalysts. Increasing the rhodium concentration to 5 wt. % resulted in an increase in the particle size to 1-2 nm for the UV reduced catalyst and *ca.* 8 nm for the thermally reduced catalyst. For Rh-P25 systems pretreated in air (70°C and 200°C) the level of Rh doping had little effect on the NO conversion rate.

It was also observed that in the presence of CO, the percentage NO conversion was higher for all the Rh-P25 systems studied compared to the unmodified P25 photocatalysts and also that the conversion rate was higher than that observed for the NO decomposition reactions over the same photocatalysts. For the other photocatalyst systems reported in this thesis (unmodified P25 and silver modified P25 photocatalysts) the presence of CO in the reaction gas resulted in a decrease in the NO conversion rate due to blocking of active sites by CO molecules.[19]

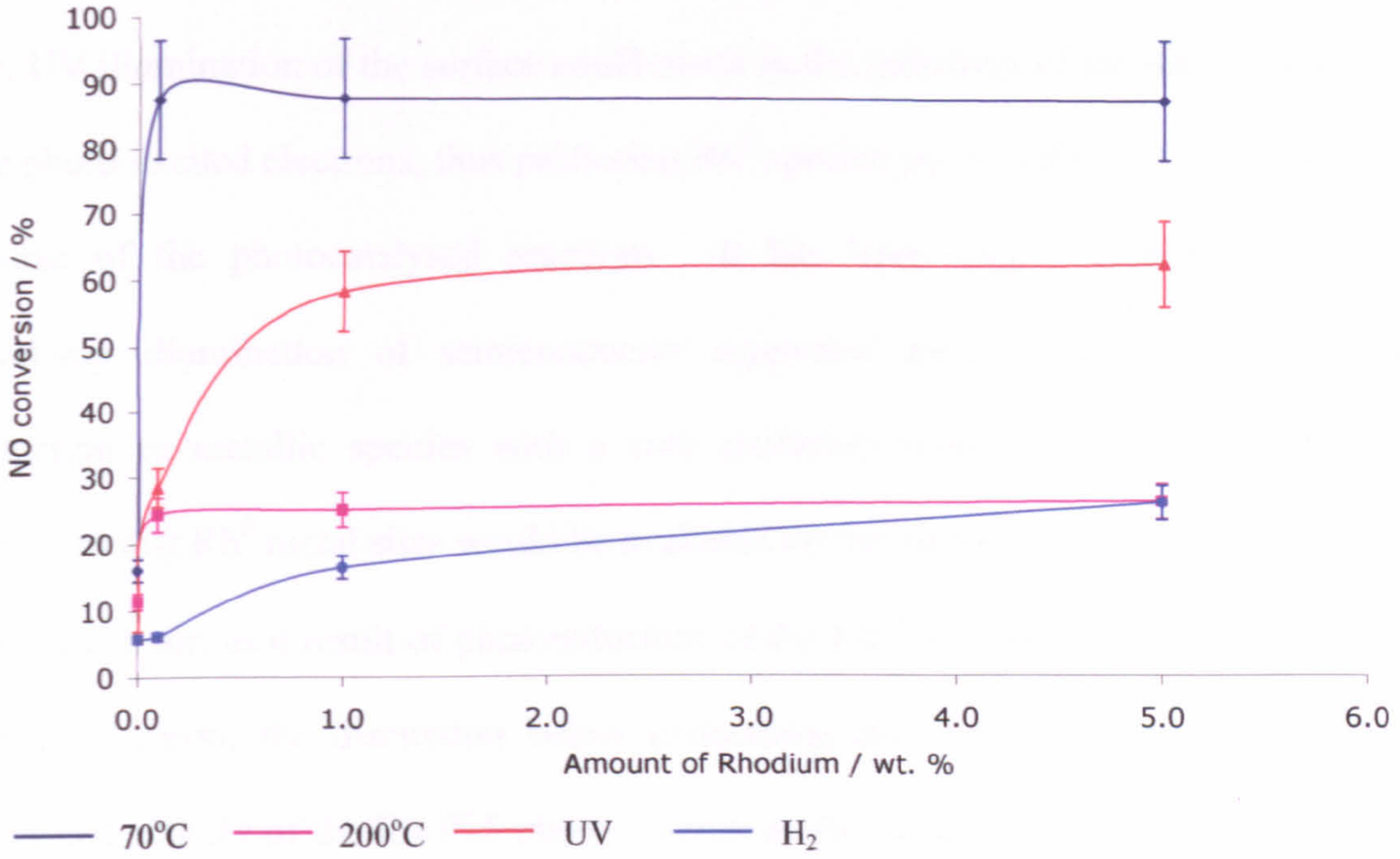


*Figure 7.2. Effect of Rh loadings on percentage NO conversion for a series of differently pretreated Rh-P25 photocatalysts. Reduction conditions: NO and CO concentrations were 909 ppm and 1818 ppm, respectively. Total flow rate of 5.5 sccm*

The increased activity of the Rh-P25 photocatalysts for NO conversion in the presence of CO may be explained by considering the exceptional charge transfer properties (both from the $TiO_2$ support to Rh centres and from Rh centres to species adsorbed on those centres) of the system.[20] Increased charge transfer from the metal centre to adsorbed NO would result in more of the adsorbed NO becoming dissociated due to the transfer of electrons into the $\pi^*$-antibonding molecular orbital of the NO molecules. Another, and probably more important, factor is that NO is more strongly adsorbed onto rhodium surfaces than CO.[14] Therefore, in comparison to unmodified P25 catalysts (in which CO is preferentially adsorbed over NO) more NO would be available to undergo surface reactions.

Before discussing the possible surface mechanisms and reaction it should be noted that although the XPS results reported in chapter 4, showed that rhodium

existed as $Rh^{3+}$ on the photocatalysts that had been pretreated at 70°C and 200°C in air, UV illumination of the surface could result in the reduction of the $Rh^{3+}$ species by the photo-excited electrons, thus producing $Rh^0$ species on the $TiO_2$ surface during the course of the photocatalysed reactions. It has been widely demonstrated that band-gap illumination of semiconductor supported metal salts results in their reduction to metallic species with a zero oxidation state.[21-23] Therefore, it was expected that $Rh^0$ metal sites would be available on the surfaces of two photocatalysts calcined in air, as a result of photoreduction of the $Rh^{3+}$ species during the reactions. For this reason, the discussion below concerning the species responsible for the enhanced activity of the Rh-P25 photocatalysts in the presence of CO is applicable to the materials that were pretreated in air.

One possible explanation for the trend observed for the NO conversion rates of NO-CO reactions over the different Rh-P25 photocatalysts is the formation of UV sensitive gem-dicarbonyl species.[24] FTIR studies of CO adsorption, without UV irradiation, on highly dispersed Rh-$TiO_2$ systems (e.g. systems with Rh particles sizes of < 4 nm) has shown that the main surface species formed are gem-dicarbonyl species, according to the reaction below:[15]

$$Rh^0 + OH_{(a)} + 2CO_{(g)} \rightleftharpoons Rh^+(CO)_2 + 1/2H_2 \qquad 7.1$$

where the $OH_{(a)}$ is present as isolated OH groups on the surface of the photocatalyst. As discussed earlier (with respect to the activity for NO decomposition) a decreasing density of surface bound OH groups could be expected for the Rh-P25 photocatalysts in the order 70°C > 200°C > UV reduced ≈ $H_2$ reduced, and hence the number of possible gem-dicarbonyl species formed would follow the same trend. EXAFS

studies by Van't Blik *et al.*[25] have shown that the formation of gem-dicarbonyl species was the result of the oxidative disruption of a $Rh_x$ cluster induced by CO adsorption, and more recent STM work has provided direct evidence for the CO-induced disintegration of Rh nano-particles of size < 4 nm.[26,27] Larger particles, however, remained intact or disintegrated only very slowly. Upon UV irradiation of the gem-dicarbonyl complexes, FTIR studies showed the formation of a species in which CO was linearly bonded to $Rh^0$, and hence it was suggested the reduction of the $Rh^+$ (formed via the oxidative disruption of $Rh^0$ clusters as discussed above) to $Rh^0$ atoms occurred.[24] The process of gem-dicarbonyl formation and the subsequent reduction of $Rh^+$ centres, therefore, results in an increase in the dispersion (and hence surface area) of $Rh^0$ species on the $TiO_2$ surface, which could then act as active sites for NO adsorption and dissociation.[28,29] Hence, this offers a possible explanation for the high activity for NO conversion observed, in the presence of CO, over the Rh-P25 photocatalysts reported here. However, if this was occurring during the course of the NO-CO reactions the NO conversion rate would be expected to increase with illumination time as a result of the increasing number of active sites available. Increasing conversion rates were, however, not observed during the 30 min. period of illumination used in the experiments reported in this thesis, so it could be that gem-dicarbonyl formation is negligible in the presence of NO, or that the oxidative disruption process occurs at a slower rate and any change to the NO conversion rate could not be observed within the 30 min. period.

Due to the good electron transfer properties of Rh, the adsorption of NO in the presence of UV irradiation results in the formation of partially negatively charged NO species ($Rh\text{-}NO^{\delta-}$), which are prone to undergo dissociation according to equation 7.2.

$$NO^{\delta-} \longrightarrow N_{(a)} + O^{\delta-}_{(a)} \qquad 7.2$$

The adsorbed N atom may then react further with another NO or CO molecule producing $N_2O_{(a)}$ and NCO species, respectively, whilst the adsorbed O atom could react with a CO molecule producing $CO_{2(a)}$.[14] Adsorbed $N_2O$ and $CO_2$ could be desorbed from the surface forming gas phase products. Hecker has shown by use of IR spectroscopy that –NCO species formed on metal sites readily migrate onto the support[30], and under UV illumination, the $TiO_2$ support can activate –NCO (according to the mechanisms shown in scheme 7.1) and replenish that site for further –NCO migration, hence leading to faster NO conversion rates. Scheme 7.1 presents the possible reaction mechanisms for NO conversion, in the presence of CO, on Rh active sites.

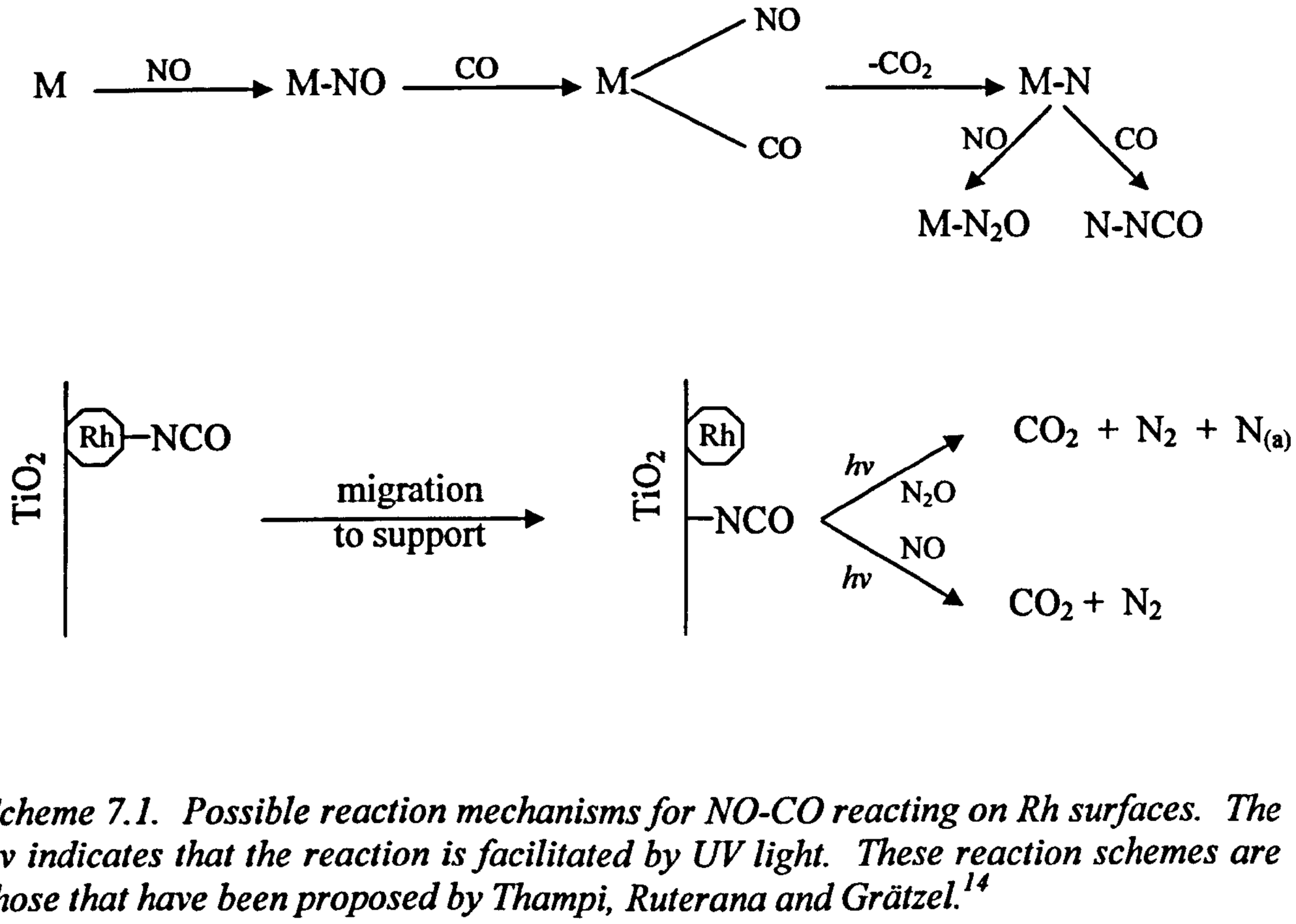


*Scheme 7.1. Possible reaction mechanisms for NO-CO reacting on Rh surfaces. The hv indicates that the reaction is facilitated by UV light. These reaction schemes are those that have been proposed by Thampi, Ruterana and Grätzel.*[14]

As the main product observed in the NO-CO photoreaction over all the Rh-P25 photocatalysts was $N_2O$, it is proposed that formation of isocyanate species (which would result in the formation of $N_2$, see scheme 7.1) is a relatively slow reaction compared to the formation of $N_2O$ by reaction of $N_{(a)}$ with gas phase NO. The increased rate of reaction in the presence of CO could be due to the CO molecules acting as scavengers of $O_{(a)}$ atoms, resulting in the desorption of $CO_2$ and leaving another active site available for NO adsorption and dissociation.

Figure 7.3 shows that under decomposition conditions, the selectivity for $N_2$ formation varied only slightly for all the rhodium loadings and pretreatments investigated. The selectivity for $N_2$ formation over the Rh-P25 photocatalysts was slightly higher than that observed for unmodified P25 photocatalysts and the highest selectivity for $N_2$ formation was observed for the UV reduced Rh-P25 photocatalysts, which contained more metallic rhodium than the other Rh containing photocatalysts. As discussed above, it could be expected that more $N_{(a)}$ would be present on the Rh-P25 photocatalysts (due to the formation and subsequent dissociation Rh-$NO^{\delta-}$ species), hence the probability of two $N_{(a)}$ species reacting together to form $N_2$ would be higher. However, it should be noted that the same reaction pathways would be available, as on the unmodified P25 surfaces, only the relative reaction rates vary in the presence of Rh. The reader is referred to chapter 5 for a list of the possible NO-NO type surface reactions.

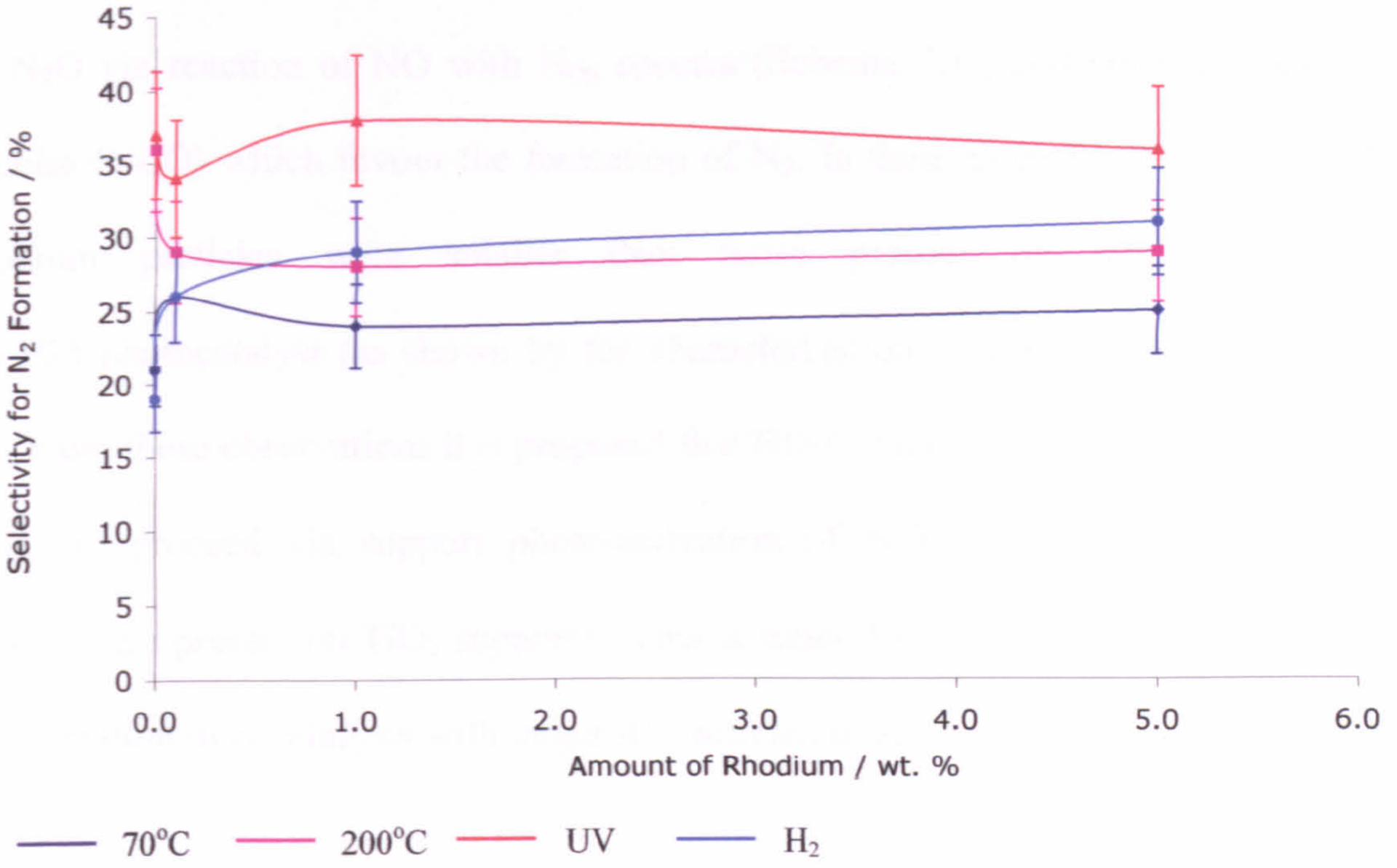


*Figure 7.3. Effect of rhodium content on the selectivity for $N_2$ formation for Rh-P25 photocatalysts that had been subjected to various pretreatment. Decomposition conditions: 909 ppm NO, Total flow rate of 5.5 sccm.*

When both NO and CO were present in the reaction stream, the selectivity for $N_2$ formation varied significantly depending on the pretreatment used (figure 7.4.). For the P25 and Rh-P25 photocatalysts that had been reduced using $H_2$ at 450°C, the selectivity for $N_2$ formation was greater than for unmodified P25 photocatalysts (40 % for $H_2$ reduced samples, compared to 25 % for unmodified P25). It could, therefore, be expected that both the migration of –NCO species to the $TiO_2$ support and the subsequent formation of $N_2$ (as described above) along with the formation of $N_2O$ via the Rh-$N_{(a)}$ intermediate, occur with nearly equal rates on the surfaces of these photocatalysts. Increased selectivity for $N_2$ formation over pre-reduced $TiO_2$ surfaces has been reported by Courbon and Pichat.[31]

The two Rh-P25 systems which had been pretreated in air (70°C and 200°C) and the UV reduced Rh-P25 system all showed similar lower selectivities for $N_2$ formation (10 %) compared to unmodified P25 photocatalysts (25 %). It is therefore

proposed that the dominate reaction pathway for these photocatalysts is the formation of $N_2O$ via reaction of NO with $N_{(a)}$ species (Scheme 7.1), and not via isocyanate species (NCO) which favour the formation of $N_2$. In these three Rh-P25 systems the rhodium particles were smaller than those present on the $H_2$ reduced Rh-P25 photocatalyst (as shown by the characterisation results presented in chapter 4). From these observations it is proposed that NO-CO reduction reactions were more likely to proceed via support photo-activation of NCO species when larger Rh particles are present on $TiO_2$ supports. This is supported by the higher selectivity for $N_2$ formation over catalysts with larger Rh particles sizes.

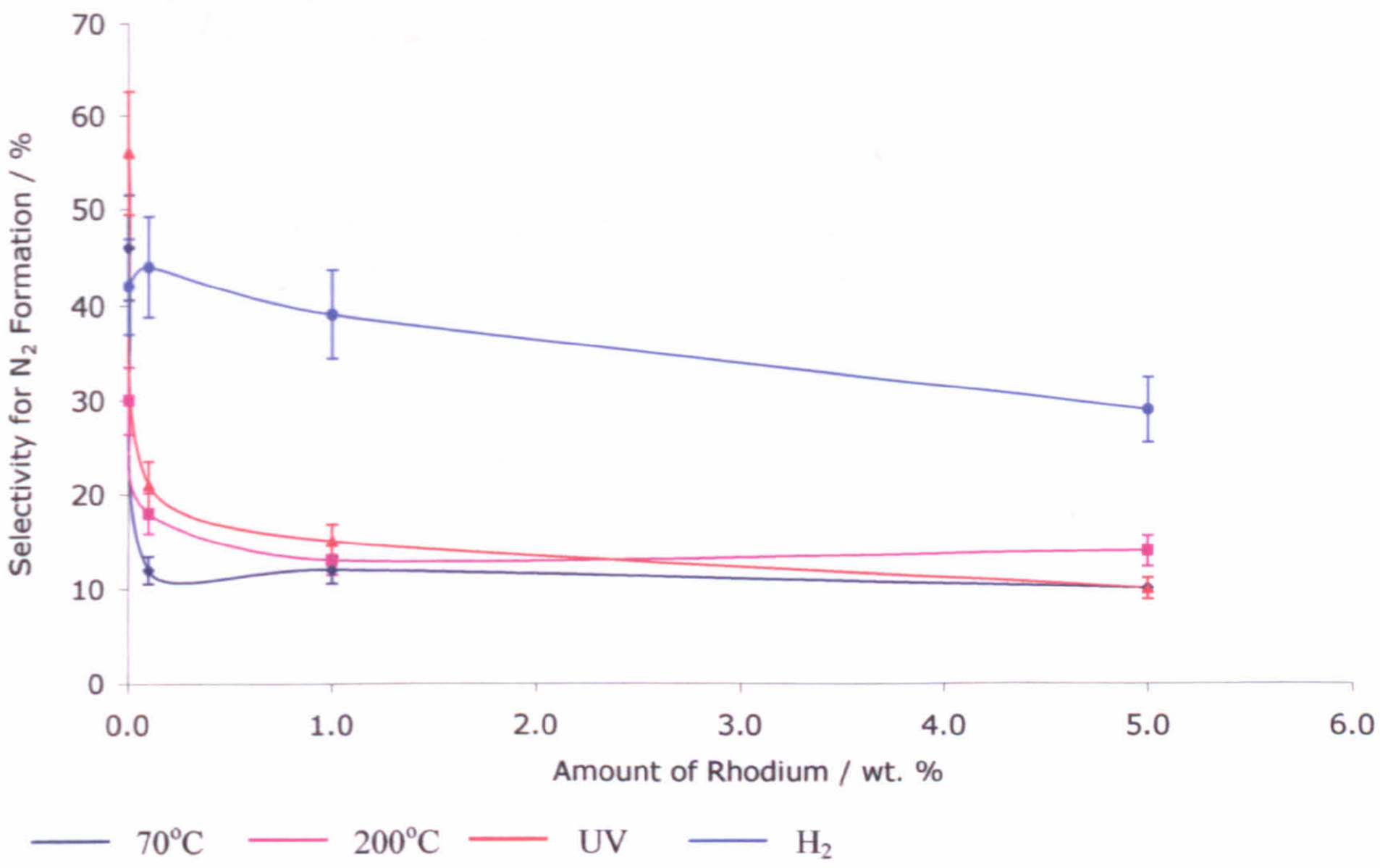


*Figure 7.4. Effect of rhodium content on the selectivity for $N_2$ formation for Rh-P25 photocatalysts that had been subjected to various pretreatment. Reduction conditions: NO and CO concentrations were 909 ppm and 1818 ppm, respectively. Total flow rate of 5.5 sccm.*

Comparing the rates of formation of $N_2$ and $N_2O$ over as-dried Rh-P25 under decomposition and reduction conditions (figure 7.5), it can be seen that both are

unaffected by the rhodium loading and that the rate of formation of $N_2O$ was very high at *ca.* 1600 μmol $h^{-1}$ $g^{-1}$ when CO was present in the reaction stream.

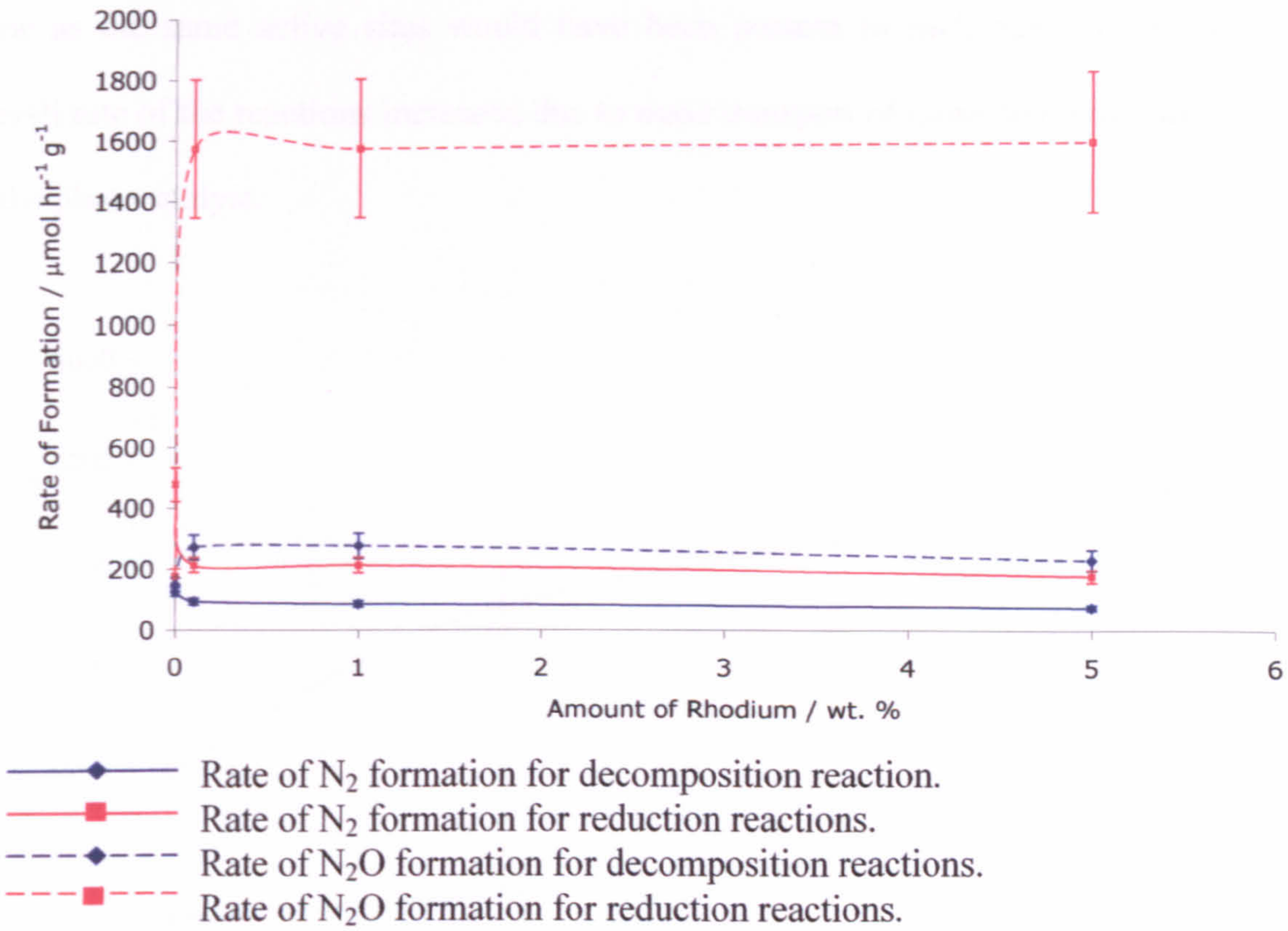


*Figure 7.5. The rates of formation of $N_2$ and $N_2O$ for NO decomposition and reduction reactions over as dried (70°C) Rh-P25 photocatalysts. Decomposition conditions: NO 909 ppm with Ar balance and total flow rate of 5.5 sccm. Reduction conditions: As for decomposition reactions plus CO at 1818 ppm.*

### 7.3.2 Effect of varying NO concentration

The effect of varying the NO concentration was investigated using the as-dried (70°C) 0.1Rh-P25 photocatalyst system and the NO conversion rate is plotted against NO concentration (figure 7.6). From the figure it is clear that the NO conversion rate increased nearly linearly with increasing NO concentration which was the same as observed for the unmodified and silver modified P25 photocatalysts.

Under decomposition conditions, the selectivity of the photoreaction products remained unaltered irrespective of the NO concentration (figure 7.7). This is as expected, because the relative rates of $N_2$ and $N_2O$ forming reactions would be the same as the same active sites would have been present in each experiment. The overall rate of the reactions increased due to mass transport of more NO to the surface of the photocatalyst.

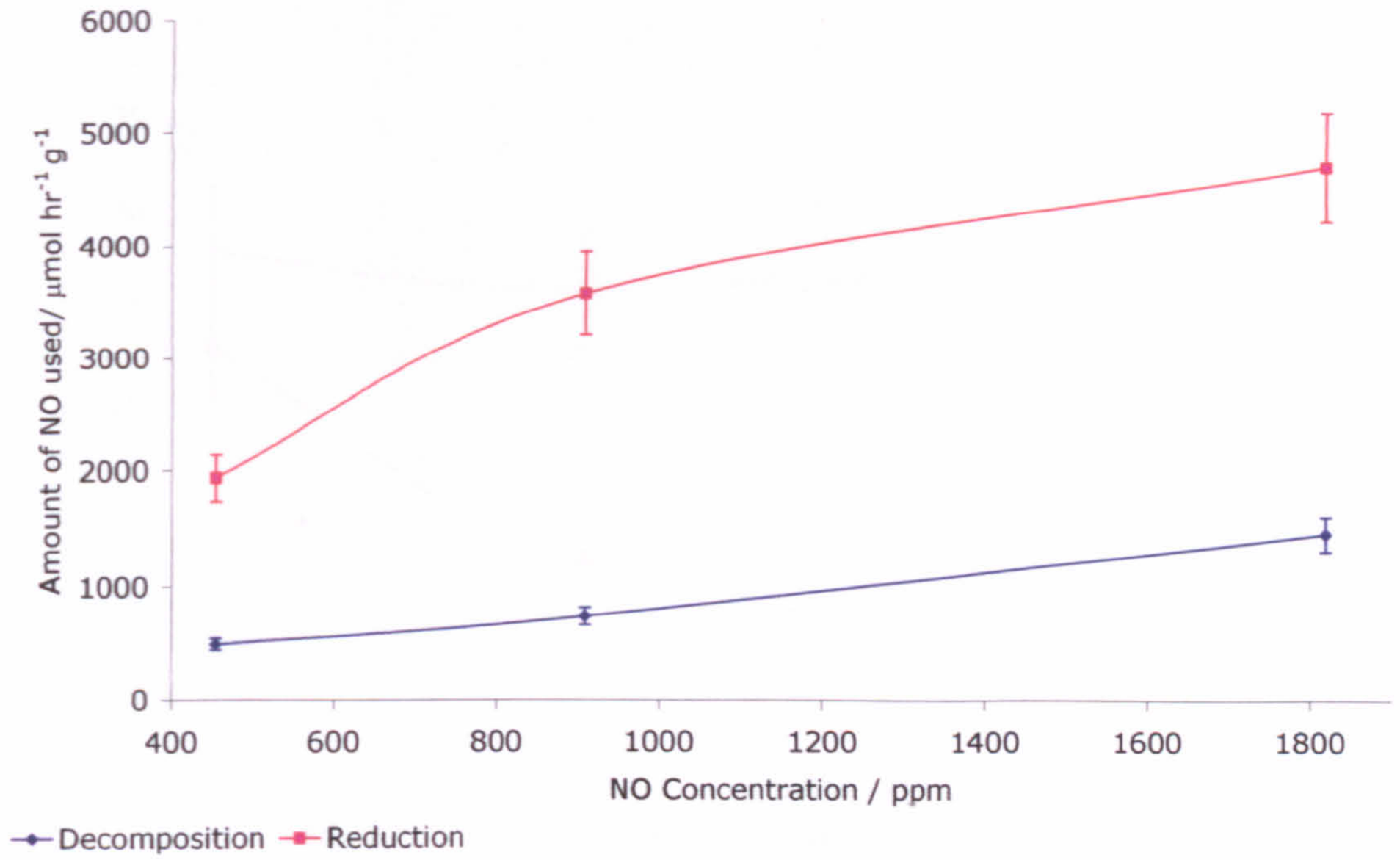


*Figure 7.6. Effect of NO concentration on the moles of NO used over as dried 0.1Rh-P25 photocatalysts. Decomposition reaction conditions: Total flow rate of 5.5 sccm. Reduction reaction conditions: Same as for decomposition reactions with a constant concentration of CO (1818 ppm).*

Under reduction conditions, the selectivity for $N_2$ formation decreased with an increase in the NO/CO ratio, i.e. with increasing NO concentration (figure 7.7). As CO was present in excess or equal concentration to the number of moles of NO, increasing the concentration of NO would result in the formation of more Rh-$N_{(a)}$ species via the route shown in scheme 7.1, and, as discussed above, this results in more prominent formation of $N_2O$ on as dried Rh-P25 photocatalysts.

The trends shown in figure 7.8 for the rates of formation of $N_2$ and $N_2O$ reflect that under decomposition conditions the rate of NO conversion increased slightly with increasing NO concentrations, whilst the selectivity of the reactions remained similar, hence the rate of formation of $N_2$ and $N_2O$ increased slightly and by comparable amounts. The substantial increase observed in the rate of formation of $N_2O$ with increasing NO concentration in the presence of CO, exemplifies the fact that the rate of NO conversion increased, whilst the selectivity for $N_2$ formation decreased.

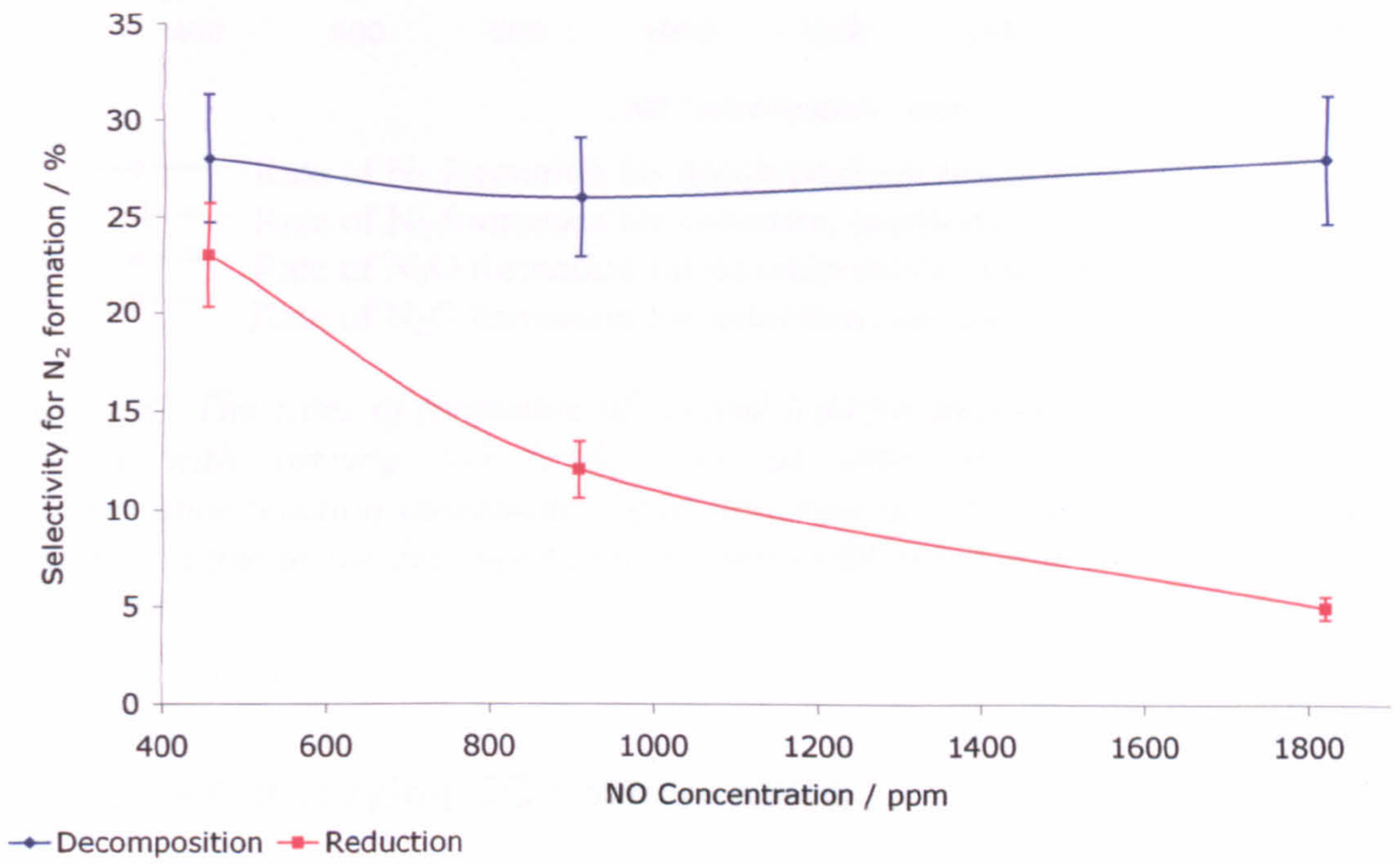


*Figure 7.7. Effect of NO concentration on the selectivity for $N_2$ formation over as dried 0.1Rh-P25 photocatalysts. Decomposition reaction conditions: Total flow rate of 5.5 sccm. Reduction reaction conditions: Same as for decomposition reactions with a constant concentration of CO (1818 ppm).*

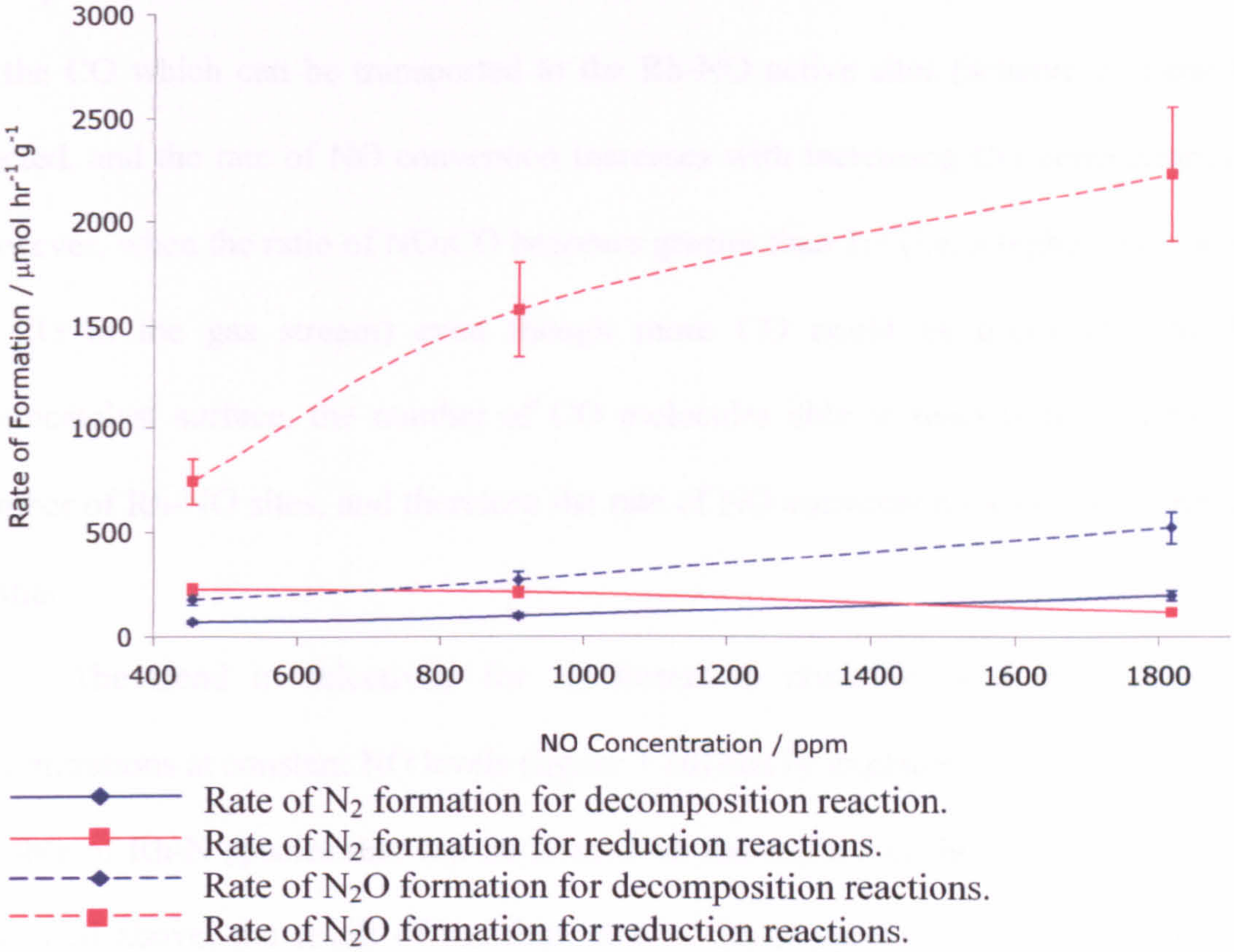


*Figure 7.8. The rates of formation of $N_2$ and $N_2O$ for decomposition and reduction reactions with varying NO levels over as dried 0.1Rh-P25 photocatalysts. Decomposition reaction conditions: Total flow rate of 5.5 sccm. Reduction reaction conditions: Same as for decomposition reactions with a constant concentration of CO (1818 ppm).*

### 7.3.3 Effect of varying CO concentration

The effect of CO concentration was investigated using as-dried (70°C) 0.1Rh-P25 photocatalyst and as shown in figure 7.9, the percentage NO conversion increased with increasing CO concentrations, up to 909 ppm. Further increasing the CO concentration to 1818 ppm (i.e. so that CO was present in excess compared to NO, which was at 909 ppm) resulted in a similar NO conversion as for reaction when NO and CO were present in a 1:1 ratio. As discussed above, the formation of Rh-$N_{(a)}$ species in the presence of CO results in enhanced NO conversion rates. When the concentration of NO is greater than the concentration of CO in the gas stream, it could

be expected that the surface concentration of NO would also be greater, and hence all of the CO which can be transported to the Rh-NO active sites (scheme 7.1) can be reacted, and the rate of NO conversion increases with increasing CO concentrations. However, when the ratio of NO:CO becomes greater than 1:1 (i.e. a higher percentage of CO in the gas stream) even though more CO could be transported to the photocatalyst surface, the number of CO molecules able to react is limited by the number of Rh-NO sites, and therefore the rate of NO conversion cannot be increased further.

The trend in selectivity for $N_2$ formation observed with increasing CO concentrations at constant NO levels (figure 7.10) can be explained by considering the number of Rh-N species that can be formed on the surface of the photocatalyst. As discussed above, the result of the formation of Rh-N species for the photocatalyst system tested here is the formation of $N_2O$, and hence if the number of Rh-N species formed increases, the selectivity for the reaction towards $N_2$ formation would decrease. When NO was present in excess (compared to CO), all of the CO molecules transported were able to react and Rh-N species can be formed. Therefore, increasing the CO concentration results in a decrease in the selectivity of the reaction for $N_2$ formation, and more $N_2O$ is formed (figure 7.11). As discussed above, when the CO concentration is greater than the NO concentration, the number of CO molecules able to react would be limited by the number of Rh-NO active sites available, and therefore further increasing the CO concentration above that of NO has no effect on the selectivity of the reactions, nor on the rates of formation of the products (figure 7.11).

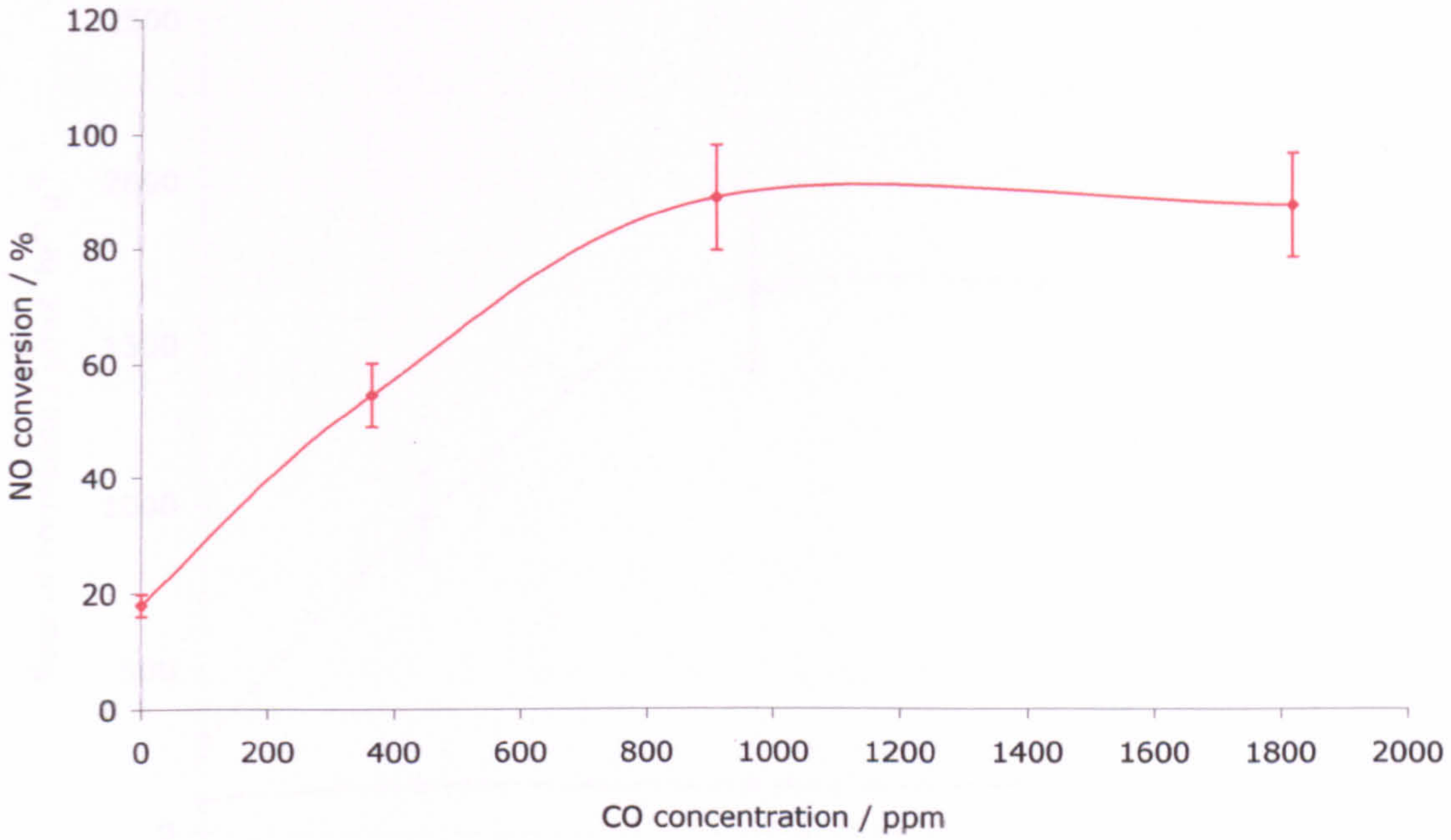


*Figure 7.9. Effect of CO concentration on the percentage NO conversion used over as dried 0.1Rh-P25 photocatalysts. Reaction conditions: NO concentration and total flow rate were kept constant at 909 ppm and 5.5 sccm respectively.*

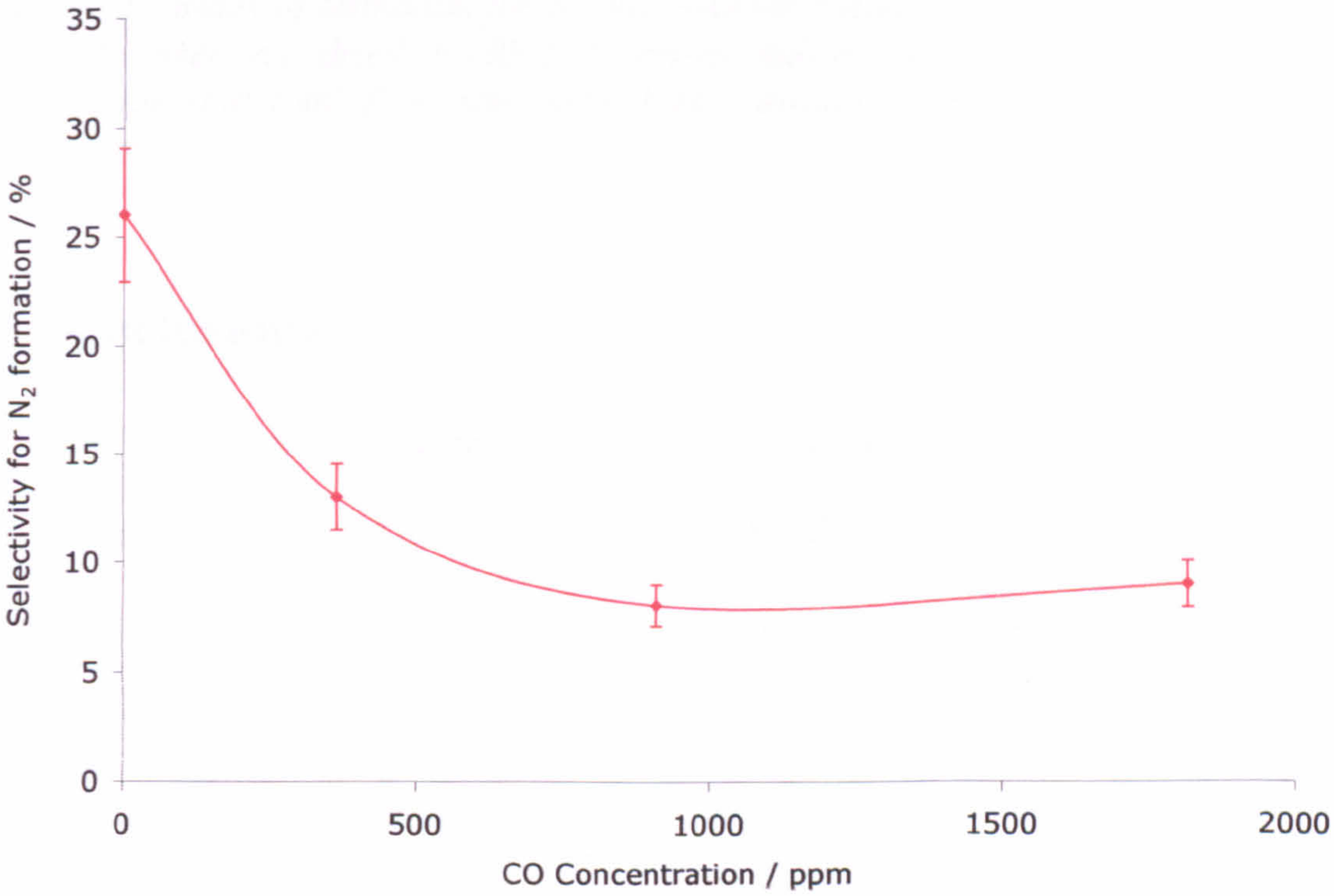


*Figure 7.10. Effect of CO concentration on the selectivity for $N_2$ formation over as dried 0.1Rh-P25 photocatalysts. Reaction conditions: NO concentration and total flow rate were kept constant at 909 ppm and 5.5 sccm respectively.*

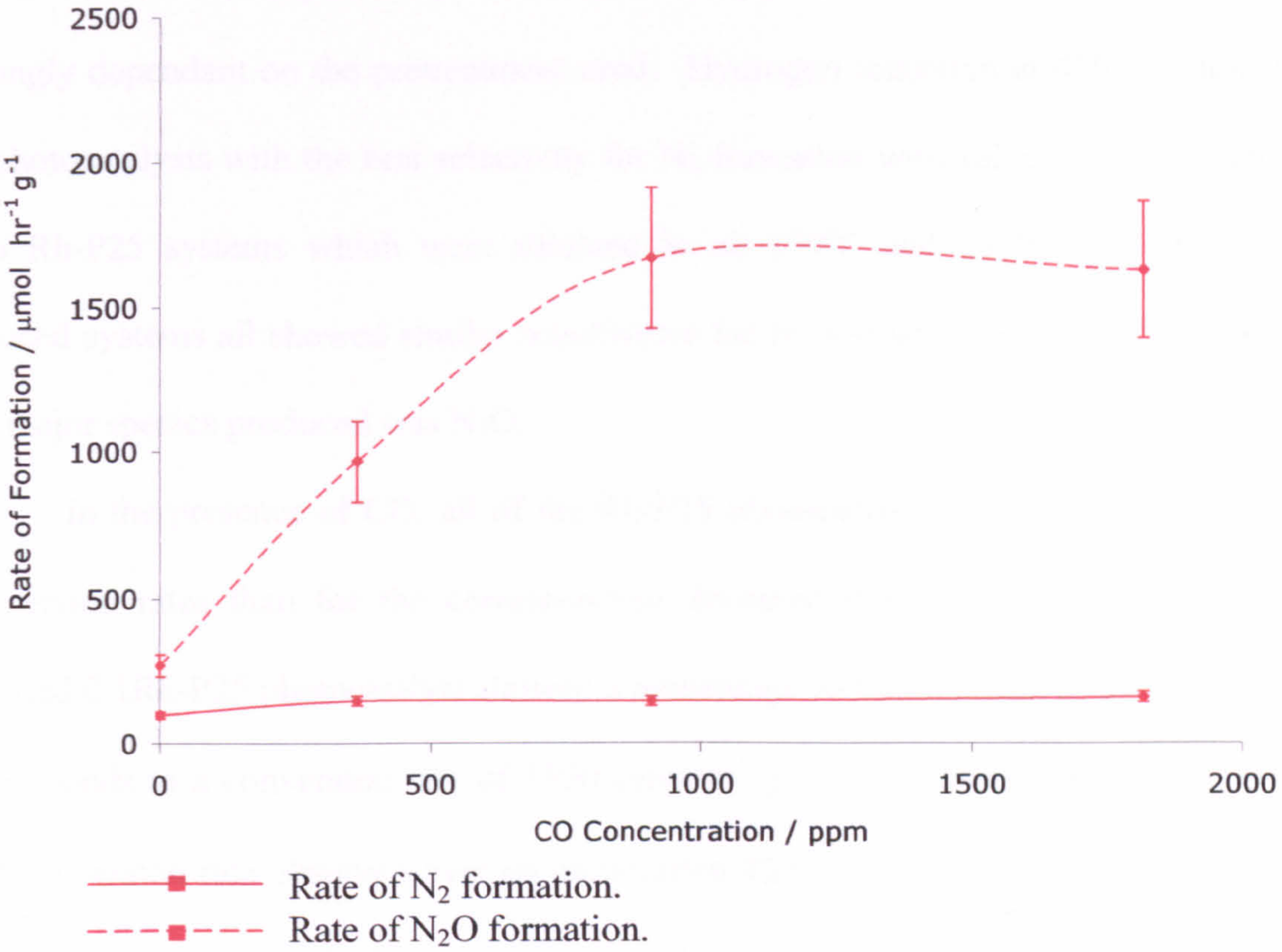


*Figure 7.11. Rates of formation for $N_2$ and $N_2O$ for reduction reactions with varying CO levels over as dried 0.1Rh-P25 photocatalyst.. Reaction conditions: NO concentration and total flow rate were kept constant at 909 ppm and 5.5 sccm respectively.*

## 7.4 Conclusions

The characteristics of the photocatalytic decomposition and reduction of NO in the presence of CO have been determined for rhodium modified Degussa P25 $TiO_2$ photocatalysts, and it has been shown that both the activity and selectivity of the NO photoreactions were dependant on the photocatalyst pretreatment conditions, hence on the nature of the deposited rhodium species.

For all of the different pretreatments undertaken in the preparation of Rh-P25 photocatalysts systems, the level of rhodium doping and the pretreatments used had little effect either on the selectivity or activity of the NO decomposition reactions,

however, the selectivity of the photocatalysts in the presence of CO was shown to be strongly dependant on the pretreatment used. Hydrogen reduction at 450°C resulted in photocatalysts with the best selectivity for $N_2$ formation with values of 40 %. The two Rh-P25 systems which were calcined in air (70°C and 200°C) and the UV reduced systems all showed similar selectivities for $N_2$ formation of *ca.* 10 %, hence the major species produced was $N_2O$.

In the presence of CO, all of the Rh-P25 photocatalysts exhibited higher NO conversion rates than for the corresponding decomposition reactions. In fact, the as-dried 0.1Rh-P25 photocatalyst showed a percentage NO conversion of 87 % which corresponds to a conversion rate of 3500 μmol $h^{-1}$ $g^{-1}$. For comparison, the highest NO conversion rate observed over an unmodified P25 photocatalyst tested under the same conditions was only 650 μmol $h^{-1}$ $g^{-1}$. Hence it can be said that Rh-P25 based photocatalysts are extremely active for NO-CO reduction reactions. It is believed that this is due to formation of reactive intermediates on the rhodium active sites, that are negligible in number on the unmodified P25 (as well as Ag-P25 ) surfaces. From the results presented here, it is proposed that the intermediate mostly likely to be responsible for the high activity is Rh-$N_{(a)}$, although other intermediates such as gem-dicarbonyls and –NCO groups could also play a part.

## 7.5 References

(1) Vanderboschdriebergen, A. G.; Kieboom, M. N. H.; Vondreumel, A.; Wolf, R. M.; Vondelft, F.; Nieuwenhuys, B. E. *Catal. Lett.* **1989**, *2*, 235.
(2) Muraki, H.; Fujitani, Y. *Ind. Eng. Chem. Prod. Res. Devel.* **1986**, *25*, 414.
(3) Kumthekar, M. W.; Ozkan, U. S. *J. Catal.* **1997**, *171*, 45.
(4) Chafik, T.; Ouassini, A.; Verykios, X. E. *J. Chim. Phys. Chim. Biol.* **1998**, *95*, 1666.
(5) Castillo, S.; Moran-Pineda, M.; Molina, V.; Gomez, R.; Lopez, T. *Appl. Catal. B Environ.* **1998**, *15*, 203.
(6) Taylor, K. C. *Catalysis Science and Technology*; springer-Verlag: Berlin, 1984; Vol. 5.

(7) Foti, G.; Lavanchy, O.; Comninellis, C. *J. Appl. Elec.* **2000**, *30*, 1223.
(8) Permana, H.; Ng, K. Y. S.; Peden, C. H. F.; Schmieg, S. J.; Lambert, D. K.; Belton, D. N. *J. Catal.* **1996**, *164*, 194.
(9) Guglielminotti, E.; Boccuzzi, F. *J. Mol. Catal. A Chem.* **1996**, *104*, 273.
(10) Granger, P.; Delannoy, L.; Lecomte, J. J.; Dathy, C.; Praliaud, H.; Leclercq, L.; Leclercq, G. *J. Catal.* **2002**, *207*, 202.
(11) Einaga, H.; Futamura, S.; Ibusuki, T. *Chem. Lett.* **2001**, 582.
(12) Kohno, Y.; Hayashi, H.; Takenaka, S.; Tanaka, T.; Funabiki, T.; Yoshida, S. *J. Photochem. Photobiol. A Chem.* **1999**, *126*, 117.
(13) Kusama, H.; Bando, K. K.; Okabe, K.; Arakawa, H. *Appl. Catal. A Gen.* **2000**, *197*, 255.
(14) Thampi, K. R.; Ruterana, P.; Gratzel, M. *J. Catal.* **1990**, *126*, 572.
(15) Chuang, S. S. C.; Tan, C. D. *Catal. Today* **1997**, *35*, 369.
(16) Peral, J.; Domenech, X.; Ollis, D. F. *J. Chem. Technol. Biotechnol.* **1997**, *70*, 117.
(17) Suda, Y.; Morimoto, T. *Langmuir* **1987**, *3*, 786.
(18) Chao, H. E.; Yu, Y.; Hu, X. F.; Larbot, A. *Appl. Surf. Sci.* **2002**, *200*, 239.
(19) Linsebigler, A.; Lu, G. Q.; Yates, J. T. *J. Phys. Chem.* **1996**, *100*, 6631.
(20) Trautmann, S.; Baerns, M. *J. Catal.* **1994**, *150*, 335.
(21) Borgarello, E.; Serpone, N.; Emo, G.; Harris, R.; Pelizzetti, E.; Minero, C. *Inorg. Chem.* **1986**, *25*, 4499.
(22) Fernandez, A.; Gonzalezelipe, A. R. *Appl. Surf. Sci.* **1993**, *69*, 285.
(23) Litter, M. I. *Appl. Catal. B Environ.* **1999**, *23*, 89.
(24) Rasko, J.; Szabo, Z.; Bansagi, T.; Solymosi, F. *Phys. Chem. Chem. Phys.* **2001**, *3*, 4437.
(25) Vantblik, H. F. J.; Vanzon, J.; Huizinga, T.; Vis, J. C.; Koningsberger, D. C.; Prins, R. *J. Am. Chem. Soc.* **1985**, *107*, 3139.
(26) Berko, A.; Solymosi, F. *J. Catal.* **1999**, *183*, 91.
(27) Berko, A.; Menesi, G.; Solymosi, F. *J. Phys. Chem.* **1996**, *100*, 17732.
(28) Bustos, V.; Unac, R.; Zaera, F.; Zgrablich, G. *J. Chem. Phys.* **2003**, *118*, 9372.
(29) Zaera, F.; Gopinath, C. S. *Phys. Chem. Chem. Phys.* **2003**, *5*, 646.
(30) Hecker, W. C.; Bell, A. T. *J. Catal.* **1984**, *85*, 389.
(31) Courbon, H.; Pichat, P. *J. Chem. Soc. Faraday Trans. I* **1984**, *80*, 3175.

# 8 Conclusions

## 8.1 Overview of results

From the results and discussion (Chapters 4-7) presented in this work, a number of key points have been observed which add to the further development of the photocatalytic elimination of $NO_x$. The characterisation and photocatalytic behaviour experiments of the transition metal modified P25 photocatalysts (Chapters 4, 6-7) compared to the results obtained from the unmodified P25 (Chapter 4-5) have illustrated that addition of modifying elements has a dramatic effect on the chemical, physical and photocatalytic properties of the prepared materials. Parallels have also been drawn between the chemical and physical nature of the materials and their corresponding photocatalytic behaviour for both NO photocatalytic decomposition and reduction reactions conducted in the presence of CO.

It is demonstrated that the addition of silver and rhodium to P25 results in more highly selective photocatalysts compared to the unmodified P25. There were significant differences though in the photocatalytic behaviour of the P25, Ag-P25 and Rh-P25 systems. NO decomposition reactions over Ag-P25 photocatalysts were generally more selective than the corresponding reactions over P25 photocatalysts. However, the activity for NO conversion was lower for the silver containing photocatalysts. In the presence of CO, the same Ag-P25 systems became highly selective for $N_2$ formation, with only small amounts of $N_2O$ produced.

In contrast to the Ag-P25 photocatalysts, rhodium modified systems were much more selective for $N_2O$ formation, for both decomposition and reduction reactions, compared to P25 photocatalysts. In the presence of CO, the Rh-P25

photocatalysts showed remarkable activities, with NO conversions of nearly 90 % being detected.

## 8.2 Conclusions from unmodified P25 photocatalysts

- XRD and TEM analysis showed that calcination at temperatures up to 600°C for 2 h did not result in a significant change in the composition of the $TiO_2$ phases and the original composition of *ca.* 20 % anatase / 80 % rutile was maintained.
- DSC analysis of as dried P25 powders led to the conclusion that as the calcination temperature increased, the density of surface bound molecular water and hydroxyl groups decreased.
- The rate of NO conversion for both photocatalytic decomposition and reduction reactions decreased as the photocatalyst pretreatment temperature was increased from 70°C to 600°C. As no phase changes occurred in the temperature range used, this was attributed to the removal of surface bound hydroxyl groups which may act as active sites for NO adsorption.
- The activity for NO conversion was less for the experiments conducted in the presence of CO, due to the preferential adsorption of CO molecules on the active NO adsorption sites.
- For decomposition reactions the major reaction product was $N_2O$ (*ca.* 75 %) with the only other product being $N_2$ (*ca.* 25 %). This product selectivity was maintained irrespective of the photocatalyst pretreatment temperature and initial NO concentration, indicating that the removal of hydroxyl groups did not effect the nature of the active sites available for NO photodecomposition.

- In the presence of CO, the selectivity for $N_2$ formation increased to *ca.* 48 % when photocatalyst pretreatment temperatures of 70°C and 120°C were used.

## 8.3 Conclusions from silver modified P25 photocatalysts

- XRD and TEM analysis of the silver modified P25 systems showed that the presence of silver reduced the onset temperature and increased the rate of the anatase-to-rutile phase transformation. For the 5Ag-P25 photocatalyst, the percentage of rutile present after calcination at 600°C for 2 h was 47 %.
- XRD analysis also showed that crystalline silver nitrate was present on the 5Ag-P25 photocatalyst after pretreatment at temperatures of up to 200°C, although the amount decreased with increasing calcination temperature. After calcination at 600°C, reflections were observed that confirmed the presence of metallic silver. It was concluded that silver nitrate was thermally reduced, forming metallic silver.
- XPS analysis of the 1Ag-P25 and 5Ag-P25 photocatalysts showed that for each of the calcination temperatures used both $Ag^+$ and $Ag^0$ were present and that the amount of $Ag^0$ (relative to the amount of $Ag^+$) increased with increasing calcination temperature.
- Increasing the silver loading and increasing the pretreatment temperature had detrimental effects on the photocatalytic activity of the photocatalysts for both NO photodecomposition and reduction reactions.
- The activity for NO conversion was less for the reduction reactions compared to the decomposition reactions for all the reaction conditions tested due to the blocking of $TiO_2$ adsorption sites by the adsorbed CO molecules.

- Although the activity of the silver modified photocatalysts was less than unmodified P25, the reactions were more selective for $N_2$ formation for all the photocatalysts tested. The NO reduction reactions over 1Ag-P25 and 5Ag-P25 that had been calcined at temperatures above 200°C were essentially 100 % selective for $N_2$ formation. Therefore these photocatalysts were efficient SCR photocatalysts for the reduction of NO with CO.

## 8.4 Conclusions from rhodium modified P25 photocatalysts

- XRD analysis of the 5Rh-P25 photocatalysts did not reveal any reflections due to rhodium containing phases and therefore no information concerning these phases could be obtained from the data. However, it was shown that the presence of rhodium had no effect on the P25 phase transformation kinetics at temperatures of 450°C.
- XPS peak positions of Rh $3d_{5/2}$ indicated that rhodium existed as $Rh^{3+}$ in the samples that were pretreated at 70°C and 200°C, whilst metallic rhodium was present for the samples which had been subjected to reduction pretreatments (both UV and hydrogen reduction).
- For all of the different pretreatments undertaken in the preparation of Rh-P25 photocatalyst systems, the level of rhodium doping and the pretreatments used had little effect either on the selectivity or activity of the NO decomposition reactions.
- In the presence of CO, all of the Rh-P25 photocatalysts exhibited higher NO conversion rates than for the corresponding decomposition reactions. In fact, the as-dried 0.1Rh-P25 photocatalyst showed a percentage NO conversion of *ca.* 87 % which corresponds to a conversion rate of *ca.* 3500 μmol $h^{-1}$ $g^{-1}$. For

comparison, the highest NO conversion rate observed over an unmodified P25 photocatalyst tested under the same conditions was only *ca.* 650 μmol $h^{-1}$ $g^{-1}$. Hence, Rh-P25 based photocatalysts are the extremely active for NO-CO reduction reactions. It is believed that this is due to formation of reactive intermediates on the rhodium active sites, that are negligible in number on the unmodified P25 (as well as Ag-P25 ) surfaces.

- Hydrogen reduction at 450°C resulted in Rh-P25 photocatalysts with the best selectivity for $N_2$ formation with values of *ca.* 40 %. The two Rh-P25 systems which were calcined in air (70°C and 200°C) and the UV reduced systems all showed similar selectivities for $N_2$ formation of *ca.* 10 %, hence the major species produced was $N_2O$.

# 9 Future Work

This is the first study concerning the use of transition metal modified $TiO_2$ photocatalysts for environmental applications that has been conducted at the University of Nottingham, and valuable results can be taken from these studies, giving the basis for future research.

The work presented in this thesis has provided a substantial amount of new information towards the effects of preparation methodology on the nature and photocatalytic properties of P25, Ag-P25 and Rh-P25 photocatalysts for the elimination of NO. Although the silver containing photocatalysts showed very high selectivity for the desired product of $N_2$, and the rhodium containing photocatalysts exhibited exceptional activities for NO conversion, there are many questions that still remain unanswered. These are mainly associated with the unambiguous identifications of the nature of the supported transition metals and the role of the available active sites in the NO decomposition and reduction surface photoreactions.

A number of further analytical techniques could be used to elucidate the nature of the transition metal dopants, where in most cases their particle sizes and/or concentration was below the detection limits for XRD and XPS analysis. Such analysis would include extended X-ray absorption fine structure (EXAFS) and time-of-flight secondary ion mass spectrometry (TOF-SIMS). EXAFS is an averaging technique that can reveal the local structure (e.g. co-ordination number, bond type and distances) in materials that do not have long range order (non-crystalline), and could therefore be used to determine the local structures of the transition metal species present after the various pre-treatments. By reference to materials of known particle sizes, EXAFS can also yield particle size information for

the species studied. Studies of the photocatalyst powders and films using TOF-SIMS could be undertaken to gain a better understanding of the chemical environment of the transition metal species.

The structural evolution with the varying pre-treatments could be further studied using *in-situ* pretreatment experiments. This approach could readily be applied to techniques such as XRD and EXAFS, where a temperature variable sample holder, within which the atmosphere could be varied, could be used. This would give a more accurate understanding of the structural evolution of the transition metal species and the $TiO_2$ phase changes observed in the doped P25 systems.

To identify the active sites and their role in the NO decomposition and reduction reactions a series of mechanistic studies needs to be undertaken. These could include further, more detailed studies of the relationship between photocatalytic activity and the photocatalyst structure. For this it would be essential to establish the nature of the surface species formed during the photo-adsorption of gases such as NO, $N_2O$, $N_2$, CO and $CO_2$. Infrared spectroscopy could readily be applied to such investigative experiments. The photocatalysts could be exposed to gases and illuminated with UV photons in an IR cell, before being evacuated and analysed using the IR source. It would yield information regarding active adsorption sites on the photocatalyst surfaces on which the various gases are adsorbed, thus elucidating potential reactions mechanisms. Similar studies could also be performed in the preparation chamber of either TOF-SIMS or XPS instruments, which would not only yield information about the preferred active sites but also reveal any structural changes that the surface of the photocatalyst may undergo during the photoreactions. By using TOF-SIMS the mechanistic studies could be investigated further by monitoring the isotopic exchange between original surface species and isotopically

labelled gases such as $^{13}CO$ and $^{15}NO$. Only after the mechanistic details of NO decomposition and reductions reactions over the photocatalyst described here are understood, can attempts be made at producing photocatalysts that are designed to give improved photocatalytic activities for NO conversion and selectivities for $N_2$ formation.

The high selectivity for $N_2$ formation of the NO photoreactions over the predominantly $Ag^0$ silver doped-P25 photocatalysts and the high NO conversions of the $Rh^{3+}$ doped photocatalysts are encouraging. A logical step would be to investigate the synergistic effects of co-doped Ag/Rh-P25 photocatalysts. Firstly Rh would be deposited onto P25 surfaces followed by the selective reduction of $Ag^+$ to form $Ag^0$ islands at the Rh sites and rather than on the surface of the P25, thus retaining the highly selective active sites of the silver doped photocatalysts and the good adsorption properties of the rhodium (and hence the high activity) without the reduction in activity due to more efficient electron-hole pair recombination at the Ag-$TiO_2$ interface.

The potential commercial application of the photocatalyst materials described here is the photo-SCR of NO in air. For this to be fulfilled, further photocatalytic evaluation is required using gas streams composed of $O_2$, NO, CO, $CO_2$, $H_2O$ vapour and a range of small hydrocarbons. Deactivation of the photocatalysts over extended periods of use should also be investigated.